# Thermalization in Periodically-Driven Interacting Quantum Systems

Thesis by
Karthik Iyengar Seetharam

In Partial Fulfillment of the Requirements for the
Degree of
Doctor of Philosophy


CALIFORNIA INSTITUTE OF TECHNOLOGY
Pasadena, California

2018
Defended May 14, 2018

Karthik Iyengar Seetharam
ORCID: 0000-0003-1928-8019

# ACKNOWLEDGEMENTS

My life has been filled with joy, comfort, adventure, and incredible intellectual growth due to the endless and unwavering support of my loving family, friends, advisor, and delightful collaborators without whom I would not be writing this thesis today. Few words can describe my debt and gratitude. My obeisance to you all.

[1]

[1] Icon made by Freepik from www.flaticon.com

# ABSTRACT

Periodically-driven (Floquet) quantum systems are ubiquitous in science and technology. For example, when a laser illuminates a material or an AC voltage is applied to a device, the system is well-described by a time-periodic Hamiltonian. In recent years, periodic driving has been proposed, not just as a tool to excite and probe devices, but actually as a mechanism of *engineering* new phases of matter, some of which have no equilibrium analog. However, with this promise comes a serious problem. Intuitively, if energy is injected into and distributed throughout a system, it is no surprise that it tends to heat up indefinitely to infinite temperature.

In this thesis, we study the mechanisms of heating, i.e. the process of thermalization, in Floquet systems and propose methods to control them. Specifically, for non-interacting Floquet systems that are coupled to external bosonic and fermionic baths (e.g. laser-driven electrons in a semiconductor that interact with phonons and an external lead), we classify the relevant scattering processes that contribute to cooling/heating in the Floquet bands and suggest methods to suppress heating via bandwidth-restrictions on the baths. We find that is possible, with appropriate dissipative engineering, to stabilize a controlled incompressible nonequilibrium steady-state resembling a ground state - a state we term the “Floquet insulator." We extend this analysis to include short-range interactions that contribute additional heating processes and show, under the same framework, that heating can be controlled with dissipation. In the process, we develop a simple effective model for the Floquet band densities that captures the essence of all the Floquet scattering processes and that is useful for ballparking experimentally-relevant estimates of heating. Next, we turn our attention to strongly-interacting closed Floquet systems and study how heating emerges through a proliferation of resonances. We find a novel integrable point governing the strong-interaction limit of the Floquet system and examine the breakdown of integrability via the proliferation of resonances. We observe two distinct scaling regimes, attributed to non-thermal and thermal behavior, and discover a power-law scaling of the crossover between them as a function of system size. The lingering ergodicity-breaking effects of the conserved quantities in the vicinity (in parameter space) of the integrable point at finite size is a phenomena we term “near-integrability.” These results suggest that small quantum systems, which are accessible currently in many platforms (e.g. trapped ions, cold atoms, superconducting devices), intrinsically host non-thermal states that one may be able to utilize to avoid heating. Furthermore, our results suggest a “dual" interpretation, in the thermodynamic limit, that a periodically-driven system exhibits prethermalization as a power-law in interaction strength.

# PUBLISHED CONTENT AND CONTRIBUTIONS

[1] Karthik Seetharam, Paraj Titum, Michael Kolodrubetz, and Gil Refael. Absence of thermalization in finite isolated interacting floquet systems. *Phys. Rev. B*, 97:014311, Jan 2018. doi: 10.1103/PhysRevB.97.014311. URL https://link.aps.org/doi/10.1103/PhysRevB.97.014311.
K.I.S. participated in the conception of the project, performed numerical simulations, made primary contributions to the results, and participated in the writing of the manuscript.

[2] Karthik I. Seetharam, Charles-Edouard Bardyn, Netanel H. Lindner, Mark S. Rudner, and Gil Refael. Controlled population of floquet-bloch states via coupling to bose and fermi baths. *Phys. Rev. X*, 5:041050, Dec 2015. doi: 10.1103/PhysRevX.5.041050. URL https://link.aps.org/doi/10.1103/PhysRevX.5.041050.
K.I.S. performed calculations and numerical simulations, made primary contributions to the results, and participated in the writing of the manuscript.

[3] Karthik I. Seetharam, Charles-Edouard Bardyn, Netanel H. Lindner, Mark S. Rudner, and Gil Refael. Floquet-ology: Steady states of interacting floquet insulators. *Arxiv (to appear)*, 2018.
K.I.S. participated in the conception of the project, performed most calculations, simulations, and analysis, and participated in the writing of the manuscript.

# TABLE OF CONTENTS

# LIST OF ILLUSTRATIONS

*Number* *Page*

# LIST OF TABLES

*Number* *Page*

*Chapter 1*

# INTRODUCTION

## 1.1 General Introduction

With recent advances in fabrication, cooling, and laser technologies, quantum physics is now at the forefront of modern science and engineering. In particular, nonequilibrium physics is a challenging frontier rife with opportunity from both a scientific and a technological perspective. Not only are universal predictions and precise quantitative statements scarce, but even the qualitative dynamical behavior of many-body systems, classical or quantum, are not fully understood. Only with a solid understanding can we hope to control quantum many-body systems. The necessity of understanding quantum dynamics is clearly exemplified by the rudimentary tasks encountered in building and operating a quantum computer. To have a fully functional device, one must be able to, with high fidelity, prepare many-qubit states of interest, execute single and two-qubit gate operations, and perform controlled measurements to observe an output, all while being robust to environmental noise. In any platform of interest (e.g. trapped ions or transmon qubits), "doing" any of these steps means altering the physical system in real-time, i.e. a dynamical or nonequilibrium process. While current efforts to build a quantum computer have shown significant progress, a thorough understanding of many-body dynamics and subsequent methods to control them is essential to usher in an age of quantum technology.

One corner of the nonequilibrium landscape is periodically-driven (Floquet) quantum systems and is the topic of this thesis. Floquet systems naturally arise in a variety of experimental platforms. For example, when a laser drives a system or when an oscillatory electrical voltage is applied to a device, the system is well-described by a time-periodic Hamiltonian. Hence, practical tools used to control, excite, and understand real devices many times fall under the broad umbrella of Floquet systems.

In recent years, periodic driving has been proposed, not just as a tool to excite and probe devices, but actually as a mechanism for *engineering* new phases of matter. These Floquet systems can not only exhibit unique phases of matter that do not exist in equilibrium, but also by construction carry the possibility of engineering states of matter in a controlled way, particularly when combined with dissipation and novel device architectures. In fact, the recent adoption of the name Floquet engineering aptly describes much of the research efforts in using periodic driving to induce and control dynamical behavior.

Floquet engineering began with proposals [35, 40, 41, 49, 56] to use a resonant driving to mix the

bands of a simple 2d semiconductor in such as a way as to obtain a nonequilibrium topological phase hosting edge states. This is known as the "Floquet Topological Insulator" (FTI) in analogy to its equilibrium counterpart. This major breakthrough stimulated and intense push to study the extent to which periodic driving could induce new phases of matter. Through this effort emerged the so-called "anomalous" Floquet phases, or rather, periodically-driven phases of matter that do not have any equilibrium counterpart. Examples of these include a quantum hall effect with no delocalized bulk modes known as the "Anomalous Floquet Anderson Insulator" [82] and the "time-crystal" [20, 90] which is a system that spontaneously breaks the periodic time translation symmetry and hosts subharmonic responses. Theoreticians have gone to great lengths to classify all the types of topological phases that exist when augmenting a system with periodic driving though concrete models and experimental proposals are a subject of ongoing work [19, 20, 28, 39, 58, 59, 63–65, 70–72, 82, 85, 86, 90].

Experimental realizations of Floquet phases are also intensely being pursued. Gedik et al. [87] illuminated the surface of a TI with laser light and showed that Floquet bands can be observed via time-resolved angle-resolved-photoemission- spectroscopy (ARPES), at least transiently. Rechtsman et al. [67] have demonstrated an analog of the FTI in photonic crystals where wave propagation is described by the paraxial Schrodinger equation. Periodic driving has also been used to induce artificial gauge fields in cold atomic systems thus providing another avenue for engineering more complex Hamiltonians useful for studying under analog quantum simulation [11, 26]. Aidelsberger et al. [4] and Miyake et al. [54] have both used this to realize the Harper-Hofstader model, and Jotzu et. al [36] have used this technique to realize the Haldane model, all in ultracold atomic gases. Time crystals have been experimentally demonstrated in diamond nitrogen vacancy (NV) centers in Choi et al. [10] and in interacting spin chain of trapped ions in Zhang et al. [92]. Finally, Parker et al. [57] utilize periodic shaking to generate spin interactions strong enough to create ferromagnetic domains.

While the intense activity in Floquet physics is warranted and exciting, there is one major impediment blocking the immediate success of Floquet engineering. If one periodically shakes or (laser) blasts a system *resonantly* thereby inputting energy, and allows that energy to be distributed throughout the system (e.g. through interactions), would the system not just heat up indefinitely? If every Floquet system just kept heating up, there would be no hope in observing new physics or having any means of control. Clearly this is an undesirable end and so one must study when this intuition is in fact true, and if so, how to avoid it. This problem of heating is what prevents a generic resonant Floquet system from becoming useful.

Recent efforts dedicated to overcoming the heating problem can be binned into a few major categories. First, one can open the Floquet system to the environment and engineer the dissipation

appropriately such that the nonequilibrium steady state (NESS) of system is controlled. This is the subject of chapters 2 and 3 and Refs. [14, 31, 32, 76].Second, one can still isolate the system but hope to find parameter regimes in which the heating process is slow compared to any desired physics of interest. This is called prethermalization, or rather finding regimes where there are long-lived transient states [2, 9, 21, 44, 52, 88, 91]. A "dual" version of prethermalization is to look for stationary states of finite systems that do not exhibit maximal entropy (heating). This is the subject of chapter 4. Third, one can study integrable, or more generally "non-ergodic," Floquet models where an extensive (in system size) number of local conserved quantities restrict mixing in the Hilbert space thereby forbidding heating - this is not a generic situation, especially in an experiment, but it serves as a good starting point for studying heating in closed systems [25, 78, 89].An example of this non-ergodic behavior is the extension of many-body localization (MBL) to the Floquet setting [1, 3, 18, 39, 48, 61, 62]. Bordia et al. [7] have periodically driven a system of cold atoms in a disordered optical lattice and demonstrated the existence of non-thermal phase. Finally, one can consider off-resonant Floquet systems in which drives are used to perturbatively modify the system but do not directly allow energetic transitions in the system. This approach has been studied using high frequency expansions as in Refs. [8, 26].

The earliest work discussing an open Floquet system was Galitski et al. [24] in 1969 in the context of a laser illuminated semiconductor. Under approximations, they noted that a resonantly driven semiconductor contains gapped quasiparticles. In modern language, these are just the approximate Floquet states of the system. Furthermore, they noted that coupling the system to a phonon bath yielded a Fermi-Dirac distribution of quasiparticles, which again, in modern language, is known as the Flouqet-Fermi-Dirac (FFD) distribution. In 2001, Kohn [43] studied open Floquet systems which he dubbed "periodic thermodynamics." He was the first to point out that scattering in Floquet systems only conserves quasienergy modulo quanta of the drive. This simple fact has major consequences for the NESS as is explored in this thesis. A few years later in 2005, Kohler et al. [42] derived master equations and studied quantum transport through periodically-driven molecular wires. Hone et al. [30] also pursued a master equation approach in the Floquet basis with particular care for the proliferation of degeneracies (or near-degeneracies) that can arise for a thermodynamically large system with a finite bandwidth (which is what happens in Floquet systems). They concluded the Floquet master equation approach can be used as long as reasonable conditions are met. Finally, Ketzmerick et al. [38] examined the steady states of a driven quartic oscillator and a kicked rotor model (both zero dimensional) and found that the two systems exhibit markedly different behavior with analogs to classical chaotic and regular dynamics.

Our work in chapter 2 builds upon these previous studies of open Floquet systems. We derive a quantum kinetic equation (*Floquet-Boltzmann* equation) for the Floquet states of an extended system

(equations hold for arbitrary dimensions) and numerically analyze its steady states (in 1d) under various conditions on the bosonic and fermionic baths taking particular note of the consequences of quasienergy non-conservation. We discuss regimes under which a FFD distribution can be approached with the help of an energy-filtered fermionic reservoir. In contrast to equilibrium systems, this quasi-thermal steady state displays incompressibility with a finite excitation density, a unique nonequilibrium characteristic leading to its name - the "Floquet insulator." One should note that though we use the term insulator in the incompressibility sense, a true transport experiment would lead to charge transport as the excited particles respond to the applied electric field [23]. Chapter 3 continues this analysis by adding short-range interactions to the system under the same kinetic equation framework. Interactions add additional forms of heating to the system but can still be controlled by the dissipation in the appropriate parameter regimes. We derive a simple effective model for the Floquet band densities that captures the essence of all types of Floquet scattering processes and can be used to ballpark heating effects in experimental settings. In the appendices, we provide a derivation of a more general kinetic equation known as the *Floquet-Redfield* equation and provide some preliminary results. This work has not been published thus far and further work is necessary to understand the role of Floquet band coherences at steady state.

In chapter 4, we turn our attention to closed systems and study heating in a non-integrable Floquet system with driven interactions. We show, using exact numerical simulations and finite size scaling, that the Floquet states of the system exhibit a power-law crossover from a non-thermal regime to a thermal (infinite temperature) regime as a function of system size. The existence of the non-thermal regime is due to what we term "near-integrability," i.e. an integrable point having lingering effects on its vicinity (in parameter space) at finite size. We find the relevant integrable point in our system to be an interesting constrained hopping model at large interaction strengths. Finally, we make predictions for the "dual" problem of prethermalization using the finite size crossover information.

## 1.2 Floquet Theory

In this section, we provide a pedagogical review of Floquet theory which is the foundation for this thesis. We begin with the statement of the Floquet theorem and examine its consequences in the subsequent sections. We show that the Floquet states serve as a natural basis to study coherent periodically-driven systems. Next, we introduce the Sambe space and discuss practical methods to compute the quasienergies and Floquet states of the system. Finally, we conclude with the simple example of a two-level system, analyzed in both the Floquet and the original bases.

*This is background section and so draws heavily upon the References [8, 16, 50, 51, 53, 74, 77]. Henceforth, they will not be explicitly cited unless necessary.*

**Floquet Theorem and Time Evolution**

Time evolution for isolated quantum systems is given by the unitary time-evolution operator on the Hilbert space $\mathcal{R}$ obeying the Schrodinger equation

$$i\partial_t U(t,t_0) = H(t)U(t,t_0) \tag{1.1}$$

where $t_0$ is the initial time point, $t$ is some later time, and $H(t)$ is the hermitian Hamiltonian operator. Application of $U(t,t_0)$ to an initial state $|\psi(t_0)\rangle \in \mathcal{R}$ yields the familiar form

$$i\partial_t |\psi(t)\rangle = H(t)|\psi(t)\rangle$$

Time-periodic (Floquet) systems have Hamiltonians with the property $H(t+T) = H(t)$ where $T$ denotes the period. The Floquet theorem states that for time-periodic Hamiltonians, the time-evolution operator can be decomposed into a static evolution piece with hermitian generator $H_F[t_0]$, known as the stroboscopic Floquet Hamiltonian for a given initial point $t_0$, and time-periodic unitary piece $P(t,t_0)$, known as the micromotion operator

$$U(t,t_0) = P(t,t_0)e^{-iH_F[t_0](t-t_0)} \tag{1.2}$$

where $P(t,t_0)$ is periodic in both arguments. Inserting this into the Schrodinger equation and rearranging yields a formula for Floquet Hamiltonian

$$\begin{aligned} H_F[t_0] &= P^\dagger(t,t_0)\left(H(t) - i\partial_t\right)P(t,t_0) \\ &= P^\dagger(t,t_0)H(t)P(t,t_0) + i\partial_t(P^\dagger(t,t_0))P(t,t_0) \end{aligned} \tag{1.3}$$

where in the last line we have used the hermiticity of $H_F[t_0]$. We may construct the general evolution operator from the decomposition guaranteed by the Floquet theorem. The stroboscopic Floquet Hamiltonian which has a gauge choice of $t_0$ yields

$$\begin{aligned} U(t_2,t_1) &= U(t_2,t_0)U(t_0,t_1) \\ &= U(t_2,t_0)U^\dagger(t_1,t_0) \\ &= P(t_2,t_0)e^{-iH_F[t_0](t_2-t_0)}e^{iH_F[t_0](t_1-t_0)}P^\dagger(t_1,t_0) \\ &= P(t_2,t_0)e^{-iH_F[t_0](t_2-t_1)}P^\dagger(t_1,t_0) \end{aligned} \tag{1.4}$$

By periodicity, $P(t_2, t_0) = P(t_2, t_0 + nT)$ and $P^\dagger(t_1, t_0) = P^\dagger(t_1 - mT, t_0)$ for some $m, n \in \mathbb{Z}$ such that $|(t_1 - mT) - t_0|, |t_2 - (t_0 + nT)| \in [0, T]$. Therefore, one can interpret the above as general "static" evolution under $H_F[t_0]$ from $t_1 \to t_2$ but with "in-period" corrections from $P$ on either end since $|t_2 - t_1|$ does not generically have to be a multiple of the period.

**Aside: Time-Dependent Change of Basis**

Consider performing a time-dependent unitary rotation with new states defined as

$$|\tilde{\psi}(t)\rangle \equiv W^\dagger(t)|\psi(t)\rangle$$

Inserting this into the Schrodinger equation, one obtains

$$\begin{aligned} i\partial_t|\tilde{\psi}(t)\rangle &= (i\partial_t(W^\dagger)W + W^\dagger HW)|\tilde{\psi}(t)\rangle \\ &\equiv \tilde{H}(t)|\tilde{\psi}(t)\rangle \end{aligned} \tag{1.5}$$

where $\tilde{H}(t)$ is Hamiltonian in the rotated frame. Note, for future reference, Sneddon's formula [66]

$$\frac{d}{dt}e^{A(t)} = \int_0^1 du e^{uA}\frac{dA}{dt}e^{(1-u)A}$$

which, for the special case of scalar function $f(t)$ times a matrix $A(t) = f(t)A$, simplifies to $\frac{d}{dt}e^{f(t)A} = A\frac{df}{dt}e^{f(t)A}$.

**Stroboscopic Kick Operators**

Equation 1.3 is exactly the change-of-basis formula for $H(t)$ with a transformation $|\tilde{\psi}(t)\rangle = P^\dagger(t, t_0)|\psi(t)\rangle$. Rearranging the definition of the time-evolution operator, we get $P(t, t_0) = U(t, t_0)e^{-iH_F[t_0](t-t_0)} \equiv e^{-iK_F[t_0](t)}$ which defines a time-dependent unitary transformation of the original basis with hermitian generator $K_F[t_0]$ known as the stroboscopic kick operator. Therefore, one may interpret the Floquet theorem as the existence of a class ($t_0$-dependent) of time-periodic unitary transformations that leads to a class ($t_0$-dependent) of static Hamiltonians that describe the system. Since $t_0$ is unique upto a period, depending on the choice of $t_0$, we have a different transformation. Choice of $t_0$ is equivalent to the choice of initial phase for the time-periodic drive. Note that $P$ is unitary by definition and since it is periodic in both arguments, so is $K_F[t_0](t)$. Furthermore, $P(t_0 + nT, t_0) = 1$ implies $K_F[t_0](t_0 + nT) = 0$ so that stroboscopically, the stroboscopic

kick operators vanish. The stroboscopic kick operators are nothing more than the one-parameter ($t_0$) set of generators of the periodic unitary transformation that transforms the problem into a static one governed by $H_F[t_0]$.

### Gauge Transformation

To make a transformation of the gauge choice $t_0$ to some other choice $t_0 + \delta$, consider the following

$$\begin{aligned} U(t_0 + nT, t_0) &= e^{-iH_F[t_0]nT} \\ &= U^\dagger(t_0 + \delta + nT, t_0 + nT)U(t_0 + \delta + nT, t_0 + \delta)U(t_0 + \delta, t_0) \\ &= U^\dagger(t_0 + \delta + nT, t_0 + nT)e^{-iH_F[t_0+\delta]nT}U(t_0 + \delta, t_0) \\ &= U^\dagger(t_0 + \delta, t_0)e^{-iH_F[t_0+\delta]nT}U(t_0 + \delta, t_0) \end{aligned}$$

where in the last line, we have used in $U(t + mT, t_0 + mT) = U(t, t_0)$ arising directly from the periodicity in $P$. Therefore,

$$e^{-iH_F[t_0+\delta]nT} = U(t_0 + \delta, t_0)e^{-iH_F[t_0]nT}U^\dagger(t_0 + \delta, t_0)$$

Noting the property of unitary transformations, $Ue^AU^\dagger = U\sum_{n=0}^{\infty}\frac{A^n}{n!}U^\dagger = \sum_{n=0}^{\infty}\frac{(UAU^\dagger)^n}{n!} = e^{UAU^\dagger}$, we obtain,

$$\begin{aligned} H_F[t_0 + \delta] &= U(t_0 + \delta, t_0)H_F[t_0]U^\dagger(t_0 + \delta, t_0) \\ &= P(t_0 + \delta, t_0)e^{-iH_F[t_0]\delta}H_F[t_0]e^{iH_F[t_0]\delta}P^\dagger(t_0 + \delta, t_0) \\ &= P(t_0 + \delta, t_0)H_F[t_0]P^\dagger(t_0 + \delta, t_0) \\ &= e^{-iK_F[t_0](t_0+\delta)}H_F[t_0]e^{iK_F[t_0](t_0+\delta)} \end{aligned} \tag{1.6}$$

Due to the periodicity of the kick operators, $H_F[t_0 + nT] = H_F[t_0]$ as expected.

### Symmetric Gauge - Kick Operators

We can perform another periodic transformation on $H_F[t_0]$ to move to an "average" gauge. This is better understood as a symmetric gauge choice and we will denote this frame with the subscript eff. Define $K(t_0)$ as the hermitian generator of the periodic transformation yielding the symmetric gauge given a choice of $t_0$.

$$H_F[t_0] = e^{-iK(t_0)} H_{\text{eff}} e^{iK(t_0)}$$

Upon inversion

$$H_{\text{eff}} = e^{iK(t_0)} H_F[t_0] e^{-iK(t_0)}$$

The spectrum of $H_{\text{eff}}$ is unchanged by the kick operators. Furthermore, the two representations

$$\begin{aligned} H_F[t_0 + \delta] &= e^{-iK(t_0+\delta)} H_{\text{eff}} e^{iK(t_0+\delta)} \\ &= P(t_0 + \delta, t_0) H_F[t_0] P^\dagger(t_0 + \delta, t_0) \\ &= P(t_0 + \delta, t_0) e^{-iK(t_0)} H_{\text{eff}} e^{iK(t_0)} P^\dagger(t_0 + \delta, t_0) \end{aligned}$$

where in the second line, we have used Eq. 1.6. This yields allows the identification

$$e^{-iK(t_0+\delta)} = P(t_0 + \delta, t_0) e^{-iK(t_0)}$$

and subsequent decomposition of the micromotion operator

$$P(t, t_0) \equiv e^{-iK_F[t_0](t)} = e^{-iK(t)} e^{iK(t_0)} \tag{1.7}$$

Utilizing Eq. 1.3, we get an expression for $H_{\text{eff}}$ in terms of a rotation on $H(t)$

$$\begin{aligned} H_{\text{eff}} &= e^{iK(t_0)} H_F[t_0] e^{-iK(t_0)} \\ &= e^{iK(t_0)} P^\dagger(t, t_0) H(t) P(t, t_0) e^{-iK(t_0)} - e^{iK(t_0)} i P^\dagger(t, t_0)(\partial_t P(t, t_0)) e^{-iK(t_0)} \\ &\equiv Q^\dagger(t, t_0) H(t) Q(t, t_0) - i Q^\dagger(t, t_0) \partial_t Q(t, t_0) \end{aligned} \tag{1.8}$$

$$Q(t, t_0) = P(t, t_0) e^{-iK(t_0)} = e^{-iK(t)}$$

where $Q$ is also periodic in $t$. Hence, this is just a different gauge choice which makes $H_{\text{eff}}$, "gauge-symmetric" by moving all the $t_0$ dependence into the modified micromotion operator $Q$. In net, we

have just performed a different periodic unitary transformation with $K(t)$, the kick operator, instead of $K_F[t_0]$, the stroboscopic kick operator. Hence, the two options now are rotation to a specific choice of $t_0$ which is generated by stroboscopic kicks or rotation to a symmetric choice of $t_0$ which is generated by the "normal" kicks. The two are related by Eq. 1.7. Since $K_F[t_0](t_0 + nT) = 0 \forall n$, $e^{-iK(t_0+nT)}e^{iK(t_0)} = 1$ which is satisfied when $K(t_0) = 0$ (by periodicity) for some $t_0$. This just corresponds to the reduction $H_{\text{eff}} = H_F[t_0]$ as per Eq. 1.8. If we are interested in evolution over a period, we have

$$\begin{aligned} U(t_0 + T, t_0) &= e^{-iH_F[t_0]T} \\ &= e^{-ie^{-iK(t_0)}H_{\text{eff}}e^{iK(t_0)}T} \\ &= e^{-iK(t_0)}e^{-iH_{\text{eff}}T}e^{iK(t_0)} \end{aligned}$$

which just corresponds to a static, but parametric on $t_0$, gauge transformation of the Floquet unitary evolution. For general evolution,

$$\begin{aligned} U(t_2, t_1) &= P(t_2, t_0)e^{-iH_F[t_0](t_2-t_1)}P^\dagger(t_1, t_0) \\ &= e^{-iK_F[t_0](t_2)}e^{-iH_F[t_0](t_2-t_1)}e^{iK_F[t_0](t_1)} \\ &= e^{-iK(t_2)}e^{-iH_{\text{eff}}(t_2-t_1)}e^{iK(t_1)} \end{aligned}$$

which is similar to Eq. 1.4 but with stroboscopic kick operators replaced by "normal" kick operators. The symmetric gauge choice and kick operators are derived in a perturbative high-frequency expansion as will be shown in chapter 4.

**Floquet States - Stroboscopically Stationary Solutions**

Consider an observable $O$ in the lab frame. We perform a change of basis

$$\begin{aligned} |\tilde{\psi}(t)\rangle &= P^\dagger(t, t_0)|\psi(t)\rangle \\ i\partial_t|\tilde{\psi}(t)\rangle &= \tilde{H}(t)|\tilde{\psi}(t)\rangle \end{aligned}$$

which by the results of the previous section, yields the static Floquet Hamiltonian $\tilde{H} = H_F[t_0]$ in the rotating frame. Define the orthonormal eigenstates of $\tilde{H} = H_F[t_0]$ thinking of $t_0$ as a parameter choice. These eigenstates are defined in the rotating frame and so we denote them with a tilde with index $\alpha = 1, ..., \dim\mathcal{R}$.

$$H_F[t_0]|\tilde{\phi}_{\alpha,t_0}(0)\rangle \equiv \mathcal{E}_{\alpha,t_0}|\tilde{\phi}_{\alpha,t_0}(0)\rangle$$

The eigenvalues are termed quasienergies by analogy to the Bloch theory of lattices. The evolution in the rotating frame is simple

$$|\tilde{\phi}_{\alpha,t_0}(t)\rangle = e^{-i\mathcal{E}_{\alpha,t_0}t}|\tilde{\phi}_{\alpha,t_0}(0)\rangle$$

In the rotating frame, the a lab frame $O$ must be modified to $\tilde{O}(t)$ given by

$$\begin{aligned}\langle\psi(t)|O|\psi(t)\rangle &= \langle\tilde{\psi}(t)|P^\dagger(t,t_0)OP(t,t_0)|\tilde{\psi}(t)\rangle \\ &\equiv \langle\tilde{\psi}(t)|\tilde{O}(t)|\tilde{\psi}(t)\rangle\end{aligned}$$

Therefore, a lab frame observable in terms of an rotating observable is $O = P(t,t_0)\tilde{O}(t)P^\dagger(t,t_0)$. Note the following property in the rotating frame,

$$\langle\tilde{\phi}_{\alpha,t_0}(t)|\tilde{O}(t)|\tilde{\phi}_{\alpha,t_0}(t)\rangle = \langle\tilde{\phi}_{\alpha,t_0}(0)|\tilde{O}(t)|\tilde{\phi}_{\alpha,t_0}(0)\rangle$$

Moving back to the lab frame we get

$$\begin{aligned}|\phi_{\alpha,t_0}(t)\rangle &= P(t,t_0)|\tilde{\phi}_{\alpha,t_0}(t)\rangle \\ &= e^{-i\mathcal{E}_{\alpha,t_0}t}P(t,t_0)|\tilde{\phi}_{\alpha,t_0}(0)\rangle\end{aligned}$$

A lab frame observable in this state is given by

$$\begin{aligned}\langle\phi_{\alpha,t_0}(t)|O|\phi_{\alpha,t_0}(t)\rangle &= \langle\tilde{\phi}_{\alpha,t_0}(t)|P^\dagger(t,t_0)P(t,t_0)\tilde{O}(t)P^\dagger(t,t_0)P(t,t_0)|\tilde{\phi}_{\alpha,t_0}(t)\rangle \\ &= \langle\tilde{\phi}_{\alpha,t_0}(t)|\tilde{O}(t)|\tilde{\phi}_{\alpha,t_0}(t)\rangle \\ &= \langle\tilde{\phi}_{\alpha,t_0}(0)|\tilde{O}(t)|\tilde{\phi}_{\alpha,t_0}(0)\rangle\end{aligned}$$

which is time-periodic due to the $P$ operators in $\tilde{O}(t)$. Therefore, the solutions $|\phi_{\alpha,t_0}(t)\rangle$ are stroboscopically stationary solutions to the Schrodinger equation and static lab frame observables are time-periodic. We redefine notation for later convenience with $|\phi_{\alpha,t_0}(t)\rangle \equiv P(t,t_0)|\tilde{\phi}_{\alpha,t_0}(0)\rangle$ and

$$|\psi_{\alpha,t_0}(t)\rangle = e^{-i\mathcal{E}_{\alpha,t_0}t}|\phi_{\alpha,t_0}(t)\rangle \tag{1.9}$$

where $|\phi_{\alpha,t_0}(t)\rangle$ is time-periodic. The $|\psi_{\alpha,t_0}(t)\rangle$ are known as the Floquet states and the $|\phi_{\alpha,t_0}(t)\rangle$ are known as the periodic Floquet modes. The existence of solutions of the form in Eq.1.9 is an alternative statement of the Floquet theorem. Importantly, since gauge transformations from $H_F[t_0] \to H_F[\tilde{t}_0]$ are unitary, they only rotate the eigenstates. The quasienergies $\mathcal{E}_\alpha$ are independent of gauge choice $t_0$.

We henceforth drop the subscript $t_0$ for brevity and assume a gauge has been chosen appropriately unless otherwise explicitly indicated or needed. The Floquet states and modes are orthonormal at equal times,

$$\begin{aligned}
\langle\psi_\beta(t)|\psi_\alpha(t)\rangle &= e^{-i(\mathcal{E}_\alpha-\mathcal{E}_\beta)t}\langle\phi_\beta(t)|\phi_\alpha(t)\rangle \\
&= e^{-i(\mathcal{E}_\alpha-\mathcal{E}_\beta)t}\langle\tilde{\phi}_\beta(0)|P^\dagger(t)P(t)|\tilde{\phi}_\alpha(0)\rangle \\
&= e^{-i(\mathcal{E}_\alpha-\mathcal{E}_\beta)t}\langle\tilde{\phi}_\beta(0)|\tilde{\phi}_\alpha(0)\rangle \\
&= \delta_{\beta\alpha}
\end{aligned}$$

and so the completeness relation over $\mathcal{R}$ is $\mathbb{I} = \sum_\alpha |\psi_\alpha(t)\rangle\langle\psi_\alpha(t)|$.

**Sambe Space Formalism**

Consider the formally enlarged Hilbert space $\mathcal{S} \equiv \mathcal{R} \otimes \mathcal{T}$, known as the Sambe space, where $\mathcal{T}$ is spanned by vectors labeled by $t \in [0, T)$. The inner product on $\mathcal{S}$ is defined as the system inner product with additional integration of $t$ over one period, i.e. we have $\frac{1}{T}\int_0^T dt \sum_\alpha$ where $\alpha$ indexes a complete set in $\mathcal{R}$. One can define the time operator (in one period) and its conjugate $P^0$ as

$$\begin{aligned}
T^0_{\mathcal{T}}|t\rangle &= t|t\rangle \\
P^0_{\mathcal{T}}|n\rangle &= n\Omega|n\rangle
\end{aligned}$$

where $\Omega = \frac{2\pi}{T}$ is the drive frequency. These two bases have the properties (note that the choice of convention for the Fourier decomposition is opposite to the usual case with $X, P$ in quantum mechanics).

$$\begin{aligned}\langle t|t'\rangle &= T\delta(t-t')\\ \langle n|n'\rangle &= \delta_{nn'}\\ \langle t|n\rangle &= e^{-in\Omega t}\end{aligned}$$

$$\begin{aligned}\langle t|T^0_{\mathcal{T}}|t'\rangle &= tT\delta(t-t')\\ \langle t|P^0_{\mathcal{T}}|t'\rangle &= iT\delta'(t-t')\\ \langle n|T^0_{\mathcal{T}}|n'\rangle &= -i\delta'_{nn'}\\ \langle n|P^0_{\mathcal{T}}|n'\rangle &= n\Omega\delta_{nn'}\end{aligned}$$

$$[T^0_{\mathcal{T}}, P^0_{\mathcal{T}}] = -i$$

$$1_{\mathcal{T}} = \frac{1}{T}\int_0^T dt|t\rangle\langle t| = \sum_n |n\rangle\langle n|$$

where $\delta'(t-t') = \partial_t\delta(t-t')$ and $\delta'_{nn'} = \partial_{n\Omega}\delta_{nn'}$. We will be cavalier about the distinction between Dirac and Kronecker delta which can be understood from context. Note the above properties make use of the mathematical facts,

$$\begin{aligned}\sum_n e^{-in\Omega(t-t')} &= T\delta(t-t')\\ \frac{1}{T}\int_0^T dt e^{-i\Omega(n-n')t} &= \delta_{nn'}\end{aligned}$$

We can extend the Hamiltonian $H_{\mathcal{R}}(t)$ (subscript $\mathcal{R}$ appended to denote its action on the original Hilbert space $\mathcal{R}$) to the Sambe space as $H_{\mathcal{S}}(t,t') \equiv \langle t|H_{\mathcal{S}}|t'\rangle = H_{\mathcal{R}}(t)T\delta(t-t')$. In fact, we can extend any time-periodic operator in $\mathcal{R}$ to $\mathcal{S}$ in the same fashion $A_{\mathcal{S}}(t,t') \equiv \langle t|A_{\mathcal{S}}|t'\rangle = A_{\mathcal{R}}(t)T\delta(t-t')$. In a compact notation, $A_{\mathcal{S}} = A_{\mathcal{R}}(t)\otimes 1_{\mathcal{T}}$ but note that there is parametric time-dependence meaning that the two pieces are not completely independent as a tensor product notation would suggest (in others words, $A_{\mathcal{S}}$ is block diagonal but not all the same block). Similarly, we can take pure $\mathcal{T}$ operators and extend them to $\mathcal{S}$: $P^0_{\mathcal{S}} = 1_{\mathcal{R}}\otimes P^0_{\mathcal{T}}$ and $T^0_{\mathcal{S}} = 1_{\mathcal{R}}\otimes T^0_{\mathcal{T}}$. In the same fashion, we may extend time-periodic kets in $\mathcal{R}$ to $\mathcal{S}$ by promoting $|\phi_\alpha(t)\rangle_{\mathcal{R}}|_{t\in[0,T)} \rightarrow \frac{1}{T}\int_0^T |t\rangle\langle t|\phi_\alpha\rangle_{\mathcal{S}}$. We

can reverse the procedure to project kets from $\mathcal{S} \rightarrow \mathcal{R}$, i.e. we can just take their time elements $|\phi_\alpha(t)\rangle_\mathcal{R} = \langle t|\phi_\alpha\rangle$.

Define the Floquet operator (also called the Floquet Hamiltonian for reasons that will become clear below)

$$H_\mathcal{S}^F \equiv H_\mathcal{S} - P_\mathcal{S}^0$$

Looking at the matrix elements in time,

$$\begin{aligned}\langle t|H_\mathcal{S}^F|t'\rangle &= H_\mathcal{R}(t)T\delta(t-t') - iT\delta'(t-t') \\ &\equiv H_\mathcal{R}^F T\delta(t-t')\end{aligned}$$

where $H_\mathcal{R}^F = (H_\mathcal{R}(t) - i\partial_t)$. Note that the matrix elements above are also just the extension of $H_\mathcal{R}^F$ to $\mathcal{S}$ as described earlier. The operator $H_\mathcal{R}^F$ is precisely the Floquet Hamiltonian on $\mathcal{R}$ which one obtains by inserting Eq.1.9 into the Schrodinger equation to obtain the eigenvalue equation $H_\mathcal{R}^F|\phi_\alpha(t)\rangle = \mathcal{E}_\alpha|\phi_\alpha(t)\rangle$. Eigenstates of $H_\mathcal{S}^F$ are defined as

$$H_\mathcal{S}^F|\phi_i\rangle = \mathcal{E}_i|\phi_i\rangle$$

where $\mathcal{E}_i$ are the quasienergies and $|\phi_i\rangle$ are the Floquet modes in $\mathcal{S}$ which are, by definition of $\mathcal{T}$, periodic functions of time when projected into $\mathcal{R}$. We can deduce more about these eigenstates by defining the Fourier-translation operators on $\mathcal{T}$ (which are trivially extended to $\mathcal{S}$ as before)

$$M_n \equiv \frac{1}{T}\int_0^T dt|t\rangle\langle t|\langle t|n\rangle$$

On $\mathcal{S}$ (the second commutation holds true on $\mathcal{S}$ and $\mathcal{T}$), we derive the following commutations

$$\begin{aligned}[H_\mathcal{S}^F, M_n] &= -n\Omega M_n \\ [P^0, M_n] &= -n\Omega M_n\end{aligned}$$

The fact $M_m M_n = M_{n+m}$ implies that

$$\begin{aligned}[M_m, M_n] &= 0 \\ [M_m^\dagger, M_n^\dagger] &= 0\end{aligned}$$

Note also,

$$[M_n, M_m^\dagger] = 0$$

Hence, $\{M_n\}$ form an abelian group. Consider the action of $P^0$ on $\mathcal{T}$ (note that $M_n$ is a pure $\mathcal{T}$ operator unless it is trivially extended).

$$\begin{aligned} P^0 M_n|m\rangle &= (M_n P^0 - n\Omega M_n)|m\rangle \\ &= (m\Omega - n\Omega)M_n|m\rangle \\ &= (m-n)\Omega M_n|m\rangle \end{aligned}$$

which further gives legitamacy to the name Fourier-translation operator. Select a particular state $|m\rangle$. Since $P^0$ has dim $\mathcal{T}$ eigenvalues labeled by $n$, acting $\{M_n\}_{n\neq m}$ can generate the entire spectrum of $P^0$. Furthermore, on $\mathcal{S}$

$$\begin{aligned} H_{\mathcal{S}}^F M_n|\phi_i\rangle &= (M_n H_{\mathcal{S}}^F - n\Omega M_n)|\phi_i\rangle \\ &= (\mathcal{E}_i - n\Omega)M_n|\phi_i\rangle \end{aligned}$$

For every eigenstate $|\phi_i\rangle$ there is another eigenstate $M_n|\phi_i\rangle$ for each $n$. Choose a set of dim $\mathcal{R}$eigenstates of $H_{\mathcal{R}}^F$ indexed with $\alpha$. Since there are dim $\mathcal{T}$, $M_n$ operators (one for each $n$), we may generate all dim $\mathcal{S}$ eigenstates by starting with $\{|\phi_\alpha\rangle\}$ and applying the "ladder" $M_n\{|\phi_\alpha\rangle\}$ $\forall n$. Hence, we may label the eigenstates as $|\phi_{\alpha n}\rangle$ and corresponding eigenvalues as $\mathcal{E}_{\alpha n}$. Note that in $\mathcal{S}$, orthonormality of eigenstates of Hermitian operators is given by $\langle\phi_{\alpha n}|\phi_{\alpha' n'}\rangle = \delta_{\alpha\alpha'}\delta_{nn'}$. From now on, greek letters $\{\alpha, \beta, ...\}$ will refer to indices labeling dim $\mathcal{R}$ values and $\{n, m...\}$ will index dim $\mathcal{T}$ values. With this eigenbasis, we can define the resolution $1_{\mathcal{S}} = \sum_{\alpha n} |\phi_{\alpha n}\rangle\langle\phi_{\alpha n}| = \frac{1}{T}\int_0^T dt \sum_\alpha |\alpha t\rangle\langle\alpha t| = \sum_n \sum_\alpha |\alpha n\rangle\langle\alpha n|$ where $|\alpha\rangle$ denotes any basis of $\mathcal{R}$, i.e. $1_{\mathcal{R}} = \sum_\alpha |\alpha\rangle\langle\alpha|$, whenever $\{\alpha, \beta, ...\}$ are not used as subscripts of $\phi$. Therefore,

$$\begin{aligned} H_{\mathcal{S}}^F|\phi_{\alpha n}\rangle &= \mathcal{E}_{\alpha n}|\phi_{\alpha n}\rangle \\ &\equiv (\mathcal{E}_\alpha + n\Omega)|\phi_{\alpha n}\rangle \end{aligned}$$

Here we define $\mathcal{E}_{\alpha n}$ as the state generated from $\mathcal{E}_\alpha$ by $M_{-n}$. We see that the eigenvalues of $H_{\mathcal{S}}^F$ are just dim $\mathcal{T}$ shifted copies of set of dim $\mathcal{R}$eigenvalues$\{\mathcal{E}_{\alpha 0}\}$. Note that the following property of the eigenstates implied by $M_{-n}$.

$$\begin{aligned}
\langle t|\phi_{\alpha(m+n)}\rangle &= \langle t|M_{-n}|\phi_{\alpha m}\rangle \\
&= \frac{1}{T}\int_0^T dt'\langle t|M_{-n}|t'\rangle\langle t'|\phi_{\alpha m}\rangle \\
&= \frac{1}{T}\int_0^T dt' T\delta(t-t')\langle t|-n\rangle\langle t'|\phi_{\alpha m}\rangle \\
&= \langle t|-n\rangle\langle t|\phi_{\alpha m}\rangle \\
&= \langle n|t\rangle\langle t|\phi_{\alpha m}\rangle
\end{aligned}$$

or in other words, on $\mathcal{R}$, $|\phi_{\alpha(m+n)}(t)\rangle = e^{in\Omega t}|\phi_{\alpha m}(t)\rangle$. For $m = 0$, this yields, $|\phi_{\alpha n}(t)\rangle = e^{in\Omega t}|\phi_{\alpha 0}(t)\rangle$. As suggested by Eq. 1.9, we can construct the Floquet states

$$\begin{aligned}
|\psi_{\alpha n}(t)\rangle &= e^{-i\mathcal{E}_{\alpha n}t}|\phi_{\alpha n}(t)\rangle \\
&= e^{-i(\mathcal{E}_{\alpha 0}+n\Omega)t}e^{in\Omega t}|\phi_{\alpha 0}(t)\rangle \\
&= e^{-i\mathcal{E}_{\alpha 0}t}|\phi_{\alpha 0}(t)\rangle \\
&= |\psi_{\alpha 0}(t)\rangle
\end{aligned}$$

and we see that only a single "Floquet zone" (a particular choice of $n$) is unique. This is expected since the real problem lies in $\mathcal{R}$ and we only expect dim $\mathcal{R}$unique Floquet states. Finally, the unique quasienergies are confined to bandwidth $\Omega$ (or alternatively quasienergies live on a circle of radius $\frac{1}{T}$) since changing $n$ shifts all the them to the next zone which is separated by $\Omega$.

**Methodology**

Suppose we have a Floquet system decomposable into a static piece and time-periodic piece $H(t) = H_0 + V(t)$ with $V(t+T) = V(t)$. Expanding the Floquet Hamiltonian in the mode basis

$$
\begin{aligned}
H^F_{\mathcal{S}} &= \frac{1}{T^2}\int_0^T dt \int_0^T dt' \sum_{nm} |m\rangle\langle m|t'\rangle\langle t'|H^F_{\mathcal{S}}|t\rangle\langle t|n\rangle\langle n| \\
&= \frac{1}{T^2}\int_0^T dt \int_0^T dt' \sum_{nm} |m\rangle e^{im\Omega t'}(H_{\mathcal{R}}(t) - i\partial_t)T\delta(t-t')e^{-in\Omega t}\langle n| \\
&= \frac{1}{T}\int_0^T dt \sum_{nm} |m\rangle e^{im\Omega t}(H_{\mathcal{R}}(t) - i\partial_t)e^{-in\Omega t}\langle n| \\
&= \sum_{nm} |m\rangle \frac{1}{T}\int_0^T dt e^{-i(n-m)\Omega t}(H_0 + V(t) - n\Omega)\langle n| \\
&= \sum_{nm} |m\rangle \left((H_0 - n\Omega)\delta_{nm} + \frac{1}{T}\int_0^T dt e^{-i(n-m)\Omega t}V(t)\right)\langle n| \\
&\equiv \sum_{nm} |m\rangle (H^F_{\mathcal{S}})_{mn}\langle n| \qquad (1.10)
\end{aligned}
$$

The Floquet Hamiltonian matrix $(H^F_{\mathcal{S}})_{mn}$ can be diagonalized to obtain the exact eigenstates $|\phi_{\alpha m}\rangle$. Choosing a single zone (i.e. a single $m$), defines the "First Floquet Zone" (FFZ) of width $\Omega$ in which the unique quasienergies live. If we choose $m = 0$ as the FFZ, the unique Floquet modes on $\mathcal{R}$ are given by the time-elements

$$
\begin{aligned}
|\phi_{\alpha 0}(t)\rangle &= \langle t|\phi_{\alpha 0}\rangle \\
&= \sum_n \langle t|n\rangle\langle n|\phi_{\alpha 0}\rangle \\
&= \sum_n e^{-in\Omega t}\langle n|\phi_{\alpha 0}\rangle \\
&\equiv \sum_n e^{-in\Omega t}|\phi^n_{\alpha 0}\rangle
\end{aligned}
$$

The associated Floquet states are

$$
\begin{aligned}
|\psi_\alpha(t)\rangle &= e^{-i\mathcal{E}_{\alpha 0}t}|\phi_{\alpha 0}(t)\rangle \\
&= \sum_n e^{-i(\mathcal{E}_{\alpha 0}+n\Omega)t}|\phi^n_{\alpha 0}\rangle \qquad (1.11)
\end{aligned}
$$

Therefore, we have an explicit method of finding the unique quasienergies and their associated Floquet states. In practice, one cannot usually diagonalize an infinite matrix and so the matrix is truncated at some finite number of zones. This serves as a good approximation to the Floquet matrix, for a sufficient number of zones, if $\frac{|V|}{\Omega} < 1$. This regime is termed weak driving.

An alternative approach to find the quasienergies is to work directly from the definition in Eq. 1.2 and note that time evolution over one period is given by $H_F[t_0]$,

$$H_F[t_0] \quad = \quad \frac{i}{T}\ln U(t_0+T,t_0)$$

If we can compute the time evolution over a single period easily (e.g. for the case of a square drive in $V(t)$), then taking a matrix logarithm provide the quasienergies and states. However, one must note that the Floquet modes obtained from this approach are of length dim $\mathcal{R}$ and so we only obtain the decomposition of Floquet modes in the original basis at stroboscopic time intervals (which is stationary). We obtain no information about harmonics (or "in-period" evolution) as is captured in the Sambe space approach.

**Example: Driven Two-Level System**

Consider a two-level system (e.g. qubit) with the following Hamiltonian

$$H(t) \quad = \quad \frac{\Delta}{2}\sigma_3 + S\cdot\sigma cos(\Omega t) \tag{1.12}$$

where $\sigma = (\sigma_1,\sigma_2,\sigma_3)$ are the three Pauli matrices. Constructing the Floquet Hamiltonian in the Sambe space as per Eq. 1.10, we have

$$H^F = \sum_{nm}|m\rangle\left((H_0-n\Omega)\delta_{nm}+\frac{1}{2}S\cdot\sigma(\delta_{n-m,1}+\delta_{n-m,-1})\right)\langle n|$$

Let us define the basis of $H_0|\nu\rangle = E_\nu|\nu\rangle$ where $E_\nu = (-1)^{\nu+1}\frac{\Delta}{2}$ for $\nu = 0,1$ denoting the lower and upper states respectively. Furthermore, let $H_0^F = \sum_{\nu n}(E_\nu - n\Omega)|\nu n\rangle\langle\nu n|$, i.e. $H_F^0|\nu n\rangle = (E_\nu - n\Omega)|\nu n\rangle$. Note that $n<0$ increases the energy. We define the ordering of a truncated Floquet matrix such that the top left corner is $n\to -N, \nu = 1$ and the bottom right corner is $n = N, \nu = 0$ with $N$ characterizing the number of zones used in the truncation. In other words, the zone index $n$ increases along row/column starting from the top left and $\nu = 1$ appears before $\nu = 0$ in the ordering. With this convention, the highest energy is in the top left and the lowest energy is in the bottom right. For example, in the case of $N = 1$ truncation,

$$H_F^0 = \begin{pmatrix} E_1+\Omega & 0 & 0 & 0 & 0 & 0 \\ 0 & E_0+\Omega & 0 & 0 & 0 & 0 \\ 0 & 0 & E_1+0 & 0 & 0 & 0 \\ 0 & 0 & 0 & E_0+0 & 0 & 0 \\ 0 & 0 & 0 & 0 & E_1-\Omega & 0 \\ 0 & 0 & 0 & 0 & 0 & E_0-\Omega \end{pmatrix}$$

Listing the energies of $|vn\rangle$ states as per $H_F^0$ ordering above,

$$\begin{pmatrix} \underline{E} \\ E_1+\Omega \\ \boldsymbol{E_0+\Omega} \\ \boldsymbol{E_1} \\ E_0 \\ E_1-\Omega \\ E_0-\Omega \end{pmatrix} \leftrightarrow \begin{pmatrix} \underline{v,n} \\ 1,-1 \\ \mathbf{0,-1} \\ \mathbf{1,0} \\ 0,0 \\ 1,1 \\ 0,1 \end{pmatrix}$$

where the bolded basis energies are where we choose to center our FFZ around as we will see below. With $S = (S_1, S_2, S_3)$, the full Floquet matrix is

$$H^F = \begin{pmatrix} E_1+\Omega & 0 & \bar{S}_3 & \bar{S}_1-i\bar{S}_2 & 0 & 0 \\ 0 & E_0+\Omega & \bar{S}_1+i\bar{S}_2 & -\bar{S}_3 & 0 & 0 \\ \bar{S}_3 & \bar{S}_1-i\bar{S}_2 & E_1+0 & 0 & \bar{S}_3 & \bar{S}_1-i\bar{S}_2 \\ \bar{S}_1+i\bar{S}_2 & -\bar{S}_3 & 0 & E_0+0 & \bar{S}_1+i\bar{S}_2 & -\bar{S}_3 \\ 0 & 0 & \bar{S}_3 & \bar{S}_1-i\bar{S}_2 & E_1-\Omega & 0 \\ 0 & 0 & \bar{S}_1+i\bar{S}_2 & -\bar{S}_3 & 0 & E_0-\Omega \end{pmatrix}$$

where we define $\bar{S} = \frac{1}{2}S$ for notational brevity. The structure above is straightforwardly extended to $N > 1$ and numerically diagonalized to the precision desired. However, to make analytical progress, it is helpful to consider the well-known Rotating Wave Approximation (RWA). In the Floquet language, the RWA approximation is to make $H^F$ block diagonal with only keeping single resonances

$$H_{\mathrm{RWA}} = \begin{pmatrix} E_1+\Omega & 0 & 0 & 0 & 0 & 0 \\ 0 & E_0+\Omega & \bar{S}_1+i\bar{S}_2 & 0 & 0 & 0 \\ 0 & \bar{S}_1-i\bar{S}_2 & E_1+0 & 0 & 0 & 0 \\ 0 & 0 & 0 & E_0+0 & \bar{S}_1+i\bar{S}_2 & 0 \\ 0 & 0 & 0 & \bar{S}_1-i\bar{S}_2 & E_1-\Omega & 0 \\ 0 & 0 & 0 & 0 & 0 & E_0-\Omega \end{pmatrix}$$

Note the block-diagonal structure decouples $H_{\mathrm{RWA}}$ into the following basis blocks which upon diagonalization provide the Floquet modes $|\phi_{\alpha m}\rangle$

$$\begin{pmatrix} |\nu=1,n=-1\rangle \\ \begin{pmatrix} |\nu=0,n=-1\rangle \\ |\nu=1,n=0\rangle \end{pmatrix} \\ \begin{pmatrix} |\nu=0,n=0\rangle \\ |\nu=1,n=1\rangle \end{pmatrix} \\ |\nu=0,n=1\rangle \end{pmatrix} \rightarrow \begin{pmatrix} \ldots \\ \begin{pmatrix} |\phi_{+,0}\rangle \\ |\phi_{-,0}\rangle \end{pmatrix} \\ \begin{pmatrix} |\phi_{+,-1}\rangle \\ |\phi_{-,-1}\rangle \end{pmatrix} \\ \ldots \end{pmatrix}$$

where, as before, $|\phi_{\alpha m}\rangle$ is the Floquet mode associated with $\mathcal{E}_\alpha + m\Omega$, and furthermore $\alpha = \pm$ denoting the two Floquet modes. We choose to define the FFZ around $|\nu = 0, n = -1\rangle$ and $|\nu = 1, n = 0\rangle$ and denote that zone as $m = 0$. Note that from comparing the two RWA blocks above, we discover

$$\langle \nu n|\phi_{\alpha 0}\rangle = \langle \nu(n-m)|\phi_{\alpha m}\rangle$$

which for $n = m$ is,

$$\langle \nu m|\phi_{\alpha 0}\rangle = \langle \nu 0|\phi_{\alpha m}\rangle$$

Consider the FFZ block,

$$H_{\mathrm{RWA}} = \begin{pmatrix} E_0+\Omega & \bar{S}_1+i\bar{S}_2 \\ \bar{S}_1-i\bar{S}_2 & E_1 \end{pmatrix}$$

which has the basis $\begin{pmatrix} |\nu=0,n=-1\rangle \\ |\nu=1,n=0\rangle \end{pmatrix}$. We shift the overall energy position (subtract $c\mathbb{I}$ for any $c \in \mathbb{R}$) to obtain

$$\begin{aligned} H_{\text{RWA}} &= \begin{pmatrix} 0 & \bar{S}_1 + i\bar{S}_2 \\ \bar{S}_1 - i\bar{S}_2 & E_1 - E_0 - \omega \end{pmatrix} + (E_0+\omega)\mathbb{I} \\ &= \begin{pmatrix} 0 & \bar{S}_1 + i\bar{S}_2 \\ \bar{S}_1 - i\bar{S}_2 & \delta \end{pmatrix} + (E_0+\omega)\mathbb{I} \\ &= \begin{pmatrix} -\tilde{\delta} & \bar{S}_1 + i\bar{S}_2 \\ \bar{S}_1 - i\bar{S}_2 & \tilde{\delta} \end{pmatrix} + \left(E_0+\omega+\frac{\delta}{2}\right)\mathbb{I} \\ &= \bar{S}_1\sigma_1 + \bar{S}_2\sigma_2 - \tilde{\delta}\sigma_3 \\ &\equiv d\cdot\sigma \end{aligned} \tag{1.13}$$

where we have the gap $\Delta = E_1 - E_0$, detuning $\delta = \Delta - \omega$, half-detuning $\tilde{\delta} = \frac{1}{2}\delta$, $d = (\bar{S}_1, \bar{S}_2, -\tilde{\delta})$, and have ignored the energy shift in the last line. The eigenvalues of such a Hamiltonian are given by

$$\mathcal{E}_\pm = \pm|d|$$

and the associated normalized eigenstates are (with $d \equiv |d| = \sqrt{d_1^2 + d_2^2 + d_3^2}$)

$$|\phi_\pm\rangle = \frac{1}{\sqrt{2d(d \pm d^3)}} \begin{pmatrix} d^3 \pm d \\ d^1 + id^2 \end{pmatrix}$$

or in spherical coordinates $\theta = \cos^{-1}(\frac{d_3}{d})$ and $\phi = \tan^{-1}(\frac{d_2}{d_1})$

$$\begin{aligned} |\phi_+\rangle &= \begin{pmatrix} \cos(\theta/2) \\ e^{i\phi}\sin(\theta/2) \end{pmatrix} \\ |\phi_-\rangle &= \begin{pmatrix} -\sin(\theta/2) \\ e^{i\phi}\cos(\theta/2) \end{pmatrix} \end{aligned}$$

For simplicity, let us assume $\bar{S}_2 = 0$ and just denote $\bar{S}_1 = \bar{S}$ to get

$$\mathcal{E}_\pm = \pm\sqrt{\tilde{\delta}^2 + \bar{S}^2}$$

$$|\phi_\pm\rangle \;=\; \frac{1}{\mathcal{N}_\pm}\begin{pmatrix} -\tilde{\delta} \pm \sqrt{\tilde{\delta}^2 + \bar{S}^2} \\ \bar{S} \end{pmatrix}$$

where we denote normalizations $\mathcal{N}_\pm = \sqrt{2d(d \pm d^3)}$. Therefore, the Floquet (quasienergy) gap in the RWA is $\Delta_A = (\mathcal{E}_+ - \mathcal{E}_-) = \sqrt{\delta^2 + S_1^2}$.

In the case where the drive is resonant with the system, i.e. $\delta = 0$, the quasienergy gap $\Delta_A = S_1$ for the case of $\delta = 0$ when the drive is resonant with the system. This is exactly the Rabi frequency which arises from the traditional RWA analysis of a driven two-level system below. The Floquet modes provide nice intuition (assuming $S_1 > 0$ for simplicity)

$$|\phi_\pm\rangle \;=\; \frac{1}{\sqrt{2}}(\pm|\nu = 0, n = -1\rangle + |\nu = 1, n = 0\rangle)$$

and so in $\mathcal{R}$,

$$\begin{aligned} |\phi_\pm(t)\rangle \;&=\; \sum_\nu (\pm\langle \nu 0|\phi_\alpha\rangle + e^{i\Omega t}\langle \nu, -1|\phi_\alpha\rangle) \\ &=\; \frac{1}{\sqrt{2}}(e^{i\Omega t}|\nu = 0\rangle \pm |\nu = 1\rangle) \end{aligned}$$

which shows that the Floquet modes are symmetric and anti-symmetric superpositions of the the original upper state and the a harmonic of the lower state.

**Aside: Rotating Wave Analysis of the Two-Level System in Original Basis**

Perform a unitary transformation with $W = e^{-iH_0 t}$ (i.e. $|\tilde{\psi}\rangle$ is the interaction picture) for the system $H = H_0 + H_1(t)$ where $H_0 = \frac{\Delta}{2}\sigma_3$ is the static part and $H_1(t) = S\sigma_1 cos(\Omega t)$ is the drive.

$$\begin{aligned} \tilde{H} \;&=\; i\partial_t(W^\dagger)W + W^\dagger H W \\ &=\; e^{iH_0 t}H_1(t)e^{-iH_0 t} \end{aligned}$$

Recalling the Pauli matrix property

$$e^{i\theta\hat{v}\cdot\sigma} \;=\; \cos(\theta)I + i\sin(\theta)(\hat{v}\cdot\sigma)$$

one can directly compute the rotated hamiltonian,

$$\tilde{H} = S\frac{1}{2}\begin{pmatrix} 0 & e^{i(\Delta+\omega)t} + e^{i(\Delta-\omega)t} \\ e^{-i(\Delta-\omega)t} + e^{-i(\Delta+\omega)t} & 0 \end{pmatrix}$$

Keeping lowest frequency terms under the RWA, we get

$$\tilde{H}_{\text{RWA}} \approx \begin{pmatrix} 0 & \frac{1}{2}Se^{i\delta t} \\ \frac{1}{2}Se^{-i\delta t} & 0 \end{pmatrix}$$

where $\delta = \Delta - \omega$ is the detuning. For $\delta = 0$ when the system is resonant $\tilde{H}_{RWA} = \frac{1}{2}S\sigma_1$ which has eigenvalues $\mathcal{E}_\pm = \pm\frac{1}{2}S$ and therefore a gap of $\Delta\mathcal{E} = S$ exactly as in the previous section. It is illuminating to consider probabilities of each state in time. Expanding $|\tilde{\psi}\rangle = \sum_n c_n(t)|n\rangle$ where $H_0|n\rangle = E_n|n\rangle$,

$$\begin{aligned} i\dot{c}_n(t) &= \sum_m e^{-i(E_m-E_n)t}\langle n|H_1(t)|m\rangle c_m(t) \\ &= \sum_m e^{-i(E_m-E_n)t} S\frac{1}{2}(e^{i\Omega t} + e^{-i\Omega t})(\sigma_1)_{nm}c_m(t) \end{aligned}$$

which explicitly is

$$\begin{aligned} i\dot{c}_0 &= e^{-i\Delta t}S\frac{1}{2}(e^{i\Omega t} + e^{-i\Omega t})c_1 \\ i\dot{c}_1 &= e^{i\Delta t}S\frac{1}{2}(e^{i\Omega t} + e^{-i\Omega t})c_0 \end{aligned}$$

where we have defined $\Delta = E_1 - E_0$. In the RWA, we throw away $\omega + \Delta$ terms as fast oscillations and defining the usual detuning $\delta = \Delta - \omega$

$$\begin{aligned} i\dot{c}_0 &= \frac{1}{2}S(e^{i(\omega-\Delta)t} + e^{-i(\omega+\Delta)t})c_1 \approx \frac{1}{2}Se^{-i\delta t}c_1 \\ i\dot{c}_1 &= \frac{1}{2}S(e^{i(\omega+\Delta)t} + e^{-i(\omega-\Delta)t})c_0 \approx \frac{1}{2}Se^{i\delta t}c_0 \end{aligned}$$

For the case of $\delta = 0$ (on-resonance), we can solve easily

$$i\partial_t \begin{pmatrix} c_0 \\ c_1 \end{pmatrix} = \begin{pmatrix} 0 & \frac{1}{2}S \\ \frac{1}{2}S & 0 \end{pmatrix} \begin{pmatrix} c_0 \\ c_1 \end{pmatrix}$$

We can solve this

$$\begin{aligned} i\ddot{c}_0 &= \frac{1}{2}S\frac{1}{2i}Sc_0 \\ \ddot{c}_0 + \frac{1}{4}S^2 c_0 &= 0 \end{aligned}$$

which is just a harmonic oscillator with frequency $\frac{1}{2}S$. Imposing the initial conditions $c_0(0) = 1$ and $c_1(0) = 0$ with the ground populated along noting proper normalization $|c_0|^2 + |c_1|^2 = 1$ yields

$$\begin{aligned} c_0(t) &= \cos(\frac{1}{2}St) \\ c_1(t) &= \sin(\frac{1}{2}St) \end{aligned}$$

The probabilities are

$$\begin{aligned} |c_0(t)|^2 &= \frac{1}{2}(1 + \cos(St)) \\ |c_1(t)|^2 &= \frac{1}{2}(1 - \cos(St)) \end{aligned} \tag{1.14}$$

which shows that the probabilities oscillate with frequency $S$ which is, by definition, the Rabi frequency. Hence, we find that the Floquet gap is the same as the Rabi frequency as stated earlier.

### 1.3 Classical Integrability, Chaos, and Statistical Mechanics

In this section, we begin from the fundamentals of classical dynamics and explore how chaos in dynamical systems emerges via the breakdown of integrability. Chaos, in turn, naturally leads to ergodicity, the foundation of statistical mechanics upon which equilibrium is defined. We show that ergodicity is naturally encoded in a maximum entropy principle that provides a simple prescription for determining the equilibrium state in any setting of interest.

*This is background section and so draws heavily upon several references. For classical mechanics, integrability, and chaos, see Ref.[6, 45, 81, 83]. For statistical mechanics, see Ref.[22, 37, 75]. Henceforth, they will not be explicitly cited unless necessary.*

**Classical Dynamics**

Classical dynamics of a physical system is governed by the least action principle. The action for $n$ degrees of freedom is described by the $n$ independent coordinates $\boldsymbol{q}$, and their associated velocities $\dot{\boldsymbol{q}}$ (not independent variables),

$$\mathcal{S} = \int_{t_0}^{t_f} L(\boldsymbol{q}, \dot{\boldsymbol{q}}, t)dt$$

with $t_0, t_f$ denoting the initial and final times. Computing the functional variation of the action with fixed end points ($\delta\boldsymbol{q}(t_f) = \delta\boldsymbol{q}(t_0) = 0$) and requiring it to vanish, $\delta\mathcal{S} = 0$, yields the Euler-Lagrange equations

$$\frac{d}{dt}\frac{\partial L}{\partial \dot{q}_i} - \frac{\partial L}{\partial q_i} = 0 \tag{1.15}$$

for $i = 1, ..., n$. This is a set of $n$ second order ordinary differential equations (ODEs). We can define $F_i \equiv \frac{\partial L}{\partial q_i}$ and $p_i \equiv \frac{\partial L}{\partial \dot{q}_i}$ as generalized forces and momenta, respectively, to obtain generalized Newton's equations $\dot{p}_i = F_i$.

We can obtain a second formulation of classical dynamics by performing a Legendre transformation where we swap $\dot{q}_i$ for $p_i$ and obtain the Hamiltonian

$$H(\boldsymbol{q}, \boldsymbol{p}) = \sum_i p_i \dot{q}_i - L(\boldsymbol{q}, \dot{\boldsymbol{q}}, t)$$

where we invert the relations $p_i = \frac{\partial L}{\partial \dot{q}_i}$ for $\dot{q}_i(\boldsymbol{p})$ and substitute this into the equation above. Invertibility is possible when $|\frac{\partial^2 L}{\partial q_i \partial q_j}| \neq 0$. Computing derivatives we get Hamilton's equations which are $2n$ first order ODEs

$$\begin{aligned} \dot{p}_i &= -\frac{\partial H}{\partial q_i} \\ \dot{q}_i &= \frac{\partial H}{\partial p_i} \end{aligned} \tag{1.16}$$

We consider $\boldsymbol{q}, \boldsymbol{p}$ as independent variables spanning the $2n$ dimensional phase space $\Gamma$ for the $n$ degrees of freedom.

Introducing the Poisson brackets

$$\{f, g\} = \sum_i \frac{\partial f}{\partial q_i}\frac{\partial g}{\partial p_i} - \frac{\partial f}{\partial p_i}\frac{\partial g}{\partial q_i}$$

one can easily rewrite Hamilton's equations

$$\begin{aligned} \dot{p}_i &= \{p, H\} \\ \dot{q}_i &= \{q, H\} \end{aligned}$$

For a more compact notation, define $\boldsymbol{z} = (q_1, ...q_n, p_1, ..., p_N)$ and the associated gradient $\nabla = (\partial_{q_1}, ..., \partial_{q_n}, \partial_{p_1}, ..., \partial_{p_n})$. Hamilton's equations are then

$$\dot{\boldsymbol{z}} = J \cdot \nabla H(\boldsymbol{z}) \tag{1.17}$$

where $J = \begin{pmatrix} 0 & \mathbb{I}_n \\ -\mathbb{I}_n & 0 \end{pmatrix}$ is the sympletic matrix in $2n$ dimensions and $\mathbb{I}_n$ is the identity matrix in $n$ dimensions.

Consider the Poincare-Cartan 1-form and its exterior derivative on the extended phase space $\mathcal{M} = \mathbb{R}^{2n+1}$ with coordinates $(\boldsymbol{p}, \boldsymbol{q}, t)$

$$\begin{aligned} \omega^{(1)}_{\text{PC}} &= \boldsymbol{p}d\boldsymbol{q} - Hdt \\ d\omega^{(1)}_{\text{PC}} &= d\boldsymbol{p} \wedge d\boldsymbol{q} - dH \wedge dt \\ &= d\boldsymbol{p} \wedge d\boldsymbol{q} - (\sum_i (\partial_{q_i} H) dq_i + (\partial_{p_i} H) dp_i) \\ &= d\boldsymbol{p} \wedge d\boldsymbol{q} + \dot{\boldsymbol{p}} d\boldsymbol{q} - \dot{\boldsymbol{q}} d\boldsymbol{p} \end{aligned}$$

where $\boldsymbol{p}d\boldsymbol{q} = \sum_i p_i dq_i$ and $d\boldsymbol{p} \wedge d\boldsymbol{q} = \sum_i dp_i \wedge dq_i$ (and assuming time-independent Hamiltonian). In odd dimensional spaces, differential 2-forms of $\omega^{(2)}$ always admits at least 1 ("null") vector $\xi \in T\mathcal{M}$ such that $\omega^{(2)}(\xi, \eta) = 0 \ \forall \eta \in T\mathcal{M}$ where $T\mathcal{M}$ is the tangent space. If there is only 1 null vector, then the 2-form is said to be nonsingular. One can use the null vector to uniquely identify a nonsingular 2-form. For a nonsingular 2-form that is exact, $\omega^{(2)} = d\omega^{(1)}$, we have that $\omega^{(1)}$ is closed, $d\omega^{(1)} = 0$, when one of the vectors provided to the 2-form is null (i.e. all oriented surfaces that have a null vector for one of their directions have $d\omega^{(1)} = 0$). Integral curves of null vector fields for nonsingular exact 2-forms are known as vortex lines in analogy to the case of $\mathbb{R}^3$ where

the null vectors are the curl vectors of $\omega^{(1)}$ (more precisely, the curl of the vector field associated to $\omega^{(1)}$ via the Euclidean metric).

The 2-form $d\omega^{(1)}_{\text{PC}}$ is nonsingular (in fact, $\omega^{(2)} = d\boldsymbol{p} \wedge d\boldsymbol{q} - \omega^{(1)} \wedge dt$ for any 1-form $\omega^{(1)}$ is nonsingular) and its null vector is $(\dot{\boldsymbol{p}}, \dot{\boldsymbol{q}}, 1)$. This is precisely the velocity vector of phase flow in Eq.1.17 on the extended phase space. Hence, vortex lines of the Poincare-Cartan 1-form $\omega^{(1)}_{\text{PC}}$ are physical dynamical trajectories (i.e., integral curves of Hamilton's equations). For a closed curve $\gamma_1$ on $\mathcal{M}$, vortex lines passing through $\gamma_1$ form a vortex tube $\sigma$. Given another closed curve $\gamma_2$ encircling the vortex tube $\sigma$, we have the boundary $\partial\sigma = \gamma_1 - \gamma_2$ for a piece of the tube. We can use Stokes' Theorem $\int_{\partial\sigma} \omega^{(1)}_{\text{PC}} = \int_{\sigma} d\omega^{(1)}_{\text{PC}} = 0$ since vortex lines are always tangent to $\sigma$ by construction. Therefore,

$$\oint_{\gamma_1} \omega^{(1)}_{\text{PC}} \;=\; \oint_{\gamma_2} \omega^{(1)}_{\text{PC}} \tag{1.18}$$

for any closed curves $\gamma_1, \gamma_2$ bounding the same vortex tube $\sigma$.

This conclusion leads to powerful results. Consider a closed curve consisting of "initial" states at the same time slice ($dt = 0$) such that $\omega^{(1)}_{\text{PC}} = \boldsymbol{p}d\boldsymbol{q}$. The image of this closed curve under phase flow (to a later time slice) leads to another closed curve. Integrations of $\boldsymbol{p}d\boldsymbol{q}$ around the initial and final closed curves have the same value by Eq. 1.18. Therefore, the (loop integral of the) 1-form $\boldsymbol{p}d\boldsymbol{q}$, known as Poincare's relative integral invariant, is conserved along phase flow/dynamics. Now consider an arbitrary oriented 2-surface $\Sigma$ with boundary $\gamma = \partial\Sigma$. By Stokes' Theorem $\oint_\gamma \boldsymbol{p}d\boldsymbol{q} = \int_\Sigma d\boldsymbol{p} \wedge d\boldsymbol{q}$, and since $\oint_\gamma \boldsymbol{p}d\boldsymbol{q}$ is conserved along phase flow, so is $\int_\Sigma \omega^{(2)}_{\text{SS}} \equiv \int_\Sigma d\boldsymbol{p} \wedge d\boldsymbol{q}$. Hence, the 2-form $\omega^{(2)}_{\text{SS}}$ is an absolute integral invariant of the phase flow and is known as the symplectic structure.

$$\int_{\Sigma} \omega^{(2)}_{\text{SS}} \;=\; \int_{g(\Sigma)} \omega^{(2)}_{\text{SS}} \tag{1.19}$$

where $g(\Sigma)$ is the image of the initial surface $\Sigma$ under evolution to some time slice $t$. Geometrically, $\omega^{(2)}_{\text{SS}}$ represents the projection of the sum of oriented areas given by $(p_i, q_i)$ onto the 2-surface $\Sigma$ and is conserved during phase flow. By taking exterior powers of the symplectic structure to get $\omega^{(2)k}_{\text{SS}}$ for $k = 1, ..., n$ (e.g. for $k = 2$,$\omega^{(2)2}_{\text{SS}} = \omega^{(2)}_{\text{SS}} \wedge \omega^{(2)}_{\text{SS}}$), we get a series of $n$ integral invariants that are conserved during phase flow. Most importantly, for $k = n$, $\omega^{(2)n}_{\text{SS}} = dp_1 \wedge ... \wedge dp_n \wedge dq_1 \wedge ... \wedge dq_n$ is the phase space volume which is conserved. This is Liouville's theorem.

A canonical transformation is a defined as a mapping $g$ that preserves the symplectic structure $\int_\Sigma \omega^{(2)}_{\text{SS}} = \int_{g(\Sigma)} \omega^{(2)}_{\text{SS}}$ for a 2-surface $\Sigma$. Since the phase flow preserves the symplectic structure by

construction, Hamiltonian dynamics are themselves canonical transformations. Physical trajectories are vortex lines of $\omega^{(1)}_{\text{PC}}$ and any new coordinate system $(\boldsymbol{P}, \boldsymbol{Q}, T)$ on $\mathbb{R}^{2n+1}$ must give rise to the same trajectories. For new functions $K(\boldsymbol{P}, \boldsymbol{Q}, T)$ and $S(\boldsymbol{P}, \boldsymbol{Q}, T)$ such that

$$\boldsymbol{p}d\boldsymbol{q} - Hdt = \boldsymbol{P}d\boldsymbol{Q} - KdT + dS$$

physical trajectories are vortex lines of $\boldsymbol{P}d\boldsymbol{Q} - KdT + dS$. Note that we can add the exterior derivative of an arbitrary function (known as the generating function of the canonical transformation) $S(\boldsymbol{P}, \boldsymbol{Q}, T)$ since $d^2 = 0$. Physical trajectories obey Hamilton's equations in the new coordinates as

$$\begin{aligned} \frac{d\boldsymbol{P}}{dT} &= -\frac{\partial K}{\partial \boldsymbol{Q}} \\ \frac{d\boldsymbol{Q}}{dT} &= \frac{\partial K}{\partial \boldsymbol{P}} \end{aligned}$$

and preserve the symplectic structure $d\boldsymbol{p} \wedge d\boldsymbol{q} = d\boldsymbol{P} \wedge d\boldsymbol{Q}$.

**Integrable Systems**

An arbitrarily function $f(\boldsymbol{q}, \boldsymbol{p}, t)$ of the phase space has evolution

$$\frac{d}{dt} f(\boldsymbol{q}, \boldsymbol{p}, t) = \{f, H\} + \frac{\partial f}{\partial t} \tag{1.20}$$

Conserved quantities (a.k.a. constants of motion) are defined as those functions $f(\boldsymbol{q}, \boldsymbol{p})$ that satisfy $\{f, H\} = 0$, i.e. their time evolution vanishes and hence are conserved along any trajectory. Two quantities are said to be in involution if their Poisson bracket vanishes. If we have $n$ quantities, one of which is the $H$, in mutual involution (i.e. all pairwise quantities are in involution), then the system is said to be completely integrable (another Liouville theorem). In this case, call these quantities $\boldsymbol{I}$, where $I_1 = H$, then the trajectories are confined to an $n$ dimensional manifold $M$ for a given choice of $\{I\}$. Define the general "velocities"

$$\boldsymbol{\xi}_i \equiv J \cdot \nabla I_i$$

Of course $\dot{\boldsymbol{z}} = \boldsymbol{\xi}_1$. All $n$ velocity vectors are tangent to $M$ (since they are gradients) and are independent (since all $F$ are in involution).

In the simplest case of $N$ free particles in one dimension, we have a $2N$ dimensional phase space with each particle's momentum conserved. Once the initial momenta are specified, the trajectory in phase space is a straight line. Physically, all the particles just run off towards $\pm\infty$. This is not a very interesting or useful case of an integrable system. More generally, if one has an open trajectory in phase space, it means that some part of the system is "running away" and is not particularly useful to consider. Therefore, out of physical interest, we restrict ourselves to systems which have confined orbits in phase space. The Poincare-Hopf theorem (hairy-ball theorem) states that the only $n$ dimensional closed manifolds with $n$ independent vector fields are those with the topology of tori. Therefore, all trajectories live on $n$-tori $\mathbb{T}^n$ once the invariants are specified.

In this case, one can move to the so-called action-angle variables via a canonical transformation. The action coordinates are none other than the conserved quantities $\boldsymbol{I}$ and the associated angle coordinates $\boldsymbol{\theta}$ characterize the trajectory on the tori. For a specific trajectory where $\boldsymbol{I}$ is specified, the dynamics are governed by $\dot{\theta}_i = \nu_i(\boldsymbol{I})t + \varphi_i$ where $\nu_i(\boldsymbol{I}) = \partial_{I_i} K(\boldsymbol{I})$ is the frequency and $\varphi_i$ is the initial condition. If the frequencies are incommensurate, then the orbits on the torus are quasiperiodic and the torus is called "non-resonant." As a result, the trajectory never overlaps itself and uniformly explores the whole torus never overlapping its previous path (though it can get arbitrarily close). The trajectories are hence ergodic on the torus: The time-average of a function $f$ along the trajectory is equal to the phase space average of a function $f$ on the torus.

$$\lim_{T\to\infty} \frac{1}{T} \int_t^{t+T} f(\boldsymbol{q}(t'), \boldsymbol{p}(t'))dt' \quad = \quad \int_{\mathbb{T}^n} d\boldsymbol{p}\, d\boldsymbol{q}\, f(\boldsymbol{q}, \boldsymbol{p}) \tag{1.21}$$

In contrast, "resonant" tori have commensurate frequencies ($\boldsymbol{k} \cdot \boldsymbol{\nu} = 0$ for some $\boldsymbol{k} \in \mathbb{Z}^n$) which eventually lead to some periodic behavior on the torus and hence no ergodicity. In the phase space $\Gamma$, the set of non-resonant and the set of resonant tori are dense. Assuming the nondegeneracy property $\det|\frac{\partial \nu_i}{\partial I_j}| \neq 0$, finding commensurability is the same as the probability of picking rational numbers in the set of real numbers; this is a set of measure zero. Hence, generically, a choice of $\boldsymbol{I}$ yields orbits on a non-resonant torus and so, ergodic behavior on the torus.

**Breaking Integrability, Mixing, and Chaos**

Suppose one adds breaks integrability by adding a small perturbation to the integrable Hamiltonian $K_0(\boldsymbol{I})$, i.e. suppose $K(\boldsymbol{I}, \boldsymbol{\theta}) = K(\boldsymbol{I}) + \varepsilon K_1(\boldsymbol{I}, \boldsymbol{\theta})$ where $\varepsilon \ll 1$. The famous theorem by Kolmogorov-Arnold-Moser (KAM) states that the irrational (non-resonant) tori survive, albeit deformed, if the perturbation is small enough; the rational (resonant) tori vanish. As the strength of the perturbation increases, even the irrational tori (containing "regular" orbits) start to vanish and trajectories

not residing on the tori become "irregular." They are not confined generically to any particular submanifold of the phase space. In many cases, this breakdown of integrability occurs when regions of phase space containing regular orbits merge into each other and then vanish leaving behind irregular motion. Irregular trajectories with nearby initial conditions often exponentially diverge in time as compared to linearly for regular motion. The exponent governing this exponential divergence is termed the Lyapunov exponent. As the tori completely vanish with energy remaining as the sole conserved quantity, a single irregular trajectory may explore the whole energy shell over time, a property known as mixing. A system displaying extreme initial condition sensitivity and mixing is called chaotic. Chaotic behavior is quite common for generic systems that do possess extensively many conserved quantitites restricting their orbits. We call these types of systems non-integrable.

A few comments are in order. A dynamical system is said to possess ergodicity if, for a function $f(\boldsymbol{q}, \boldsymbol{p})$ on the phase space $\Gamma$,

$$\lim_{T\to\infty} \frac{1}{T} \int_t^{t+T} f(\boldsymbol{q}(t'), \boldsymbol{p}(t'))dt' \quad = \quad \int_{\mathcal{P}} d\boldsymbol{p}\, d\boldsymbol{q}\, f(\boldsymbol{q}, \boldsymbol{p}) \tag{1.22}$$

where $\mathcal{P} \subseteq \Gamma$ is possibly a subset of the phase space, e.g. the energy shell associated to the particular trajectory considered on the left hand side. Furthermore, a dynamical system is mixing if it possesses the stronger property

$$\lim_{t\to\infty} f(\boldsymbol{q}(t), \boldsymbol{p}(t)) \quad = \quad \int_{\mathcal{P}} d\boldsymbol{p}\, d\boldsymbol{q}\, f(\boldsymbol{q}, \boldsymbol{p}) \tag{1.23}$$

Importantly, mixing systems are ergodic but not necessarily the other way around. For example, regular orbits on tori are ergodic but not mixing since a small local region of initial conditions on the torus stays the same throughout evolution, i.e. it is just translated through phase space. There is no exponential sensitivity to initial conditions and hence no deformation of a region of initial conditions upon evolution.

**Statistical Mechanics**

In practical instances of macroscopic objects ($\sim 10^{23}$ degrees of freedom), it is impossible to measure a single phase space trajectory given a particular initial condition. It makes more sense to consider all possible initial conditions, or microstates, consistent with the macroscopic properties of the object, e.g. total energy, total momentum, total particle number, etc. After all, we are interested in properties of a generic large macroscopic object, not a single particular instance of it.

As stated nicely in [22], we want to understand and predict what a generic liter of water does, not a single specific liter that you have prepared with full knowledge of the system (if you could even do so!). This is the purpose and triumph of statistical mechanics - to describe the properties of macroscopic objects without having to track all the dynamical details of the constituent degrees of freedom.

To this end, one defines an ensemble as $\mathcal{N}$ points in phase, i.e. a "cloud" of points in phase space. In the limit of very large $\mathcal{N}$, we can approximate this cloud of points with a density function $\rho(\boldsymbol{q}, \boldsymbol{p})$. The density function can be normalized by dividing by $\mathcal{N} = \int_\Gamma d\boldsymbol{q} d\boldsymbol{p} \rho(\boldsymbol{q}, \boldsymbol{p})$ which counts the number of points in the cloud. We henceforth assume this has be done and now we can interpret $\rho$ as the probability density of the ensemble. The function $\rho$ represents the "state" (ensemble) of the system which evolves in time and so we append $t$ to its argument. Since, Hamiltonian dynamics are canonical transformations that preserve phase space volume, Liouville's theorem dictates

$$\frac{d}{dt}\rho = \{\rho, H\} + \frac{\partial \rho}{\partial t} = 0 \tag{1.24}$$

Defining $j = \rho(\dot{\boldsymbol{q}}, \dot{\boldsymbol{p}}) = \rho \dot{\boldsymbol{z}}$ as the probability current, Eq. 1.24 is just the continuity equation for probability $\partial_t \rho = -\nabla \cdot j$. Intuitively, if we start with some $\mathcal{N}$ points in the ensemble, we must still maintain $\mathcal{N}$ points after evolution.

Ensemble averages (or state averages) of a function $f(\boldsymbol{q}, \boldsymbol{p})$ over phase space $\mathcal{P} \subseteq \Gamma$ can be defined

$$\langle f \rangle_{\mathcal{P}}^{\text{ens}}(t) \equiv \int_{\mathcal{P}} d\boldsymbol{q} d\boldsymbol{p} \rho(\boldsymbol{q}, \boldsymbol{p}, t) f(\boldsymbol{q}, \boldsymbol{p})$$

For example, we may choose $\mathcal{P} = \Gamma_E$, the energy shell $\Gamma_E = [E, E + \Delta]$ for $\Delta \ll E$. Defining the long-time average of a function (we shall assume there is no issue with commuting limits and integrals below)

$$\begin{aligned}
\langle f \rangle_{\mathcal{P}}^{\text{time}} &= \lim_{T \to \infty} \int_t^{t+T} dt' f(\boldsymbol{q}(t'), \boldsymbol{p}(t')) \\
&= \lim_{T \to \infty} \int_t^{t+T} dt' \int_{\mathcal{P}} d\boldsymbol{p} d\boldsymbol{q} \rho(\boldsymbol{q}, \boldsymbol{p}, t') f(\boldsymbol{q}, \boldsymbol{p}) \\
&= \int_{\mathcal{P}} d\boldsymbol{p} d\boldsymbol{q} \left( \lim_{T \to \infty} \int_t^{t+T} dt' \rho(\boldsymbol{q}, \boldsymbol{p}, t') \right) f(\boldsymbol{q}, \boldsymbol{p}) \\
&\equiv \int_{\mathcal{P}} d\boldsymbol{p} d\boldsymbol{q} \langle \rho(\boldsymbol{q}, \boldsymbol{p}) \rangle^{\text{time}} f(\boldsymbol{q}, \boldsymbol{p})
\end{aligned}$$

which is just the ensemble average of $f$ with respect to the time-averaged density $\bar{\rho} \equiv \langle \rho(\boldsymbol{q}, \boldsymbol{p}) \rangle^{\text{time}}$, i.e. $\langle f \rangle_{\mathcal{P}}^{\text{time}} = \langle \langle f \rangle_{\mathcal{P}}^{\text{ens}}(t) \rangle^{\text{time}}$. The phase space average of a function is given by

$$\langle f \rangle_{\mathcal{P}}^{\text{space}} = \int_{\mathcal{P}} d\boldsymbol{q} d\boldsymbol{p} f(\boldsymbol{q}, \boldsymbol{p})$$

Using Eq. 1.22 and Eq. 1.23 with the above definitions we see that a system with ergodicity would require

$$\langle f \rangle_{\mathcal{P}}^{\text{time}} = \langle f \rangle_{\mathcal{P}}^{\text{space}}$$

which implies that $\langle \rho(\boldsymbol{q}, \boldsymbol{p}) \rangle^{\text{time}}$ is constant. A mixing system would require

$$\lim_{t \to \infty} \langle f \rangle_{\mathcal{P}}^{\text{ens}}(t) = \langle f \rangle_{\mathcal{P}}^{\text{space}}$$

which can be satisfied if $\lim_{t \to \infty} \rho(\boldsymbol{q}, \boldsymbol{p}, t)$ is constant. Constant $\rho$ means a uniform distribution across $\mathcal{P}$. A generic Hamiltonian system is not necessarily integrable or ergodic but the idea that chaos can lead to mixing is powerful enough that we hypothesize that many dynamical systems with large numbers of degrees of freedom, at long times, are ergodic. This is often called the ergodic hypothesis or the fundamental postulate of statistical mechanics. Mixing automatically implies the weaker notion of ergodicity. Therefore, in the simplest case where only total energy is conserved, we can just assume a constant density function over an energy shell for any appreciable time scales of interest.

$$\begin{aligned} \rho_{\text{MC}} &= \frac{1}{\mathcal{N}} \delta(H(\boldsymbol{q}, \boldsymbol{p}) - E) \\ \mathcal{N} &= \int_{\Gamma} d\boldsymbol{q} d\boldsymbol{p} \delta(H(\boldsymbol{q}, \boldsymbol{p}) - E) \end{aligned} \tag{1.25}$$

where the delta function restricts the integral to $\Gamma_E$. The idea here is that the chaotic orbits of the phase space cloud described by $\rho$ at long times (and averaged) have sufficiently mixed and so tend to $\rho_{\text{MC}}$. This is known as the microcanonical ensemble.

One can also derive Eq. 1.25 from a different and very useful perspective. Define the von-Neumann entropy function

$$S(\rho) = -k \text{Tr}(\rho \ln \rho) \tag{1.26}$$

where $k$ is Boltzmann's constant and $\mathrm{Tr}(\cdot) = \int_\Gamma d\boldsymbol{q}d\boldsymbol{p}(\cdot)$. If we maximize $S$ on an energy shell (i.e. restrict $\mathrm{Tr}(\cdot)$ to $\Gamma_E$) with respect to $\rho$ subject to the ensemble normalization constraint that $\mathrm{Tr}(\rho) = 1$, we obtain$\rho_{\mathrm{MC}}$. The entropy in this state is

$$S_{\mathrm{MC}} = k\ln(\mathcal{N})$$

which is just the natural logarithm of the number of points in the ensemble. If we only had a single microstate in the ensemble, then the entropy would vanish. This result is equivalent to the thermodynamic (Boltzmann) entropy. Just as the dynamical equations of motion can be recast into a variational principle, we now *define* the equlibrium state as that state $\rho$ which is found by maximizing the entropy $S$ subject to $\mathrm{Tr}(\rho) = 1$ and any other constraints of interest. By construction, this state is time-independent, i.e. stationary as expected in equilibrium. With this procedure, we are equating ergodicity characterizing equilibrium and maximal entropy.

Consider an ensemble with the additional constraint of fixed average energy $U = \langle H\rangle_\Gamma^{\mathrm{ens}}$. Maximization yields

$$\begin{aligned} \rho_{\mathrm{C}} &= \frac{1}{Z}e^{-\beta H} \\ Z &= \mathrm{Tr}(e^{-\beta H}) \end{aligned} \tag{1.27}$$

where $U = \mathrm{Tr}(\rho_C(\beta)H)$ fixes the value of $\beta$, so far just a Lagrange multiplier for the average energy constraint. This is known as the canonical ensemble. Furthermore, the entropy in this state is

$$S_C = k\beta U + k\ln Z$$

and therefore

$$\beta = \frac{1}{k}\frac{\partial S_C}{\partial U} \equiv \frac{1}{kT}$$

Hence, we see that $\beta$ corresponds to rate of change of objective function (entropy) with respect to the constraint variable (average energy) - note that this is the general property of Lagrange multipliers which we have demonstrated explicitly above. The quantity $T$ is the temperature. One also obtains the usual result

$$dU = TdS_{\mathrm{C}}$$

One can trade the constrained maximization of $S$ for unconstrained minimization of a quantity known as the free energy. The free energy $F$ is the (negative) Legendre transformation of $U$ which swaps $S$ for $T$ which is now considered a free parameter instead of $S$.

$$\begin{aligned} F &\equiv U - TS \\ &= \mathrm{Tr}(\rho H) + kT\mathrm{Tr}(\rho \ln \rho) \end{aligned} \tag{1.28}$$

The minimization problem of the free energy subject to only the normalization constraint yields Eq. 1.27. At equilibrium, we find

$$\begin{aligned} F_{\mathrm{C}} &= U - TS_{\mathrm{C}} = -\frac{1}{\beta} \ln Z \\ Z &= e^{-\beta F_C} \end{aligned}$$

Furthermore, we obtain the total differential

$$dF_C = -S_{\mathrm{C}} dT$$

$$S_C = -\frac{\partial F_{\mathrm{C}}}{\partial T}|_U$$

which suggests that one can determine the size of the equilibrium phase space (entropy) if we can measure temperature dependence of the free energy.

One more case of interest is when both the average particle number $\bar{N} \equiv \langle N \rangle_{\Gamma}^{\mathrm{ens}}$ and the average energy $U = \langle H \rangle_{\Gamma}^{\mathrm{ens}}$ is fixed. This is known as the grand canonical ensemble

$$\begin{aligned} \rho_{\mathrm{GC}} &= \frac{1}{\mathcal{Z}} e^{-\beta(H-\mu N)} \\ \mathcal{Z} &= \mathrm{Tr}(e^{-\beta(H-\mu N)}) \end{aligned}$$

from which we obtain

$$S_{\mathrm{GC}} = k\beta U - k\beta\mu\bar{N} + kln\mathcal{Z}$$

$$\begin{aligned}\beta &= \frac{1}{k}\frac{\partial S_{\rm GC}}{\partial U}\\ \mu &= -\frac{1}{T}\frac{\partial S_{\rm GC}}{\partial \bar{N}}\end{aligned}$$

The free energy $\mathcal{F}$ may be computed via a similar Legendre transformation where $S, N$ are swapped for $T, \mu$ as free parameters

$$\mathcal{Z} = e^{-\beta\mathcal{F}}$$

$$\begin{aligned}\mathcal{F}_{\rm GC} &= -\frac{1}{\beta} ln\mathcal{Z}\\ &= U - TS_{\rm GC} - \mu\bar{N}\end{aligned}$$

$$d\mathcal{F}_{GC} = -S_{\rm GC}dT - \bar{N}d\mu$$

which yields

$$\begin{aligned}S_{\rm GC} &= -\frac{\partial \mathcal{F}_{\rm GC}}{\partial T}\\ \bar{N} &= -\frac{\partial \mathcal{F}_{\rm GC}}{\partial \mu}\end{aligned}$$

In all of these ensembles, in the thermodynamic limit (TDL) of $n \to \infty$, the fluctuations around the averages are negligible as a consequence of the central limit theorem (variance around average values die as $\frac{1}{n}$). Hence, all ensembles are equivalent in the thermodynamic limit.

### 1.4 Quantum Thermalization

The formalism developed in the previous section can easily be extended to the quantum realm by promoting the phase space density $\rho$ describing the state of the classical system to the quantum density matrix, Poisson brackets to commutators, and classical observables (e.g. energy, particle number) to hermitian operators. We discuss ideas in quantum integrability and its breakdown to quantum chaos, which address the question as to how *isolated* quantum systems appear thermal,

even under unitary (purity-conserving) evolution. Next, we discuss thermalization as the approach to equilibrium, or perhaps a nonequilibrium steady-state, and give an example of a non-interacting Fermi gas weakly coupled to a bosonic heat bath. Finally, we discuss an important recently discovered phenomena known as many-body localization (MBL) currently under investigation for its unique ergodicity-breaking properties.

### Quantum Dynamics and Statistical Mechanics

Promoting the phase space density to the quantum density matrix

$$\rho \quad = \quad \sum_{\alpha} p_{\alpha} |\psi_{\alpha}\rangle\langle\psi_{\alpha}|$$

where $|\psi_{\alpha}\rangle$ are pure quantum states on a Hilbert space $\mathcal{R}$ and $\alpha$ indexes the pure states involved in the mixture. The $\mathrm{Tr}(\cdot)$ function is now the usual matrix trace. Conservation of probability requires $\mathrm{Tr}(\rho) = 1$.

Ensemble averages of an observable $O$ on $\mathcal{R}$ are given by

$$\langle O \rangle \quad = \quad \mathrm{Tr}(O)$$

and dynamics are given by

$$i\frac{\partial \rho}{\partial t} \quad = \quad [H, \rho]$$

where $\hbar = 1$ unless explicitly noted. The (Schrodinger picture) evolution equation above is just Liouville's theorem with Poisson brackets replaced with commutators (see Eq. 1.20), hence the name the quantum Liouville equation. Entropy is defined exactly as before in Eq. 1.26 and the canonical and grand canonical ensembles are defined by promoting $H, N$ etc. to operators on $\mathcal{R}$.

### Quantum Integrability

The notion of integrability for quantum systems is more subtle and is still an active area of research [60]. For our purposes, and in direct analogy to the definition of classical integrability, we define a integrable quantum system as one in which there is an extensive (polynomial in system size, logarithmically with Hilbert space size) number of *local* (additive) conserved quantities. Locality is an important ingredient in this definition since one can take any quantum Hamiltonian and

diagonalize it in terms of mutually commuting projectors onto eigenstates. However, for a generic system, these would be non-local and so enforcing locality is a necessity. Concretely, we means $H = \sum_\alpha I_\alpha$, $[I_\alpha, I_\beta] = 0$ where $\alpha$ is extensive, and that $\{I\}$ have sub-extensive support in the system size. Note that these conserved quantities should be mutually independent, i.e. one conserved quantity cannot be formed from the others (e.g. cannot just use powers of $I$). Just as with classical integrable systems, the large number of conserved quantities restrict mixing between states in the Hilbert space during unitary evolution. As a result, observables heavily depend on the conserved quantities, even for eigenstates of similar energy or other macroscopic properties. Examples of quantum integrable models include free particle systems ($I$ are just momentum modes), Luttinger liquids, the Transvere field Ising model, and more recently, (at least non-ergodic if not integrable) many-body localized (MBL) systems. Other examples, which have a variant known as Bethe ansatz integrability, are the Lieb-Liniger Bose gas and the XXZ spin chain.

We have defined equilibrium for various ensembles in the previous sections. One can easily generalize the constrained entropy maximization/free energy minimization formalism to account for arbitrary constraints resulting in the Generalized Gibbs Ensemble (GGE) [60, 84]

$$\rho_{\text{GGE}} = \frac{e^{-\sum_\alpha \lambda_\alpha I_\alpha}}{\text{Tr}(e^{-\sum_\alpha \lambda_\alpha I_\alpha})} \tag{1.29}$$

where $\{I\}$ are the conserved quantities and $\{\lambda\}$ are their Lagrange multipliers. The GGE, with an extensive number of local conserved quantities, has been proposed as describing the long time states of quantum integrable models. The GGE is heavily restricted maximal entropy state and can, in a sense, be thought of as the quantum analog of the irrational ergodic tori in classical integrable systems. While the GGE has had a fair amount of success, there are still open investigation on its applicability. Furthermore, in the thermodynamic limit, a quantum analog of the KAM theorem is yet to be found, i.e. for infinite integrable systems, does adding a small perturbation completely destroy the integrability? More generally, do all non-integrable systems thermalize? These are open questions in the field.

### Quantum Chaos

If one introduces integrability-breaking terms, one might expect "quantum chaos," i.e. heavy mixing among states to be allowed. Consequently, the system may exhibit some universal behavior among states sharing a few "macroscopic" properties, such as energy or particle number. This is precisely what is captured in the *Eigenstate Thermalization Hypothesis* (ETH) [13, 15, 55, 68, 69, 79, 80] which states that, for closed conservative systems, eigenstates of similar (finite) energy have similar values of *local* (additive) observables. Again the notion of a local observable is important. If one

looks at global observables of two neighboring (in energy) eigenstates, there is no reason to expect them to be similar - after all, the two eigenstates are globally orthogonal.

This idea was initially captured by Srednicki [79, 80] by the following ansatz for the matrix elements of a generic local observable $\langle a|A|b\rangle$ in many-body eigenstates $|a\rangle$ with energy $E_a$ (assume non-degeneracy such that $E_a = E_b$ only if $\delta_{ab}$)

$$\langle a|A|b\rangle \approx \mathcal{A}(E)\delta_{ab} + e^{-S(E)/2} f(E,\omega) R_{ab} \tag{1.30}$$

where $\mathcal{A}(E)$ and $f(E,\omega)$ are smooth functions of the average energy $E = \frac{1}{2}(E_a + E_b)$ and energy difference $\omega = E_a - E_b$, $S(E)$ is the thermodynamic entropy, and $R_{\alpha\beta}$ is a random complex number drawn from a normal distribution of zero mean and unit variance. Note that the factor $e^{S(E)} = \ln N_E$ where $N_E$ is the number of eigenstates present around $E$. For a system of $n$ degrees of freedom, $N_E$ grows exponentially with $n$, or in other words, $S(E) \sim n$ because entropy is extensive. The second term attempts to capture, in an "average" way, the multiplicity of various off-diagonal matrix elements.

Consider the dynamics of $A$ in a generic pure state $|\psi\rangle = \sum_a c_a |a\rangle$ with $\sum_a |c_a|^2 = 1$ where $H|a\rangle = E_a|a\rangle$ and $\langle H\rangle = E$ is fixed with with small energy fluctuations

$$\langle A(t)\rangle = \sum_{ab} c_b^* c_a e^{-i(E_a - E_b)t} A_{ba}$$

Upon time-averaging the observable, we notice that the phases approximately die out upto a statistical factor that dies exponentially as $n \to \infty$,

$$\begin{aligned}
\overline{\langle A\rangle} &= \lim_{T\to\infty} \int_t^{t+T} dt' \langle A(t')\rangle \\
&= \sum_a |c_a|^2 \mathcal{A}(E) + O(e^{-S/2}) \\
&\approx \sum_a |c_a|^2 \mathcal{A}(E) \\
&= \mathcal{A}(E)
\end{aligned} \tag{1.31}$$

By defining the diagonal mixed state $(\rho_{\text{diag}})_{aa} = |c_a|^2$, the above statement can also be written as

$$\overline{\langle A\rangle} \approx \text{Tr}(\rho_{\text{diag}} A) = \sum_a |c_a|^2 A_{aa} \tag{1.32}$$

where we notice the ansatz in Eq. 1.30 has just identified $A_{aa} = \mathcal{A}(E)$ or rather that the eigenstate expectation values of $A$ are smooth functions of energy, i.e. the ETH. Equation 1.31 and Eq. 1.32 also indicate that one may use the ETH to *effectively replace* $\rho_{\text{diag}} \to \rho_{\text{MC}}$ an obtain the thermal equilibrium result

$$\overline{\langle A \rangle} = \text{Tr}(\rho_{\text{diag}} A) = \text{Tr}(\rho_{\text{MC}} A) \tag{1.33}$$

Note that this argument about dephasing is simple and intuitive but Ref. [69] shows more precisely that the off-diagonal matrix elements are smaller upon time-averaging and hence can be ignored. Importantly, Eq. 1.32 shows that time-averaging leads to a loss of phase information although the energy of the ensemble remains constant (unlike the case in an open system). For chaotic systems with additional sub-extensive constraints beyond just energy conservation, we can replace the diagonal ensemble with the appropriate Gibbs ensemble - a "GGE" with sub-extensive number of integrals of motion. Examining the average temporal fluctuations around $\overline{\langle A \rangle}$ yields

$$\overline{\langle (A(t) - \overline{\langle A \rangle})^2 \rangle} = \sum_{a,b \neq a} |c_a|^2 |c_b|^2 |A_{ab}|^2 = O(e^{-S})$$

which again dies exponentially in system size $n$.

The structure of eigenstates obeying the ETH (a.k.a. ergodic states) have important properties. Suppose one perturbs an ETH hamiltonian (a system whose eigenstates obey ETH) $H \to H + \varepsilon B$ with some operator $B$ whose typical amplitude is $J$. The strength of the perturbation $\varepsilon J$ is generically still larger (assuming $\varepsilon$ isn't exponentially small) than the exponentially decreasing many-body energy spacing $Je^{-S}$. Hence, its effect on any eigenstates is therefore non-perturbative and generically will have a non-local effect. Therefore, the eigenstates of an ETH hamiltonian are very sensitive to perturbation, another signature characteristic of "chaos." [1]. Finally, eigenstates obeying ETH have "volume" law entanglement of the reduced density matrix since they are well-described by a thermal density matrix (Eq. 1.33) on the region of support for the local observable.

The ETH provides one avenue for which a closed quantum system with unitary dynamics can exhibit thermal observations consistent with statistical mechanics. An alternative approach is that of canonical typicality which states that a subsystem of a typical pure state can be well-approximated by $\rho_{\text{MC}}$ [17, 27]. Note that this is a direct statement about the reduced density matrix of the subsystem which is based on the idea that the entanglement of a local subsystem with its complement is sufficient for the complement to act as a bath for the subsystem.

What is the analog of the ETH for Floquet systems? Energy is no longer a conserved quantity and so instead of thorough mixing over a shell $E$, the system may mix overall $E$. This means that the nonequilibrium steady state of the system, upon time-averaging, tends to a completely uniform average over the whole Hilbert space, i.e. an infinite temperature/maximal entropy Gibbs state

$$\rho_{\text{SS}}^{\text{Floq}} \sim \mathbb{I} \tag{1.34}$$

which is what we define as the "Floquet-ETH." This is the generic expectation for a non-integrable Floquet system and intuitively captures the notion of "heating." If one drives the system and the system mixes well without any restrictions, it will heat up indefinetly [12, 46, 47]no matter the structure of the Floquet states (or any basis). As before, if the model is integrable, then heating will not occur [47, 73]. Hence, if one hopes to acheive success with engineering interesting real (generically non-integrable) Floquet phases of matter, then it is of paramount importance to quell this heating and control the nonequilibrium steady state in a desired way.

**Thermalization**

We have described how quantum chaos leads to "equilibrium" behavior for local observables via the ETH in *closed* systems. For the case of an *open* system, equilibrium does not have any restrictions on local observables etc. The global state of the system $\rho$ is a Gibbs state which arises due to exchange of energy, particles, etc. with the environment. In either case, what has been omitted so far was how a generic state of the system achieves (or not!) such an equilibrium state under evolution. In the most general sense, a nonequilibrium state is one in which

$$\rho \neq \rho_{\text{Gibbs}}$$

where $\rho_{\text{Gibbs}}$ corresponds to the appropriate maximal entropy state for a given system. Systems may begin out of equilibrium but as a function of time, approach a nonequilibrium steady state (NESS) denote $\rho_{\text{SS}} \equiv \lim_{t\to\infty} \rho(t)$ (with implicit time-averaging as needed). This process is called *thermalization*. There is no guarantee that $\rho_{\text{SS}} = \rho_{\text{Gibbs}}$, although many times it does (hence the utility of statistical mechanics). In the most general case, $\rho_{\text{SS}}$ does not need to be time-independent for appreciable, but not infinite, time-averaging (e.g. limit cycles). Describing the dynamics and long-time behavior of nonequilibrium systems in a variety of settings is a very active area of research.

Nonequilibrium systems can violate the fundmental ergodic hypothesis of statistical mechanics but all hope of understanding isn't immediately lost. It is certainly possible that dynamics of certain

systems can be well-approximated, perhaps on larger length/time scales or in particular parameter regimes, by effective macroscopic variables obeying partial differential equations, a notion known as hydrodynamics. Another possibility is that observables of interest behave in simple fashion - for example, when making approximations about the correlations in the system. The important point is that nonequilibrium systems require problem-specific analysis and there universal principles governing their behavior are rare.

How does one describe the process of thermalization, either to equilibrium or to a nonequilibrium steady state? One must describe the evolution of the system, usually under approximations with respect to some observables of interest - this approximate evolution is the topic of quantum kinetics. If quantum kinetic approaches are insufficient, then one must resort to direct simulation of full quantum dynamics of the system. Both approaches are utilized in this thesis.

**Example: Quantum Kinetics in Open Systems**

An open system can exchange energy, particles, information, etc. with the environment and eventually settle into a steady state. A simple example capturing this behavior is dynamics of a free Fermi gas that is wealky coupled to a thermal bosonic reservoir which exchanges energy with the system. In this case, the only unique observable (recall Wick's theorem) is the single fermion occupation function $F_a$, where $a$ denotes a particular state of the system, and its evolution is well-described by the semi-classical quantum Boltzmann equation (QBE) [29].

$$\begin{aligned}\dot{F}_a &= \frac{2\pi}{\hbar}\sum_{a_2}|G^a_{a_2}|^2\left(F_{a_2}(1-F_a)N_\omega - F_a(1-F_{a_2})(1+N_\omega)\right)\delta(E_a-E_{a_2}-\hbar\omega)\\ &+ \frac{2\pi}{\hbar}\sum_{a_2}|G^a_{a_2}|^2\left(F_{a_2}(1-F_a)(1+N_\omega) - F_a(1-F_{a_2})N_\omega\right)\delta(E_a-E_{a_2}+\hbar\omega)\end{aligned} \tag{1.35}$$

where $N_\omega$ is the Bose-Einstein distribution of the bosonic bath temperature $T$ and $|G^a_{a_2}|^2$ is the strength of a scattering process $a_2 \to a$ where the fermion absorbs boson of energy $\omega$ - energy conservation is strictly enforced by the delta function. Morever, Fermi statistics appear in the occupation factors in that particle scattering can only happen if there is a particle in the initial state and empty space in the final state. If one is interested in the steady state, we may solve for when $\dot{F}_a = 0$. This solution is the Fermi-Dirac distribution independent of the rates $|G|^2$ and even independent of initial condition (upto having $\mu$ below fixed by the initial number of particles in the system)

$$F_a^{\mathrm{SS}} = \frac{1}{e^{\beta(E_a-\mu)}+1} \tag{1.36}$$

where $\beta = \frac{1}{kT}$ is the inverse bath temperature. Hence, one obtains the fermion distribution expected from an equilibrium state, independent of initial condition and microscopic rate details. One can numericaly evolve the QBE in Eq. 1.35, and see how it approachs $F_a^{\mathrm{SS}}$. Analytical progress can be made by linearizing the Boltzmann equation around steady state $F_a = F_a^{\mathrm{SS}} + \delta_a$. This amounts to a system of linear differential equations for $\delta_a$ which yields exponentially decaying solutions towards equilibrium.

The following chapters examine what happens to the QBE and more general kinetics in the presence of periodic driving. Much of the work will focus the Floquet-Boltzmann equation, the cousin of the QBE responsible for semi-classical kinetics in Floquet systems. Derivations of Floquet-Kinetic equations are provided in appendix.

**An exotic case: Many-Body Localization**

*Much of this section follows the review [1] and henceforth, it will not be explicitly cited unless necessary.*

Many-body localization (MBL) is a remarkable example of ergodicity-breaking (non-ETH) in a system one might intuitively guess is non-integrable/thermalizes. In addition, MBL is a purely quantum mechanical effect which displays a unique type of *quasi-local* integrability that is slightly different from the definition discussed earlier. To understand these statements, it is important to review the first notion of localization discovered by Anderson [5]. He studied a simple hopping model of free fermions in a disordered potential landscape which intuitively was expected to be a dirty metal exhibiting diffusive transport. The results were markedly different. All single particle eigenstates were found to be exponentially localized in space, i.e. $\psi(x) \sim e^{-\frac{|x|}{\xi}}$ where $\xi$ is known as the localization length. This holds true for dimension $d \leq 2$ but for $d \geq 3$, there is a critical strength of the disorder above which the eigenstates delocalize. In fact, even in the localized phase for $d = 3$, there is a separation of the single particle spectrum called the mobility edge below which states are localized and above which states are delocalized (and so conduct). The delocalization transition point is when the mobility edge has vanished and all states are delocalized. This surprising effect is purely a result of destructive quantum interference induced by the disordered potential. Localization implies that the system does not conduct charge and retains memory of its initial state under dynamics since mixing is forbidden.

A natural question is to ask if this localization phenomena survives the introduction of interactions. Intuitively, if the particles are now allowed to scatter from eachother due to interactions over some

spatial range, then one might expect the single particle states to mix across space and hence form delocalized many-body eigenstates. Again, we end up with a surprise - the many-body eigenstates are localized even at infinite temperature, i.e. the full spectrum is localized. This is the celebrated MBL "phase." The prototypical model used to understand such behavior is the random field XXZ chain

$$H_{\mathrm{XXZ}} = J_\perp \sum_{ij} (\sigma_i^x \sigma_{i+1}^x + \sigma_i^y \sigma_{i+1}^y) + J_z \sum_i \sigma_i^z \sigma_{i+1}^z + \sum_i h_i \sigma_i^z \tag{1.37}$$

where $h_i \in [-W, W]$ is a random variable (disorder) drawn from a uniform distribution with max amplitude $W$. Under Jordan-Wigner transformation, this model is equivalent to a hopping ( $J_\perp$) model with nearest-neighbor interactions ($J_z$) and a random chemical potential ($h_i$). Hence, in the limit $J_z \to 0$, one recovers the Anderson insulator. It turns out that for fixed interaction strength, the system is fully localized through the whole spectrum above a critical disorder strength $W^*$ . Even below the critical disorder $W < W^*$, a many-body mobility edge is found to appear. Hence, even in 1d, there is delocalization transition. On the flip side, for fixed disorder strength, below a critical interaction strength $J_z^*$, the system remains fully localized. In the Heisenberg limit where $J_z = J_\perp = J$, the critical disorder point is found to be $W^* = 3.5J$.

These are highly non-trivial observations and lead to several important consequences. First, the MBL-thermal transition is dynamical in that the localization properties explicitly deal with *excited* states, not just ground states as in usual phase transitions. Second, there exists an extensive number of constraints on the system preventing mixing. Third, in contrast to the previous notions of integrability where a small perturbation starts to destroy the local conserved quantities and mixing immediately begins, an MBL system is *robust* to perturbations and the non-ergodic behavior persists for a finite regime in the parameter space of Hamiltonians. Fourth, the localized eigenstates deep inside a region space do not mix with any states near the edge of the region. Consequently, the entanglement entropy grows with the boundary of the region. This is known as the area law and is in stark contrast to the volume law entanglement for thermal states. Finally, local perturbations only affect the states localized in that region.

These statement motivate the idea the MBL eigenstates host localized "quasiparticle" states. We can make this more precise by considering the eigenstates of Eq. 1.37 in the limit of $J_\perp = 0$. In this limit, $H_{\mathrm{XXZ}}$ commutes with all local $\sigma_i^z$, which are hence the local conserved quantities, and so eigenstates are labeled by product states of $\sigma_i^z$ eigenvalues of $\pm 1$ on each site. Turning on a small $J_\perp \neq 0$ yields the MBL phase. The crucial idea is by making *quasi-local* unitary operations $U$ (with finite depth) on the original conserved quantities to get $\tau_i^z \equiv U^\dagger \sigma_i^z U$, one obtains the

new *quasi-local* conserved quantities of the MBL Hamiltonian. The MBL eigenstates are then just product states in this new quasiparticle basis. More specifically,

$$\tau_i^z = C\sigma_i^z + \sum_n V_i^n O_i^n$$

where $O_i^n$ contains upto $2n+1$ body operators from sites around $i$, i.e. an operator with max range upto $n$ around $i$. The coefficient $C$ denotes the *finite* overlap with the original conserved quantity. Furthermore, the coefficients $V_i^n \sim e^{-n/\xi}$ and $\xi$ is termed the localization length hence the usage of "quasi-local" to denote exponential suppression. The operators $\tau_i^z$ are now the quasi-local conserved quantites of the MBL phase and are known commonly as $l$-bits (or quasiparticles in analogy to Fermi-liquid theory). In this basis, an MBL phase is well-described by the universal Hamiltonian

$$H_{\text{MBL}} = \sum_i \tilde{h}_i \tau_i^z + \sum_{ij} J_{ij} \tau_i^z \tau_j^z + \sum_{ijk} J_{ijk} \tau_i^z \tau_j^z \tau_k^z + \ldots \tag{1.38}$$

where $J_{ij}, J_{ijk}, \ldots$ are exponentially suppressed in distance (quasi-local). The details of the coefficients $\tilde{h}, J$ depend on the particular form of the disorder. Weak perturbations would affect the parameters in $H_{\text{MBL}}$ but not change the phase. Hence, one can think of the stability of the MBL phase as a quantum analogue of the KAM theorem where $H_{\text{MBL}}$ is the analog of the "action-angle" representation. Importantly, if one couples an MBL system to a heat bath (e.g. phonons), then the system will delocalize and restore charge transport. This last property distinguishes the MBL from a glassy phase which is reselient to a heat bath. Two final noteworthy properties are that the steady state of an MBL system is believed to be a GGE with the $\tau_i^z$ as the conserved quantities, and that the entanglement entropy grows logarithmically in time after a quench, as opposed to ballistic spreading in thermal states. All of these properties have been tested in finite size simulations and by RG methods. It has even been proven that MBL in 1d can be achieved by quasi-local unitary transformations [33, 34]. However, the fate of MBL in higher dimension (and in the continuum limit) is an open question.

These ideas can be extended to the periodically-driven setting where we get the Floquet-MBL phase. The Floquet states remain localized in the presence of a period drive so long as the drive frequency is high enough. For low frequencies that causes resonances, delocalization immediately occurs with even small drive amplitude. Hence, MBL can be used to prevent uncontrolled heating in a Floquet system with some restrictions on drive frequency. The Floquet-MBL phase was used as a basis for the so-called time-crystal where the periodic time-translation invariance of the system is broken and observables exhibit subharmonic responses.

## References


[1] D. A. Abanin, E. Altman, I. Bloch, and M. Serbyn. Ergodicity, Entanglement and Many-Body Localization. *ArXiv e-prints*, April 2018.

[2] Dmitry Abanin, Wojciech De Roeck, Wen Wei Ho, and Francois Huveneers. A rigorous theory of many-body prethermalization for periodically driven and closed quantum systems. *Communications in Mathematical Physics*, 354(3):809–827, September 2017.

[3] Adhip Agarwala and Diptiman Sen. Effects of interactions on periodically driven dynamically localized systems. *Phys. Rev. B*, 95:014305, Jan 2017. doi: 10.1103/PhysRevB.95.014305.

[4] M. Aidelsburger, M. Atala, M. Lohse, J. T. Barreiro, B. Paredes, and I. Bloch. Realization of the hofstadter hamiltonian with ultracold atoms in optical lattices. *Phys. Rev. Lett.*, 111: 185301, Oct 2013. doi: 10.1103/PhysRevLett.111.185301.

[5] P. W. Anderson. Absence of diffusion in certain random lattices. *Phys. Rev.*, 109:1492–1505, Mar 1958.

[6] V I Arnold. *Mathematical Methods of Classical Mechanics*. Springer, 1997.

[7] Pranjal Bordia, Henrik Luschen, Ulrich Schneider, Michael Knap, and Immanuel Bloch. Periodically driving a many-body localized quantum system. *Nature Physics*, 13(5):460–464, 05 2017.

[8] Marin Bukov, Luca D'Alessio, and Anatoli Polkovnikov. Universal high-frequency behavior of periodically driven systems: from dynamical stabilization to floquet engineering. *Advances in Physics*, 64(2):139–226, 2015. doi: 10.1080/00018732.2015.1055918.

[9] Marin Bukov, Sarang Gopalakrishnan, Michael Knap, and Eugene Demler. Prethermal floquet steady states and instabilities in the periodically driven, weakly interacting bose-hubbard model. *Phys. Rev. Lett.*, 115:205301, Nov 2015. doi: 10.1103/PhysRevLett.115.205301.

[10] Soonwon Choi, Joonhee Choi, Renate Landig, Georg Kucsko, Hengyun Zhou, Junichi Isoya, Fedor Jelezko, Shinobu Onoda, Hitoshi Sumiya, Vedika Khemani, Curt von Keyserlingk, Norman Y. Yao, Eugene Demler, and Mikhail D. Lukin. Observation of discrete time-crystalline order in a disordered dipolar many-body system. *Nature*, 543(7644):221–225, 2017.

[11] N. R. Cooper, J. Dalibard, and I. B. Spielman. Topological Bands for Ultracold Atoms. *ArXiv e-prints*.

[12] Luca D'Alessio and Marcos Rigol. Long-time behavior of isolated periodically driven interacting lattice systems. *Phys. Rev. X*, 4:041048, Dec 2014.

[13] Luca D'Alessio, Yariv Kafri, Anatoli Polkovnikov, and Marcos Rigol. From quantum chaos and eigenstate thermalization to statistical mechanics and thermodynamics. *Advances in Physics*, 65(3):239–362, 2016.

[14] Hossein Dehghani, Takashi Oka, and Aditi Mitra. Dissipative floquet topological systems. *Phys. Rev. B*, 90:195429, Nov 2014. doi: 10.1103/PhysRevB.90.195429.

[15] J. M. Deutsch. Quantum statistical mechanics in a closed system. *Phys. Rev. A*, 43:2046–2049, Feb 1991. doi: 10.1103/PhysRevA.43.2046.

[16] T. Dittrich, P. Hänggi, G.-L. Ingold, B. Kramer, G. Schön, and W. Zwerger. *Quantum Transport and Dissipation*. Wiley-WCH, 1998. ISBN 978-3527292615.

[17] Anatoly Dymarsky, Nima Lashkari, and Hong Liu. Subsystem eigenstate thermalization hypothesis. *Phys. Rev. E*, 97:012140, Jan 2018.

[18] Luca D'Alessio and Anatoli Polkovnikov. Many-body energy localization transition in periodically driven systems. *Annals of Physics*, 333(Supplement C):19 – 33, 2013. ISSN 0003-4916.

[19] Dominic V. Else and Chetan Nayak. Classification of topological phases in periodically driven interacting systems. *Phys. Rev. B*, 93:201103, May 2016. doi: 10.1103/PhysRevB.93.201103.

[20] Dominic V. Else, Bela Bauer, and Chetan Nayak. Floquet time crystals. *Phys. Rev. Lett.*, 117: 090402, Aug 2016.

[21] Dominic V. Else, Bela Bauer, and Chetan Nayak. Prethermal phases of matter protected by time-translation symmetry. *Phys. Rev. X*, 7:011026, Mar 2017. doi: 10.1103/PhysRevX.7.011026.

[22] Eric. Statistical mechanics. Lecture Notes, September 2012. URL `http://www.pa.ucla.edu/content/eric-dhoker-lecture-notes`.

[23] I. Esin, M. S. Rudner, G. Refael, and N. H. Lindner. Steady states and edge state transport in topological Floquet-Bloch systems. *ArXiv e-prints*, October 2017.

[24] V. M. Galitskii, S. P. Goreslavskii, and V. F. Elesin. Electric and magnetic properties of a semiconductor in the field ofa strong electromagnetic wave. *Sov. Phys. JETP*, 30:117, 1970.

[25] James R. Garrison, Ryan V. Mishmash, and Matthew P. A. Fisher. Partial breakdown of quantum thermalization in a hubbard-like model. *Phys. Rev. B*, 95:054204, Feb 2017. doi: 10.1103/PhysRevB.95.054204.

[26] N. Goldman and J. Dalibard. Periodically driven quantum systems: Effective hamiltonians and engineered gauge fields. *Phys. Rev. X*, 4:031027, Aug 2014. doi: 10.1103/PhysRevX.4.031027.

[27] Sheldon Goldstein, Joel L. Lebowitz, Roderich Tumulka, and Nino Zanghì. Canonical typicality. *Phys. Rev. Lett.*, 96:050403, Feb 2006.

[28] Fenner Harper and Rahul Roy. Floquet topological order in interacting systems of bosons and fermions. *Phys. Rev. Lett.*, 118:115301, Mar 2017. doi: 10.1103/PhysRevLett.118.115301.

[29] Antti-Pekka Jauho Hartmut Haug. *Quantum Kinetics in Transport and Optics of Semiconductors*. Springer-Verlag Berlin Heidelberg, 2008.

[30] Daniel W. Hone, Roland Ketzmerick, and Walter Kohn. Statistical mechanics of floquet systems: The pervasive problem of near degeneracies. *Phys. Rev. E*, 79:051129, 2009.

[31] Thomas Iadecola and Claudio Chamon. Floquet systems coupled to particle reservoirs. *Phys. Rev. B*, 91:184301, May 2015. doi: 10.1103/PhysRevB.91.184301.

[32] Thomas Iadecola, Titus Neupert, and Claudio Chamon. Occupation of topological floquet bands in open systems. *Phys. Rev. B*, 91:235133, Jun 2015. doi: 10.1103/PhysRevB.91.235133.

[33] John Z. Imbrie. Diagonalization and many-body localization for a disordered quantum spin chain. *Phys. Rev. Lett.*, 117:027201, Jul 2016.

[34] John Z. Imbrie. On many-body localization for quantum spin chains. *Journal of Statistical Physics*, 163(5):998–1048, Jun 2016.

[35] Liang Jiang, Takuya Kitagawa, Jason Alicea, A. R. Akhmerov, David Pekker, Gil Refael, J. Ignacio Cirac, Eugene Demler, Mikhail D. Lukin, and Peter Zoller. Majorana fermions in equilibrium and in driven cold-atom quantum wires. *Phys. Rev. Lett.*, 106:220402, Jun 2011. doi: 10.1103/PhysRevLett.106.220402.

[36] Gregor Jotzu, Michael Messer, Rémi Desbuquois, Martin Lebrat, Thomas Uehlinger, Daniel Greif, and Tilman Esslinger. Experimental realization of the topological haldane model with ultracold fermions. *Nature*, 515:237–240, Nov 2014. doi: 10.1038/nature13915.

[37] Mehran Kardar. *Statistical Physics of Fields*. Cambridge University Press, 2007.

[38] Roland Ketzmerick and Waltraut Wustmann. Statistical mechanics of floquet systems with regular and chaotic states. *Phys. Rev. E*, 82:021114, 2010.

[39] Vedika Khemani, Achilleas Lazarides, Roderich Moessner, and S. L. Sondhi. Phase structure of driven quantum systems. *Phys. Rev. Lett.*, 116:250401, Jun 2016.

[40] Takuya Kitagawa, Erez Berg, Mark Rudner, and Eugene Demler. Topological characterization of periodically driven quantum systems. *Phys. Rev. B*, 82:235114, 2010.

[41] Takuya Kitagawa, Takashi Oka, Arne Brataas, Liang Fu, and Eugene Demler. Transport properties of nonequilibrium systems under the application of light: Photoinduced quantum hall insulators without landau levels. *Phys. Rev. B*, 84:235108, Dec 2011. doi: 10.1103/PhysRevB.84.235108.

[42] Sigmund Kohler, Jörg Lehmann, and Peter Hänggi. Driven quantum transport on the nanoscale. *Phys. Rep.*, 406:379–443, Feb 2005. doi: 10.1016/j.physrep.2004.11.002.

[43] Walter Kohn. Periodic thermodynamics. *Journal of Statistical Physics*, 103:417–423, 2001. doi: 10.1023/A:1010327828445.

[44] Tomotaka Kuwahara, Takashi Mori, and Keiji Saito. Floquet-magnus theory and generic transient dynamics in periodically driven many-body quantum systems. *Annals of Physics*, 367:96–124, April 2016.

[45] E. M. Lifshitz L. D. Landau. *Mechanics*. Butterworth-Heinemann, 1976.

[46] Achilleas Lazarides, Arnab Das, and Roderich Moessner. Equilibrium states of generic quantum systems subject to periodic driving. *Phys. Rev. E*, 90:012110, Jul 2014.

[47] Achilleas Lazarides, Arnab Das, and Roderich Moessner. Periodic thermodynamics of isolated quantum systems. *Phys. Rev. Lett.*, 112:150401, Apr 2014.

[48] Achilleas Lazarides, Arnab Das, and Roderich Moessner. Fate of many-body localization under periodic driving. *Phys. Rev. Lett.*, 115:030402, Jul 2015.

[49] N. H. Lindner, G. Refael, and V. Galitski. Floquet topological insulator in semiconductor quantum wells. *Nature Physics*, 7:490–495, Mar 2011. doi: 10.1038/nphys1926.

[50] Radu Paul Lungu. The floquet theory of the time-periodic hamiltonian systems i. the pseudo-evolution method. *Romanian Reports in Physics*, 52(3-4):233–263, 2000.

[51] Radu Paul Lungu. The floquet theory of the time-periodic hamiltonian systems ii. fermion system at zero temperature. *Romanian Reports in Physics*, 52(3-4):265–316, 2000.

[52] F. Machado, G. D. Meyer, D. V. Else, C. Nayak, and N. Y. Yao. Exponentially slow heating in short and long-range interacting floquet systems. *ArXiv e-prints*, August 2017.

[53] M. Matti Maricq. Application of average hamiltonian theory to the nmr of solids. *Phys. Rev. B*, 25:6622–6632, Jun 1982. doi: 10.1103/PhysRevB.25.6622. URL `https://link.aps.org/doi/10.1103/PhysRevB.25.6622`.

[54] Hirokazu Miyake, Georgios A. Siviloglou, Colin J. Kennedy, William Cody Burton, and Wolfgang Ketterle. Realizing the harper hamiltonian with laser-assisted tunneling in optical lattices. *Phys. Rev. Lett.*, 111:185302, Oct 2013. doi: 10.1103/PhysRevLett.111.185302.

[55] Rahul Nandkishore and David A. Huse. Many-body localization and thermalization in quantum statistical mechanics. *Annual Review of Condensed Matter Physics*, 6(1):15–38, 2015.

[56] Takashi Oka and Hideo Aoki. Photovoltaic hall effect in graphene. *Phys. Rev. B*, 79:081406, Feb 2009. doi: 10.1103/PhysRevB.79.081406.

[57] Colin Parker, Li-Chung Ha, and Cheng Chin. Direct observation of effective ferromagnetic domains of cold atoms in a shaken optical lattice. *Nature Physics*, 2013.

[58] Hoi Chun Po, Lukasz Fidkowski, Takahiro Morimoto, Andrew C. Potter, and Ashvin Vishwanath. Chiral floquet phases of many-body localized bosons. *Phys. Rev. X*, 6:041070, Dec 2016. doi: 10.1103/PhysRevX.6.041070.

[59] Hoi Chun Po, Lukasz Fidkowski, Ashvin Vishwanath, and Andrew C. Potter. Radical chiral floquet phases in a periodically driven kitaev model and beyond. *Phys. Rev. B*, 96:245116, Dec 2017. doi: 10.1103/PhysRevB.96.245116. URL https://link.aps.org/doi/10.1103/PhysRevB.96.245116.

[60] Anatoli Polkovnikov, Krishnendu Sengupta, Alessandro Silva, and Mukund Vengalattore. Colloquium. *Rev. Mod. Phys.*, 83:863–883, Aug 2011. doi: 10.1103/RevModPhys.83.863.

[61] Pedro Ponte, Anushya Chandran, Z. Papić, and Dmitry A. Abanin. Periodically driven ergodic and many-body localized quantum systems. *Annals of Physics*, 353:196–204, Nov 2014. doi: 10.1016/j.aop.2014.11.008.

[62] Pedro Ponte, Z. Papić, Francois Huveneers, and Dmitry A. Abanin. Many-body localization in periodically driven systems. *Phys. Rev. Lett.*, 114:140401, 2015.

[63] A. C. Potter, A. Vishwanath, and L. Fidkowski. An infinite family of 3d floquet topological paramagnets. *ArXiv e-prints*, June 2017.

[64] Andrew C. Potter and Takahiro Morimoto. Dynamically enriched topological orders in driven two-dimensional systems. *Phys. Rev. B*, 95:155126, Apr 2017. doi: 10.1103/PhysRevB.95.155126.

[65] Andrew C. Potter, Takahiro Morimoto, and Ashvin Vishwanath. Classification of interacting topological floquet phases in one dimension. *Phys. Rev. X*, 6:041001, Oct 2016. doi: 10.1103/PhysRevX.6.041001.

[66] Ravinder R. Puri. *Mathematical Methods of Quantum Optics*. Springer-Verlag Berlin Heidelberg, 2001.

[67] M. C. Rechtsman, J. M. Zeuner, Y. Plotnik, Y. Lumer, D. Podolsky, F. Dreisow, S. Nolte, M. Segev, and A. Szameit. Photonic floquet topological insulators. *Nature*, 496:196–200, Apr 2013. doi: 10.1038/nature12066.

[68] Marcos Rigol. Breakdown of thermalization in finite one-dimensional systems. *Phys. Rev. Lett.*, 103:100403, Sep 2009. doi: 10.1103/PhysRevLett.103.100403. URL https://link.aps.org/doi/10.1103/PhysRevLett.103.100403.

[69] Marcos Rigol, Vanja Dunjko, and Maxim Olshanii. Thermalization and its mechanism for generic isolated quantum systems. *Nature*, 2008.

[70] Rahul Roy and Fenner Harper. Abelian floquet symmetry-protected topological phases in one dimension. *Phys. Rev. B*, 94:125105, Sep 2016. doi: 10.1103/PhysRevB.94.125105.

[71] Rahul Roy and Fenner Harper. Floquet topological phases with symmetry in all dimensions. *Phys. Rev. B*, 95:195128, May 2017. doi: 10.1103/PhysRevB.95.195128.

[72] Mark S. Rudner, Netanel H. Lindner, Erez Berg, and Michael Levin. Anomalous edge states and the bulk-edge correspondence for periodically driven two-dimensional systems. *Phys. Rev. X*, 3:031005, Jul 2013. doi: 10.1103/PhysRevX.3.031005.

[73] Angelo Russomanno, Alessandro Silva, and Giuseppe E. Santoro. Periodic steady regime and interference in a periodically driven quantum system. *Phys. Rev. Lett.*, 109:257201, Dec 2012.

[74] Hideo Sambe. Steady states and quasienergies of a quantum-mechanical system in an oscillating field. *Phys. Rev. A*, 7:2203–2213, Jun 1973. doi: 10.1103/PhysRevA.7.2203.

[75] Franz Schwabl. *Statistical Mechanics*. Springer-Verlag Berlin Heidelberg, 2006.

[76] Karthik I. Seetharam, Charles-Edouard Bardyn, Netanel H. Lindner, Mark S. Rudner, and Gil Refael. Controlled population of floquet-bloch states via coupling to bose and fermi baths. *Phys. Rev. X*, 5:041050, Dec 2015. doi: 10.1103/PhysRevX.5.041050.

[77] Jon H. Shirley. Solution of the schrödinger equation with a hamiltonian periodic in time. *Phys. Rev.*, 138:B979–B987, May 1965. doi: 10.1103/PhysRev.138.B979.

[78] A. Smith, J. Knolle, D. L. Kovrizhin, and R. Moessner. Disorder-free localization. *Phys. Rev. Lett.*, 118:266601, Jun 2017. doi: 10.1103/PhysRevLett.118.266601.

[79] Mark Srednicki. Chaos and quantum thermalization. *Phys. Rev. E*, 50:888–901, Aug 1994. doi: 10.1103/PhysRevE.50.888.

[80] Mark Srednicki. The approach to thermal equilibrium in quantized chaotic systems. *Journal of Physics A: Mathematical and General*, 32(7):1163, 1999.

[81] Michael Tabor. *Chaos and Integrability in Nonlinear Dynamics - An Introduction*. Wiley-Interscience, 1989.

[82] Paraj Titum, Erez Berg, Mark S. Rudner, Gil Refael, and Netanel H. Lindner. Anomalous floquet-anderson insulator as a nonadiabatic quantized charge pump. *Phys. Rev. X*, 6:021013, May 2016.

[83] A. Avez V.I. Arnold. *Ergodic Problems of Classical Mechanics*. Addison-Wesley Publishing Co., 1989.

[84] Lev Vidmar and Marcos Rigol. Generalized gibbs ensemble in integrable lattice models. *Journal of Statistical Mechanics: Theory and Experiment*, 2016(6):064007, 2016.

[85] C. W. von Keyserlingk and S. L. Sondhi. Phase structure of one-dimensional interacting floquet systems. i. abelian symmetry-protected topological phases. *Phys. Rev. B*, 93:245145, Jun 2016. doi: 10.1103/PhysRevB.93.245145.

[86] C. W. von Keyserlingk and S. L. Sondhi. Phase structure of one-dimensional interacting floquet systems. ii. symmetry-broken phases. *Phys. Rev. B*, 93:245146, Jun 2016.

[87] Y. H. Wang, H. Steinberg, P. Jarillo-Herrero, and N. Gedik. Observation of floquet-bloch states on the surface of a topological insulator. *Science*, 342(6157):453–457, 2013. ISSN 0036-8075. URL `http://science.sciencemag.org/content/342/6157/453`.

[88] Simon A. Weidinger and Michael Knap. Floquet prethermalization and regimes of heating in a periodically driven, interacting quantum system. *Scientific Reports*, 7, 2017.

[89] N. Y. Yao, C. R. Laumann, J. I. Cirac, M. D. Lukin, and J. E. Moore. Quasi-many-body localization in translation-invariant systems. *Phys. Rev. Lett.*, 117:240601, Dec 2016. doi: 10.1103/PhysRevLett.117.240601.

[90] N. Y. Yao, A. C. Potter, I.-D. Potirniche, and A. Vishwanath. Discrete time crystals: Rigidity, criticality, and realizations. *Phys. Rev. Lett.*, 118:030401, Jan 2017.

[91] Tian-Sheng Zeng and D. N. Sheng. Prethermal time crystals in a one-dimensional periodically driven floquet system. *Phys. Rev. B*, 96:094202, Sep 2017. doi: 10.1103/PhysRevB.96.094202.

[92] J. Zhang, P. W. Hess, A. Kyprianidis, P. Becker, A. Lee, J. Smith, G. Pagano, I.-D Potirniche, A. C. Potter, A. Vishwanath, N. Y. Yao, and C. Monroe. Observation of a discrete time crystal. *Nature*, 543(7644):217–220, 03 2017.

*Chapter 2*

# NON-INTERACTING OPEN FLOQUET SYSTEMS

Karthik I. Seetharam, Charles-Edouard Bardyn, Netanel H. Lindner, Mark S. Rudner, and Gil Refael. Controlled population of floquet-bloch states via coupling to bose and fermi baths. *Phys. Rev. X*, 5:041050, Dec 2015. doi: 10.1103/PhysRevX.5.041050. URL https://link.aps.org/doi/10.1103/PhysRevX.5.041050.
K.I.S. performed calculations and numerical simulations, made primary contributions to the results, and participated in the writing of the manuscript.

## 2.1 Introduction

The availability of coherent driving fields such as lasers opens many exciting possibilities for controlling quantum systems. In particular, the recent realization that the topological characteristics of Bloch bands can be modified through periodic driving [42, 50, 55, 69] sparked a wave of proposals [19, 23, 25, 27, 29, 30, 37, 43, 47, 48, 51, 56, 59, 65] and experiments [38, 39, 44, 58, 67] to realize various types of "Floquet topological insulators" in solid state, atomic, and photonic systems. Here topology emerges in the basis of Floquet states, time-periodic eigenstates of the driven system's single-particle evolution operator [24, 60, 64].

Floquet states provide a convenient basis for describing the evolution of driven systems, in many ways analogous to the Hamiltonian eigenstates of non-driven systems. However, the powerful thermodynamic rules that govern the level occupations of static systems in thermal equilibrium in general *cannot* be directly translated into the inherently non-equilibrium context where Floquet states are defined [33, 40, 45, 46]. Photon-assisted scattering processes in which energy is exchanged with the driving field produce heating and violate the reversibility conditions that give rise to the Boltzmann distribution in equilibrium [15]. This crucial difference brings up many intriguing and important questions about the steady-state physical properties of open Floquet-Bloch systems. Importantly, the steady state governs the transport and response properties of the system on timescales longer than those on which the system-bath coupling acts. In particular, in order to realize the promise of non-equilibrium topological phenomena, one of the major outstanding problems is to identify which types of systems, baths, and system-bath couplings can lead to non-equilibrium steady states enabling Floquet topological insulators to exhibit behaviors similar to those of their equilibrium counterparts [21, 22].

Floquet-Bloch steady-state distributions are currently known for certain special cases. A closed driven system tends to heat up to a maximal entropy (infinite temperature) steady state [20, 49],

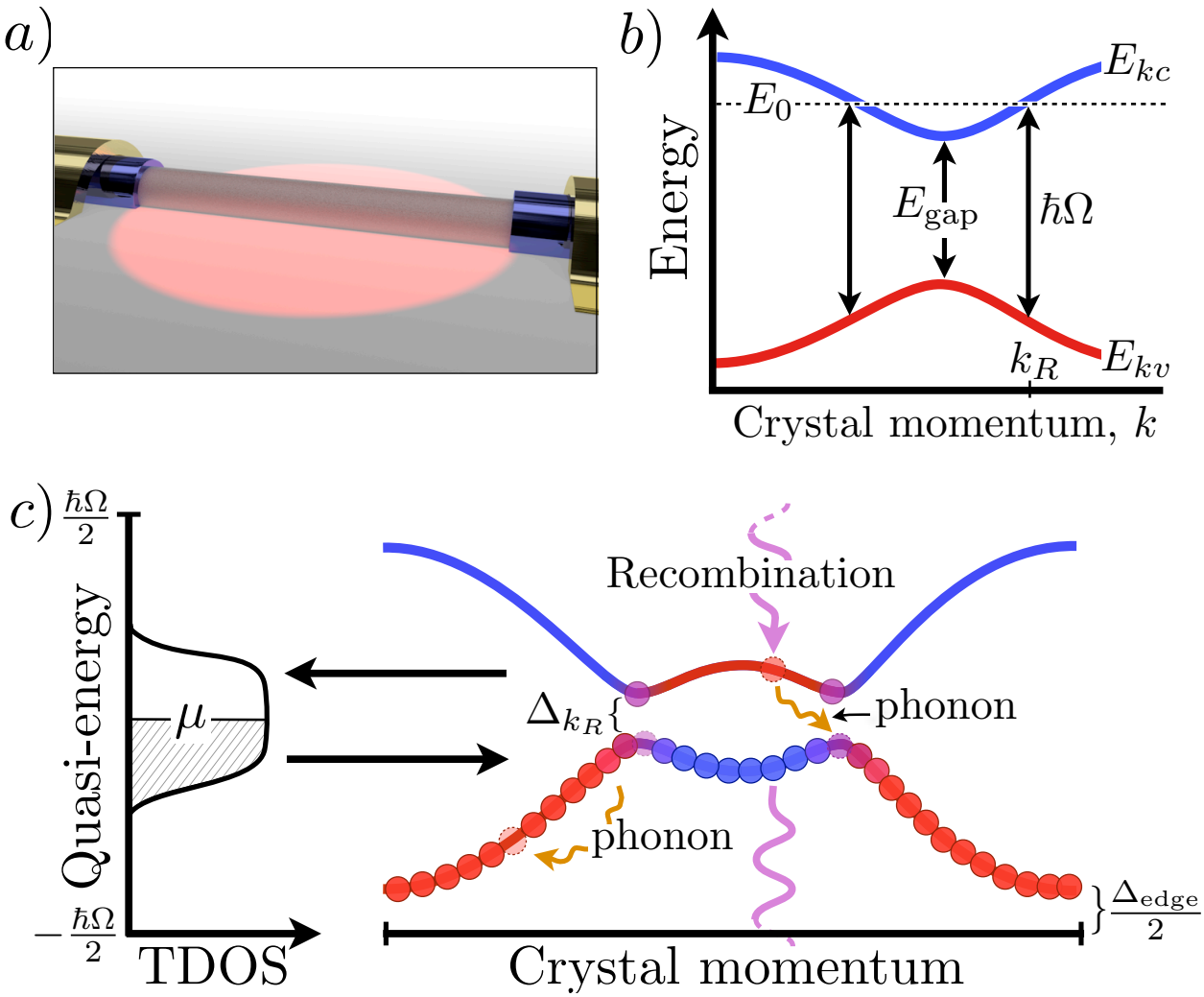


Figure 2.1: Carrier kinetics in a Floquet-Bloch system coupled to Bose and Fermi reservoirs. a) One dimensional semiconductor wire coupled to an energy-filtered fermionic reservoir. Energy filtering is achieved by coupling the system and reservoir via a deep impurity band in a large bandgap semiconductor. b) Band structure of the non-driven system. The driving field photon energy $\hbar\Omega$ exceeds the bandgap $E_{\text{gap}}$, causing resonant coupling at crystal momentum values $\pm k_R$. c) Floquet band structure, indicating the character of the Floquet band in terms of the original conduction (blue) and valence (red) bands. Coupling to acoustic phonons mediates electronic momentum and energy relaxation (orange arrows), while radiative recombination scatters electrons vertically between conduction and valence band like states (purple arrow). At half filling, the steady state resembles that of an insulator with a small density of excited electrons and holes.

in the absence of integrability or many-body localization [13, 57]. In contrast, an open driven system connected to a thermal bath need not reach such an end. Indeed, when the system and system-bath coupling Hamiltonians can be made time-independent through a simple rotating frame transformation, Gibbs-type steady states are expected [26, 35, 52, 63]. More generically, however, even spontaneous emission into a zero temperature bath may cause heating due to the possibility of absorbing energy from the driving field. How to control the steady states of driven systems, and, in particular, under what conditions they may be used to explore novel topological phenomena, pose challenging questions.

Our aim in this work is to uncover new means to control the steady state occupations of Floquet-Bloch states in driven systems. Here we focus on the dissipative open-system dynamics governed by the system's coupling to external baths; the complicated problem of electron-electron interactions will be addressed in future work. In particular we target the case of a half-filled fermionic system, where we seek to obtain an insulator-like steady state in which the lower Floquet band is filled and the upper Floquet band is empty. We refer to this state as a Floquet insulator. We investigate how this state can be approached through the relaxation of momentum and energy, enabled by connection to low temperature bosonic and fermionic baths, see Fig. 2.1. For a semiconductor-based realization, these baths naturally correspond to phonons and the electromagnetic environment (bosonic baths), and to a lead connected to the system (fermionic bath); analogous couplings can be arranged, e.g., in cold atomic systems [18, 28].

Several dynamical processes and their interplay govern the density of particle-hole "excitations" above the ideal Floquet insulator state[2]. Radiative recombination constitutes an important mechanism for generating excitations. In a non-driven system, recombination allows electrons in the conduction band to annihilate with holes in the valence band via the spontaneous emission of a photon. For resonant driving, as illustrated for the case of a one-dimensional system in Fig. 2.1b, the Floquet bands feature a band inversion: states with crystal momenta between the two resonance values $\pm k_R$ in the *lower* Floquet band are primarily formed from *conduction band* states of the non-driven system, while in the same interval the upper Floquet band is comprised of *valence band* states. Therefore, radiative recombination results in transitions from the *lower* to the *upper* Floquet band, thus increasing the density of excitations, see Fig. 2.1c. Phonon scattering, on the other hand, enables relaxation of momentum and quasi-energy within and between Floquet bands, and may balance the recombination-induced heating. A fermionic reservoir provides additional channels for removing excitations from the system, and also gives means to tune its total carrier density. Importantly, photon-assisted electron-phonon scattering, as well as photon-assisted tunneling to/from the Fermi reservoir, generally also contribute to heating[34, 45], see Fig. 2.2.

Our main message is that the driven electronic system can approach the Floquet insulator steady state

when appropriately coupled to phonon and Fermi reservoirs. In order for this to work, the coupling to the fermionic reservoir must be "engineered" to avoid the deleterious effects of photon-assisted tunneling. This can be accomplished by connecting the system to the reservoir via a narrow-band energy filter (see Fig. 2.2 and Sec. 2.4). We also discuss regimes in which photon-assisted electron-phonon scattering can be suppressed. Most remarkably, at low temperatures and with energy-filtered coupling to a fermionic reservoir, we find that the driven system exhibits incompressible and insulating behavior. This implies that a steady-state Floquet topological insulator phase may be within reach.

**Structure of the paper and main results**

Before beginning the analysis, we briefly summarize the structure of the text to follow. Keeping in mind our motivation of realizing Floquet topological insulators, our main focus in this work is on achieving Floquet insulator steady states.

First, in Sec. 2.2 we introduce the Floquet states of the periodically-driven lattice system, with band structure depicted schematically in Fig. 2.1b. After defining the Floquet states, we introduce the Floquet kinetic equation, Eq. (2.4), which forms the basis for the description of many-body population dynamics throughout this work. The kinetic equation can be obtained systematically from the exact (infinite) hierarchy of equations of motion for multi-particle correlators (see Appendix 2.A), and at our level of approximation takes on a simple intuitive form in terms of incoming and outgoing rates for each state.

Next, in Sec. 2.3 we study the steady states when the system is coupled only to the bosonic baths. Here our aim is to elucidate the competition between heating due to radiative recombination and momentum/energy relaxation by phonons in a particle number conserving system. When the electron-phonon scattering rates (ignoring Pauli blocking) are large compared to the recombination rate, we find that the driven system approaches a Floquet insulator state, with separate particle and hole densities in the upper and lower Floquet bands, respectively, see Fig. 2.3 below. The steady state excitation density depends on the ratio of phonon-assisted inter-Floquet-band relaxation and recombination rates, becoming small for fast interband relaxation. Using rather general arguments, we show that the steady state excitation density scales with the square root of the recombination rate in the limit of fast interband relaxation. As a result, even strong electron-phonon coupling may be insufficient to fully deplete excited carriers from the system.

In Sec. 2.4 we introduce coupling to a fermionic reservoir. In Fig. 2.4 we display the steady states for both wide-band and energy-filtered reservoirs. We show that coupling to a wide-band reservoir increases the density of excitations, due to photon-assisted tunneling. The energy-filtered system-reservoir coupling suppresses all photon-assisted tunneling, and our results demonstrate that it can

further *reduce* the density of excitations. We discuss two coupling geometries, where the Fermi reservoir is either coupled to the system at a single point (as a lead), or uniformly throughout the system. For homogeneous coupling, when the chemical potential of the filtered reservoir is set inside the Floquet gap, the excitation density may be highly suppressed, thus bringing the system close to the ideal Floquet insulator state. Interestingly, even when the steady state hosts a finite density of excitations, the system is incompressible in the sense that the excitation density is unaffected by small shifts of the chemical potential of the reservoir, see Fig. 2.5. For a lead coupled at a single point, the steady state distribution is necessarily inhomogeneous. We provide an estimate for the "healing length" over which the distribution can be affected by such coupling. Beyond this length, the steady state is set by the competition between recombination and electron-phonon coupling, as described in Sec. 2.3.

Finally, in Sec. 2.5 we summarize the main results and discuss implications for transport experiments. We discuss the corresponding observables and the conditions under which insulating behavior could be observed.

## 2.2 Floquet-Bloch kinetic equation for the driven two-band system

In this section we describe the single-particle properties of an isolated periodically-driven system. We first give the Hamiltonian of the system without driving, and then discuss the form of driving and the resulting Floquet states. We then introduce the kinetic equation for Floquet-state occupation numbers, which is the foundation for the description of many-body dynamics used throughout this work. The section concludes with a brief overview of the dynamical processes described by the kinetic equation.

### System Hamiltonian and Floquet-Bloch states

We now introduce the single-particle Hamiltonian and Floquet-Bloch states for the periodically-driven system that we consider. Many of the features that we describe, including the form of the kinetic equation, hold quite generally, independent of dimensionality. For concreteness, and to allow comparison with detailed numerical simulations, we focus on the case of a one-dimensional system with two bands.

The single particle Hamiltonian of the driven system is defined as follows. We assume that the driving field is spatially uniform, thus maintaining the translational symmetry of the lattice. In this case the crystal momentum $k$ is conserved. For each $k$ the evolution within the corresponding $2\times 2$ Bloch space is given by the Hamiltonian $H(k) = H_0(k) + V(t)$, with

$$H_0(k) = \tfrac{1}{2}E_k\,(\boldsymbol{d}_k\cdot\boldsymbol{\sigma}), \quad V(t) = \tfrac{1}{2}V_0\,(\boldsymbol{g}\cdot\boldsymbol{\sigma})\cos\Omega t, \tag{2.1}$$

where $\pm\frac{1}{2}E_k$ are the energies of the conduction and valence bands, $\boldsymbol{d}_k$ and $\boldsymbol{g}$ are unit vectors, $V_0$ and

$\Omega$ are the amplitude and angular frequency of the drive, and $\boldsymbol{\sigma}$ is a vector of Pauli matrices acting in the two-component orbital space (in this work we ignore spin). For now we leave the values of $\boldsymbol{d}_k$ and $\boldsymbol{g}$ unspecified, giving explicit forms when discussing numerical results below.

To understand the nature of the coupling induced by driving, we rotate to the basis of conduction and valence band states, i.e., to the basis which diagonalizes $H_0(k)$. Specifically, the Bloch eigenstates in the conduction and valence bands of the non-driven system satisfy $H_0(k)|u_{kc}\rangle = \frac{1}{2}E_k|u_{kc}\rangle$ and $H_0(k)|u_{kv}\rangle = -\frac{1}{2}E_k|u_{kv}\rangle$. The driving term $V(t)$ in Eq. (2.1) is expressed in the basis of lattice orbitals, and naturally does not depend on $k$. However, after rotating to the basis of conduction and valence band states for each $k$, the driving picks up a non-trivial $k$-dependent matrix structure

$$\tilde{H}_0(k) = \tfrac{1}{2}E_k\sigma_z, \quad \tilde{V}(k,t) = \tfrac{1}{2}V_0(\tilde{\boldsymbol{g}}_k \cdot \boldsymbol{\sigma})\cos\Omega t, \tag{2.2}$$

where tildes indicate operators in the basis of conduction and valence bands, and $\tilde{\boldsymbol{g}}_k = \tilde{g}_{k,\parallel}\hat{\boldsymbol{z}} + \tilde{\boldsymbol{g}}_{k,\perp}$ is a unit vector determined by the relative orientations of $\boldsymbol{d}_k$ and $\boldsymbol{g}$ in Eq. (2.1), broken down to $z$ and $x-y$ components.

When the system is isolated, the Floquet-Bloch states $\{|\psi_{k\pm}(t)\rangle\}$ provide a convenient basis for describing its evolution. Each state $|\psi_{k\pm}(t)\rangle$ can be expressed as a sum over harmonics:

$$|\psi_{k\pm}(t)\rangle = \sum_{n=-\infty}^{\infty} e^{-i(\mathcal{E}_{k\pm}+n\hbar\Omega)t/\hbar}|\phi^n_{k\pm}\rangle, \tag{2.3}$$

where $\mathcal{E}_{k\pm}$ is the quasi-energy of $|\psi_{k\pm}(t)\rangle$ and $\{|\phi^n_{k\pm}\rangle\}$ is a *non-normalized* (and over-complete) set of states found by Fourier transforming the time-dependent $2\times 2$ Schrödinger equation [60, 64] in the Bloch space for crystal momentum $k$. The quasi-energies $\{\mathcal{E}_{k\pm}\}$ and harmonics $\{|\phi^n_{k\pm}\rangle\}$ in Eq. (2.3) are only uniquely defined up to the gauge freedom $\mathcal{E}'_{k\pm} = \mathcal{E}_{k\pm} + m\hbar\Omega$, $|\phi'^n_{k\pm}\rangle = |\phi^{n+m}_{k\pm}\rangle$. Here we fix the gauge by choosing $\mathcal{E}_{k\pm}$ within a single Floquet-Brillouin zone centered around a specific *energy* $E_0$, $E_0 - \hbar\Omega/2 \le \mathcal{E}_{k\pm} < E_0 + \hbar\Omega/2$.

Before discussing many-body dynamics, a few comments on the nature of the Floquet bands are in order. We are interested in the case where the driving field photon energy $\hbar\Omega$ exceeds the bandgap $E_{\text{gap}}$ of the non-driven system, see Fig. 2.1b. In the Floquet picture, the leading-order influence of the driving can be understood by first shifting the valence band up by the photon energy $\hbar\Omega$. After shifting, the bands become degenerate at the resonance points [7] $\pm k_R$ in the Brillouin zone where $E_{k_R} = \hbar\Omega$. Here the driving opens avoided crossings, resulting in a gap $\Delta_{k_R} \approx V_0|\tilde{\boldsymbol{g}}_{k_R,\perp}|$ between the two Floquet bands. The resulting band structure is depicted in Fig. 2.1c. We center the Floquet zone on these resonances in the conduction band, setting $E_0 = \frac{1}{2}\hbar\Omega$. Throughout we assume that the bandwidth is narrow enough such that the two-photon resonance condition is never satisfied [11], i.e., $E_k < 2\hbar\Omega$ for all $k$.

As discussed in the introduction, the resonant driving introduces a *band inversion* in the Floquet bands. Furthermore, near the resonant momenta $k_R$ the Floquet bands are strongly hybridized superpositions of conduction and valence band states. Away from the resonant momenta, the Floquet states are only slightly perturbed with respect to the Bloch eigenstates of the non-driven system. We will refer to Floquet states which predominantly overlap with valence band states as having valence band character, and vice versa. These features of the Floquet bands have important consequences both for controlling band topology [14, 31] and for the nature of many-body dynamics in the system, as we describe below.

**The Floquet kinetic equation**

Below we use the Floquet basis of single-particle states to describe the many-body dynamics of the driven system when it is coupled to bosonic and fermionic baths. In particular, we aim to characterize the steady states of the system in terms of the Floquet state occupation numbers $F_{k\alpha} = \langle f^\dagger_{k\alpha}(t) f_{k\alpha}(t)\rangle$, where $f^\dagger_{k\alpha}(t)$ creates an electron in the state $|\psi_{k\alpha}(t)\rangle$ at time $t$, with $\alpha = \pm$. Focusing on the dynamics for time scales much longer than the driving period, we develop a kinetic equation in the Floquet basis to describe the net rate of change of the population in the Floquet state $|\psi_{k\alpha}\rangle$ due to electron-phonon scattering, radiative recombination, and tunneling to and from the fermionic reservoir:

$$\dot{F}_{k\alpha} \;=\; I^{\mathrm{ph}}_{k\alpha}(\{F\}) + I^{\mathrm{rec}}_{k\alpha}(\{F\}) + I^{\mathrm{tun}}_{k\alpha}(F_{k\alpha}). \tag{2.4}$$

Here the "collision integrals" $I^{\mathrm{ph}}$, $I^{\mathrm{rec}}$, and $I^{\mathrm{tun}}$ describe electron-phonon scattering, recombination, and tunnel coupling to the reservoir, respectively, and $\{F\}$ indicates the set of occupation factors for all momentum and band index values. The key processes associated with each of these terms are represented schematically in Fig. 2.1c.

The derivation of Eq. (2.4) is rather technical, so here we briefly summarize the approach (for details, see Appendix 2.A and, e.g., Ref. [41]). We begin by considering the equations of motion for the single-particle correlators $\langle f^\dagger_{k\alpha}(t) f_{k\alpha}(t)\rangle$. Coupling to the bath degrees of freedom generates an infinite hierarchy of equations of motion involving correlators of higher and higher order. We focus on a homogeneous system, in the regime where coherences between different Floquet states can be neglected (see below). Using a standard cluster-expansion approach, we systematically truncate the equation of motion hierarchy and obtain transition rates which coincide with those given by the "Floquet Fermi's golden rule." Below we frame the discussion in terms of these golden-rule transition rates, which provide a clear intuitive picture for all terms contributing to Eq. (2.4). We will use the rates to build up the specific forms of the collision integrals $I^{\mathrm{ph}}$, $I^{\mathrm{rec}}$, and $I^{\mathrm{tun}}$.

In describing the dynamics of the system, it is important to note that the occupation factors $F_{k\alpha}$ do

not generally give a complete description of the steady state. However, off-diagonal correlations such as $\langle f^{\dagger}_{k\alpha}(t) f_{k\alpha'}(t)\rangle$ are suppressed in the steady state for $(\Delta_{k_R}\tau_{\rm scat})^{-1} \ll 1$, see Appendix 2.D. Here, $\tau_{\rm scat}$ is the scattering time in the steady state of the system. As above $\Delta_{k_R}$ is the Floquet gap, which is proportional to the driving amplitude. Crucially, even if the scattering rates are large when the system is far from the steady state, Pauli blocking in the steady state can strongly suppress the phase space for scattering. Indeed, such suppression occurs in the steady states that we find in this work. For these states, we estimate $\tau_{\rm scat}$ to be similar to the scattering rate in the non-driven system in equilibrium at an elevated temperature (see Appendix 2.D for more details).

It follows from the above discussion that, in the regime $(\Delta_{k_R}\tau_{\rm scat})^{-1} \ll 1$, Eq. (2.4) can provide a good description of the steady state, even in parameter regimes where it does not give a faithful description of the transient dynamics. The requirement that the steady state scattering rates remain small compared with the Floquet gap $\Delta_{k_R}$ provides an important consistency check, which we apply to all numerical simulations discussed below.

Finally, we note that the non-unitary dynamics of the kinetic equation derived using the cluster expansion can be equivalently obtained using a master equation approach (see Appendix 2.D). The cluster expansion provides a powerful framework that can be used to incorporate the roles of interactions, coherences and non-Markovian dynamics, going beyond the regime studied here[61].

### 2.3 Electron-phonon coupling and recombination

In this section we discuss the steady states of the electronic system which result from the competition between radiative recombination and coupling to the phonon bath. Both processes arise from the coupling of electrons to a bosonic bath, comprised of photons in the former case and phonons in the latter. Formally, the collision integrals $I^{\rm rec}$ and $I^{\rm ph}$ describing these processes are very similar. However, it is important to understand that they act in competition. During recombination, an electron transitions from the non-driven conduction band to the valence band, while emitting a photon. In terms of the Floquet bands, this process *promotes* an electron from the lower to the upper Floquet band (see Fig. 2.1), thereby heating the electronic system and increasing the total number of excitations. On the other hand, electron-phonon scattering primarily relaxes excited electrons to the bottom of the upper Floquet band (and similarly relaxes holes to the top of the lower Floquet band), and allows excited electrons to relax back to the lower Floquet band, thereby reducing the number of excitations.

Note that the electron-phonon interaction may also play an adverse role in the system: photon-assisted scattering processes may increase the number of excitations. We show that these processes can be effectively eliminated under suitable conditions on the phononic spectrum and the form of the drive. Even when these processes are eliminated, radiative recombination remains as a source

of heating in our model.

The competition between electron-phonon scattering and recombination determines the steady state of the system. We show that these steady states feature Fermi seas of excited electrons and holes, with separate chemical potentials and a temperature equal to that of the phonon bath. Below we first analyze the kinetic equation in the presence of a generic bosonic bath. We then input the specific details needed to describe recombination and scattering by acoustic phonons, and analyze the resulting steady states. Finally, through an analytical estimate we show that for fixed electron-phonon coupling the steady state excitation density grows with the square root of the radiative recombination rate.

**Collision integral for a generic bosonic bath**

The bosonic bath is described by the Hamiltonian $H_{\mathrm{b}} = \sum_{\boldsymbol{q}} \hbar\omega_{\boldsymbol{q}}\, b^{\dagger}_{\boldsymbol{q}} b_{\boldsymbol{q}}$, where $b^{\dagger}_{\boldsymbol{q}}$ and $b_{\boldsymbol{q}}$ are the creation and annihilation operators for a bosonic excitation carrying (crystal) momentum $\boldsymbol{q}$, and $\omega_{\boldsymbol{q}}$ is the corresponding frequency. Using the creation and annihilation operators $\{c^{\dagger}_{k\nu}, c_{k\nu}\}$ for electrons in the bands of the non-driven system, defined below Eq. (2.1), we describe the "electron-boson" interaction via $H_{\mathrm{int}} = \sum_{\boldsymbol{q}} H_{\mathrm{int}}(\boldsymbol{q})$, with

$$H_{\mathrm{int}}(\boldsymbol{q}) = \sum_{kk'} \sum_{\nu,\nu'} G^{k'\nu'}_{k\nu}(\boldsymbol{q}) c^{\dagger}_{k',\nu'} c_{k\nu} (b^{\dagger}_{\boldsymbol{q}} + b_{-\boldsymbol{q}}). \tag{2.5}$$

Here $G^{k'\nu'}_{k\nu}(\boldsymbol{q})$ is the matrix element for scattering an electron with crystal momentum $k$ in band $\nu$ to crystal momentum $k'$ in band $\nu'$, with the emission (absorption) of a boson of momentum $\boldsymbol{q}$ ($-\boldsymbol{q}$). We take the bath to be three dimensional, and the electronic system to lie along the $x$-axis. Note that for an infinite, translation invariant system, momentum conservation enforces $k' = k - q_x$. To allow the possibility of describing a system of finite size, where the bath momenta may not be commensurate with the allowed values of the discrete crystal momentum of the system, we keep the general form for $G^{k'\nu'}_{k\nu}(\boldsymbol{q})$ in Eq. (2.5).

As a fundamental building block for constructing the many-body collision rates, we calculate the rate $W^{k'\alpha'}_{k\alpha}$ for a *single electron* in an otherwise empty system to scatter from crystal momentum $k$ in Floquet band $\alpha$ to crystal momentum $k'$ in Floquet band $\alpha'$. For transparency, we focus on zero temperature; the analogous expressions at finite temperature are given in Appendix 2.A. For simplicity we take the matrix elements in Eq. (2.5) to depend only on $q_x$, i.e., $G^{k'\nu'}_{k\nu}(\boldsymbol{q}) = G^{k'\nu'}_{k\nu}(q_x)$; the discussion that follows can be easily generalized beyond this assumption, but the qualitative results will not be affected.

Due to the harmonic structure of the time-dependent Floquet state wave functions, Eq. (2.3), the transition rate is given by a sum over many contributions, $W^{k'\alpha'}_{k\alpha} = \sum_n W^{k'\alpha'}_{k\alpha}(n)$. In terms of the

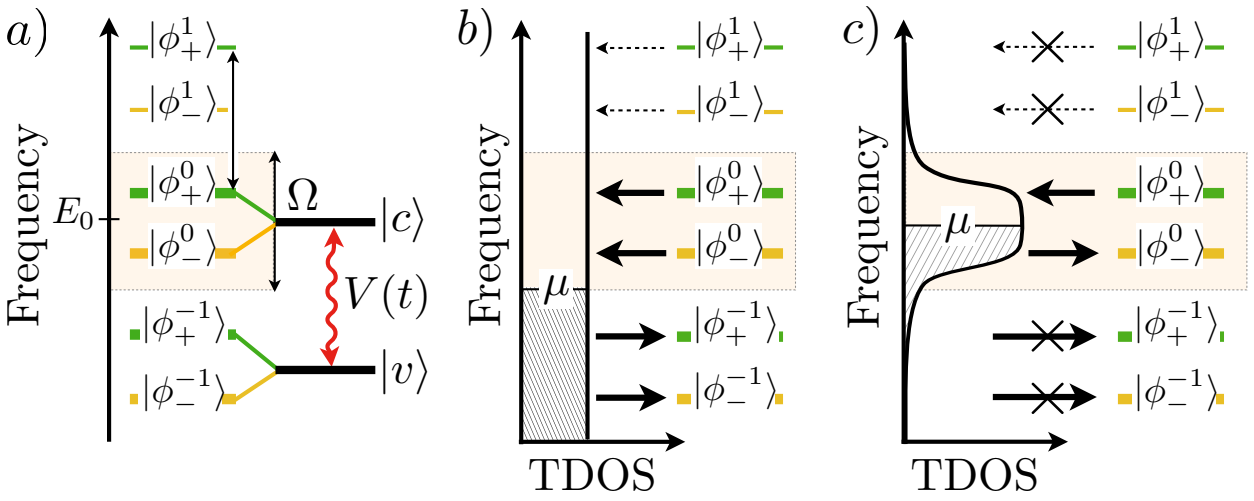


Figure 2.2: Harmonic structure of Floquet states and energy-filtered reservoir coupling. a) Floquet harmonics of a two-level system with states $|v\rangle$ and $|c\rangle$ coupled by an *on-resonance* driving field $V(t)$. The Floquet zone (shaded) is centered at the energy $E_0$, set equal to the energy of the resonant state $|c\rangle$. In the special case of a rotating-field, $V(t) = \frac{1}{2}V_0 e^{-i\Omega t}|c\rangle\langle v| + \text{h.c.}$, we have $|\phi^0_\pm\rangle = |c\rangle$, $|\phi^{-1}_\pm\rangle = \pm|v\rangle$ and $\mathcal{E}_\pm = E_0 \pm \frac{1}{2}V_0$, see Eq. (2.3). Away from resonance, the relative normalizations of $|\phi^n_+\rangle$ and $|\phi^n_-\rangle$ will change. For a more general form of weak driving, the dominant harmonics are shown in bold. b) The Floquet states $|\psi_\pm(t)\rangle$ are both coupled to filled and empty states of a wide-band reservoir via the harmonics $\{|\phi^n_\pm\rangle\}$, see Eq. (2.10). Here the reservoir chemical potential is set in the gap of the non-driven system. c) When coupling is mediated by a narrow-band energy filter, the tunneling density of states (TDOS) and photon-assisted tunneling are suppressed outside the filter window. By setting the reservoir chemical potential inside the Floquet gap, centered around the energy $E_0$ in the original conduction band (see Fig. 2.1b), the lower and upper Floquet bands are selectively filled and emptied, respectively.

electronic operator $\hat{G}(q_x) \equiv \sum_{k,k'}\sum_{\nu,\nu'} G^{k'\nu'}_{k\nu}(q_x) c^\dagger_{k',\nu} c_{k\nu'}$, these contributions are

$$W^{k'\alpha'}_{k\alpha}(n) = \frac{2\pi}{\hbar}\sum_{q_x}\Big|\sum_m \langle\phi^{m+n}_{k'\alpha'}|\hat{G}(q_x)|\phi^m_{k\alpha}\rangle\Big|^2 \rho_{q_x}(-\Delta\mathcal{E}_n), \tag{2.6}$$

where $\Delta\mathcal{E}_n = \Delta\mathcal{E} + n\hbar\Omega$, and $\Delta\mathcal{E} = \mathcal{E}_{k'\alpha'} - \mathcal{E}_{k\alpha}$ is the quasi-energy difference between final and initial electronic states. Here $\rho_{q_x}(\omega)$ is the boson density of states at frequency $\omega$ for a fixed value of the boson's longitudinal momentum component $q_x$. Note that for a monotonic boson dispersion, $\rho_{q_x}(\omega)$ is only nonzero if $\omega > \omega_{\boldsymbol{q}_0}$, where $\boldsymbol{q}_0 = (q_x, 0, 0)$. The scaling of the individual rates $W^{k'\alpha'}_{k\alpha}$ with system size is discussed in Appendix 2.B.

The structure of the transition rates in Eq. (2.6) can be understood heuristically as follows. Superficially, $|\psi_{k\pm}(t)\rangle$ in Eq. (2.3) takes the form of a superposition over a ladder of states $|\phi^n_{k\pm}\rangle$ with "energies" $\mathcal{E}_{k\pm} + n\hbar\Omega$, see illustration in Fig. 2.2a. Viewing these harmonics $|\phi^n_{k\pm}\rangle$ as independent states, the net transition rate $W^{k'\alpha'}_{k\alpha} = \sum_n W^{k'\alpha'}_{k\alpha}(n)$ is found by summing the contributions from all

pairs of initial and final states, while taking into account "energy" conservation. The appearance of $n\hbar\Omega$ inside the density of states in Eq. (2.6) expresses the fact that quasi-energy is a periodic variable, and therefore Floquet scattering processes need only conserve quasi-energy *up to multiples of the driving field photon energy* $\hbar\Omega$. If a boson is emitted and an electron *decreases* its quasi-energy, $\Delta\mathcal{E} < 0$, then the scattering rate can be non-zero for $n = 0$. Interestingly, the scattering rate can also be non-zero if a boson is emitted and an electron *increases* its quasi-energy, $\Delta\mathcal{E} > 0$, if $n < 0$.

The collision integrals in Eq. (2.4) are given by the differences between the total rates for scattering into and out of the state $|\psi_{k\alpha}(t)\rangle$, due to recombination or coupling to acoustic phonons. In turn, these rates are obtained by multiplying the bare rates in Eq. (2.6) by products of occupation factors $F_{k\alpha}$, $\bar{F}_{k'\alpha'} \equiv (1 - F_{k'\alpha'})$, etc., to account for the filling of the initial and final states:

$$I_{k\alpha} = \sum_{k'\alpha'} \left[ W^{k\alpha}_{k'\alpha'} \bar{F}_{k\alpha} F_{k'\alpha'} - W^{k'\alpha'}_{k\alpha} \bar{F}_{k'\alpha'} F_{k\alpha} \right]. \tag{2.7}$$

The corresponding expressions for nonzero bath temperature are shown in the Appendix 2.A.

Equations (2.6) and (2.7) support what we refer to as "Floquet-Umklapp" processes, in which quasi-energy conservation is satisfied with $n \neq 0$. Such processes generically heat the system when they are allowed within the kinematic constraints imposed by the bath and Floquet-system spectra (i.e. by energy and momentum conservation). For example, even at zero bath temperature, an electron may spontaneously jump from the *lower* Floquet band to the *upper* one while *emitting* a bosonic excitation (see Fig. 2.1c). As we show below, such processes cause deviations from the ideal Floquet insulator state.

Fortunately, Floquet-Umklapp processes are suppressed under appropriate conditions on the dispersion of the bath bosons. In fact, Floquet-Umklapp processes are completely suppressed if the bath bandwidth is limited such that $W^{k'\alpha'}_{k\alpha}(n)$ strictly vanishes for all $n \neq 0$. Practically speaking, this means that the maximal boson energy $\hbar\omega_D$ must be smaller than the quasi-energy gap at the Floquet zone edge (i.e., the gap around $\hbar\Omega/2$ in Fig. 2.1c), such that the energy conservation condition $-\Delta\mathcal{E} - \hbar\omega_{\boldsymbol{q}} - n\hbar\Omega = 0$ cannot be satisfied with $n \neq 0$. Below we will show how Floquet-Umklapp processes are manifested in radiative recombination and phonon scattering processes, and discuss methods to suppress them.

**Radiative recombination**

Having established the general framework for coupling the driven system to a bosonic bath, we now use it to study specific dissipation mechanisms which are relevant for driven semiconductor systems. We start by considering radiative recombination.

In non-driven systems, radiative recombination occurs when an excited particle in the conduction band relaxes to fill a hole in the valence band. This results from the interaction of electrons

with the electromagnetic environment, which is represented by a bosonic bath in our model. In typical semiconductors, the electromagnetic interaction leads to transitions between states of *different* bands. This restriction on the transitions arises due to two important factors: 1) the large speed of light implies that energy and momentum conserving transitions are practically "vertical" (i.e. the electronic momentum is conserved), and 2) the electromagnetic dipole matrix elements couple states from *different* atomic orbitals. To impose this restriction in our model we describe the interaction with the electromagnetic environment using matrix elements of the form $G^{\mathrm{rec}} \propto (1 - \delta_{\nu\nu'})$. For simplicity, in the simulations below we model vertical recombination via [6] $G^{\mathrm{rec}} = g^{\mathrm{rec}}(1 - \delta_{\nu\nu'})\delta_{q_x,0}\delta_{k,k'}$, and take a constant density of states $\rho_0$ for photons with energies $\hbar\omega \gtrsim E_{\mathrm{gap}}$.

We now describe the processes resulting from the coupling to the electromagnetic environment in the *driven* system that we consider. The most dominant of these involve transitions from Floquet states of predominantly conduction band character to final states of predominantly valence band character, and follow directly from processes present in the non-driven case. Due to the band inversion described in detail in Sec. 2.2, the − Floquet band has conduction band character for momenta $|k| < k_R$. Therefore, spontaneous transitions from the − to the + Floquet band are active for states in this momentum range. Note that these Floquet-Umklapp processes *increase* the total electronic quasi-energy, and play an important role in determining the density of excitations in the steady state of the system (see Sec. 2.3). The rates of these processes may be controlled to some extent by placing the system in a cavity or photonic crystal, which modifies the photon density of states. In addition, spontaneous transitions from the + to the − Floquet band are allowed in the momentum region $|k| > k_R$, where the + Floquet band has predominantly conduction band character. These processes help to reduce the total electronic quasi-energy, but will play a minor role near the steady state where the + Floquet band is mostly empty.

The processes described above follow directly from those that are active in a non-driven system. However, in a driven system an electron may also transition from a state of valence band character to one of conduction band character, by emitting a photon to the environment while absorbing energy from the drive. Such processes are possible for initial states in the − Floquet band with $|k| > k_R$, and for initial states in the + Floquet band with $|k| < k_R$. Both cases involve a spontaneous emission and the absorption of two photons from the driving field. Due to the latter, the matrix elements for such processes[8] are suppressed by $[V_0/(\hbar\Omega)]^2$ for weak driving, and hence their rates are suppressed as $[V_0/(\hbar\Omega)]^4$.

| Phonon-assisted scattering regime | Phonon bandwidth, $\hbar\omega_D$ |
|---|---|
| No Floquet-Umklapp scattering | $\hbar\omega_D < \Delta_{\text{edge}}$, $\Delta_{\text{edge}} \leq \hbar\omega_D < \hbar\Omega + \Delta_{\text{edge}}$, $\tilde{g}_{\parallel} = 0$ |
| Intraband scattering only | $\hbar\omega_D < \Delta_{\text{k}_\text{R}}$ |
| Intraband and interband scattering | $\Delta_{\text{k}_\text{R}} < \hbar\omega_D$ |

Table 2.1: Summary of the different regimes of scattering processes assisted by acoustic phonons. Interband and Floquet-Umklapp processes are active or inactive depending on the relation between the phonon bandwidth $\hbar\omega_D$ and the relevant Floquet gap: $\Delta_{k_R}$ is the Floquet gap at $\mathcal{E} = 0$, while $\Delta_{\text{edge}}$ is the Floquet gap at the Floquet zone edge, $\mathcal{E} = \hbar\Omega/2$. The drive parameter $\tilde{g}_{\parallel}$ is defined through Eq. (2.2).

**Scattering due to acoustic phonons**

The interaction between the electronic system and a bath of acoustic phonons plays a key role in setting the steady state of the driven system. Phonon-mediated scattering quickly relaxes excited electrons (holes) to the bottom (top) of the respective Floquet band. In addition, phonon-mediated scattering allows these excitations to relax across the Floquet gap. The competition between the latter interband scattering processes and radiative recombination sets the steady state density of excitations, as we discuss below.

In our model we assume that the electron-phonon coupling conserves the band index $\nu$ of the non-driven system, $G^{\text{ph}} \propto \delta_{\nu\nu'}$, as is typical for wide gap semiconductors [41, 62, 71]. The coherent drive hybridizes the bands near the resonances $\pm k_R$, thus enabling both intraband *and* interband scattering in the Floquet bands (see Fig. 2.1c). Note that the scattering crucially involves the exchange of both crystal momentum and quasi-energy between the phonons and the electrons, thus allowing relaxation of these quantities. We take the matrix elements to conserve lattice momentum, $G^{k'\nu'}_{k\nu}(q_x) = g(q_x)\delta_{\nu\nu'}\delta_{q_x,k-k'}$. In principle, the $q_x$ dependence of $g(q_x)$ depends on the specific type of electron-phonon coupling. For simplicity, we take the matrix elements to be independent of $q_x$, but have numerically verified that other choices do not change the qualitative results.

Besides helping to relax excitations, photon-assisted electron-phonon scattering can increase the excitation density. Such Floquet-Umklapp scattering transfers electrons from the lower to the upper Floquet band, and can occur even for a zero temperature phonon bath.

Phonon-related Floquet-Umklapp processes can be suppressed in several ways. First, as discussed in Sec. 2.3, limiting the bandwidth for the phonons to be smaller than the quasi-energy gap at the Floquet zone edge, $\Delta_{\text{edge}}$, efficiently suppresses Floquet-Umklapp phonon scattering. Note, however, that the phonon bandwidth should remain bigger than the Floquet gap emerging at the

resonance momenta, $\Delta_{k_R}$, as otherwise phonons would be unable to facilitate relaxation between the upper and lower Floquet bands. An optimal phonon bandwidth $\omega_D$ would therefore satisfy $\Delta_{k_R} < \hbar\omega_D < \Delta_{\text{edge}}$. The bandwidth for the phonon bath depends on material parameters, however, and may not be easily tunable.

Interestingly, additional routes are available for suppressing Floquet-Umklapp processes involving phonons. If the boson bandwidth allows the energy conservation condition $-\Delta\mathcal{E} - \hbar\omega_{\boldsymbol{q}} - n\hbar\Omega = 0$ to be satisfied for $|n| \leq 1$ (but not for $|n| > 1$), the rates $W^{k'\alpha'}_{k\alpha}(n)$ with $n = \pm 1$ can be controlled by the choice of driving. In particular, for harmonic driving they vanish as $\tilde{g}_{\parallel} \to 0$ (see Appendix 2.A). For many experimentally-relevant materials driven by optical fields, $\tilde{g}_{\parallel}$ is indeed small for momenta near $k = 0$. Additionally, even when none of the conditions above are met, the amplitudes of the Floquet harmonics $\{|\phi^n_{k\alpha}\rangle\}$ (and hence the rates $W^{k'\alpha'}_{k\alpha}(n)$) are generically suppressed for large $n$. Hence, although heating inevitably accompanies coupling to a bosonic bath, there are many ways to control or limit the corresponding effects on the steady state distribution (see below and also Refs. [26, 35, 52, 63]). For a summary of the different regimes of phonon-assisted scattering, see Table 2.1.

**Steady state**

The steady state of the driven model described above results from the competition between the two main dissipation mechanisms: radiative recombination and acoustic phonon scattering. To gain a more quantitative picture of the behavior, we numerically solve for the steady states of the kinetic equation (2.4) in the model outlined above, with the parameter values given in Table 2.2. We take acoustic phonons to have a linear dispersion in three dimensions, $\omega^{\text{ph}}_{\boldsymbol{q}} = c_s|\boldsymbol{q}|$, up to a "Debye frequency" cutoff $\omega_D$. We focus on the situation where $\Delta_{k_R} < \hbar\omega_D < \Delta_{\text{edge}}$, which allows inter-Floquet-band scattering, but forbids Floquet-Umklapp phonon scattering processes. The rates $\{W^{k\alpha}_{k'\alpha'}\}$ are calculated using the form for the matrix elements described in Sections 2.3 and 2.3. Our results are summarized in Fig. 2.3.

The main result of the numerical simulation is the steady state distribution $F_{k+}$ of excited carriers in the upper Floquet band, which is shown in Fig. 2.3a, for a total density of particles corresponding to half-filling. Due to particle-hole symmetry, the distribution of holes in the lower Floquet band, $\bar{F}_{k-}$, is identical to that above. We examine the behavior of the steady state distribution while tuning the ratio of the phonon scattering and radiative recombination rates. Specifically, we fix the parameters for electron-phonon coupling, and vary the overall scale of the matrix elements for recombination.

As seen in Fig. 2.3a, in all cases the upper Floquet band hosts a finite density of excited Floquet carriers, localized around the two band minima. For relatively weak electron-phonon coupling

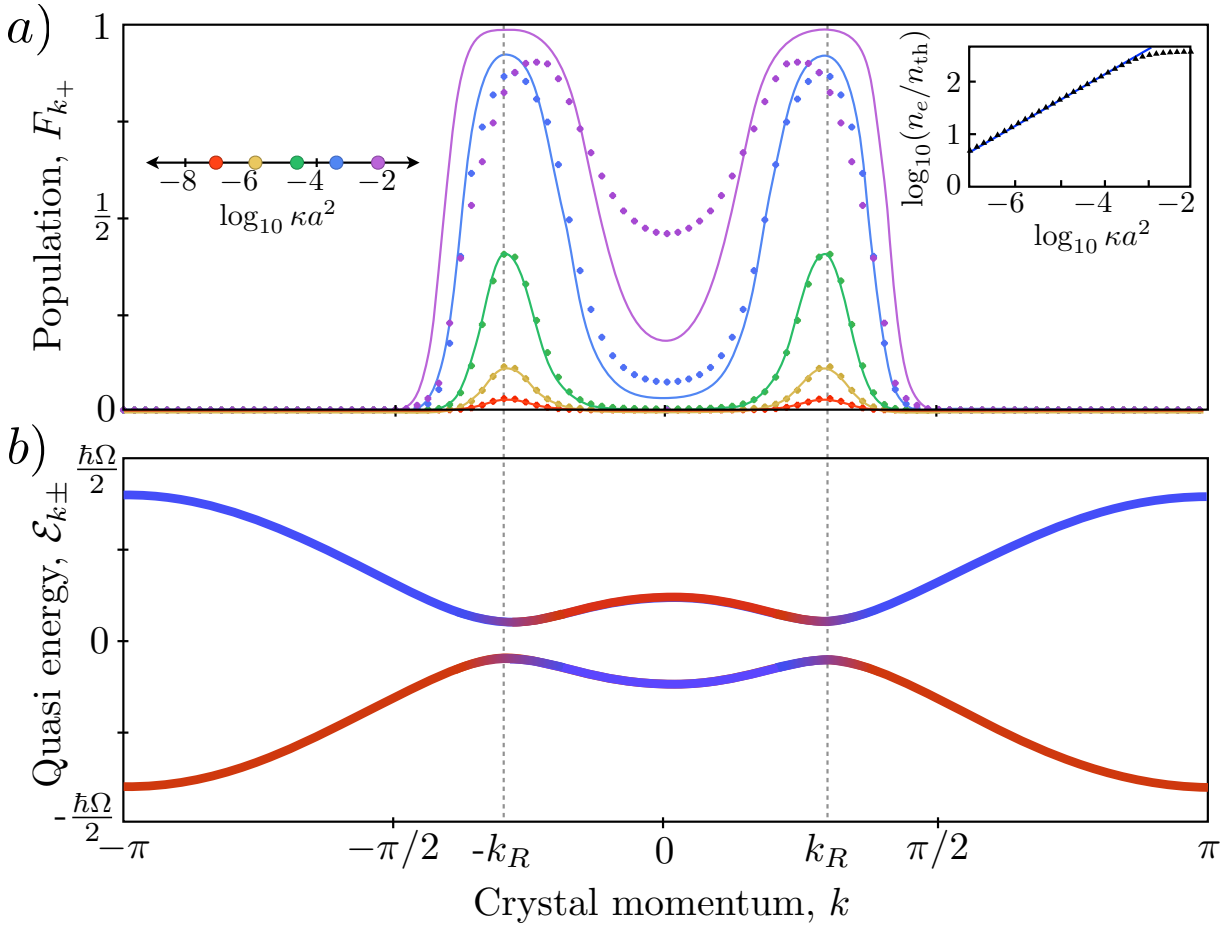


Figure 2.3: Numerically obtained steady states with radiative recombination and coupling to acoustic phonons. Here the density is set to half-filling, and we use a 3D acoustic phonon bath with $\hbar\omega_D$ smaller than the gap $\Delta_{\rm edge}$ at the Floquet zone edge. The phonon temperature is set to $k_B T = 10^{-2}\hbar\Omega$. We keep the phonon and photon densities of states fixed, and only vary an overall scale for the coupling matrix elements. The full details of the model can be found in Table 2.2. (a) Distribution of electrons in the upper Floquet band, $F_{k+} = \langle f^\dagger_{k+} f_{k+}\rangle$, for several values of $\kappa = k_R \overline{W}^{\rm rec}/\pi\Lambda^{\rm inter}$, see Eq. (2.9) and Appendix 2.C for definitions. The distributions are fitted to a Floquet-Fermi-Dirac distribution at temperature $T$ (solid lines). Due to particle-hole symmetry, the distributions of holes in the lower Floquet band, $1 - F_{k-}$, are identical to the distributions shown. *Inset*: Log-Log plot showing the total density of electrons in the upper Floquet band, $n_e$ as a function of $\kappa$. The density $n_e$ is normalized to the "thermal density" $n_{\rm th} = 6.8 \times 10^{-4}$ (see text). The plot demonstrates the square root behavior predicted in Eq. (2.9). Note that for large $n_e$, the recombination rates saturate due to Pauli blocking. The Floquet band structure is shown in panel (b).

| $A$ | $E_{\text{gap}}$ | $\mathbf{g}$ | $\mathbf{d_k}$ | $V_0$ |
|---|---|---|---|---|
| $0.25\hbar\Omega$ | $0.8\hbar\Omega$ | $(1,0,0)$ | $(0,0,1)$ | $0.1\hbar\Omega$ |

| $c_s$ | $\hbar\omega_D$ | $2\pi(G_0^{ph})^2\bar{\rho}^{\text{ph}}$ | $k_BT$ |
|---|---|---|---|
| $\frac{0.05}{\pi\sqrt{3}}a\Omega$ | $0.15\hbar\Omega$ | $\left(2\times10^{-2}\right)\hbar\Omega$ | $0.1\Delta_{k_R}$ |

Table 2.2: Parameters fixed in all simulations. Top row: parameters of the electronic Hamiltonian, Eq. (2.1), with $E_k = 2A[1-\cos(ka)] + E_{\text{gap}}$, where $a$ is the lattice constant. The drive is spatially uniform, $V(t) = \frac{1}{2}V_0(\mathbf{g}\cdot\boldsymbol{\sigma})\cos\Omega t$. Bottom row: parameters of the three dimensional acoustic phonon bath, where $c_s$ is the phonon velocity, and $\omega_D$ is the Debye frequency. In all simulations, the overall scale of the phonon matrix elements is set by fixing the ratio $2\pi(G_0^{ph})^2\bar{\rho}^{\text{ph}}/(\hbar\Omega)$, where $\bar{\rho}^{\text{ph}}$ is the phonon density of states at zero momentum and energy $\hbar c_s(\pi/a)$. For convergence, in the simulations we keep the phonon bath at a small temperature, $k_BT \approx 10^{-2}\hbar\Omega$.

the excitation density is large, but is limited by saturation of the recombination rates due to Pauli exclusion above a given density. Notably, when electron-phonon coupling is relatively strong, the excitation density is significantly suppressed. Moreover, in this regime the distribution of excited carriers is well described by a Floquet-Fermi-Dirac distribution with an effective chemical potential $\mu_e$ (a fit parameter) and temperature corresponding to that of the phonon bath (solid lines). By "Floquet-Fermi-Dirac distribution" we refer to a distribution of particles in Floquet states, which is described by a Fermi-Dirac distribution taken as a function of quasi-energy. The distribution of holes in the lower Floquet band (not shown) takes an identical form with an effective chemical potential $\mu_h = \mu_e$ due to particle-hole symmetry of the model. To check the consistency of our approach, we verify that the scattering rates in the steady state are significantly smaller than the Floquet gap $\Delta_{k_R}$. This condition is satisfied in particular for momenta around $k_R$ where the electron and hole excitation densities are localized. A more detailed discussion of the scattering rates is provided in Appendix 2.D.

The above form for $F_{k+}$ can be understood by considering the dynamics of the electrons coupled to the photon and phonon baths. When an electron is excited to the upper Floquet band via a recombination process, it quickly "trickles down" via repeated intraband scattering from acoustic phonons until eventually reaching one of the minima of the band. There it joins the Fermi gas of excited electrons. Relaxation from the upper to the lower band via phonon emission is only substantial near the band bottom, where the original valence and conduction bands are strongly hybridized. The total density of excited carriers is determined by a balance between the interband excitation and relaxation process.

As seen in Fig. 2.3a, even for relatively large electron-phonon coupling strengths the density of excited electrons remains appreciable. As we now explain, this situation arises from a bottleneck in interband relaxation due to the suppression of phonon emission rates for small excitation densities.

The relaxation bottleneck can be understood by considering the rate of change of the excitation density $n_e = \int \frac{dk}{2\pi} F_{k+}$ of excited electrons in the upper Floquet band. In a heuristic model for the regime of low excitation density, recombination transfers electrons from the mostly filled states in the "valley" between maxima of the lower Floquet band (centered around $k = 0$), to the mostly-empty "hump" in the upper band, providing a constant source term for the excitations (see Fig. 2.1c): $\dot{n}_e^{\text{rec}} = \gamma^{\text{rec}}$, with

$$\gamma^{\text{rec}} \approx \int_{-k_R}^{k_R} \frac{dk}{2\pi} \mathcal{W}_k^{\text{rec}}. \tag{2.8}$$

Here, $\mathcal{W}_k^{\text{rec}} \equiv \sum_{k'} W_{k-}^{k'+}$ is the total rate for an electron, initially in the lower Floquet band with momentum $k$, to "decay" to the upper Floquet band with *any* final momentum (within the constraints of quasi-energy and crystal momentum conservation). Thus $\mathcal{W}_k^{\text{rec}}$ is simply the recombination rate for a single electron. When we compute $\gamma^{\text{rec}}$ using $\mathcal{W}_k^{\text{rec}}$, we take the occupations in the lower and upper Floquet bands in the interval $-k_R \leq k \leq k_R$ to be one and zero, respectively. It is convenient to define an average recombination rate in this interval, $\overline{\mathcal{W}}^{\text{rec}}$, whereby Eq. (2.8) becomes $\gamma^{\text{rec}} \approx (k_R/\pi)\overline{\mathcal{W}}^{\text{rec}}$.

Relaxation via *interband* electron-phonon scattering occurs for momenta in narrow regions around $\pm k_R$, from the bottom of the upper Floquet band to the top of the lower Floquet band. In these momentum regions the bands are strongly hybridized, giving nonzero matrix elements for the electron-phonon coupling which is diagonal in the bands of the non-driven system. For simplicity, in the discussion below we set $W_{k+}^{k'-} = \overline{W}^{\text{inter}}$, where $\overline{W}^{\text{inter}}$ is an average value for the transition rates in the active regions around $\pm k_R$. The *total rate* of electrons relaxing from the upper to the lower Floquet band is found by summing the transition rates from occupied states in the upper band to empty states in the lower band. The corresponding change to the excitation *density* goes as $\dot{n}_e^{\text{inter}} \approx \frac{1}{L} \sum_k \sum_{k'} \overline{W}^{\text{inter}} F_{k+} \bar{F}_{k'-}$. Using particle-hole symmetry of the distribution, and $\sum_k F_{k+} = L n_e$, we obtain $\dot{n}_e^{\text{inter}} \approx -\Lambda^{\text{inter}} n_e^2$, where $\Lambda^{\text{inter}} \equiv L\overline{W}^{\text{inter}}$.

The two powers of excitation density appearing in the expression for $\dot{n}_e$ come from 1) the density of excited electrons available to decay and 2) the density of final states available for each electron. Note that the above discussion assumed zero temperature of the bath. However, when the phonon bath is at finite temperature, the picture above gives a good approximation when $n_e$ exceeds the thermal excitation density (see below).

Importantly, despite the system size $L$ appearing explicitly in the definition of $\Lambda^{\text{inter}}$, the net relaxation rate is in fact *system size independent*. As explained in Appendix 2.B, the individual rates $W_{k\alpha}^{k'\alpha'}$ to scatter between specific momentum values $k$ and $k'$ generically scale as $1/L$. The system size independence is restored by the increasing number of final states, which scales as $L$.

Combining the recombination and interband phonon scattering terms, we obtain $\dot{n}_e = \gamma^{\text{rec}} - \Lambda^{\text{inter}} n_e^2$.

The condition $\dot{n}_e = 0$ yields an approximate relation for the steady state excitation density, $n_e = n_{\text{steady}}$, where:

$$n_{\text{steady}} = \left( \frac{k_R}{\pi} \frac{\overline{\mathcal{W}}^{\text{rec}}}{\Lambda^{\text{inter}}} \right)^{1/2} . \tag{2.9}$$

The square root dependence in Eq. (2.9) is clearly exhibited in our simulations[9], as shown in the inset of Fig. 2.3a.

Note that in our simulations the bath temperature was set to $k_B T = 0.1\Delta_{k_R}$. At this temperature, a "global" Floquet-Fermi-Dirac distribution with its chemical potential set in the middle of the Floquet gap would have a small density of excited electrons, $n_{\text{th}}$ (and similarly for holes). Here we define the "global" Floquet-Fermi-Dirac distribution as a single distribution describing the electronic occupations in both bands of the system. For very low recombination rates, the square root behavior should saturate when $n_e \approx n_{\text{th}}$. However, throughout the parameter range used for Fig. 2.3a, $n_e \gg n_{\text{th}}$, and therefore the effect of the finite temperature of the bath on the square root behavior is negligible. Thus we see that even for zero bath temperature the deviation from the global Floquet-Fermi Dirac distribution remains, and is given by Eq. (2.9).

To summarize this section, when radiative recombination and other Floquet-Umklapp processes are absent, the system approaches the ideal Floquet insulator state (at half filling). Importantly, our analysis shows that Floquet-Umklapp processes cannot be ignored: the steady state excitation density rises rapidly when the recombination rate is increased from zero. In order to further reduce the excitation density, additional controls are needed. Coupling the system to a Fermi reservoir can provide such a control, which we shall study in detail in the next section.

## 2.4 Coupling to a Fermi reservoir

In this section we consider the steady state of the system upon coupling it to an external fermionic reservoir. Our motivation here is twofold: the reservoir serves as an additional effective control over the steady state of the system, and is a necessary component of transport experiments. However, as we show below, when the driven system is coupled to a standard fermionic reservoir with a wide bandwidth, photon assisted tunneling significantly increases the density of excitations. In addition, even in the ballistic regime, photon assisted tunneling opens extra channels for transport [30, 43, 45, 47, 48]. We will discuss how such processes can be suppressed using energy filtering, thereby allowing for the possibility to control and probe the driven system using external fermionic reservoirs.

In the discussion below we first assume that the distribution remains homogeneous under coupling to the reservoir. This can be approximately satisfied for small systems with point-like coupling to a lead, or for systems where the coupling is extended rather than pointlike. Next we focus on the

scenario of a lead coupled at a point, where we will discuss the role of inhomogeneities and the length scale over which the steady state distribution is controlled by the lead.

**Collision integral for a fermionic reservoir**

The Hamiltonian of the isolated reservoir is given by $H_{\rm res} = \sum_\ell E_\ell\, d_\ell^\dagger d_\ell$, where $d_\ell^\dagger$ creates an electron in state $|\ell\rangle$ of the reservoir with energy $E_\ell$. Throughout this work we assume that the periodic driving acts only on the system, and does *not* affect the reservoir. We describe tunneling between the reservoir and states of the (undriven) system by the Hamiltonian $H_{\rm tun} = \sum_{\ell,k\nu} J_{\ell,k\nu}\,(d_\ell^\dagger c_{k\nu} + c_{k\nu}^\dagger d_\ell)$. The values of the tunneling matrix elements $J_{\ell,k\alpha}$ depend on the precise forms of the reservoir states $\{|\ell\rangle\}$, the Bloch wave functions of the undriven system, and the details of the coupling.

The Floquet states $|\psi_{k\pm}\rangle$ are coupled to the Fermi reservoir via the harmonics $|\phi_{k\pm}^n\rangle$, as shown in Fig. 2.2b,c. These harmonics are spread over a large range of frequencies $\mathcal{E}_{k\pm} + n\hbar\Omega$. As a result, both the upper and lower Floquet bands are coupled to reservoir states in a wide range of energies. This coupling is directly mirrored in the collision integral for the reservoir. Following the spirit of the discussion surrounding Eq. (2.6), we define the "bare" rate $\Gamma_{k\alpha}^n$ for a single electron to tunnel from a (filled) reservoir into the Floquet state $|\psi_{k\alpha}(t)\rangle$, via the harmonic $|\phi_{k\alpha}^n\rangle$,

$$\Gamma_{k\alpha}^n = \frac{2\pi}{\hbar}\sum_\ell |\langle\phi_{k\alpha}^n|H_{\rm tun}|\ell\rangle|^2\delta(\mathcal{E}_{k\alpha} + n\hbar\Omega - E_\ell). \tag{2.10}$$

Next, we assume that the reservoir is in equilibrium, with the occupation of a state with energy $E_\ell = \mathcal{E}_{k\alpha} + n\hbar\Omega$ given by the Fermi-Dirac distribution $D(E_\ell)$ with chemical potential $\mu_{\rm res}$ and temperature $T_{\rm res}$. To build up the integral $I_{k\alpha}^{\rm tun}$ in the kinetic equation (2.4), we supplement the rates $\{\Gamma_{k\alpha}^n\}$ in Eq. (2.10) with the occupation factors $F_{k\alpha}$ and $D(\mathcal{E}_{k\alpha}^n)$, with $\mathcal{E}_{k\alpha}^n \equiv \mathcal{E}_{k\alpha} + n\hbar\Omega$:

$$I_{k\alpha}^{\rm tun} = \sum_n \Gamma_{k\alpha}^n\left[\bar{F}_{k\alpha}D(\mathcal{E}_{k\alpha}^n) - F_{k\alpha}\bar{D}(\mathcal{E}_{k\alpha}^n)\right]. \tag{2.11}$$

The first and second terms of Eq. (2.11) correspond to electrons tunneling into and out of the system, respectively.

**Steady state with fermionic and bosonic baths**

How does the coupling to the reservoir influence the steady state of the system? The possibility of photon-assisted tunneling of particles between the system and the reservoir makes the behavior of the driven system strikingly different from its equilibrium behavior.

To understand the effect of the reservoir, it is instructive to first look at the steady state distribution $\tilde{F}_{k\alpha}$ of Eq. (2.4) in the absence of recombination and electron-phonon scattering, $I^{\rm rec} = I^{\rm ph} = 0$. Staying within the homogeneous regime and setting the left hand side of Eq. (2.4) to zero while

using Eq. (2.11) for $I^{\text{tun}}_{k\alpha}$ yields

$$\tilde{F}_{k\alpha} = \frac{\sum_n \Gamma^n_{k\alpha} D(\mathcal{E}^n_{k\alpha})}{\sum_n \Gamma^n_{k\alpha}}. \tag{2.12}$$

For a typical metallic reservoir with a wide bandwidth (greater than $\hbar\Omega$), the photon-assisted tunneling rates $\Gamma^n_{k\alpha}$ in Eq. (2.10) may be significant for $n \neq 0$. Consequently, the sum over $n$ in Eq. (2.12) leads to steady state occupations which differ substantially from those given by a simple Floquet-Fermi-Dirac distribution $F_{k\alpha} = D(\mathcal{E}_{k\alpha})$.

We now directly illustrate the difficulties which arise from coupling the periodically-driven system to a wide-band fermionic reservoir, in the more general case where the system is also subject to electron-phonon coupling and radiative recombination, $I^{\text{rec}}$, $I^{\text{ph}} \neq 0$. In Fig. 2.4a we plot steady state distributions for several values of the coupling strength to the reservoir. The parameters of the bosonic bath (phonons and recombination) are held fixed, with values identical to those yielding the green (middle) curve of Fig. 2.3a. We start at half filling, with the chemical potential of the reservoir set in the middle of the bandgap of the non-driven system, i.e., we set $\mu_{\text{res}} = E_0 - \hbar\Omega/2$, see Fig. 2.1. The system-reservoir coupling $J_{\ell,k\nu}$ as well as the reservoir density of states are taken to be constant [12]. As the reservoir coupling increases, the steady state distribution becomes "hotter", with a higher and higher density of excitations.

The heating effects of the reservoir can be understood as follows. In terms of the original (non-driven) bands, Fig. 2.1b, the leading order effect of the reservoir is to populate valence-band-like states and to empty conduction-band-like states. In terms of the Floquet bands, this in particular entails removing electrons from states in the lower Floquet band within the momentum window $-k_R < k < k_R$, and injecting electrons into states of the upper Floquet band in the same momentum window. Qualitatively, this is similar to the effect of radiative recombination, compare to Fig. 2.3. Strong coupling to the reservoir thus leads to a large density of excitations in the Floquet bands. To achieve an insulator-like distribution, as needed for the realization of a Floquet topological insulator, these excitations must be suppressed.

**Energy filtered fermionic reservoirs**

Interestingly, photon-assisted tunneling can be effectively suppressed if the system-reservoir coupling is mediated through a narrow band of "filter" states (realizations are discussed below). For illustration, let us imagine that the system is connected to the reservoir via an energy filter: a device with a finite density of states in a restricted energy range, whose states couple strongly to the electron reservoir. The filter states hybridize with the reservoir states to produce a peak in the continuum density of states within the filter energy window. When the system is coupled to the fermionic reservoir only via the filter, the transition rates in Eq. (2.10) are controlled by the effective tunneling density of states (TDOS), $\rho_{\text{tun}}(\mathcal{E}) \equiv \sum_\ell |\langle x_{\text{filter}}|\ell\rangle|^2 \delta(\mathcal{E} - E_\ell)$. Here $\langle x_{\text{filter}}|\ell\rangle$

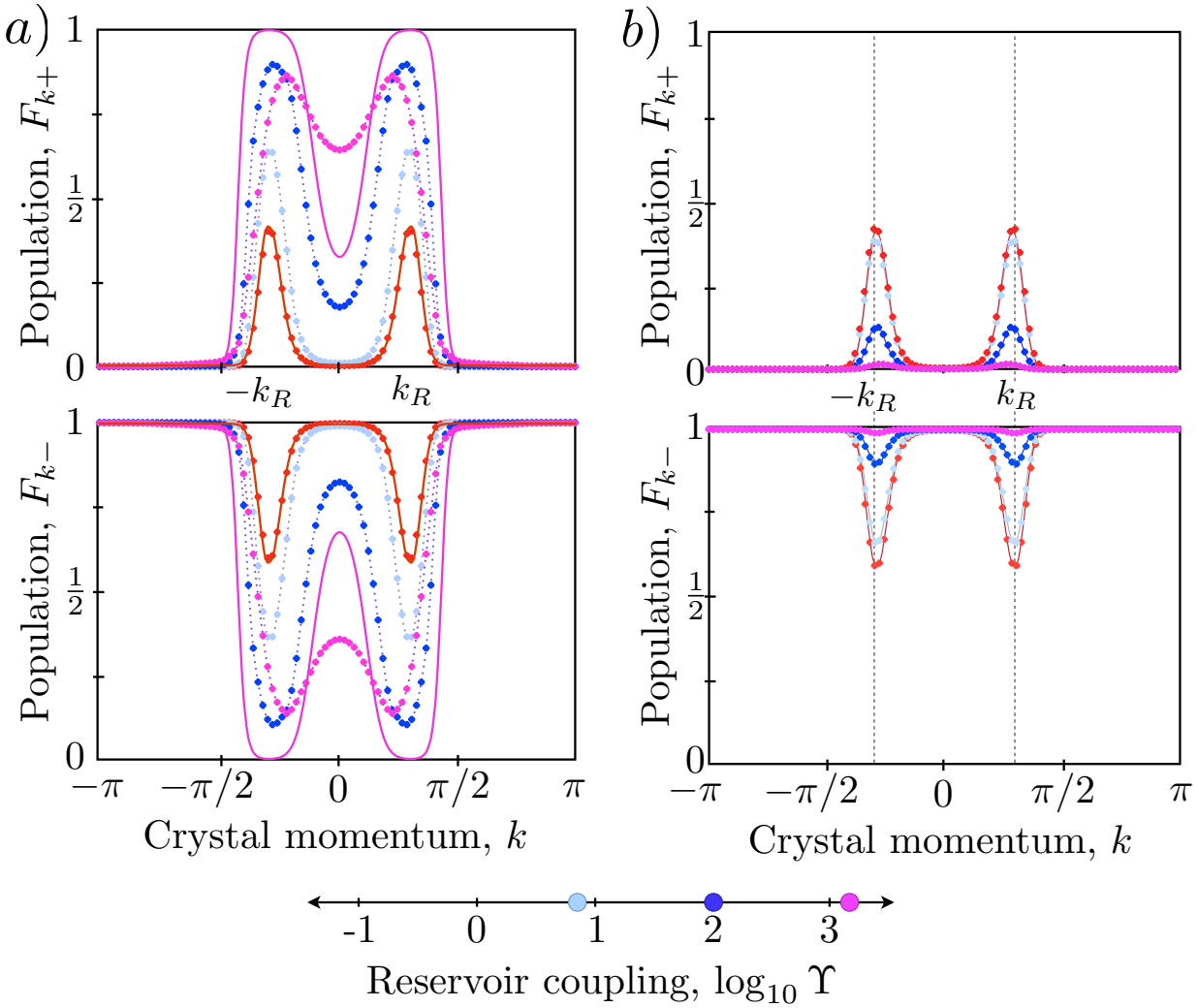


Figure 2.4: Numerically obtained steady states of the system coupled to both bosonic and fermionic baths. The top and bottom panels show the distributions of electrons in the Floquet + and - bands, respectively, for increasing strength of the coupling to the Fermi reservoir. We characterize the coupling strength by the ratio of tunneling and recombination rates, $\Upsilon = 2\Gamma^0_{k_R,+}/\overline{\mathcal{W}}^{\text{rec}}$ (see Eqs. (2.8) and (2.10) for definitions of the rates). Two types of Fermi reservoirs are studied. (a) *Wide-band* Fermi reservoir, whose Fermi level lies in the middle of the original bandgap (the bandgap of $H_0$). An increase in the coupling strength to such a reservoir leads to a substantial increase in the electron and hole densities $n_e$ and $n_h$, due to photon assisted tunneling. (b) *Energy filtered* Fermi reservoir, whose Fermi level lies at the resonance energy $E_0$ in the original conduction band, i.e., in the middle of the Floquet gap of the driven system. The electron and holes densities $n_e$ and $n_h$ are suppressed via the coupling to the narrow-band Fermi reservoir. In all panels, the red data points are for a half filled system which is disconnected from the Fermi reservoir. The other colors correspond to the values of $\Upsilon$ indicated at the bottom. The solid lines are fits to Floquet-Fermi-Dirac distributions, with separate chemical potentials for electrons and holes in the Floquet + and − bands, respectively. The temperature taken for the fits is identical to the phonon and reservoir temperature, $k_B T = 10^{-2}\hbar\Omega$. In these simulations, the parameters for the photon (recombination) and phonon baths were kept fixed at the values yielding the green curve in Fig. 2.3, while we vary the overall scale of the coupling strength to a homogeneously coupled fermionic reservoir.

is the amplitude of the continuum state $|\ell\rangle$ (formed of hybridized filter and reservoir states) at the position of the filter, $x_{\text{filter}}$, where tunneling occurs. The factor $|\langle x_{\text{filter}}|\ell\rangle|^2$ is part of the squared matrix element in Eq. (2.10). Note that in the above discussion we assumed that the filter is not subject to the external drive[3].

As a concrete example, consider resonant tunneling through a single filter level at energy $E_{\text{filter}}$. Here we find tunneling rates with a Lorentzian dependence on energy: $\Gamma^n \sim \gamma J_n^2/[(\mathcal{E}_{k\alpha} + n\hbar\Omega - E_{\text{filter}})^2 + (\hbar\gamma/2)^2]$, where $\gamma$ is the level broadening of the filter state due to its coupling to the continuum of reservoir modes, and $J_n$ characterizes the matrix elements for coupling into the $n$-th harmonic of the system's Floquet state. Consider, for example, setting $E_{\text{filter}} = \frac{1}{2}\hbar\Omega = E_0$ (i.e., at the conduction band resonance energy). Then, in the limit $\Omega \gg \gamma$, photon-assisted tunneling rates ($n \neq 0$) are strongly suppressed. If the energy filter consists of multiple resonant levels connected in series, or a narrow band of states, a sharper "box-like" transmission window can be obtained (see, e.g., Ref. [68]). In addition to this filtering effect on the effective TDOS, note that the rates $\Gamma^n$ for large $n$ are suppressed via $J_n$ due to the negligible admixture of very high harmonics in the Floquet state wave functions (this suppression also occurs for the case of no filtering).

In practice, the energy filter may be realized by coupling the system to the reservoir via a section of large bandgap material hosting a narrow band of impurity states deep inside its gap. The intermediate band should satisfy three essential requirements: (i) The Fermi level should lie inside it, (ii) The band should be narrower than the width $\hbar\Omega$ of a single Floquet zone, as discussed above, and (iii) it should be separated from the conduction and valence bands of the host material by more than $\hbar\Omega$, to avoid the direct absorption of photons from the driving field. Highly mismatched alloys featuring narrow bands of extended states in their bandgaps have been realized in the context of intermediate-band solar cells [53, 54, 70]. We expect similar methods to allow for the realization of the energy filter introduced in this work. Energy filtering through quantum dots could provide an alternative approach. Due to their large size as compared to atoms, however, achieving a level spacing exceeding $\hbar\Omega$ may prove challenging (especially at optical frequencies) [54].

**Steady state with filtered reservoir**

We now investigate how coupling to an energy-filtered reservoir affects the steady state of the system. We start with the case where phonons and radiative recombination are absent, $I^{\text{rec}} = I^{\text{ph}} = 0$. Throughout the discussion below we assume a box-like filter, such that the tunneling density of states is strictly zero outside the filter window.

When the filter window (bandwidth) is narrower than $\hbar\Omega$, photon-assisted processes are suppressed. According to Eq. (2.12), the occupation distribution in the reservoir, taken as a function of energy, is then directly mapped into the occupation distribution of the driven system, taken as a function of

*quasi-energy* (i.e., the occupation $F_{k\alpha}$ of each Floquet state $|\psi_{k\alpha}\rangle$ is determined by a single term, $D(\mathcal{E}_{k\alpha})$ with fixed $n$, on the right hand side). In the case of the wide-band reservoir, half-filling was ensured by placing the chemical potential of the reservoir in the middle of the gap of the non-driven system. Here, the best choice is to center the filter window around the energy of the resonance in either the conduction band or the valence band, $\mu_{\rm res} = \pm\hbar\Omega/2$, and also to set the chemical potential $\mu_{\rm res}$ close to the resonance value (for the simulations below, we center the filter window around the resonance in the conduction band). In this way, the reservoir chemical potential will end up inside the Floquet gap. Note that although the chemical potential $\mu_{\rm res}$ is set to an energy within the conduction the bands of the non-driven system, the filtering prevents a large inflow or outflow of electrons which would otherwise push the density far away from half-filling. Due to the fact that this is a highly non-equilibrium situation, however, some density shifts away from half-filling are generically expected (see discussion below).

The ideal Floquet insulator distribution can be achieved in the situation where the reservoir chemical potential is set inside the Floquet gap, and where the filter window is wide enough to cover the full bandwidth of the Floquet-Bloch band structure, but narrower than the driving field photon energy $\hbar\Omega$ such that photon-assisted processes are still suppressed. More generically, however, the filter window will be narrower than the bandwidth of the Floquet-Bloch bands, as depicted in Fig. 2.1c. In this case the kinetic equation (2.4) with $I^{\rm rec} = I^{\rm ph} = 0$ does not have a unique steady state, as excited electrons and holes above and below the filter edges, respectively, have no way to relax. However, this is an unstable situation: any small scattering rate due to acoustic phonons will allow electrons to "trickle down" and fill up all Floquet states below the bottom of the filter window. In the absence of Floquet-Umklapp processes, the resulting steady state will correspond to that of an insulator at finite temperature (assuming the same temperature for the phonons and the Fermi reservoir). More specifically, the electronic distribution for both bands will be described by a global Floquet-Fermi-Dirac distribution with a single chemical potential, which is set by that of the reservoir.

Once we include the contributions of Floquet-Umklapp processes such as recombination, the steady state hosts densities of excited electrons and holes, $n_e$ and $n_h$, respectively (which are generally large compared with the thermal density $n_{\rm th}$). In the limit of a weakly coupled reservoir, the combined density of electrons and holes $\bar{n} = n_e + n_h$ is determined solely by the recombination and phonon scattering rates, as discussed in Sec. 2.3. The steady state excitation density is further suppressed with increasing coupling to the reservoir, as we demonstrate below (see Fig. 2.4b).

While the steady state electron and hole excitation densities are equal for a half-filled system without coupling to a Fermi reservoir (Sec. 2.3), $n_e$ and $n_h$ need not be equal when the reservoir is present, even when the chemical potential of the filtered reservoir is placed in the middle of the Floquet gap.

To see why, note that here the Fermi level of the filtered reservoir is aligned with the resonance energy $\frac{1}{2}\hbar\Omega$ in the conduction band of the non-driven system. The asymmetric placement of the energy window of the reservoir with respect to the non-driven band structure generically breaks any effective particle-hole symmetry, and yields a shift of the total density away from half-filling. Importantly, the shift $\Delta n = n_e - n_h$ can be small, being bounded by $\bar{n}$. More careful considerations (see Appendix 2.E) show that $\Delta n$ is in fact expected to be significantly lower than $\bar{n}$, which is confirmed by our numerical simulations (see Fig. 2.5d).

Staying within the regime of a weakly coupled reservoir, let us now consider what happens when the reservoir's Fermi energy is shifted away from the center of the Floquet gap. As long as the Fermi level of the reservoir remains within the Floquet gap, the occupation factors $D(\mathcal{E}_{k\alpha})$ in Eq. (2.11) change only weakly, due to the finite temperature of the reservoir. Since the rates $\Gamma^n_{k\alpha}$ are independent of the occupation of the reservoir, the changes in $I^{\text{tun}}_{k\alpha}$ are only "thermally activated" by the reservoir's temperature. We therefore expect the steady state of the system to be only weakly affected. This implies that an interesting situation has been obtained, in which the driven system becomes *incompressible*, with respect to changes of the reservoir's Fermi level. Interestingly, this incompressibility occurs in the presence of a finite excitation density. Once the Fermi level enters, say, the upper Floquet band, the density of excited electrons in the band is greatly affected. If we approximate the distribution of excited electrons by a Fermi function, we can expect its Fermi level to track the Fermi level of the reservoir.

As the strength of the coupling to the reservoir is increased, we expect the Fermi reservoir to become more dominant in setting the steady state of the system. In the limit where the coupling to the reservoir dominates all other scattering mechanisms, we expect the steady state to be described by a global Floquet-Fermi-Dirac distribution, with the same chemical potential as that of the filtered reservoir. Note that in this limit, a non-zero coupling to the phonon bath is still important in order to allow electrons to fill up states from the bottom of the lower Floquet band up to the reservoir's Fermi level.

The above considerations are confirmed by our numerical simulations, which are given in Figs. 2.4 and 2.5. In these simulations, we fix the matrix elements describing the coupling to the photon (recombination) and acoustic phonon baths as in the green (middle) curve of Fig. 2.3a, and vary the overall scale of the couplings $J_{\ell,k\nu}$ to the Fermi reservoir (which are taken to be uniform). The reservoir density of states is taken to be constant in a window of width $\hbar\Omega/2$ placed symmetrically around $E_0 = \frac{1}{2}\hbar\Omega$. The distributions of electrons $\langle f^\dagger_{k\alpha} f_{k\alpha}\rangle$ in the two bands are plotted in Fig. 2.4, and are separately fitted to Floquet-Fermi-Dirac distributions with independent chemical potentials $\mu_e$ and $\mu_h$ for electrons and holes, as in Sec. 2.3.

Figure 2.4 clearly demonstrates that for a wide-band reservoir, panel (a), the density of excitations

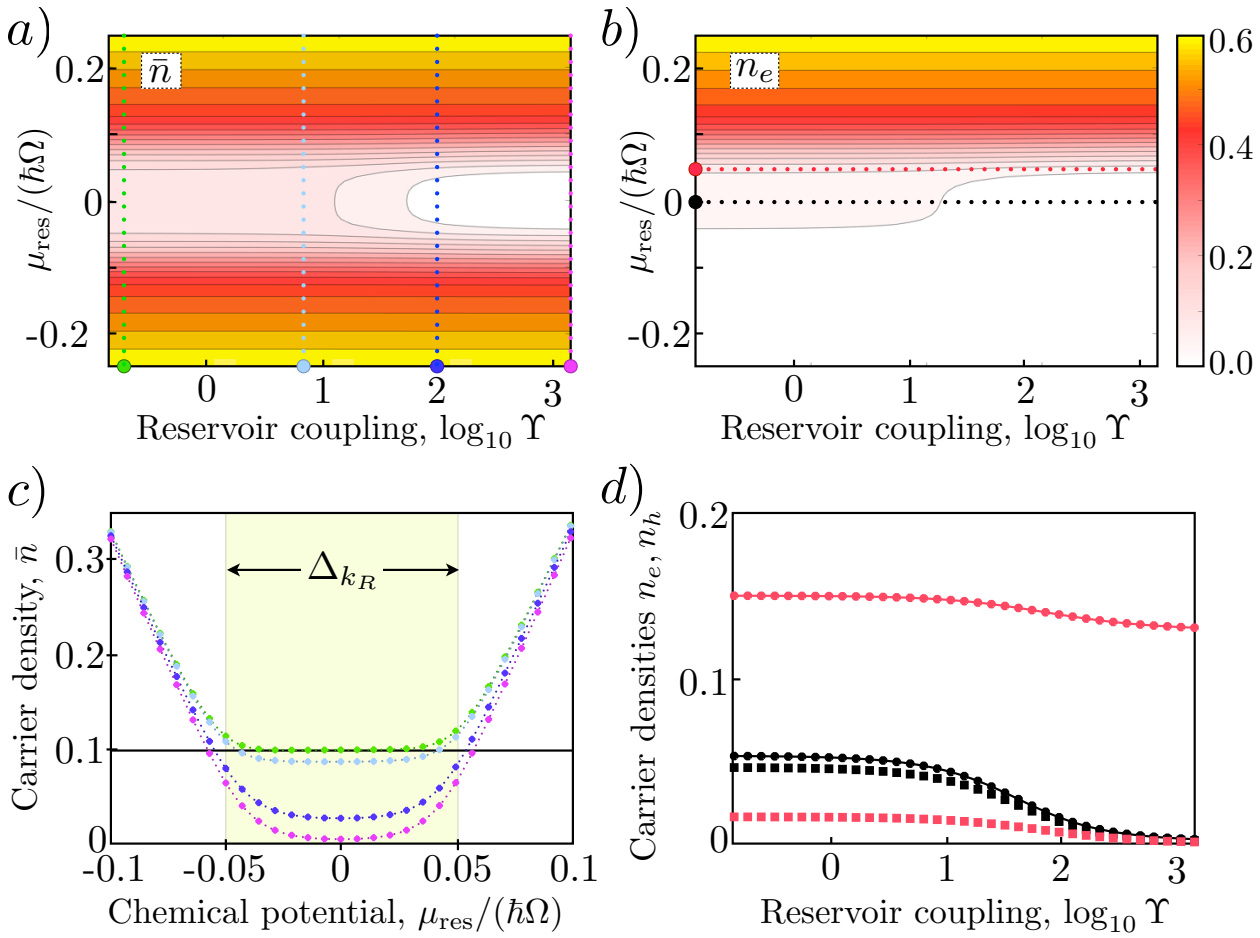


Figure 2.5: Electron and holes densities $n_e$ and $n_h$ in the steady state of the system coupled to bosonic baths (acoustic phonons and recombination) and an *energy filtered* fermionic reservoir. The figure clearly demonstrates that (1) the steady state densities $n_e$ and $n_h$ are insensitive to small shifts of the reservoir's chemical potential $\mu_{\rm res}$ near the middle of the Floquet gap, and (2) a sufficiently strong coupling to the reservoir can effectively suppress the electron and hole densities when $\mu_{\rm res}$ is within the Floquet gap. Panel (a) shows the total density $\bar{n} = n_e + n_h$ as a function of the Fermi level of the reservoir $\mu_{\rm res}$ and the coupling strength ratio $\Upsilon = 2\Gamma^0_{k_R,+}/\overline{\mathcal{W}}^{\rm rec}$. As long as $\mu_{\rm res}$ is within the Floquet gap, $n_e$ and $n_h$ remain low. Once $\mu_{\rm res}$ enters the Floquet + or − bands, the system becomes metallic and the electron (hole) density $n_e$ ($n_h$) is set by the Fermi level of the reservoir. This behavior is seen in in panel (b), where we plot $n_e$. To further demonstrate the incompressible regime, in (c) we show $\bar{n}$ as a function of $\mu_{\rm res}$ for several coupling strengths to the reservoir, corresponding to the dotted lines in panel (a). Panel (d) gives the the electron and hole densities, $n_e$ (circles) and $n_h$ (squares) for two values of $\mu_{\rm res}$: in the middle of the Floquet gap (black) and at the edge of the + Floquet band (red). In the first case, the results explicitly demonstrate the suppression of the excitation densities $n_e$ and $n_h$ with increasing reservoir coupling. Model parameters are the same as in Fig. 2.4.

*increases* when the coupling to the reservoir is increased; in contrast, for a filtered reservoir, panel (b), the density of excitations *decreases* with increasing coupling strength to the reservoir. For the filtered reservoir, the chemical potential sits at the resonance energy in the conduction band, $\frac{1}{2}\hbar\Omega$. In all fits in Fig. 2.4 we set the temperatures of the Floquet-Fermi-Dirac distributions to be identical to the phonon and reservoir temperature. While we obtain excellent fits at weak reservoir coupling, the fits become less accurate when the coupling to the reservoir is increased. This arises due to the non-uniform way in which the reservoir is coupled to the Floquet bands. As in Sec. 2.3, we verify that the scattering rates in the numerically obtained steady states are significantly smaller than the Floquet gap $\Delta_{k_R}$ for all reservoir coupling strengths used (see Appendix 2.D).

In Fig. 2.5 we study the densities $n_e$ and $n_h$ as functions of the strength of the coupling to the reservoir and its chemical potential. The figure demonstrates two important points. First, the steady state densities $n_e$ and $n_h$ are insensitive to small shifts of the Fermi level of the reservoir away from the middle of the Floquet gap, yielding an "incompressible" behavior $dn_{e,h}/d\mu_{\rm res} \approx 0$. This is demonstrated most clearly by panel (c), which shows $\bar{n}$ vs. $\mu_{\rm res}$ (similar plots of $\Delta n$ can be found in Appendix 2.E). Second, when the Fermi level of the reservoir lies within the Floquet gap, a sufficiently strong coupling to the reservoir can effectively suppress the electron and hole densities, giving a steady state close to an ideal Floquet insulator.

The coupling strength at which the reservoir is expected to significantly affect the steady state excitation density can be estimated as follows. Radiative recombination acts to increase the excitation density with the rate $\dot{n}_e^{\rm rec} = \gamma^{\rm rec}$ defined in Eq. (2.8). As above, we approximate $\gamma^{\rm rec}$ by $\gamma^{\rm rec} \approx (k_R/\pi)\overline{\mathcal{W}}^{\rm rec}$, where $k_R/\pi$ represents the fraction of states that participate in the recombination process and $\overline{\mathcal{W}}^{\rm rec}$ is the average recombination rate in this interval. Meanwhile, the reservoir can extract excitations at a rate $\dot{n}_e^{\rm tun} \approx -\Gamma^0 n_e$, where $\Gamma^0 \equiv \Gamma^0_{k_R,+}$ characterizes the rate for a single electron to tunnel in or out of the system. When the reservoir is weakly coupled, the steady state excitation density is controlled by the rate of phonon-mediated interband relaxation, as discussed around Eq. (2.8). The reservoir begins to play an important role when $\Gamma^0 n_e \gtrsim (k_R/\pi)\overline{\mathcal{W}}^{\rm rec}$, or equivalently when

$$\Upsilon \equiv (2\Gamma^0/\overline{\mathcal{W}}^{\rm rec}) \gtrsim k_R/(\pi n_e). \tag{2.13}$$

This relation is indeed borne out in Fig. 2.5d, where $n_e \approx 0.05$ and $k_R/\pi \approx 0.3$, and the excitation density is suppressed for $\log_{10}\Upsilon \gtrsim 1$. Note that Fig. 2.5d also shows a small non-zero value of $\Delta n \ll \bar{n}$ when the Fermi level is in the middle of the Floquet gap (black symbols in Fig. 2.5d), arising from the asymmetry of the coupling of the reservoir to the two Floquet bands.

**Point coupling to a lead**

In many experimentally relevant situations, the system is coupled to a lead at a single point. What is the spatial dependence of the steady state in this situation? So far we have discussed *homogeneous* steady state distribution functions $\{\tilde{F}_{k\alpha}\}$, which depend on momentum and band indices but not on position. A *homogeneous* steady state can arise in several situations. For the bosonic baths discussed earlier, we assumed a uniform coupling throughout the system. Therefore by themselves the bosonic baths yield a spatially homogeneous steady state distribution. Clearly, if in addition we introduce a fermionic reservoir which is coupled homogeneously throughout the system, a spatially homogeneous steady state is expected. In addition, for a lead coupled at a single point, there are still two limits in which the steady state remains uniform: (1) in the absence of any other sources of dissipation; and (2) in the limit of a small system size. In the latter case, a uniform distribution is obtained when the level spacing of the system's single particle states is larger than the tunneling rate to and from the reservoir; this corresponds to a tunneling time that exceeds the time required for an electron to traverse the system.

For larger system sizes, where the stringent criterion above is not met, the steady state need not be spatially homogeneous. If the tunneling rates are comparable to or larger than the level spacing, the coupling to the reservoir can yield nonzero values of the "coherence" terms $\langle f^\dagger_{k\alpha} f_{k'\beta}\rangle$, which generically cause spatial inhomogeneity. Calculating the full set of such coherences is a formidable task. Fortunately, we can gain an intuitive understanding of the form of the inhomogeneous steady state by considering the dynamics of a spatially-dependent excitation densities $n_e(x,t)$ and $n_h(x,t)$. Close to the lead, placed at $x = 0$, the excitation density will be affected by the lead and will roughly correspond to that found for a homogeneous system-reservoir coupling. Far from the lead, we expect the excitation densities to relax to bulk values $n_e^{\text{bulk}}$ and $n_h^{\text{bulk}}$. Below we estimate the "healing length" over which this transition occurs.

Due to fast intraband electron-phonon scattering (which is still slow compared with the driving frequency and the on-resonance Rabi frequency $\Delta_{k_R}/\hbar$), carrier motion on time scales much larger than the driving period is expected to be diffusive. The corresponding diffusion constant can be estimated as $D = \bar{v}^2/W^{\text{intra}}$, where $\bar{v}$ is a typical velocity of the excitations [5] and $W^{\text{intra}}$ is a typical *intraband* scattering rate from acoustic phonons, both taken in the steady state. Focusing on the situation near half-filling and incorporating the source and sink terms due to recombination and interband phonon scattering discussed in Sec. 2.3, we obtain two reaction-diffusion equations for the electron and hole densities, $\partial_t n_\lambda = D\,\partial_x^2 n_\lambda + \gamma^{\text{rec}} - \Lambda^{\text{inter}} n_e n_h$, with $\lambda = e, h$. Adding and subtracting these equations, we find the reaction-diffusion equations governing the total and offset

densities $\bar{n}$ and $\Delta n$,

$$\begin{aligned} \partial_t \bar{n} &= D\,\partial_x^2 \bar{n} + 2\gamma^{\mathrm{rec}} - \tfrac{1}{2}\Lambda^{\mathrm{inter}}\left(\bar{n}^2 - \Delta n^2\right), \\ \partial_t \Delta n &= D\,\partial_x^2 \Delta n. \end{aligned} \tag{2.14}$$

For the boundary conditions for the above equations, we use $\Delta n(x = 0)$ and $\bar{n}(x = 0)$ which are set by the lead, as well as $\partial_x \Delta n = \partial_x \bar{n} = 0$ for $x \gg 0$, which corresponds to no net flow of particles into the system. Eq. (2.14) entails two main consequences for the spatial distribution of the steady state, $\partial_t n_\lambda(x, t) = 0$. First, the shift of the total density of electrons from half filling, $\Delta n$, is in fact homogeneous across the system, and set by the lead. Furthermore, linearizing Eq. (2.14) around the bulk steady state gives the healing length

$$\xi = \left(\frac{D\bar{n}^{\mathrm{bulk}}}{4\gamma^{\mathrm{rec}}}\right)^{1/2}, \tag{2.15}$$

where we can approximate $\bar{n}_{\mathrm{bulk}} = 2\sqrt{k_R \overline{\mathcal{W}}^{\mathrm{rec}}/\pi\Lambda^{\mathrm{inter}}}$ from Eq. (2.9). Here we neglect corrections due to a small $\Delta n$. For system sizes smaller than $\xi$, a lead coupled at a point can be effective in setting the distribution throughout the system. In such a system, for a sufficiently strong point coupling to a filtered lead, a Floquet insulator distribution can be achieved, as was shown for the homogeneous case in Sec. 2.4.

### 2.5 Summary and Discussion

The ability to control and probe non equilibrium quantum many body systems poses one of the most outstanding challenges in modern condensed matter physics. In this paper, we analyzed steady states in a model for a periodically driven semiconductor, and demonstrated the means through which these steady states can be controlled. We considered the open system dynamics of a resonantly driven electronic system coupled to acoustic phonons and the electromagnetic environment, as well as to an external fermionic reservoir. The couplings to these baths have two complementary roles: they allow energy relaxation, but may also induce processes which lead to heating. Motivated by the prospect of realizing Floquet topological insulators, our goal was to find the conditions under which the steady state resembles a band insulator. Importantly, we focused on the regime where the scattering rates in the steady state are smaller than the drive-induced Floquet gap. Only in this regime could we expect to observe effects requiring quantum coherence, such as drive-induced topological phenomena.

Starting with the case where the system is coupled only to the bosonic baths, we have shown that the system can approach a Floquet insulator steady state with an added density of excitations in the two Floquet bands. The density of excitations is controlled by the ratio of radiative recombination and

| | Parameter regime | Steady state | Excitation density, $n_e$ |
|---|---|---|---|
| No Floquet-Umklapp | $\mathcal{W}^{\rm rec} = 0$ | GFFD | $n_e = n_{\rm th}$ |
| Phonon dominated | $\mathcal{W}^{\rm rec}/\Lambda^{\rm inter} \ll 1$ | FFD | $n_e \approx n_{\rm steady}$ |
| Filtered Fermi reservoir dominated | $\pi\Upsilon n_{\rm steady}/k_R \gg 1$ | FFD | $n_e \approx n_{\rm th}$ |

Table 2.3: Summary of main results for the steady state distributions in different regimes. FFD denotes a steady state in which electrons and holes in Floquet bands + and − are described by separate Fermi-Dirac distributions with independent chemical potentials (at the bath temperature). GFFD stands for a global Floquet-Fermi-Dirac distribution, with a single chemical potential. Other symbols: $n_{\rm th}$ stands for the thermal excitation density, while $n_{\rm steady}$ is defined in Eq. (2.9). The parameter $\Upsilon$ characterizing the tunneling rate to the Fermi reservoir is defined in Eq. (2.13), and $\mathcal{W}^{\rm rec}$ and $\Lambda^{\rm inter}$ characterizing recombination and phonon mediated interband relaxation rates are defined below Eq. (2.8).

electron-phonon scattering rates, and can be small for experimentally-relevant parameter values. We found a square root dependence of the excitation density on the above ratio, see Eq. (2.9), which implies that additional controls are needed to fully suppress the deviations from the Floquet insulator state. Next, we considered the effects of coupling to an external Fermi reservoir, which plays two important roles in our setup. First, the reservoir is a crucial component for transport experiments. Importantly, we show this coupling significantly increases the density of excitations, unless the reservoir is coupled through an energy filter. Second, the energy-filtered reservoir can serve as an additional control to *reduce* the density of excitations, bringing the system closer to the ideal Floquet insulator state. Our main results are summarized in Table 2.3.

A main motivation for our work is the prospect of obtaining a Floquet topological insulator: a driven system with an insulating bulk but with conductive edge and surface modes. What are the implications of our results for transport? Our findings are relevant for system sizes which are larger than the electronic inelastic mean free path (transport in the complementary ballistic regime has been studied previously in a number of works, see for example Refs. [25, 30, 43]). Interestingly, we find that even in the presence of a finite density of excitations, the steady state of the driven system can exhibit an "incompressible" behavior: the steady state is unaffected by small changes in the chemical potential of the *energy filtered* reservoir, as long as it situated near the middle of the Floquet gap [4]. This behavior is shown in Fig. 2.5. In addition, when energy filtered leads are used for transport, photon-assisted conduction channels are suppressed. In the case of neutral particles, the incompressibility implies insulating behavior: no current would result from a small source-drain bias between two spatially-separated energy-filtered leads. This follows from the insensitivity of the steady state to the leads' chemical potentials.

When we consider charged particles, however, the electric field which accompanies the source-drain bias may drive a current due to the non-zero density of excited carriers.Thus, here we expect a finite

resistivity even in the parameter range corresponding to the insulating regime above. Given the diffusive nature of particle motion in the system, we estimate the local resistivity $\sigma^{-1}(x)$ using the Drude form: $\sigma^{-1}(x) = |m_*|W^{\text{intra}}/[e^2\bar{n}(x)]$, where $m_*$ is the effective mass around the Floquet upper (lower) band minimum (maximum), $e$ is the electric charge. Consider now a two-terminal transport measurement using energy filtered leads, through such a system of charged carriers. If the system is small enough such that the steady state is spatially homogeneous, a sufficiently strong coupling to energy filtered leads can, in fact, suppress the density of excited carriers and yield nearly-insulating behavior. For larger systems, with a spatially inhomogeneous steady state, the total resistance $R$ is given by the sum of series resistances, $R = \int_0^L dx\, \sigma^{-1}(x)$. The bulk of the system gives an extensive contribution $R_{\text{bulk}} \approx L|m_*|W^{\text{intra}}/\left[e^2\bar{n}^{\text{bulk}}\right]$. Interestingly, if the lead coupling is strong, the excitation density near the ends of the system will become very small and thus give a large contribution $R_{\text{end}}$ to the resistance. Therefore, for a fixed system size, the system may obtain insulating behavior in a two-terminal measurement upon increasing the coupling strength of the lead.

The analysis of steady states in driven electronic systems is currently the subject of intense activity (see e.g., Refs. [21, 34]). In Ref. [21], time evolution and steady states after a quench were studied for a 2D semiconductor with a topological Floquet spectrum. There, the authors considered open system dynamics with momentum conserving interactions with a bosonic bath, and found regimes exhibiting quantized Hall conductivity. In addition, Ref. [34] studied a resonantly-driven electronic system where the only relaxation pathway was through an external fermionic lead, and found that a grand canonical distribution could be obtained under finely-tuned conditions[1]. In our work, we considered the combined effects of momentum and energy relaxation through the coupling to acoustic phonons and the coupling to an external fermionic reservoir. Notably, we included the inevitable effects of heating due to Floquet-Umklapp processes, as exemplified by radiative recombination. Importantly, momentum relaxation plays a crucial role in establishing the Floquet insulator steady state under these conditions.

To make a connection with experimentally relevant regimes, we compare our model parameters with those accessible in solid state systems. Consider a drive frequency of $\Omega = 2\pi \times 100$ THz, which translates to 0.4 eV in energy units. Correspondingly, the parameters used in Sec. 2.3 yield a Floquet gap of $\Delta_{k_R}/\hbar \approx 2\pi \times 10$ THz (translating to 40 meV), and a characteristic phonon relaxation time scale of $[\sum_{k'} W^{k'+}_{k=0,-}]^{-1} = 500$ fs. This is the total relaxation rate out of the state $k = 0$ in the upper band. The recombination time scales, $(\mathcal{W}^{\text{rec}}_{k=0})^{-1}$ used to obtain the steady state distribution in Fig. 2.3, are [1 $\mu$s, 60 ns, 3 ns, 180 ps, 10 ps]. When coupling to the fermionic reservoir was introduced in Sec. 2.4, we fixed the recombination time scale at 3 ns; the steady state distributions in Fig. 2.4 correspond to tunneling times $(\Gamma_{k=0,-})^{-1}$ of approximately [200 ps, 30 ps, 3 ps]. In

Fig. 2.5, the tunneling time from the reservoir varies from 30 ns to 3 ps. Note that these values are in line with those in typical semiconductor nanostructures, where tunneling times can vary widely[62].

Although our model is inspired by resonantly-driven semiconductors, we expect our conclusions and formalism to be relevant to a broad variety of driven-dissipative systems including cold atomic gases. Our results also have important implications for Floquet topological insulators. Indeed, they provide a roadmap towards the practical realization of the Floquet insulator state, which is key to observing quantized transport in Floquet topological insulators. We expect engineered reservoirs of carriers to be particularly useful in this context, allowing to perform transport measurements while stabilizing insulating-like steady states.

Several aspects of the problem require further study. In this work we have not addressed the effect of inter particle interactions. Floquet-Umklapp processes involving inter-particle scattering give an additional channel for the system to absorb energy from the driving field and increase the number of excitations. However, our current work demonstrates that coupling to a bath of phonons can help keep the heating and excitation density under control. Another important direction is a careful study of the inhomogeneous steady states of Floquet topological insulators, which is crucial in order to predict the edge and surface responses of these systems.

The authors would like to thank A. İmamoğlu, C. Grenier, A. Srivastava, and L.I. Glazman for insightful discussions. Financial support from the Swiss National Science Foundation (SNSF) is gratefully acknowledged. MR acknowledges support from the Villum Foundation and from the People Programme (Marie Curie Actions) of the European Union's Seventh Framework Programme (FP7/2007-2013) under REA grant agreement PIIF-GA-2013-627838. NL acknowledges support from the Israel-US Binational Science Foundation, and I-Core, the Israeli excellence center "Circle of Light". GR and KS are grateful for support from NSF through DMR-1410435, as well as the Institute of Quantum Information and matter, an NSF Frontier center funded by the Gordon and Betty Moore Foundation, and the Packard Foundation. KS is grateful for support from NSF Graduate Research Fellowship Program.

# APPENDIX

## 2.A Kinetic equation in the Floquet basis

In this appendix we discuss the key points in the derivation of the Floquet kinetic equation, represented schematically in Eq. (2.4) of the main text. Specifically, the aim is to derive a system of differential equations which describe the time evolution of the Floquet state occupation factors $F_{k\alpha}(t) = \langle f^\dagger_{k\alpha}(t) f_{k\alpha}(t)\rangle$, where $f^\dagger_{k\alpha}(t)$ and $f_{k\alpha}(t)$ are the creation and annihilation operators for Floquet states as defined above Eq. (2.4). The time derivative $\dot{F}_{k\alpha} = \frac{d}{dt}\langle f^\dagger_{k\alpha}(t) f_{k\alpha}(t)\rangle$ couples to an infinite hierarchy of higher and higher order correlation functions. The main approximation is to truncate this hierarchy at the lowest non-trivial order, and obtain a closed system of evolution equations. We now outline the required steps.

### Basis transformation and dressed matrix elements

The first important step is to express the electronic terms in the Hamiltonian in terms of the Floquet creation and annihilation operators. Using Eq. (2.3), the transformation is made via

$$\begin{aligned} c^\dagger_{k\nu} &= \sum_\alpha \sum_n e^{i(\mathcal{E}_{k\alpha}+n\Omega)t} \langle \phi^n_{k\alpha}|\nu k\rangle f^\dagger_{k\alpha}(t), \\ c_{k\nu} &= \sum_\beta \sum_m e^{-i(\mathcal{E}_{k\beta}+m\Omega)t} \langle \nu k|\phi^m_{k\beta}\rangle f_{k\beta}(t), \end{aligned} \tag{2.16}$$

where $|\nu k\rangle$ is the Bloch function corresponding to crystal momentum $k$ in band $\nu$ of the non-driven system, and $f^\dagger_{k\alpha}(t)$ and $f_{k\alpha}(t)$ are creation and annihilation operators for the Floquet state $|\psi_{k\alpha}(t)\rangle$ (we simplify notations by setting $\hbar = 1$ here and everywhere below). Using these relations, we write the electron-boson interaction and system-reservoir tunneling Hamiltonians as

$$H_{\rm int} = \sum_{k\boldsymbol{q}} \sum_{\alpha\alpha'} \sum_n e^{i(\mathcal{E}_{k-q_x,\alpha'}-\mathcal{E}_{k\alpha})t} e^{in\Omega t} \mathcal{G}^{(n)}_{\alpha'\alpha}(k,q_x) f^\dagger_{k-q_x,\alpha'}(t) f_{k\alpha}(t)(b_{-\boldsymbol{q}} + b^\dagger_{\boldsymbol{q}}), \tag{2.17}$$

$$H_{\rm tun} = \sum_{k\ell} \sum_n \left( e^{i\mathcal{E}_{k\alpha}t} e^{in\Omega t} \mathcal{J}^{(n)}_{\ell,k\alpha} f^\dagger_{k\alpha}(t) d_\ell \; + \; \text{h.c.} \right), \tag{2.18}$$

with "dressed" matrix elements

$$\mathcal{G}^{(n)}_{\alpha'\alpha}(k,q_x) = \sum_\nu \sum_m G^{k-q_x\nu'}_{k\nu}(q_x) \langle \phi^{m+n}_{k-q_x,\alpha'}|\nu', k-q_x\rangle \langle \nu k|\phi^m_{k\alpha}\rangle, \tag{2.19}$$

$$\mathcal{J}^{(n)}_{\ell,k\alpha} = \sum_\nu J_{\ell,k\nu} \langle \phi^n_{\alpha k}|\nu k\rangle. \tag{2.20}$$

Here we use $\mathcal{G}$ and $\mathcal{J}$ to indicate the coupling matrix elements in the Floquet basis.

Note that in Eq. (2.19) we have imposed lattice momentum conservation of the electron-phonon interaction, $G^{k'\nu'}_{k\nu}(q_x) \propto \delta_{q_x,k-k'}$. Equations (2.17) and (2.19) arise from Eq. (2.5) of the main text. Sets of equivalent scattering processes can be identified based on the following useful relation:

$$\mathcal{G}^{(n)}_{\alpha'\alpha}(k, q_x) = [\mathcal{G}^{(-n)}_{\alpha\alpha'}(k + q_x, -q_x)]^*. \tag{2.21}$$

The explicit form of the dressed matrix elements shows that the overlaps $\langle \phi^m_{k\alpha} | k\nu \rangle$ between the original states and the Fourier components $|\phi^m_{k\alpha}\rangle$ of the Floquet modes are crucial in determining the rates of the different Floquet scattering processes, as discussed in the main text.

**Matrix elements for Floquet-Umklapp processes**

An interesting situation occurs when the coupling to the driving field is defined by a vector $\mathbf{g}$ [see Eq. (2.1)] such that $\tilde{g}_\parallel = 0$ [see Eq. (2.2) for the definition of $\tilde{\mathbf{g}}$]. This commonly occurs in experimentally relevant materials driven by optical fields. Here, the Fourier harmonics $|\phi^m_{k\alpha}\rangle$ have a fixed band character for $m$ of fixed parity: for example, in the convention used throughout the paper and set below Eq. (3), $|\phi^m_{k\alpha}\rangle$ is proportional to $|kv\rangle$ for $m$ odd and proportional to $|kc\rangle$ for $m$ even, see Fig. 2a. Additionally, note that scattering by phonons preserves the band character, $G_{\nu\nu'} \propto \delta_{\nu\nu'}$. As a consequence, under these conditions Floquet-Umklapp processes involving phonons are forbidden for $n$ odd. Therefore, if in addition to $\tilde{g}_\parallel = 0$ the phonon bandwidth is less than the driving frequency $\Omega$, all Floquet-Umklapp processes, including both even and odd $n$, are not allowed.

**Equations of motion**

We now study the equations of motion for the Floquet state populations $F_{k\alpha} = \langle f^\dagger_{k\alpha}(t) f_{k\alpha}(t) \rangle$. The populations are the diagonal part of the "polarization matrix" $P^{k'\alpha'}_{k\alpha}(t) = \langle f^\dagger_{k'\alpha'}(t) f_{k\alpha}(t) \rangle$. In addition to the populations, this matrix also characterizes coherence between Floquet states with different crystal momenta and/or band indices. This off-diagonal part may be important for the dynamics and for characterizing steady states. In the main text we focus on steady states in a regime where the off-diagonal part of the polarization matrix can be neglected. Here we derive the kinetic equation in a more general context, including the full polarization matrix, and discuss when and how the off-diagonal parts may be neglected.

As a preliminary, we note the following important property of the Floquet state creation operators $f^\dagger_{k\alpha}(t)$. Similar relations hold for the annihilation operators. Let $U(t, t')$ be the single particle time evolution operator corresponding to the Schrödinger equation $i\frac{d}{dt}|\psi\rangle = H(t)|\psi\rangle$, with the Hamiltonian $H(t) = \sum_k c^\dagger_{k\nu} H_{\nu\nu'}(k, t) c_{k\nu'}$, where $H(k, t) = H_0(k) + V(t)$ is defined in Eq. (2.1) in the text. The operator $f^\dagger_{k\alpha}(t)$ satisfies $f^\dagger_{k\alpha}(t) = U(t, t') f^\dagger_{k\alpha}(t') U^\dagger(t, t')$, which can be written in the

differential form:

$$i\partial_t f^\dagger_{k\alpha}(t) = [H(t), f^\dagger_{k\alpha}(t)]. \tag{2.22}$$

This expression will be used below.

The derivation of the kinetic equation proceeds along standard lines, as explained in detail in, e.g., Ref. [41]. The main difference from the usual case (i.e., for non-driven systems) is the appearance of the "dressed" matrix elements in the interaction Hamiltonians. Below we set up the calculation and point out where these terms appear, and where special considerations are needed to complete the derivation for the case of a periodically driven system.

We seek the time evolution of the Floquet state populations $F_{k\alpha}(t)$. However, since these populations are special cases of the polarizations $P^{k'\alpha'}_{k\alpha}(t)$ defined above, for $k = k'$, $\alpha = \alpha'$, we begin with the more general expression for the time derivative of $P^{k'\alpha'}_{k\alpha}(t)$:

$$i\partial_t \langle f^\dagger_{k'\alpha'}(t) f_{k\alpha}(t)\rangle = \langle [f^\dagger_{k'\alpha'}(t) f_{k\alpha}(t), H_{\rm tot} - H(t)]\rangle, \tag{2.23}$$

where $H(t)$ is the full single particle Hamiltonian (including driving) as defined above, and $H_{\rm tot} = H(t) + H_{\rm b} + H_{\rm int} + H_{\rm res} + H_{\rm tun}$ is the total Hamiltonian including the baths and the system-bath coupling. The commutator in Eq. (2.23) includes two types of contributions, arising from: (1) the time derivative acting on the state with respect to which the average is taken, and (2) from the explicit time dependence of the operators $f^\dagger_{k'\alpha'}(t)$ and $f_{k\alpha}(t)$. The latter are given by Eq. (2.22) and its Hermitian conjugate.

To simplify the expressions below, we introduce a more compact notation in which $k$ and the Floquet band index $\alpha$ are compressed into a single index $a$. In this notation, the dressed electron-phonon coupling matrix elements will be written as $\mathcal{G}^{(n)}_{\alpha'\alpha}(k, q_x) \equiv \mathcal{G}^{(n)}_{a'a}(q_x)$. The commutator in Eq. (2.23) has two non-trivial terms related to the system-boson and system-reservoir couplings $H_{\rm int}$ and $H_{\rm tun}$, $[f^\dagger_a(t) f_b(t), H_{\rm int}]$ and $[f^\dagger_a(t) f_b(t), H_{\rm tun}]$, respectively. The system-boson coupling produces the following contribution:

$$\begin{aligned}\langle [f^\dagger_a(t) f_b(t), H_{\rm int}]\rangle &= \sum_{a'\boldsymbol{q}}\sum_n e^{i(\mathcal{E}_b - \mathcal{E}_{a'})t} e^{in\Omega t} \mathcal{G}^{(n)}_{ba'}(q_x)\, \langle f^\dagger_a(t) f_{a'}(t)(b_{-\boldsymbol{q}} + b^\dagger_{\boldsymbol{q}})\rangle \\ &- \sum_{a'\boldsymbol{q}}\sum_n e^{i(\mathcal{E}_{a'} - \mathcal{E}_a)t} e^{in\Omega t} \mathcal{G}^{(n)}_{a'a}(q_x) \langle f^\dagger_{a'}(t) f_b(t)(b_{-\boldsymbol{q}} + b^\dagger_{\boldsymbol{q}})\rangle, \end{aligned} \tag{2.24}$$

while the system-reservoir coupling leads to

$$\begin{aligned}\langle [f^\dagger_a(t) f_b(t), H_{\rm res}]\rangle &= \sum_\ell \sum_n e^{i\mathcal{E}_b t} e^{in\Omega t} \mathcal{J}^{(n)}_{\ell,b}\, \langle f^\dagger_a(t) d_\ell\rangle \\ &- \sum_\ell \sum_n e^{-i\mathcal{E}_a t} e^{-in\Omega t} \mathcal{J}^{(n)*}_{\ell,a}\, \langle f_b(t) d^\dagger_\ell\rangle. \end{aligned} \tag{2.25}$$

Note the appearance of "mixed" correlators such as $\langle f_a^\dagger(t) f_{a'}(t)(b_{-\boldsymbol{q}} + b_{\boldsymbol{q}}^\dagger)\rangle$ and $\langle f_a^\dagger(t) d_\ell\rangle$ involving both system and bath degrees of freedom, which appear in Eqs. (2.24) and (2.25). The expressions are very similar to those that would be obtained for a non-driven system, except that here we find an additional sum over $n$ which accounts for the harmonic structure of the Floquet state wave functions.

In order to describe scattering between Floquet states, we need to solve for the equations of motion of these mixed correlators. To do so, we must evaluate expressions such as

$$\begin{aligned} i\partial_t \langle f_a^\dagger(t) f_b(t) b_{-\boldsymbol{q}}\rangle &= \langle [f_a^\dagger(t) f_b(t) b_{-\boldsymbol{q}}, H_{\rm tot} - H(t)]\rangle \\ i\partial_t \langle f_a^\dagger(t) d_\ell\rangle &= \langle [f_a^\dagger(t) d_\ell, H_{\rm tot} - H(t)]\rangle . \end{aligned} \tag{2.26}$$

Similar expressions are also needed for $i\partial_t \langle f_a^\dagger(t) f_b(t) b_{\boldsymbol{q}}^\dagger\rangle$ and $i\partial_t \langle f_b(t) d_\ell^\dagger\rangle$.

The commutators in Eq. (2.26) generate many terms. The corresponding calculation is straightforward, but somewhat tedious. As above, the primary difference from the textbook case of a non-driven system [41] is the appearance of sums over Floquet harmonic indices.

Mathematically, the crucial point is that the commutators in Eq. (2.26) give rise to higher order correlation functions such as $\langle f_a^\dagger f_c^\dagger f_b f_d\, b_{\boldsymbol{q}}^\dagger b_{\boldsymbol{q}'}\rangle$ and $\langle f_a^\dagger f_b d_\ell^\dagger d_{\ell'}\rangle$. In the first case we split the averages into products of averages of fermionic and bosonic bilinear operators: $\langle f_a^\dagger f_c^\dagger f_b f_d\, b_{\boldsymbol{q}}^\dagger b_{\boldsymbol{q}'}\rangle \approx \langle f_a^\dagger f_d\rangle\langle f_c^\dagger f_b\rangle\langle b_{\boldsymbol{q}}^\dagger b_{\boldsymbol{q}'}\rangle - \langle f_a^\dagger f_b\rangle\langle f_c^\dagger f_d\rangle\langle b_{\boldsymbol{q}}^\dagger b_{\boldsymbol{q}'}\rangle$, etc. The fermionic averages involving system operators just give the polarizations $P_a^{a'}$ defined above. We take the averages of the bosonic operators with respect to a thermal distribution with inverse temperature $\beta$: $\langle b_{\boldsymbol{q}}^\dagger b_{\boldsymbol{q}'}\rangle = \delta_{\boldsymbol{q}\boldsymbol{q}'} N(\omega_{\boldsymbol{q}})$, where $N(\varepsilon) = 1/(1 - e^{-\beta\varepsilon})$ and $\omega_{\boldsymbol{q}}$ is the frequency of bosonic mode $\boldsymbol{q}$. Likewise, we split the averages involving reservoir degrees of freedom as $\langle f_a^\dagger f_b d_\ell^\dagger d_{\ell'}\rangle \approx \langle f_a^\dagger f_b\rangle\langle d_\ell^\dagger d_{\ell'}\rangle$. For the Fermi reservoir, we take $\langle d_\ell^\dagger d_{\ell'}\rangle = \delta_{\ell\ell'} D(E_\ell)$, where $D(E)$ is the Fermi-Dirac function with temperature $T$ and chemical potential $\mu_{\rm res}$. For brevity, below we use $D_\ell = D(E_\ell)$.

Through the above approximations we close the equation of motion hierarchy. After splitting the averages on the right hand sides of Eq. (2.26), we integrate them from time 0 to $t$ to find the correlation functions $\langle f_a^\dagger(t) f_b(t) b_{\boldsymbol{q}}\rangle(t)$ and $\langle f_a^\dagger(t) d_\ell\rangle(t)$ needed as input for the equations of motion of the polarizations, Eqs. (2.23), (2.24) and (2.25).

To give an explicit example, we focus on one term which arises from the system-reservoir coupling,

$$i\partial_t \langle f_a^\dagger d_\ell\rangle = E_\ell \langle f_a^\dagger d_\ell\rangle + \sum_b \sum_n e^{-i\mathcal{E}_b t} e^{-in\Omega t} \mathcal{J}_{\ell,b}^{(n)*} \left[P_b^a(1 - D_\ell) - (\delta_{ab} - P_b^a) D_\ell\right] . \tag{2.27}$$

The calculation for other terms yields similar expressions. A straightforward formal integration,

taking $\langle f_a^\dagger d_b\rangle(t=0)=0$, then yields

$$\langle f_a^\dagger d_\ell\rangle = \frac{1}{i}\sum_b\sum_n \mathcal{J}^{(n)*}_{\ell,b} e^{-iE_\ell t}\int_0^t dz e^{-i(\mathcal{E}_b-E_\ell)z}e^{-in\Omega z}\left[P^a_b(1-D_\ell)-(\delta_{ab}-P^a_b)D_\ell\right] \quad (2.28)$$

The next step is to introduce this result and its counterpart for $\langle d_\ell^\dagger f_a\rangle$ into Eq. (2.25), for the contribution of the system-reservoir coupling to the evolution of the population $P^{a'}_a$, Eq. (2.23). Doing so, we obtain:

$$\begin{aligned}\langle[f_a^\dagger f_{a'}, H_{\rm tun}]\rangle &= \frac{1}{i}\sum_{\ell b}\sum_{mn}\mathcal{J}^{(n)}_{\ell,a'}\mathcal{J}^{(m)*}_{\ell,b}e^{i(\mathcal{E}_{a'}-E_\ell)t}e^{in\Omega t}\int_0^t dz e^{-i(\mathcal{E}_b-E_\ell)z}e^{-im\Omega z}\left[P^a_b(1-D_\ell)-(\delta_{ab}-P^a_b)D_\ell\right]\\ &- \frac{1}{i}\sum_{\ell b}\sum_{mn}\mathcal{J}^{(n)*}_{\ell,a}\mathcal{J}^{(m)}_{\ell,b}e^{-i(\mathcal{E}_a-E_\ell)t}e^{-in\Omega t}\int_0^t dz e^{i(\mathcal{E}_b-E_\ell)z}e^{im\Omega z}\left[(\delta_{a'b}-P^b_{a'})D_\ell - P^b_{a'}(1-D_\ell)\right]\\ &. \end{aligned} \quad (2.29)$$

Importantly, notice that the right hand side of Eq. (2.29) couples the evolution of the population $F_a = P^a_a$ to both the diagonal and off-diagonal polarizations $P^a_b$. Thus in principle we do not have a closed set of equations for the populations alone. In particular, for transient behavior (e.g., at early times when the driving is just switched on) such terms can not be ignored.

Close to the steady state, we may expect the off-diagonal polarizations (coherences) to be small under certain circumstances. For a homogeneous system where the steady state maintains translational invariance, the polarizations in the steady state are diagonal in the electronic crystal momentum, $P^{k'\alpha'}_{k\alpha} \propto \delta_{kk'}$. Furthermore, coherences between the two Floquet bands can be suppressed in the steady state under suitable conditions, which are discussed at length in Appendix 2.D. These conditions are expected to be met for weak system-bath coupling, and we have verified that the steady states resulting from our simulations are indeed in this regime (see Appendix 2.D).

For strong system-bath coupling, the conditions discussed in Appendix 2.D might not be met, and a more complicated situation may arise. There, the particular form of system-bath coupling may try to drive the system towards specific states other than the Floquet states. For example, relaxation may occur into the eigenstates of the non-driven system. The competition between driving and relaxation may then lead to steady states featuring significant inter-Floquet-band coherences.

In this work we focus on the case of homogeneous steady states, with weak (but nonetheless realistic) system bath coupling. We neglect all off-diagonal coherences, setting $P^a_b \propto \delta_{ab}$ in Eq. (2.29) and similarly for all other terms in the equations of motion. Additionally, in the sums over Fourier harmonics we only keep the terms for which $n = m$; when the Floquet state populations evolve

slowly on the timescale of the driving period, the terms with $n \neq m$ give rise to fast oscillations and thus produce negligible contributions. With these two simplifications, the standard Markovian approximation yields the full Floquet kinetic equation:

$$\partial_t F_{k\alpha} \quad = \quad I^{\mathrm{ph}}_{k\alpha} + I^{\mathrm{rec}}_{k\alpha} + I^{\mathrm{tun}}_{k\alpha}, \tag{2.30}$$

with the collision integral for electron-phonon scattering given by

$$\begin{aligned} I^{\mathrm{ph}}_{k\alpha} \quad = \quad & \frac{2\pi}{\hbar} \sum_{\alpha' \boldsymbol{q}} \sum_n |\mathcal{G}^{(n)}_{\alpha'\alpha}(k, q_x)|^2 \left[ F_{k-q_x\alpha'} \bar{F}_{k\alpha} N(\hbar\omega_{\boldsymbol{q}}) - F_{k\alpha} \bar{F}_{k-q_x\alpha'} (1 + N(\hbar\omega_{\boldsymbol{q}})) \right] \\ & \delta(\mathcal{E}_{k\alpha} - \mathcal{E}_{k-q_x\alpha'} - \hbar\omega_{\boldsymbol{q}} - n\hbar\Omega) \\ + \quad & \frac{2\pi}{\hbar} \sum_{\alpha' \boldsymbol{q}} \sum_n |\mathcal{G}^{(n)}_{\alpha'\alpha}(k, q_x)|^2 \left[ F_{k-q_x\alpha'} \bar{F}_{k\alpha} (1 + N(\hbar\omega_{\boldsymbol{q}})) - F_{k\alpha} \bar{F}_{k-q_x\alpha'} N(\hbar\omega_{\boldsymbol{q}}) \right] \\ & \delta(\mathcal{E}_{k-q_x\alpha'} - \mathcal{E}_{k\alpha} - \hbar\omega_{\boldsymbol{q}} + n\hbar\Omega). \end{aligned} \tag{2.31}$$

Tunneling in and out of the Fermi reservoir is described by (see Eqs. (2.10) and (2.11) in the main text):

$$I^{\mathrm{tun}}_{k\alpha} = \frac{2\pi}{\hbar} \sum_\ell \sum_n |\mathcal{J}^{(n)}_{\ell,k\alpha}|^2 \left[ \bar{F}_{k\alpha} D(E_\ell) - F_{k\alpha} (1 - D(E_\ell)) \right] \delta(\mathcal{E}_{k\alpha} - E_\ell + n\hbar\Omega). \tag{2.32}$$

The collision integral corresponding to radiative recombination looks identical to that for electron-phonon scattering in Eq. (2.31), with the matrix elements $\mathcal{G}^{(n)}_{\alpha'\alpha}(k, q_x)$ replaced by the appropriate ones for coupling to the electromagnetic environment. In our model, the matrix element for coupling to bath photons is purely off-diagonal in the basis of the conduction and valence bands of the non-driven system. This model is motivated by the form of radiative transitions for electrons near $k = 0$ in many experimentally relevant materials. For simplicity, we modeled recombination as "vertical" transitions [6], giving $G^{\mathrm{rec}} = g^{\mathrm{rec}}(1 - \delta_{\nu\nu'})\delta_{q_x,0}\delta_{k,k'}$.

According to our convention in Eq. (2.3), the fact that $G^{\mathrm{rec}} \propto (1 - \delta_{\nu\nu'})$ requires a coupling between $|\phi^m_{k\alpha}\rangle$ and $|\phi^{m'}_{k\alpha'}\rangle$, where $m$ and $m'$ are separated by an odd integer for the case $\tilde{g}_\parallel = 0$. Furthermore, the conservation of energy expressed by the delta function in Eq. (2.31) requires $n$ to be *negative*. Therefore, in our model recombination only acts through terms in Eq. (2.31) with $n < 0$ odd. The dominant contribution comes for $n = -1$ for weak driving. Correspondingly, the emitted photon energy is large (on the order of the driving frequency), and hence we set all Bose occupation factors for photons to zero (i.e., only spontaneous emission is included).

Finally, to get the collision integral (2.31) into the form of Eq. (2.7) in the text, we integrate over the delta function to get the density of states for bosons with momentum $q_x$ parallel to the system. This gives

$$I^{\rm ph}_{k\alpha} = \frac{2\pi}{\hbar}\sum_{k'\alpha'}\sum_{n}|\mathcal{G}^{(n)}_{\alpha'\alpha}(k,q_x)|^2\left[F_{k'\alpha'}\bar{F}_{k\alpha}N(\Delta\mathcal{E}_n)-F_{k\alpha}\bar{F}_{k'\alpha'}(1+N(\Delta\mathcal{E}_n))\right]\rho_{q_x}(\Delta\mathcal{E}_n) \quad (2.33)$$
$$+ \frac{2\pi}{\hbar}\sum_{k'\alpha'}\sum_{n}|\mathcal{G}^{(n)}_{\alpha'\alpha}(k,q_x)|^2\left[F_{k'\alpha'}\bar{F}_{k\alpha}(1+N(-\Delta\mathcal{E}_n))-F_{k\alpha}\bar{F}_{k'\alpha'}N(-\Delta\mathcal{E}_n)\right]\rho_{q_x}(-\Delta\mathcal{E}_n),$$

where in the above $q_x = k - k'$ and $\Delta\mathcal{E}_n = \mathcal{E}_{k\alpha} - \mathcal{E}_{k'\alpha'} - n\hbar\Omega$.

### 2.B System size scaling of transition rates

In this section we discuss the scaling of the electron-boson scattering rates $W^{k'\alpha'}_{k\alpha}$ with the system size. We will show that in the limit of a large system, the rates scale as $\sim 1/L$. As we explain below, this implies that both $\gamma^{\rm rec}$ and $\Lambda^{\rm inter} = L\overline{W}^{\rm inter}$, defined in Eq. (2.8) and the discussion below, are independent of system size. An important consequence is that the excitation density $n_{\rm steady}$ is also *independent* of the system size, as one would naturally expect. We first focus our discussion on radiative recombination, i.e. the interaction with a photon bath, and then explain how it can be easily applied also to a bath of phonons. To simplify the discussion, we illustrate the scaling using a non-driven toy model, but the discussion can be easily generalized for transition rate between Floquet states in a driven system.

We consider an electronic Bloch Hamiltonian of the form $H_0(k) = \left[2A\left(1-\cos(ka)\right) + E_{\rm gap}\right]\sigma_z$. We define the Bloch states as $|k\alpha\rangle = \frac{1}{\sqrt{N}}\sum_{x=0}^{(N-1)a} e^{ikx}|x,\alpha\rangle$, where $c, v$ correspond to the positive and negative eigenvalues of $\sigma_z$, $a$ is the lattice constant and $L = Na$ is the electronic system size.

The electron photon interaction Hamiltonian, in the rotating wave approximation, is given by $H_{\rm int} = \sum_{\boldsymbol{q}} H_{\rm int}(\boldsymbol{q})$, with

$$H_{\rm int}(\boldsymbol{q}) = \sum_x M_{\boldsymbol{q}} e^{i\boldsymbol{q}\cdot\boldsymbol{r}}\left(c^\dagger_{x,v}c_{x,c}b^\dagger_{\boldsymbol{q}} + c^\dagger_{x,c}c_{x,v}b_{-\boldsymbol{q}}\right) + h.c., \quad (2.34)$$

where in the above $c^\dagger_{x,\alpha}$ are creation and annihilation operators for Wannier states in the conduction and valence bands, and $|M_{\boldsymbol{q}}|$ depends on the volume of the electromagnetic environment as $|M_{\boldsymbol{q}}| \sim 1/\sqrt{V_{\rm env}}$. Note that $H_{\rm int}(\boldsymbol{q})$ is diagonal in the lattice coordinate $x$. The rate for recombination from $|k,c\rangle$ to $|k',v\rangle$ is then given by

$$W^{k'v}_{kc} = \frac{2\pi}{\hbar}\sum_{\boldsymbol{q}}\left|M_{\boldsymbol{q}}\sum_x\frac{e^{i(k-k'+q)x}}{N}\right|^2\delta(E_{kc}-E_{k'v}-\hbar\omega_{\boldsymbol{q}}), \quad (2.35)$$

where $\{E_{k\alpha}\}$ are the eigenenergies of $H_0(k)$. Importantly, the photon momentum lives on a *different reciprocal lattice* than the momenta of the electronic system, $q = \frac{2\pi}{L_{\rm env}}n$. For simplicity, we drop

the $\boldsymbol{q}$ dependence of $M_{\boldsymbol{q}}$. Summing over the *transverse* photon momenta $\boldsymbol{q}_\perp$ yields a 2D density of states for the transverse modes with $q_x$ held fixed,

$$W_{kc}^{k'v} = \frac{2\pi}{\hbar} \sum_{q_x} \frac{|M|^2}{N^2} \left| \sum_x e^{i(k-k'+q)x} \right|^2 \rho_{q_x}(E_{kc} - E_{k'v}). \tag{2.36}$$

Note that $\rho_{q_x}(E_{kc} - E_{k'v})$ has dimensions of $\frac{1}{\text{Energy}}$ and scales as $L_{\text{env}}^2$. The photons emitted by the radiative recombination transition have a typical energy of $E_{\text{gap}}$, and therefore the corresponding photon momentum $\hbar q_* = E_{\text{gap}}/c$ plays an important role in the calculation of the rates. For simplicity, we set the density of states $\rho_{q_x}(E_{kc} - E_{k'v})$ to be a constant $\rho_0^{(2D)}$ for $|q_x| \leq q_*$, and zero otherwise. This gives

$$W_{kc}^{k'v} = \frac{2\pi}{\hbar} \frac{M^2 \rho_0^{(2D)}}{N^2} \sum_{q_x=-q_*}^{q_*} \left| \sum_x e^{i(k-k'+q)x} \right|^2 . \tag{2.37}$$

Assuming a large environment volume, we can write

$$W_{kc}^{k'v} = \frac{2\pi}{\hbar} \frac{M^2 \rho_0^{(2D)} L_{\text{env}}}{N^2} \int_{-q_*}^{q_*} \frac{dq}{2\pi} \left| \frac{1 - e^{iqL}}{1 - e^{i(k-k'+q)a}} \right|^2 . \tag{2.38}$$

Recalling that $M \sim 1/\sqrt{V_{\text{env}}}$ we see that the factor $M^2 \rho_0^{(2D)} L_{\text{env}}$ is *independent of environment size*.

The calculation now amounts to evaluating the integral in Eq. (2.38). Using integers to represent momenta as in $k = \frac{2\pi}{L} n$, we denote this integral by $g_N(n - n')$, where the $N$ subscript denotes the fact that the integral depends on the system size $L = Na$. We are interested in the scaling of this integral with $N$. We define the dimensionless variable $\tilde{q} = qL$, and divide by $N^2$ for later convenience, whereby the integral becomes

$$\frac{g_N(m)}{N^2} = \frac{1}{L} \int_{-q_* Na}^{q_* Na} d\tilde{q} \frac{\sin^2(\tilde{q}/2)}{N^2 \sin^2(\frac{1}{2N}[2\pi m + \tilde{q}])}. \tag{2.39}$$

Note that in the prefactor on the right hand side above, $L$ is the *electronic system* size. In order for $W_{kc}^{k'v} \sim 1/L$, which guarantees that e.g. $n_{\text{steady}}$ remains independent of system size, one has to have that $\frac{g_N(m)}{N^2} \sim 1/L$.

In the following, we assume $q_* a = \frac{E_{gap} a}{\hbar c} \ll 1$, which means the photon wavelength is much larger then the lattice spacing of the system. We furthermore consider the limit where the system size is larger than the photon wavelength, $N \gg 1/(q_* a)$. We start again from Eq. (2.39). Clearly, for $g_N(m)/N^2$ to be of order $1/L$, we must have $2\pi|m| \lesssim N q_* a$, which guarantees that the integral picks the contribution where the sin function in the denominator of (2.39) vanishes. Physically, this corresponds to the requirement that $|k - k'| \lesssim q_*$.

We now need to check how the integral in Eq. (2.39) scales with $N$. We do this explicitly for $m = 0$; the result can be generalized for any $2\pi|m| \lesssim N q_* a$. We break the integral into three integration

regions: (1) $\left[-\sqrt{q_*Na}, \sqrt{q_*Na}\right]$ (2) $\left[\sqrt{q_*Na}, q_*Na\right]$ and (3) $\left[-q_*Na, -\sqrt{q_*Na}\right]$. In region (2), we can give an upper bound to the integral by

$$\int_{\sqrt{q_*Na}}^{q_*Na} d\tilde{q} \frac{1}{N^2 \sin^2(\sqrt{q_* a/4N})} \xrightarrow{N\to\infty} C, \tag{2.40}$$

where $C$ is a constant. The same result applies to the integral in region (3). In region (1), we expand the denominator to obtain

$$\int_{-\sqrt{q_*Na}}^{\sqrt{q_*Na}} d\tilde{q} \frac{\sin^2(\tilde{q}/2)}{\frac{1}{4}\tilde{q}^2} \left(1 - \frac{\tilde{q}^2}{12N^2} + ...\right). \tag{2.41}$$

The first term in the above expansion clearly gives an order 1 contribution, while the remaining terms vanish in the limit of large $N$.

The result of the above analysis is that $g_N(m) \approx \frac{N^2}{L}\bar{g}(m)$, where $\bar{g}(m)$ is independent of system size. The full expression for $g_N(m)$ may contain terms that scale slower than $N^2/L$ with the system size. Finally, inserting this result this back into Eq. (2.38), we arrive at the scaling $W_{kv}^{k'c} \sim 1/L$ of rates with the system size, in the limit of a large system.

Putting this into the definition of the *total rate* of recombination out of the state $|k, c\rangle$, defined by $\mathcal{W}_k^{rec} = \sum_{k'} W_{kc}^{k'v}$, we get

$$\mathcal{W}_k^{rec} = L \int \frac{dk'}{2\pi} W_{kc}^{k'v} \approx L \frac{E_{gap}}{\pi\hbar c} W_{kc}^{kv}. \tag{2.42}$$

Therefore $\mathcal{W}_k^{rec}$ is *independent* of system size, as promised. Likewise, the *total rate density*, $\gamma^{\text{rec}} = \frac{1}{L}\sum_{k,k'} W_{kc}^{k'v} = \int \frac{dk}{2\pi} \mathcal{W}_k^{rec}$ is *independent* of system size. Note that the factor $\frac{E_{gap}}{\pi\hbar c}$ in Eq. (2.42) accounts for the photon density of states in the longitudinal direction, whereby $\rho^{3\text{D}} = \frac{E_{gap}}{\pi\hbar c}\rho^{2\text{D}}$.

**Scaling of phonon matrix elements**

The treatment of the phonon matrix elements follows along the same lines as above. Let us treat the longitudinal size (along the direction of the one dimensional system) of the phonon bath to be equal to the system size $L$. This ensures the conservation of crystal momentum, $k' + q = k$. We start from the analogue of Eq. (2.35), for phonon scattering rates. Performing the sum over $x$ we obtain a factor of $N^2\delta_{k'-k,q_x}$. In this case, however, the factor $M^2\rho_0^{2D}$ scales as $\sim 1/L$. Therefore, $W_{k'\alpha}^{k'\alpha'} \sim 1/L$.

## 2.C Numerical simulations

In our numerical simulations, the steady state distributions were obtained by direct evolution of Eq. (2.4). The results are independent of the initial distribution $\{F_{k\alpha}(t = 0)\}$.

In Sec. 2.3 we discussed the square root dependence of the excitation density $n_{\text{steady}}$ on the ratio $\pi\overline{\mathcal{W}}^{\text{rec}}/k_R W^{\text{inter}}$. This behaviour was observed in our numerical simulations, as shown in Fig. 2.3. Below we discuss how each factor in the above ratio was calculated from the numerical data. For recombination, the quantity $\overline{\mathcal{W}}^{\text{rec}}$ is calculated by averaging the quantity $\mathcal{W}_k^{\text{rec}}$ [defined below Eq. (2.8)], in the interval $[-k_R, k_R]$. Since $\mathcal{W}_k^{\text{rec}}$ becomes negligible far outside of this interval, we define $\overline{\mathcal{W}}^{\text{rec}} = \pi/(k_R L)\sum_k \mathcal{W}_k^{\text{rec}}$, with

$$\mathcal{W}_k^{\text{rec}} = \frac{2\pi}{\hbar}|g^{\text{rec}}|^2\rho_0 \sum_{n=1}^{\infty}\Big|\sum_m \langle\phi_{k+}^{m-n}|kv\rangle\langle kc|\phi_{k-}^{m}\rangle\Big|^2. \tag{2.43}$$

To estimate the typical *interband* scattering rate from phonons, we evaluate $\overline{W}^{\text{inter}}$ by taking an average interband phonon scattering rate near the resonances $\pm k_R$. The explicit form for $\overline{W}^{\text{inter}}$ we used is

$$\overline{W}^{\text{inter}} = \frac{2}{N_\varepsilon^2}\sum_{k=k_R-\varepsilon}^{k_R+\varepsilon}\sum_{k'=k_R-\varepsilon}^{k_R+\varepsilon} W_{k+}^{k'-} \tag{2.44}$$

In the above, the rates $W_{k+}^{k'-} = W_{k+}^{k'-}(0)$, defined in Eq. (2.6), corresponds to interband transitions from the upper to the lower Floquet band, through the energetically allowed phonon *emission* processes in the model that we studied numerically. The factor of 2 comes from summing over transitions at momenta around $\pm k_R$. Furthermore, in Eq. (2.44), we denote by $N_\varepsilon$ the number of $k$-points corresponding to the region near $k_R$ set by $\varepsilon = \frac{\pi}{10a}$. The excitation density, normalized to the thermal density, is fitted using nonlinear least squares, to the form $\log_{10}(\frac{n_e}{n_{th}}) = p\log_{10}\left(\frac{k_R}{\pi}\frac{\mathcal{W}^{\text{rec}}}{W^{\text{inter}}}\right) + (b - \log_{10}(n_{th}))$ to obtain $p = 0.49$ and $b = 0.95$ with a standard error of 0.001 in the region away from saturation.

## 2.D Populations vs. coherences in the steady state

Throughout this paper we have used the basis of single particle Floquet states to describe the steady state of the driven system. We focused on a regime in which the quadratic correlators in the steady state are approximately diagonal in the Floquet state basis, (i.e., where the "off diagonal" correlations of the form $\langle f_{k\alpha}^\dagger(t) f_{k'\beta}(t)\rangle$, and higher order correlations, are negligible for $k \neq k'$ and/or $\alpha \neq \beta$). In this regime, the steady state of the system can be efficiently described in terms of occupation numbers of the single particle Floquet states.

In this appendix we obtain a criterion for the system to be in the "diagonal" regime described above. The criterion can be summarized as $1/(\Delta_{k_R}\tau_{\text{scat}}) \ll 1$, where $\tau_{\text{scat}}$ is a typical scattering time in the steady state of the system (see below for a formal definition). To relate this condition to experimentally relevant quantities, first recall that $\Delta_{k_R}$, the Floquet gap at the resonance momentum,

is directly proportional to the drive amplitude: $\Delta_{k_R} = V_0|\tilde{\boldsymbol{g}}_{k_R,\perp}|$, see Eq. (2.2). Heuristically, the value of $\tau_{\text{scat}}$ is comparable to the scattering time of charge carriers in the same system studied throughout this paper, at thermal equilibrium in the absence of driving, and with an effective temperature yielding a similar excitation density as in the steady state of the driven system.

**Criterion for the diagonal regime**

Our approach is to derive a Markovian master equation for the reduced density matrix describing the modes with momentum $k_0$, for each $k_0$. In the limit $1/(\Delta_{k_R}\tau_{\text{scat}}) \to 0$, we will show that the self-consistent solution to this set of equations yields the steady state obtained in the main text. In particular, all of the "off diagonal" correlations such as $\langle f^\dagger_{k\alpha}(t) f_{k'\beta}(t)\rangle$ with $\alpha \neq \beta$ strictly vanish in this limit.

To set up the approach we consider the Hilbert space associated with a specific momentum $k_0$, which can be spanned by the state $|e\rangle \equiv |0\rangle$, where $|0\rangle$ is the vacuum for the single particle modes at momentum $k_0$, $|-\rangle \equiv f^\dagger_{k_0,-}(t)|0\rangle$, $|+\rangle \equiv f^\dagger_{k_0,+}(t)|0\rangle$ and $|2\rangle \equiv f^\dagger_{k_0,+}(t) f^\dagger_{k_0,-}(t)|0\rangle$. Accordingly, the reduced density matrix $\rho(k_0)$ in this space (given by tracing out the electronic degrees of freedom at all other momenta) is given by a $4\times 4$ matrix. Importantly, there are no off-diagonal correlations between states with different occupation numbers[10]. Therefore, the only non zero elements in $\rho(k_0)$ are $\rho_{jj}(k_0)$ with $j = \{e, +, -, 2\}$, and $\rho^*_{+-}(k_0) = \rho_{-+}(k_0)$. As in the cluster expansion approach (see appendix 2.A), we assume that four-point correlators can be well approximated by factorization into products of two-point correlators. The relation between the density matrix $\rho(k_0)$ and the two-point correlators $\langle f^\dagger_{k_0\alpha} f_{k_0\alpha'}\rangle$ is simple: For the diagonal elements of $\rho(k_0)$, we have $\rho_{ee}(k_0) = \bar{F}_{k_0,+}\bar{F}_{k_0,-}$, $\rho_{--}(k_0) = F_{k_0,-}\bar{F}_{k_0,+}$, $\rho_{++}(k_0) = F_{k_0,+}\bar{F}_{k_0,-}$ and $\rho_{22}(k_0) = F_{k_0,+}F_{k_0,-}$. The off-diagonals are given by $\rho_{+-}(k_0) = \langle f^\dagger_{k_0-} f_{k_0+}\rangle$. In the following, we will denote $\rho \equiv \rho(k_0)$.

The derivation of the Markovian master equation follows a standard weak coupling procedure (for a reference discussing the master equation for periodically driven systems, see Ref. [32]). In our case the bath consists of the bosonic baths discussed in Sec. 2.3, the fermionic reservoir discussed in Sec. 2.4, as well as the electrons at all other momenta $k \neq k_0$. Here we assume that the electrons with $k \neq k_0$ are in a time-periodic steady state $\rho_{\text{steady}}$, which is determined self-consistently by the solutions to the master equations for all values of $k_0$. This time dependence of the bath's density matrix is an important difference between the situation in this work and the one described in Ref. [32]. Making the appropriate minor modifications, we obtain an evolution equation for the "coherence vector" $\boldsymbol{\rho} = (\rho_{ee}, \rho_{--}, \rho_{++}, \rho_{22}, \rho_{+-}, \rho_{-+})^T$:

$$\dot{\boldsymbol{\rho}} = \mathcal{L}\boldsymbol{\rho}, \qquad \mathcal{L} = \begin{pmatrix} R & V \\ V' & C \end{pmatrix}. \tag{2.45}$$

Generically, the Liouvillian $\mathcal{L}$ in Eq. (2.45) depends periodically on time, $\mathcal{L}(t) = \sum_m e^{im\omega t}\mathcal{L}_m$. As

in Ref. [32], here we keep only the zero frequency component, $\mathcal{L} = \mathcal{L}_0$, which is justified when $\boldsymbol{\rho}$ changes slowly in time. The dimensions of the sub-matrices $R$, $V$, $V'$ and $C$ are $4\times4$, $4\times2$, $2\times4$ and $2\times2$, respectively. Note that the matrix $\mathcal{L}$ depends on the occupation factor of all other momentum states, $k \neq k_0$.

In the formulation above, Eq. (2.45), the evolution described by the kinetic equation (2.4) is incorporated in the sub-matrix $R$. The collision integrals $I_{k\alpha}$ in (2.4) can be written in terms of the matrix elements of $R$ by taking the time derivative of the identity $F_{k_0\alpha} = \rho_{\alpha\alpha} + \rho_{22}$. Therefore, if we restrict Eq. (2.45) to the first four components of $\boldsymbol{\rho}$ for each momentum, the solution for this set of equations will be identical to the solution to the kinetic equation, Eq. (2.4).

To study the coherences $\rho_{+-}$, $\rho_{-+}$, we need to take into account the sub-matrices $V$, $V'$ and $C$. The matrix $C$ takes the form

$$C = \begin{pmatrix} i\Delta\mathcal{E} & C_{+-,-+} \\ C_{-+,+-} & -i\Delta\mathcal{E} \end{pmatrix} \tag{2.46}$$

where $\Delta\mathcal{E} = \mathcal{E}_{k_0,+} - \mathcal{E}_{k_0,-}$.

We now investigate the role of the coherences in Eq. (2.45) using perturbation theory for small $|V|/\Delta\mathcal{E}$ and $|V'|/\Delta\mathcal{E}$, where $|V| = \max_{i,j}|V_{ij}|$. In the limit $|V|/\Delta\mathcal{E}$, $|V'|/\Delta\mathcal{E} \to 0$, the zero-order steady state solution $\mathcal{L}\boldsymbol{\rho} = 0$ reduces to $R\boldsymbol{\rho} = 0$, where $\boldsymbol{\rho}$ is restricted to the first four components, the remaining two being zero. As discussed above, this solution is identical to the solution of the kinetic equation used in the main text.

For finite but small values of $|V|/\Delta\mathcal{E} \sim |V'|/\Delta\mathcal{E}$, we compute corrections to the steady state solution, i.e., changes to the zero eigenvector of $\mathcal{L}$ due to mixing in contributions from the $\rho_{+-}$, $\rho_{-+}$ subspace. Here, $\Delta\mathcal{E}$ serves as an "energy denominator" which effectively decouples the populations from the coherences.

We now show that the matrix elements of the submatrices $V$ and $V'$ are similar in magnitude to the matrix elements of $R$. Therefore, our perturbative approach is justified when $|R|/\Delta\mathcal{E} \ll 1$. This allows us to formulate the criterion for the applicability of the kinetic equation purely in terms of the rates discussed in the main text.

To see why the matrix elements of $V$, $V'$ and $R$ are similar in magnitude, we consider as an example the matrix element $V_{ee,+-}$ for the case of zero temperature:

$$V_{ee,+-} = \bar{F}_{k'\alpha'} \sum_{k'\alpha'} \left( V_+^{k'\alpha'} + V_-^{k'\alpha'} \right), \tag{2.47}$$

where

$$V_{\pm}^{k'\alpha'} = \frac{\pi}{\hbar}\sum \langle \phi_{k'\alpha'}^{m+n}|\hat{G}(q_x)|\phi_{k\pm}^{m}\rangle \left(\langle \phi_{k'\alpha'}^{m'+n}|\hat{G}(q_x)|\phi_{k\mp}^{m'}\rangle\right)^* \times \rho_{q_x}(-\Delta\mathcal{E}_n^{(\pm)} + n\hbar\Omega). \quad (2.48)$$

Following the notation in Eq. (2.6), we denote $\Delta\mathcal{E}_n^{(\beta)} = \mathcal{E}_{k',\alpha} - \mathcal{E}_{k_0,\beta} + n\hbar\Omega$, and the sum is taken over $q_x, m, m', n$. In comparison, the matrix element $R_{ee,++}$ is given by

$$R_{ee,++} = \sum_{k'\alpha'} \bar{F}_{k'\alpha'} W_{k_0+}^{k'\alpha'}, \quad (2.49)$$

where $W_{k_0+}^{k'\alpha'}$ is defined using Eq. (2.6). Equations (2.6) and (2.48) are of a very similar form [note that in Eq. (2.48), the $\pm$ and $\mp$ signs prevent a completion to a square as in Eq. (2.6)]. Comparing the two equations, we see that $|V_{ee,+-}| \sim |R_{ee,++}|$.

In summary, the above discussion gives a clear criterion for the regime in which the off-diagonal coherences $\rho_{+-}$ and $\rho_{-+}$ can be neglected. We define $\tau_{\rm scat}^{-1} = |R|$, where $R$ is computed in the the self-consistent steady state solution of Eqs. (2.45) for all momenta $k_0$, at zeroth order in $|V|/\Delta\mathcal{E}$. Intuitively, $\tau_{\rm scat}^{-1}$ signifies the typical scattering rate in or out of the momentum state at $k_0$, in the steady state. Furthermore, the quasienergy difference $\Delta\mathcal{E}$ is bounded from below by the Floquet gap, $\Delta\mathcal{E} \geq \Delta_{k_R}$. From the discussion above we see that the coherences $\rho_{+-}$ and $\rho_{-+}$ can be neglected in the limit $(\Delta_{k_R}\tau_{\rm scat})^{-1} \ll 1$.

**Comparison between $\tau_{\rm scat}$ and scattering rates in non-driven systems**

What is the typical magnitude of $(\Delta_{k_R}\tau_{\rm scat})^{-1}$? The Floquet gap $\Delta_{k_R}$ depends on driving power, and may be on the order of $0.5\,\mathrm{ps}^{-1}$ or even larger in experimentally accessible setups (see, e.g., Refs. [66, 67]). Our model includes three scattering mechanisms: electron-phonon interaction, radiative recombination, and the coupling to the Fermi reservoir. Typically in semiconductors, radiative recombination rates are on the order of $1\,\mathrm{ns}^{-1}$, and can therefore be neglected in comparison to $\Delta_{k_R}$. Phonon scattering rates can be appreciably larger. An order of magnitude for the "bare" phonon scattering rate, (not suppressed, e.g., by Pauli blocking), is on the order of $1\,\mathrm{ps}^{-1}$.

In non-driven systems, Pauli blocking and phase space considerations can significantly reduce the scattering rates for the populated states, relative to their bare values. As we discuss below, a similar suppression of the scattering rates occurs in the driven system. Therefore, we can expect $\tau_{\rm scat}^{-1}$ in the steady state to be of similar magnitude to the scattering rate in an equilibrium semiconductor at a temperature which supports a similar excitation density. Importantly, even when the coupling to the reservoir is strong enough to significantly suppress the densities of excited electrons and holes,

it may induce tunneling rates to and from the reservoir which are still significantly smaller than the "bare" rate for scattering from phonons.

To see how Pauli blocking suppresses the scattering rates in the steady state of the driven system, we focus our attention to regions near the resonance momenta, $\pm k_R$, where the distributions of excited electrons $n_e(k) = \langle f^\dagger_{k+} f_{k+} \rangle$ and holes $n_h(k) = 1 - \langle f^\dagger_{k-} f_{k-} \rangle$ are concentrated. In the regime of low excitation densities studied in this paper, the fermionic distributions $n_e(k)$ and $n_h(k)$ are far from *degenerate* (see Fig 2.4). Since $n_e(k)$ and $n_h(k)$ are highly peaked around the minima and maxima of the Floquet bands, *intraband* scattering from acoustic phonons is suppressed due to reduced phase space for these processes. The *interband* phonon scattering rates are also reduced because of phase space arguments: recall that an electron in the upper Floquet band can only relax to momentum states around $k_R$ in the lower Floquet band. These are the considerations which led us to the square root behavior in Eq. (2.9). In conclusion, for the momentum regions near the resonances we expect a suppression of the scattering rate $\tau^{-1}_{\rm scat}$ compared to its "bare" value, making it comparable to the scattering rate of electrons (or holes) near the band minimum (maximum) in the *non-driven* system, at an effective temperature supporting a comparable excitation density.

In other regions in momentum space, $|k| \gg k_R$ and $|k| \ll k_R$, the steady state has $F_{k+} \approx 1$ and $F_{k-} \approx 0$. The coherences appearing in the pertubative corrections to the steady state must be suppressed in the limit $F_{k+} \to 1$ and $F_{k-} \to 0$, simply by the fact that $\rho(k_0)$ is a positive matrix (i.e., the magnitude of a coherence between two states is limited by the geometric mean of the probabilities for being in those two states). This conclusion also follows from examining the scattering rate in these momentum regions, as we discuss below.

**Numerical evaluation of $\Delta\mathcal{E}\tau_{\rm scat}$**

In order to compare the scattering rates in the steady state to the Floquet gap, we numerically evaluate the scattering rate $\tau^{-1}_{\rm scat}$ (or equivalently, $|R|$) in the steady state of the system for the same parameter regime analyzed in the main text. We denote $R_\alpha(k) \equiv |R_{\alpha\alpha,\alpha\alpha}(k)|$, c.f. Eq. (2.45). Recall that the structure of the matrix $R$ requires that $R_\alpha(k)$ is the sum of the off-diagonal matrix elements of $R$ in the column $\alpha\alpha$. Therefore, it is larger than each one of them separately. The value of $R_\alpha(k)$ is just the inverse lifetime of a test particle which we initialize in a Floquet state $\alpha$ at momentum $k$,

$$\begin{aligned} R_\alpha(k) &= \sum_{k'\alpha'} \left\{ W^{k'\alpha'}_{k\alpha} \left[1 + N(\mathcal{E}_{k\alpha} - \mathcal{E}_{k'\alpha'})\right] + W^{k\alpha}_{k'\alpha'} N(\mathcal{E}_{k'\alpha'} - \mathcal{E}_{k\alpha}) + \mathcal{W}^{\rm rec}_k \delta_{kk'} \delta_{\alpha-} \delta_{\alpha'+} \right\} \left(\bar{F}_{k'\alpha'}\right) \\ &+ \Gamma^0_{k\alpha} \left[1 - D(\mathcal{E}_{k\alpha})\right]. \end{aligned} \tag{2.50}$$

In the above, the first two terms correspond to electron-photon scattering. In the first term, the rates $W^{k'\alpha'}_{k\alpha} = W^{k'\alpha'}_{k\alpha}(0)$, defined in Eq. (2.6), correspond to the energetically allowed phonon *emission*

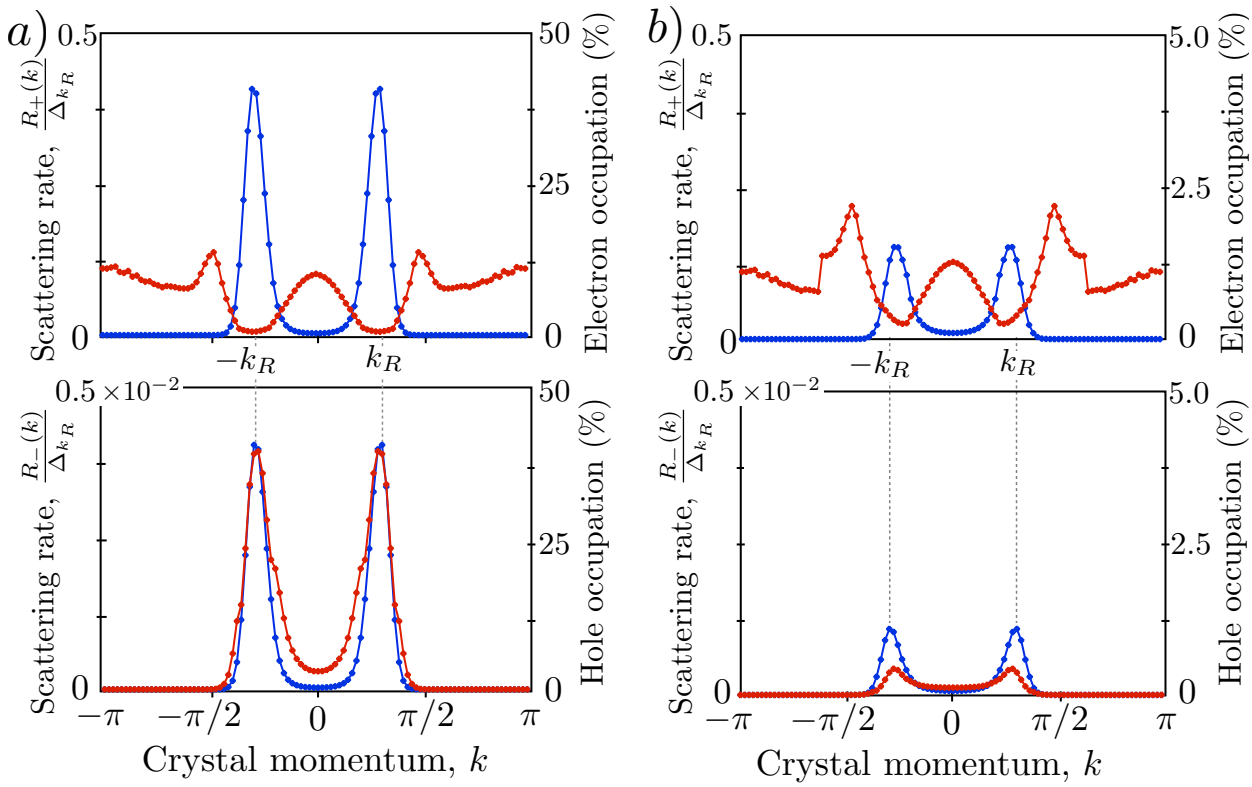


Figure 2.D.1: Scattering rates (red), $R_\alpha(k)$, [see Eq. (2.50)] in the steady state of the system. The top (bottom) plot corresponds to the upper (lower) Floquet band. Also shown (blue) are the distributions $n_e(k)$ an $n_h(k)$ in each Floquet band. In panel (a), we show the case of half-filling, with no reservoir coupling (corresponding to Fig. 2.3 in the main text) while in (b) we take $\log_{10}(\Upsilon) = 3.15$. Other model parameters are the same as for the green (middle) curve in Fig. 2.3. Note the enhanced scale for the rates in the bottom plots, and the enhanced scale for the distributions in panel (b).

processes in the model we studied numerically. Note that $W^{k'\alpha'}_{k\alpha} = 0$ when $\mathcal{E}_k - \mathcal{E}_{k'} < 0$, due to the requirement for a nonzero density of states for the phonons. The second term in Eq. (2.50) corresponds to phonon *absorption*, described by the rates $W^{k\alpha}_{k'\alpha'} = W^{k\alpha}_{k'\alpha'}(0)$ which vanish when $\mathcal{E}_k - \mathcal{E}_{k'} > 0$. Furthermore, in Eq. (2.50), $\mathcal{W}^{\text{rec}}_k$ [see Eq. (2.43)] is the radiative recombination rate out of the state $k, -$ to the state $k, +$ (recall that we model recombination with "vertical" transitions). The results are given in Fig. 2.D.1, which shows $R_\alpha(k)$ normalized to the Floquet gap $\Delta_{k_R}$ in both Floquet bands, for two representative values of the coupling strength to an energy filtered Fermi reservoir. The chemical potential of the reservoir is placed in the middle of the Floquet gap. In the same figures, we plot the numerically obtained distributions of electrons $n_e(k)$ and holes $n_h(k)$.

Let us first examine the situation when the system is not coupled to the Fermi reservoir, Fig. 2.D.1a. Consider the scattering rates in the lower Floquet band (shown in the lower panel). For values of $|k|$ which are significantly larger than $k_R$, the scattering rate vanishes. This is due to Pauli

blocking, which prohibits scattering from phonons. Other scattering mechanisms are absent in this momentum region: for small $\tilde{g}_{\|}$ or for weak driving, the radiative recombination rate out of these states is strongly suppressed. Likewise, since these states are coupled to filled states of the filtered reservoir, the reservoir does not introduce any further scattering out of these states. Therefore, overall we expect negligibly small scattering rate in the lower Floquet band for $|k| \gg k_R$. In the momentum region $|k| < k_R$, recombination is active. For the simulations shown, the "bare" recombination rate (defined without taking into account the occupations $F_{k\alpha}$) is taken to be $\mathcal{W}_k^{\mathrm{rec}} = 3 \times 10^{-5} \Delta_{k_R}$, in line with experimentally accessible parameter regimes. Therefore, a small nonzero $R_\alpha(k)$, set by the recombination rate, can be seen in Fig. 2.D.1a. Finally, for momenta $|k| \approx k_R$, more significant scattering rates can be observed, due to the nonzero density of holes and the possibility for scattering from phonons. However, due to phase space restrictions, the scattering rate is strongly suppressed relative to its "bare" value (see below), and therefore it is significantly smaller than the Floquet gap (note the scale of the vertical axis in the lower panel of Fig. 2.D.1a).

Next, we examine the rates in the upper Floquet band (upper panels of Fig. 2.D.1a). In this band, momentum states with $|k| \gg k_R$ and $|k| \ll k_R$ are mostly unoccupied, and therefore a test particle initialized in these momentum states is expected to exhibit the "bare" phonon scattering rate. This "bare" scattering rate is the predominant contribution to the maximal scattering rate appearing in Fig. 2.D.1. Importantly, near the resonances $k \approx k_R$ the scattering rate is significantly suppressed compared with this bare scattering rate due to reduced phase space for phonon scattering, and therefore is significantly smaller than the Floquet gap.

Finally, we consider the scattering rates when the system is connected to an energy filtered Fermi reservoir. We note that increasing the coupling strength to the Fermi reservoir increases the scattering rates in the upper Floquet band for states with $|k| \lesssim k_R$. This is a result of the significant original conduction band component in these Floquet states, which is coupled to predominantly empty reservoir states (up to thermally induced corrections). The rates in the lower Floquet band are only weakly affected, as this band is coupled to predominantly filled reservoir states.

In summary, near the resonances $k \approx k_R$ the criterion $(\Delta_{k_R} \tau_{\mathrm{scat}})^{-1} \ll 1$ strictly holds. Away from the resonances, $(\Delta_{k_R} \tau_{\mathrm{scat}})^{-1} < 1$. As we discussed above, the positivity of the density matrix $\rho(k)$ implies a strong suppression of any corrections in $(\Delta_{k_R} \tau_{\mathrm{scat}})^{-1}$. Indeed, when pertubatively computing the corrections to the steady state, the bare rates appearing for $|k| \gg k_R$ and $|k| \ll k_R$ in the upper Floquet band have negligible effects since the occupations in the upper Floquet band at these momenta are negligible (as indicated Fig. 2.D.1).

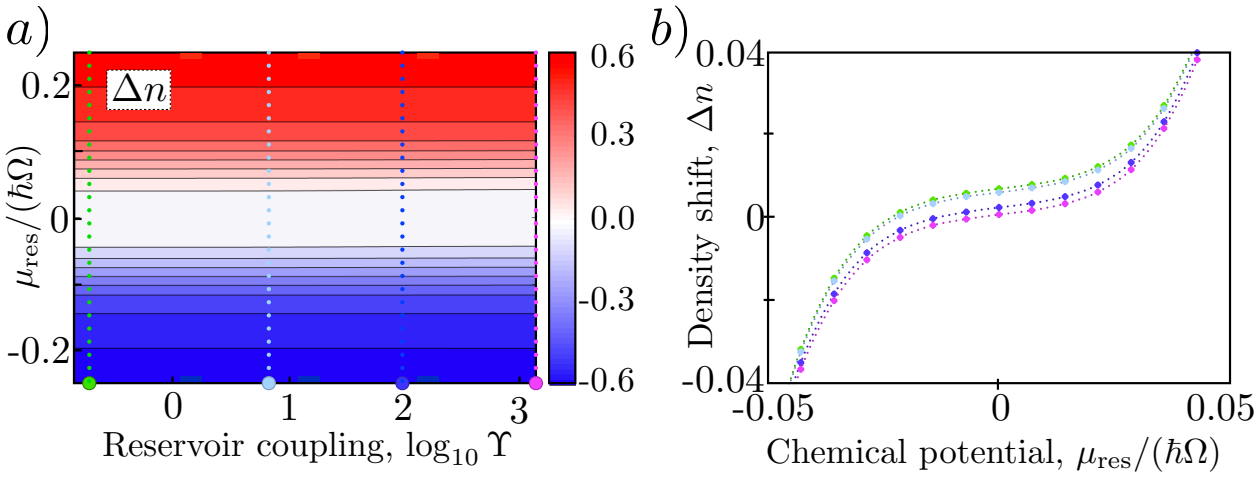


Figure 2.E.1: The offset density $\Delta n$. Panel (a) shows $\Delta n$ as a function of the reservoir chemical potential $\mu_{\rm res}$, and the coupling of the Fermi reservoir $\log_{10}\Upsilon$. Incompressible behavior can be seen when $\mu_{\rm res} \approx 0$. (b) Vertical cuts of panel (a), showing $\Delta n$ as a function of $\mu_{\rm res}$ for several coupling strengths to the Fermi reservoir, with values indicated by the dashed lines in panel (a). The small slope can be attributed to activated behavior due to the finite temperature of the reservoir.

## 2.E Particle-hole asymmetry due to an energy filtered lead

In Sec. 2.4, we studied the situation where the system is coupled to an energy filtered Fermi reservoir with its chemical potential $\mu_{\rm res}$ placed in the middle of the Floquet gap. Here we generically find a nonzero difference between the densities of excited electrons and holes, $\Delta n = n_e - n_h$, despite the symmetry of the Floquet band structure. This highlights one of the interesting features of driven systems, where steady state level occupations depend *both* on the state of the bath, as well as on the detailed form of the system-bath coupling.

To see how a nonzero $\Delta n$ arises, we first note that in order to have $\mu_{\rm res}$ in the middle of the Floquet gap, we aligned it with the resonant energy $\frac{1}{2}\hbar\Omega$ in the conduction band. This placement manifestly breaks the particle hole symmetry of the system. Consider how the Floquet states $|\psi_{k\alpha}(t)\rangle$ are coupled to the reservoir, as depicted in Fig. 2.2. Because the reservoir is energy filtered, within our convention for defining the quasi-energy zone the available reservoir states only couple to the $|\phi^0_{\pm}\rangle$ harmonics of the Floquet states, i.e., only the rates with $n = 0$ in Eq. (2.10) are nonzero. Consider the situation now for weak driving or small $\tilde{g}_{\parallel}$. The $n = 0$ harmonics are then predominantly formed from conduction band components, $|\phi^0_{k\pm}\rangle \approx |c, k\rangle$. Therefore, in the lower Floquet band, only states with momenta $-k_R \lesssim k \lesssim k_R$ have an appreciable $|\phi^0_{k-}\rangle$ component, and therefore only those are coupled to the reservoir. The situation in the upper Floquet band is reversed: only states with $|k| \gtrsim k_R$ have an appreciable $|\phi^0_{k+}\rangle$ component, and are therefore coupled to the reservoir.

From the above considerations, we see that the rates $\Gamma^0_{k+}$ and $\Gamma^0_{k-}$ are not equal in the regions around the resonance momenta $k_R$. As a consequence, the following rates are not equal: (1) the rate for

excited electrons in the distribution $n_e(k)$ to tunnel to the reservoir, and (2) the rate for electrons in the reservoir to tunnel into empty states of the distribution $n_h(k)$. The difference between these rates leads to the non-zero value of $\Delta n$.

To conclude this section, we examine how $\Delta n$ behaves as $\mu_{\text{res}}$ is shifted away from the middle of the Floquet gap. In Sec. 2.4 we discussed an incompressible behavior of the system. Specifically, Fig. 2.5c showed that $\bar{n} = n_e + n_h$, which characterizes the number of "free carriers," is unchanged by small shifts of $\mu_{\text{res}}$ around the middle of the Floquet gap. Here, we complement this result by plotting the behavior for $\Delta n$ in Fig. 2.E.1. The small slope of $\Delta n(\mu_{\text{res}})$ can be attributed to an activated behavior due to the finite temperature of the reservoir. Note that $|\Delta n|$ decreases as the coupling to the fermionic reservoir is increased. This is expected as $|\Delta n| < |\bar{n}|$.

## References


[1] . A further study including dissipation appeared online after this work was submitted, see Ref. [36].

[2] . While there is no notion of a ground state for the driven system, we use the term "excitation" over the ideal steady state to make connection to the analogous states of equilibrium systems.

[3] . If this criterion is not met, photon assisted tunneling rates will not be strictly suppressed, but rather will be controlled by the amplitude at which the filter is driven.

[4] . When the reservoir is at finite temperature activated behavior can be expected as thermal excitations in the lead overlap with Floquet bands of the system.

[5] . When we discuss observables such as the current in the steady state, we refer to their average values over a cycle. In order to compute these, one has to recall the explicit time dependence of the Floquet states as well as that of the observable itself, see, e.g., Refs. [16, 17].

[6] . For systems larger than the photon wavelength, non "vertical" recombination rates $W^{k'+}_{k-}$ may be non zero. Here we use a single rate $W^{k+}_{k-}$ to account for the combined contribution of all processes, as $\sum_{k'} W^{k'+}_{k-}$ is expected to be independent of system size (see Appendix 2.B).

[7] . In higher dimensions, the resonance points generically become curves (2D) or surfaces (3D).

[8] . We assume that the photon density of states at energies on the order of the Floquet gap $\Delta_{k_R}$ is negligible, and only consider emission of photons with energies $\hbar\omega \gtrsim E_{\text{gap}}$.

[9] . Note that $\overline{\mathcal{W}}^{\text{rec}}$ is size-independent (see Appendix 2.B), and therefore the density $n_{\text{steady}}$ is also size-independent.

[10] . Taking into account global particle number conservation, states with different occupation numbers at momentum $k_0$ must be associated with different particle number states in the bath. Therefore the off-diagonal terms vanish under the partial trace.

[11] . The condition $E_k < 2\hbar\Omega$ ensures that the two photon resonance condition is never satisfied for a two-band system.

[12] . In practice, the density of state is taken to be nonzero only in a window of width $11\Omega$ placed symmetrically around $E = 0$.

[13] D. Abanin, W. De Roeck, and F. Huveneers. A theory of many-body localization in periodically driven systems. *arXiv:1412.2752*, 2014.

[14] B. Andrei Bernevig, Taylor L. Hughes, and Shou-Cheng Zhang. Quantum spin hall effect and topological phase transition in hgte quantum wells. *Science*, 314(5806):1757–1761, 2006.

[15] Thomas Bilitewski and Nigel R. Cooper. Scattering theory for floquet-bloch states. *arXiv:1410.5364*, 2014.

[16] Marin Bukov and Anatoli Polkovnikov. Stroboscopic versus nonstroboscopic dynamics in the floquet realization of the harper-hofstadter hamiltonian. *Phys. Rev. A*, 90:043613, 2014.

[17] Marin Bukov, Luca D'Alessio, and Anatoli Polkovnikov. Universal high-frequency behavior of periodically driven systems: from dynamical stabilization to floquet engineering. *arXiv:1407.4803*, 2014.

[18] Lawrence W. Cheuk, Ariel T. Sommer, Zoran Hadzibabic, Tarik Yefsah, Waseem S. Bakr, and Martin W. Zwierlein. Spin-injection spectroscopy of a spin-orbit coupled fermi gas. *Phys. Rev. Lett.*, 109:095302, 2012.

[19] Jan P. Dahlhaus, Benjamin M. Fregoso, and Joel E. Moore. Magnetization signatures of light-induced quantum hall edge states. *Phys. Rev. Lett.*, 114:246802, 2015.

[20] Luca D'Alessio and Marcos Rigol. Long-time behavior of isolated periodically driven interacting lattice systems. *Phys. Rev. X*, 4:041048, 2014.

[21] Hossein Dehghani, Takashi Oka, and Aditi Mitra. Dissipative floquet topological systems. *Phys. Rev. B*, 90:195429, 2014.

[22] Hossein Dehghani, Takashi Oka, and Aditi Mitra. Out of equilibrium electrons and the hall conductance of a floquet topological insulator. *arXiv:1412.8469*, 2014.

[23] Pierre Delplace, Álvaro Gómez-León, and Gloria Platero. Merging of dirac points and floquet topological transitions in ac-driven graphene. *Phys. Rev. B*, 88:245422, Dec 2013. doi: 10.1103/PhysRevB.88.245422.

[24] T. Dittrich, P. Hänggi, G.-L. Ingold, B. Kramer, G. Schön, and W. Zwerger. *Quantum Transport and Dissipation*. Wiley-WCH, 1998. ISBN 978-3527292615.

[25] L.E.F. Foa Torres, P.M. Perez-Piskunow, C.A. Balseiro, and Gonzalo Usaj. Multiterminal conductance of a floquet topological insulator. *Phys. Rev. Lett.*, 113:266801, 2014.

[26] V. M. Galitskii, S. P. Goreslavskii, and V. F. Elesin. Electric and magnetic properties of a semiconductor in the field ofa strong electromagnetic wave. *Sov. Phys. JETP*, 30:117, 1970.

[27] N. Goldman and J. Dalibard. Periodically driven quantum systems: Effective hamiltonians and engineered gauge fields. *Phys. Rev. X*, 4:031027, Aug 2014. doi: 10.1103/PhysRevX.4.031027.

[28] Ch. Grenier, A. Georges, and C. Kollath. Peltier cooling of fermionic quantum gases. *Phys. Rev. Lett.*, 113:200601, Nov 2014. doi: 10.1103/PhysRevLett.113.200601.

[29] Adolfo G. Grushin, Álvaro Gómez-León, and Titus Neupert. Floquet fractional chern insulators. *Phys. Rev. Lett.*, 112:156801, Apr 2014. doi: 10.1103/PhysRevLett.112.156801.

[30] Zhenghao Gu, H. A. Fertig, Daniel P. Arovas, and Assa Auerbach. Floquet spectrum and transport through an irradiated graphene ribbon. *Phys. Rev. Lett.*, 107:216601, Nov 2011. doi: 10.1103/PhysRevLett.107.216601.

[31] M. Z. Hasan and C. L. Kane. *Colloquium* : Topological insulators. *Rev. Mod. Phys.*, 82: 3045–3067, 2010.

[32] Daniel W. Hone, Roland Ketzmerick, and Walter Kohn. Statistical mechanics of floquet systems: The pervasive problem of near degeneracies. *Phys. Rev. E*, 79:051129, 2009.

[33] Daniel W. Hone, Roland Ketzmerick, and Walter Kohn. Statistical mechanics of floquet systems: The pervasive problem of near degeneracies. *Phys. Rev. E*, 79:051129, May 2009.

[34] Thomas Iadecola and Claudio Chamon. Grand canonical treatment of open floquet systems. *arXiv:1412.5599*, 2014.

[35] Thomas Iadecola, David Campbell, Claudio Chamon, Chang-Yu Hou, Roman Jackiw, So-Young Pi, and Silvia Viola Kusminskiy. Materials design from nonequilibrium steady states: Driven graphene as a tunable semiconductor with topological properties. *Phys. Rev. Lett.*, 110:176603, 2013.

[36] Thomas Iadecola, Titus Neupert, and Claudio Chamon. Occupation of topological floquet bands in open systems. *arXiv:1502.05047*, 2015.

[37] Liang Jiang, Takuya Kitagawa, Jason Alicea, A. R. Akhmerov, David Pekker, Gil Refael, J. Ignacio Cirac, Eugene Demler, Mikhail D. Lukin, and Peter Zoller. Majorana fermions in equilibrium and in driven cold-atom quantum wires. *Phys. Rev. Lett.*, 106:220402, Jun 2011. doi: 10.1103/PhysRevLett.106.220402.

[38] K. Jiménez-García, L. J. LeBlanc, R. A. Williams, M. C. Beeler, C. Qu, M. Gong, C. Zhang, and I. B. Spielman. Tunable spin-orbit coupling via strong driving in ultracold atom systems. *arXiv:1410.5364*, 2014.

[39] Gregor Jotzu, Michael Messer, Rémi Desbuquois, Martin Lebrat, Thomas Uehlinger, Daniel Greif, and Tilman Esslinger. Experimental realization of the topological haldane model with ultracold fermions. *Nature*, 515:237–240, Nov 2014. doi: 10.1038/nature13915.

[40] Roland Ketzmerick and Waltraut Wustmann. Statistical mechanics of floquet systems with regular and chaotic states. *Phys. Rev. E*, 82:021114, 2010.

[41] Mackillo Kira and Stephan W. Koch. *Semiconductor Quantum Optics*. Cambridge University Press, 2012. ISBN 978-0521875097.

[42] Takuya Kitagawa, Erez Berg, Mark Rudner, and Eugene Demler. Topological characterization of periodically driven quantum systems. *Phys. Rev. B*, 82:235114, 2010.

[43] Takuya Kitagawa, Takashi Oka, Arne Brataas, Liang Fu, and Eugene Demler. Transport properties of nonequilibrium systems under the application of light: Photoinduced quantum hall insulators without landau levels. *Phys. Rev. B*, 84:235108, Dec 2011. doi: 10.1103/PhysRevB.84.235108.

[44] Takuya Kitagawa, Matthew A. Broome, Alessandro Fedrizzi, Mark S. Rudner, Erez Berg, Ivan Kassal, Alán Aspuru-Guzik, Eugene Demler, and Andrew G. White. Energy-filtered cold electron transport at room temperature. *Nat. Comm.*, 3(882), Jun 2012. doi: 10.1038/ncomms1872.

[45] Sigmund Kohler, Jörg Lehmann, and Peter Hänggi. Driven quantum transport on the nanoscale. *Phys. Rep.*, 406:379–443, Feb 2005. doi: 10.1016/j.physrep.2004.11.002.

[46] Walter Kohn. Periodic thermodynamics. *Journal of Statistical Physics*, 103:417–423, 2001. doi: 10.1023/A:1010327828445.

[47] Arijit Kundu and Babak Seradjeh. Transport signatures of floquet majorana fermions in driven topological superconductors. *Phys. Rev. Lett.*, 111:136402, 2013.

[48] Arijit Kundu, H.A. Fertig, and Babak Seradjeh. Effective theory of floquet topological transitions. *Phys. Rev. Lett.*, 113:236803, 2014.

[49] A. Lazarides, A. Das, and R. Moessner. *Phys. Rev. Lett*, 112:150401, 2014.

[50] N. H. Lindner, G. Refael, and V. Galitski. Floquet topological insulator in semiconductor quantum wells. *Nat. Phys.*, 7:490–495, Mar 2011. doi: 10.1038/nphys1926.

[51] Netanel H. Lindner, Doron L. Bergman, Gil Refael, and Victor Galitski. Topological floquet spectrum in three dimensions via a two-photon resonance. *Phys. Rev. B*, 87:235131, Jun 2013. doi: 10.1103/PhysRevB.87.235131.

[52] Dong E. Liu. Thermalization mechanism for time-periodic finite isolated interacting quantum systems. *arXiv:1410.2962*, 2014.

[53] N. López, L. A. Reichertz, K. M. Yu, K. Campman, and W. Walukiewicz. Engineering the electronic band structure for multiband solar cells. *Phys. Rev. Lett.*, 106:028701, Jan 2011. doi: 10.1103/PhysRevLett.106.028701.

[54] Antonio Luque, Antonio Marti, and Colin Stanley. Understanding intermediate-band solar cells. *Nat. Photon.*, 6:146–152, Feb 2012. doi: 10.1038/nphoton.2012.1.

[55] Takashi Oka and Hideo Aoki. Photovoltaic hall effect in graphene. *Phys. Rev. B*, 79:081406, Feb 2009. doi: 10.1103/PhysRevB.79.081406.

[56] P. M. Perez-Piskunow, Gonzalo Usaj, C. A. Balseiro, and L. E. F. Foa Torres. Floquet chiral edge states in graphene. *Phys. Rev. B*, 89:121401, 2014.

[57] Pedro Ponte, Anushya Chandran, Z. Papić, and Dmitry A. Abanin. Periodically driven ergodic and many-body localized quantum systems. *Annals of Physics*, 353:196–204, Nov 2014. doi: 10.1016/j.aop.2014.11.008.

[58] M. C. Rechtsman, J. M. Zeuner, Y. Plotnik, Y. Lumer, D. Podolsky, F. Dreisow, S. Nolte, M. Segev, and A. Szameit. Photonic floquet topological insulators. *Nature*, 496:196–200, Apr 2013. doi: 10.1038/nature12066.

[59] Mark S. Rudner, Netanel H. Lindner, Erez Berg, and Michael Levin. Anomalous edge states and the bulk-edge correspondence for periodically driven two-dimensional systems. *Phys. Rev. X*, 3:031005, Jul 2013. doi: 10.1103/PhysRevX.3.031005.

[60] Hideo Sambe. Steady states and quasienergies of a quantum-mechanical system in an oscillating field. *Phys. Rev. A*, 7:2203–2213, Jun 1973. doi: 10.1103/PhysRevA.7.2203.

[61] K. I. Seetharam, C.-E. Bardyn, N. H. Lindner, M. S. Rudner, and G. Refael. *to appear*, 2015.

[62] J. Shah. *Ultrafast Spectroscopy and Semiconductors and Semiconductor Nanostructures*. Springer, 1999. ISBN 978-3540642268.

[63] Tatsuhiko Shirai, Takashi Mori, and Seiji Miyashita. On the condition for emergence of the floquet-gibbs state in periodically driven open systems. *arXiv:1410.0464*, 2014.

[64] Jon H. Shirley. Solution of the schrödinger equation with a hamiltonian periodic in time. *Phys. Rev.*, 138:B979–B987, May 1965. doi: 10.1103/PhysRev.138.B979.

[65] Gonzalo Usaj, P. M. Perez-Piskunow, L. E. F. Foa Torres, and C. A. Balseiro. Irradiated graphene as a tunable floquet topological insulator. *Phys. Rev. B*, 90:115423, 2014.

[66] Q. T Vu, H. Haug, O. D Mücke, T. Tritschler, M. Wegener, G. Khitrova, and H. M. Gibbs. Light-induced gaps in semiconductor band-to-band transitions. *Physical Review Letters*, 92: 217403, 2004.

[67] Y. H. Wang, H. Steinberg, P. Jarillo-Herrero, and N. Gedik. Observation of floquet-bloch states on the surface of a topological insulator. *Science*, 342(6157):453–457, 2013. doi: 10.1126/science.1239834.

[68] Robert S. Whitney. Most efficient quantum thermoelectric at finite power output. *Phys. Rev. Lett.*, 112:130601, Apr 2014. doi: 10.1103/PhysRevLett.112.130601.

[69] Wang Yao, A. H. MacDonald, and Qian Niu. Optical control of topological quantum transport in semiconductors. *Phys. Rev. Lett.*, 99:047401, 2007.

[70] K. M. Yu, W. Walukiewicz, J. Wu, W. Shan, J. W. Beeman, M. A. Scarpulla, O. D. Dubon, and P. Becla. Diluted ii-vi oxide semiconductors with multiple band gaps. *Phys. Rev. Lett.*, 91:246403, Dec 2003. doi: 10.1103/PhysRevLett.91.246403.

[71] Peter Yu and Manuel Cardona. *Fundamentals of Semiconductors: Physics and Materials Properties*. Springer, 2010. ISBN 978-3642007095.

*Chapter 3*

# WEAKLY-INTERACTING OPEN FLOQUET SYSTEMS

Karthik I. Seetharam, Charles-Edouard Bardyn, Netanel H. Lindner, Mark S. Rudner, and Gil Refael. Floquet-ology: Steady states of interacting floquet insulators. *Arxiv (to appear)*, 2018. K.I.S. participated in the conception of the project, performed most calculations, simulations, and analysis, and participated in the writing of the manuscript.

## 3.1 Introduction

Floquet engineering has emerged as an exciting tool for controlling the properties of quantum systems. A periodic drive, it was shown, could give rise to topological phases in graphene [20, 25] as well as in trivial spin-orbit coupled semiconductors [23]. Subsequent work revealed a wealth of new phases without analogues in equilibrium[2, 3, 9, 10, 16, 17, 19, 26–30, 36–39]; these phases exhibit exotic features such as time-translation symmetry breaking[3, 10, 38, 39], topologically-protected chiral edge states in the presence of a completely localized bulk [36], or fractionalized edges carrying a quantized flow of entropy [26].

In many-body systems, Floquet engineering faces an important challenge due to electron-electron interactions. Interactions provide an efficient conduit for the system to absorb energy from the drive. In the absence of a bath, such energy absorption drives the system towards a maximum-entropy, infinite-temperature state [1, 4, 13, 21, 22]. Therefore, in order to assess the viability of Floquet engineering in electronic systems, it is crucial to determine the conditions under which a heat bath can stabilize a low-entropy steady state with certain key properties of interest. In particular, in the context of trying to realize Floquet topological insulators, it is important that the steady state is well described in terms of electronic populations in the single-particle Floquet states. Moreover, in order to observe the topological features of the system, we seek a population distribution corresponding to an insulator-like steady state.

Recently, several works have considered the steady states of non-interacting Floquet topological insulators in contact with external baths[5–8, 14, 15, 24, 32–34] These works showed that, under appropriate conditions on the driving and the system-bath coupling (such as phonon bandwidth[15, 32], lead density of states[14, 32], etc.), the topological features of the Floquet system may be observed through both the bulk Hall conductivity[8] and edge state transport[11]. However, in the presence of interactions, it remains an open question whether the bath engineering strategies outlined in the works above are sufficient to control heating and stabilize the desired steady states.

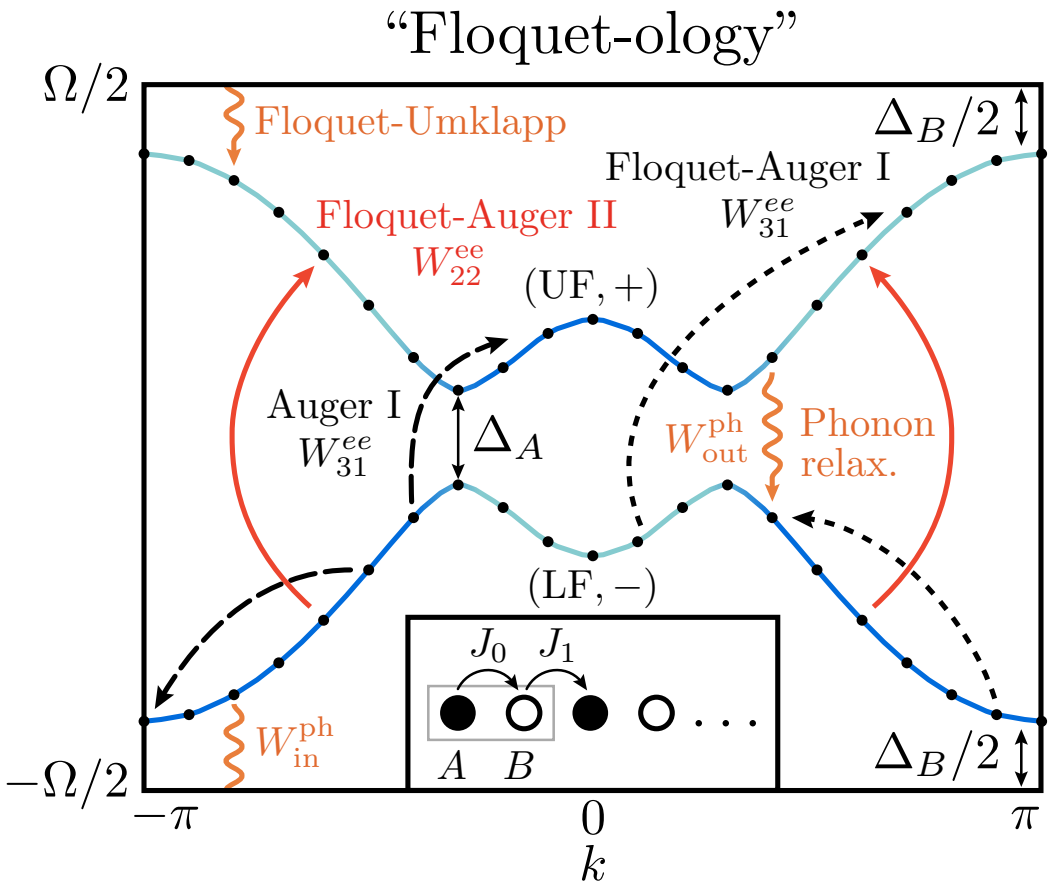


Figure 3.1: Quasienergy band structure and interband scattering processes. Electron-electron interactions yield three different types of interband processes: Auger, and Floquet-Auger (FA) of types I and II (see text) depicted by dashed, dotted, and solid lines, respectively. In the Floquet-Auger processes, the sums of quasienergies of the electrons in the initial and final states differ by an integer multiple of the driving frequency, $\hbar\Omega$. Interband scattering resulting from electron-phonon interactions yields two important processes: (i) relaxation from the upper to the lower band via phonon emission, and (ii) excitation from the lower to the upper band. This process can occur even at zero temperature, as a Floquet-Umklapp (FU) process, which involves phonon emission and absorption of $\hbar\Omega$ from the driving field.

In this work we consider the following question: can an insulatorlike filling of quasienergy bands be achieved in an interacting electronic system in which a periodic drive is used to induce a topological transition via a band inversion? In this situation, the desired Floquet topological insulator (FTI) steady state is strikingly different from the ground state of the nondriven system: the FTI features a significant population inversion when viewed in terms of the valence and conduction bands of the host material. Thus, in such a resonantly driven system, stabilizing the FTI steady state brings additional challenges compared to other protocols (e.g., based on high frequency driving).

To answer this question, here we consider a one-dimensional (1D) interacting, open, periodically-driven electronic system. We derive the Floquet-Boltzmann equation (FBE) for the electronic populations of the quasienergy states of the open interacting system [13, 32]. We numerically solve these equations for a system coupled to a bosonic bath of acoustic phonons, and show that, despite the interactions, the phononic bath still provides effective means for cooling the interacting driven system, even for experimentally realistic parameters. We develop a simple effective model for the Floquet band densities that captures the essence of all the Floquet scattering channels and that shows good numerical agreement with the exact FBE results for a large regime in parameter space.

### 3.2 Microscopic model

To investigate dynamics of a periodically driven 1D electronic system, we employ a tight-binding model for spinless electrons with time-dependent hopping parameters and nearest-neighbor electron-electron interactions. We consider a two-band model, with each unit cell of the lattice containing two sites (labeled $A$ and $B$, see inset of Fig. 3.1). The system's evolution is governed by the Hamiltonian $H = H_0(t) + H_{\text{int}}$, where the single-particle Hamiltonian

$$H_0(t) = \sum_x \left( [J_0 + \delta J(t)] c^\dagger_{x,A} c_{x,B} + J_1 c^\dagger_{x,B} c_{x+1,A} \right) + \text{h.c.} \tag{3.1}$$

defines the system's band structure and driving, and

$$H_{\text{int}} = V_0 \sum_x \left( n_{x,A} n_{x,B} + n_{x,A} n_{x-1,B} \right) \tag{3.2}$$

describes the nearest-neighbor interactions. Here, $c^\dagger_{x,A}$ and $c_{x,A}$ (likewise $c^\dagger_{x,B}$ and $c_{x,B}$) denote the spinless electron creation and annihilation operators on site $x$ of sublattice $A$ ($B$); the corresponding on-site densities are given by $n_{x,A} = c^\dagger_{x,A} c_{x,A}$ and $n_{x,B} = c^\dagger_{x,B} c_{x,B}$, respectively. The intracell and intercell hopping parameters $J_0$ and $J_1$ as well as the interaction strength $V_0$ are taken to be positive and constant in time; throughout this work we take a modulation of the form $\delta J(t) = S \cos \Omega t$, where $\Omega$ is the drive (angular) frequency and $S$ is the driving strength.

The single-particle Hamiltonian $H_0(t)$ in Eq. (3.1) is translationally invariant, and is therefore diagonal in crystal momentum. We introduce an index $\nu$ to label the bands of the system

in the absence of driving, i.e., for $S = 0$. In this basis, Eq. (3.1) takes the form $H_0(t) = \sum_{k\nu\nu'} c^\dagger_{k\nu} \left[E_k \sigma^z_{\nu\nu'} + \cos(\Omega t)(\boldsymbol{S}_k \cdot \boldsymbol{\sigma})_{\nu\nu'}\right] c_{k\nu'}$, where $E_k = |J_k|$ and $S_k = S(0, -\sin\theta_k, \cos\theta_k)$, with $J_k = J_0 + e^{ika} J_1 \equiv |J_k| e^{i\theta_k}$. Here, $\boldsymbol{\sigma} = (\sigma_x, \sigma_y, \sigma_z)$ is the vector of Pauli matrices, and $a$ is the lattice constant of the system. We take the driving frequency $\Omega$ to be larger than the band gap of the nondriven system, $E_{\text{gap}} = |J_0 - J_1|$, such that resonances are induced at crystal momenta $k_R$ satisfying $2E_{k_R} = \Omega$.

In the presence of driving, the system is conveniently described in terms of its Floquet-Bloch band structure (see Fig. 3.1). We apply Floquet's theorem to find a complete basis of states $|\psi_{k\alpha}(t)\rangle = e^{-i\mathcal{E}_{k\alpha}t} |\phi_{k\alpha}(t)\rangle$ that satisfy Schrödinger's equation with Hamiltonian $H_0(t)$, where $|\phi_{k\alpha}(t+T)\rangle = |\phi_{k\alpha}(t)\rangle$ is periodic with $T = 2\pi/\Omega$ and $\alpha = \pm$ labels the Floquet-Bloch bands with quasienergies $\mathcal{E}_{k\alpha}$. Importantly, the $T$-periodic function $|\phi_{k\alpha}(t)\rangle$ can be expressed in terms of a discrete set of Fourier harmonics $\{|\phi^n_{k\alpha}\rangle\}$, as $|\phi_{k\alpha}(t)\rangle = \sum_n e^{-in\Omega t} |\phi^n_{k\alpha}\rangle$. The structure of these harmonic coefficients plays an important role in determining the rates of the various scattering processes that will be considered below.

Equations (3.1) and (3.2) prescribe the dynamics of the electronic system in isolation. In the presence of a periodic drive, the system's coupling to the enviroment plays a crucial role in determining its steady state. We therefore consider the electronic system's coupling to a bath of acoustic phonons. We take the system to be embedded in a three-dimensional (3D) medium which supports phonon modes, playing the role of the substrate supporting the 1D quantum wire. The phonon bath and electron-phonon coupling Hamiltonians are given by

$$H_{\text{b}} = \sum_{\boldsymbol{q}} \omega_{\boldsymbol{q}} b^\dagger_{\boldsymbol{q}} b_{\boldsymbol{q}}, \tag{3.3}$$

$$H_{\text{el-ph}} = \sum_{\boldsymbol{q}} \sum_{\substack{k\nu \\ k'\nu'}} G^{\nu'k'}_{\nu k}(\boldsymbol{q})\, c^\dagger_{k'\nu'} c_{k\nu} (b_{\boldsymbol{q}} + b^\dagger_{-\boldsymbol{q}}). \tag{3.4}$$

Here, $\boldsymbol{q} = (q, \boldsymbol{q}_\perp)$ is the phonon momentum (with components $q$ parallel to the 1D electronic system, and $\boldsymbol{q}_\perp$ in the transverse direction), and $\omega_{\boldsymbol{q}} = C|\boldsymbol{q}|$ defines the phonon spectrum, taken to be linear and isotropic with speed of sound $C$, up to a frequency cutoff $\Omega_D$. The electron-phonon interaction amplitude $G^{\nu'k'}_{\nu k}(\boldsymbol{q})$ corresponds to an electronic transition $\nu k \to \nu' k'$ via absorption of a phonon with momentum $\boldsymbol{q}$ (or emission with $-\boldsymbol{q}$); this amplitude is proportional to $\sum_n \delta(k' - k - q + 2\pi l/a)$, with $l$ ranging over all integers, ensuring crystal-momentum conservation along the direction of the electronic system. For simplicity, in this work we choose the matrix elements multiplying the momentum delta function in the phonon scattering amplitude to be $G_0 \sigma^3_{\nu\nu'}$; i.e., the electron-phonon coupling conserves the band index of the non-driven system. The qualitative features of our results

do not depend on the exact form of the electron-phonon coupling. The Debye cutoff frequency $\Omega_D$ is an important parameter of the model, which we use to control the types of possible scattering processes (see below).

We seek the steady states of the interacting driven system coupled to the bosonic (phonon) bath described by Eqs. (3.3) and (3.4). We define the population of the single-particle Floquet mode $k\alpha$ as $F_{k\alpha}(t) = \langle f^\dagger_{k\alpha}(t) f_{k\alpha}(t)\rangle$, where the operator $f^\dagger_{k\alpha}(t) = \sum_{\nu,n} e^{-i(\mathcal{E}_{k\alpha}+n\Omega)t}\langle k\nu|\phi^n_{k\alpha}\rangle c^\dagger_{k\nu}$ creates an electron in the Floquet state $|\psi_{k\alpha}\rangle$ at time $t$. We focus on the regime where scattering rates in the steady state are small compared with the gaps between Floquet-Bloch bands, translation invariance is maintained, and strong multi-particle correlations (e.g., excitons) are absent. In this regime, the steady state is well represented in terms of the populations $F_{k\alpha}(t)$ of the single-particle Floquet states. We use the Floquet-Boltzmann equation (FBE) [1, 13, 32] to evolve these populations:

$$\dot{F}_{k\alpha} = I^{\rm ph}_{k\alpha}(\{F\}) + I^{\rm ee}_{k\alpha}(\{F\}), \tag{3.5}$$

where $I^{\rm ph}_{k\alpha}$ and $I^{\rm ee}_{k\alpha}$ are the collision integrals that capture the net rates of electron scattering into Floquet mode $k\alpha$ due to electron-phonon and electron-electron interactions, Eqs. (3.4) and (3.2), respectively. Explicit expressions for these collision integrals and the Fermi's golden rule transition rates inside them are given in Appendix 3.A.

*Simple model for population kinetics* – Before examining the numerical solution of the full FBE, we first develop and discuss a simple effective model that captures the basic qualitative features of the steady states of Eq. (3.5). Specifically, we focus on the interplay between electron-electron and electron-phonon scattering in determining the net populations of the two Floquet-Bloch bands,

$$n_\alpha = \frac{1}{N}\sum_k F_{k\alpha}, \tag{3.6}$$

where $\alpha = -, +$ denotes the lower/upper Floquet (LF/UF) bands, respectively (see Fig. 3.1), and $N$ is the number of unit cells in the system. At half filling, which is our focus in this work, the number of excitations in the upper Floquet band is equal to the number of holes in the lower Floquet band; this implies $n_+ = 1 - n_- \equiv n$.

Due to the periodicity of quasienergy, the designation of "upper" and "lower" Floquet bands amounts to a gauge choice. However, the rates of dissipative processes are sensitive to the characters of the Floquet band wave functions (valence-band-like or conduction-band-like), and provide a natural orientation for the bands (see, e.g., Refs. [11, 32]). Our choice follows this natural orientation, picked in anticipation of the results below.

We construct the model by characterizing the rates of all possible inter-Floquet-band transitions facilitated by electron-phonon scattering and electron-electron interactions. The rates of the various

scattering processes depend on incoming and outgoing crystal momentum and band indices, as well as the full distribution of Floquet state populations, $\{F_{k\alpha}\}$, see Eq. (3.5). Therefore, the evolution of the excitation density $n$ generally cannot be written as a function of $n$ alone. As a crude approximation, a closed dynamical equation for $n$ can be obtained by making a "uniform" approximation on the FBE, replacing all $k$-dependent rates by their band-averaged values (see Appendix 3.A). Crucially, this model retains the essential structure of phase-space restrictions on different classes of processes, which we describe in detail below. Comparing to numerical simulations of the full FBE, we will show that the simple model captures and provides insight into the qualitative dependence of the steady-state excitation density on the fundamental parameters of the system.

Consider first the possible electron-phonon scattering processes. Phonon-mediated transitions *out* of the UF band (and into the LF band) require an excited particle in the UF band to scatter into a hole in the LF band. This requirement constrains the phase space for such processes, which thus provides a sink for density in the UF band with rate $W^{\mathrm{ph}}_{\mathrm{out}} n_+(1-n_-) = W^{\mathrm{ph}}_{\mathrm{out}} n^2$. We refer to processes that reduce the density of excitations as "cooling" processes. Similarly, phonon-mediated transitions from the LF band *into* the UF band require a particle in the LF band to scatter into an empty state in the UF band. Such processes provide a source for the excited population, with rate $W^{\mathrm{ph}}_{\mathrm{in}}(1-n_+)n_- = W^{\mathrm{ph}}_{\mathrm{in}}(1-n)^2$. We refer to processes that increase the density of excitations as "heating" processes.

Importantly, the competition between phonon-mediated "heating" and "cooling" processes, captured by the rates $W^{\mathrm{ph}}_{\mathrm{in}}$ and $W^{\mathrm{ph}}_{\mathrm{out}}$, depends on the driving strength and frequency, as well as the bandwidth of the phonon bath, $\Omega_D$. We consider the case where the phonon bandwidth is larger than the resonance-induced Floquet gap centered at quasi-energy $\mathcal{E} = 0$, denoted by $\Delta_A$ in Fig. 3.1. Under this condition, the sink rate $W^{\mathrm{ph}}_{\mathrm{out}}$ in Eq. (3.7) is nonzero; excited particles in the UF band can scatter into available holes in the LF band, while emitting a phonon to conserve quasienergy. In contrast, at zero temperature (and assuming $\Omega_D < E_{\mathrm{gap}}$), scattering processes contributing to the bare rate $W^{\mathrm{ph}}_{\mathrm{in}}$ in the source term are always of "Floquet-Umklapp" type: the scattered electron's quasienergy in the final state differs from its initial value by $\hbar\Omega - \hbar\omega_{\mathbf{q}}$, where $\hbar\omega_{\mathbf{q}}$ is the energy of the emitted phonon. Therefore the rate $W^{\mathrm{ph}}_{\mathrm{in}}$ is suppressed in comparison to $W^{\mathrm{ph}}_{\mathrm{out}}$ by a factor of $(S/\Omega)^4$ (where $S$ is the drive strength, and $\Omega$ is its frequency), see App. 3.A. Thus for weak driving, $(S/\Omega) \ll 1$, heating due to electron-phonon scattering is naturally a weak effect (see Fig. 3.A.1 for more details).

Electron-electron interactions may give rise to two types of "Auger" processes that can change the populations in the two Floquet bands: (I) two particles in the same Floquet band may scatter to a final state which has one particle in each of the Floquet bands, and (II) two particles in the

same Floquet band may simultaneously scatter to the opposite Floquet band. Examples of these processes are depicted in Fig. 3.1 (see also Fig. 3.A.1).

Electron-electron scattering conserves total crystal momentum and quasi-energy. Similar to conservation of crystal momentum, conservation of quasienergy can either be "direct," with the sum of initial and final single particle quasienergies being equal, or "Umklapp"-like, where the sum of single particle quasienergies in the final state differs from its initial value by $\hbar\Omega$. Processes of type (I) can be either direct or Floquet-Umklapp-like; we label such processes "Auger I" and "Floquet-Auger I," respectively. Processes of type (II), which we label "Floquet-Auger II," are necessarily of the Umklapp type. For weak driving, the rates of these Floquet-Umklapp processes are suppressed by a factor $(S/\Omega)^2$ (for specific Floquet-Umklapp process, the suppression can be even stronger).

We now characterize the rates for electron-electron scattering processes, taking into account the phase-space requirements for the corresponding transitions. Processes of type I require two particles in the initial band to scatter into two empty states, one in each band. If the two particles are initially in the LF band, we obtain a source term for the excitation density (a "heating" process) with rate $W_{31}^{\mathrm{ee}} n_-^2(1-n_+)(1-n_-) = W_{31}^{\mathrm{ee}}(1-n)^3 n$. Note that this rate includes the contributions of both Auger-I and Floquet-Auger I processes. If both particles are initially in the UF band, we obtain a sink term for the density of excitations with a rate of $W_{31}^{\mathrm{ee}} n_+^2(1-n_+)(1-n_-) = W_{31}^{\mathrm{ee}} n^3(1-n)$. Due to particle-hole symmetry, the same bare rate $W_{31}^{\mathrm{ee}}$ appears for both the source and sink terms.

Using similar considerations, we find that processes of type II contribute a source term for $n$ with rate $W_{22}^{\mathrm{ee}} n_-^2(1-n_+)^2 = (1-n)^4$, and a sink term with rate $W_{22}^{\mathrm{ee}} n_+^2(1-n_-)^2 = n^4$. In the primary regime of interest the excitation density will be small. Therefore, the *sink terms* arising from electron-electron scattering will be suppressed (relative to the source terms), as they involve higher powers of $n$.

Combining all source and sink terms, the rate of change of the excitation density $n$ is approximately given by

$$\begin{aligned} \dot{n} &= W_{\mathrm{in}}^{\mathrm{ph}}(1-n)^2 - W_{\mathrm{out}}^{\mathrm{ph}} n^2 + W_{31}^{\mathrm{ee}}[n(1-n)^3 - n^3(1-n)] \\ &\quad + W_{22}^{\mathrm{ee}}[(1-n)^4 - n^4]. \end{aligned} \tag{3.7}$$

We obtain the steady-state population of the UF band by solving $\dot{n} = 0$. This condition yields a cubic equation for the steady-state excitation density [1], which is supplemented by the condition $0 \le n \le 1$. In App. 3.B we present a generalization of Eq. (3.7) which incorporates the role of a fermionic reservoir.

[1] While such a relation in principle admits for multistability, we find only a single physical solution in all regimes studied.

Although Eq. (3.7) can be solved exactly using the general solution for the roots of a cubic polynomial, it is instructive to examine the behavior perturbatively around specific limits of interest. In the absence of phonons, $W^{\rm ph}_{\rm in} = W^{\rm ph}_{\rm out} = 0$, interactions drive the system toward a high-entropy state with $n^* = 1/2$. In the more general scenario, the phonon bath can extract entropy and energy from the system, yielding a non-trivial steady state.

A nontrivial steady state with a Floquet-band-insulator-like distribution is obtained when the heating rates due to electron-phonon and electron-electron interactions are small compared with the rate of relaxation by the phonon bath. To characterize this regime, it is useful to define the dimensionless quantities $\kappa_{31} = W^{\rm ee}_{31}/W^{\rm ph}_{\rm out}$, $\kappa_{22} = W^{\rm ee}_{22}/W^{\rm ph}_{\rm out}$ and $\kappa_{\rm ph} = W^{\rm ph}_{\rm in}/W^{\rm ph}_{\rm out}$. As explained above, we expect $\kappa_{\rm ph} \ll 1$. For weak interactions, we may also have $\kappa_{22}, \kappa_{31} \ll 1$. Within this limit, the excitation density in the steady state will be small, $n \ll 1$. To lowest order in $n$, the heating rate in Eq. (3.7) arising from electron-electron scattering is $W^{\rm ee}_{22}$. Therefore, if $\kappa_{22} \gg \kappa_{\rm ph}$, electron-electron scattering provides the main source of heating and we find $n^* \sim \sqrt{\kappa_{22}}$. When electron-phonon scattering dominates the heating rate, $\kappa_{\rm ph} \gg \kappa_{22}$, we expect $n^* \sim \sqrt{\kappa_{\rm ph}}$.

### 3.3 Results

We now discuss numerical results for the solution of the full Floquet Boltzmann equation, Eq. (3.5), and their comparison with the predictions of the simple model described above. In Fig. 3.1 we show the full momentum-resolved steady-state populations in the UF band, for several ratios of the electron-phonon ($G_0$) and electron-electron ($V_0$) coupling strengths [see Eq. (3.2) and text below Eq. (3.4)].

To start from a conceptually simple case, in Fig. 3.1 we take a restricted phonon bandwidth $\Omega_D < \Delta_B$ (see Fig. 3.1), which ensures that phonon-mediated Floquet-Umklapp processes are energetically forbidden. Under this condition, the only source terms for excitation density (i.e., "heating processes") are electron-electron-mediated Floquet-Umklapp processes and thermally-activated phonon absorption. The rates of the latter are suppressed by a factor $e^{-\Delta_A/T_{\rm ph}} \approx 5 \times 10^{-5}$ for $T_{\rm ph} = \Delta_A/10$, as used in the simulations. To a very good approximation, in this regime, $G_0$ controls cooling and $V_0$ directly controls heating.

As a function of the ratio $G_0^2/V_0^2$ we observe a clear transition from a "hot" state with nearly uniform populations, $F_{k\pm} \approx 0.5$ for all $k$, to a "cold" state in which the LF (UF) band is nearly completely filled (empty). The "cold" state hosts a small density of excitations near the band extrema around $\mathcal{E} = 0$. We fit the populations $F_{k\pm}$ using two separate Floquet-Fermi-Dirac distributions, with independent chemical potentials $\mu^*_+$ and $\mu^*_-$ for electrons and holes in the upper and lower Floquet bands, respectively. By particle-hole symmetry, $\mu^*_- = -\mu^*_+$. The fits are shown as solid lines in Fig. 3.1. The effective temperature $T^*$ and chemical potential $\mu^*_+$ extracted from these fits are shown

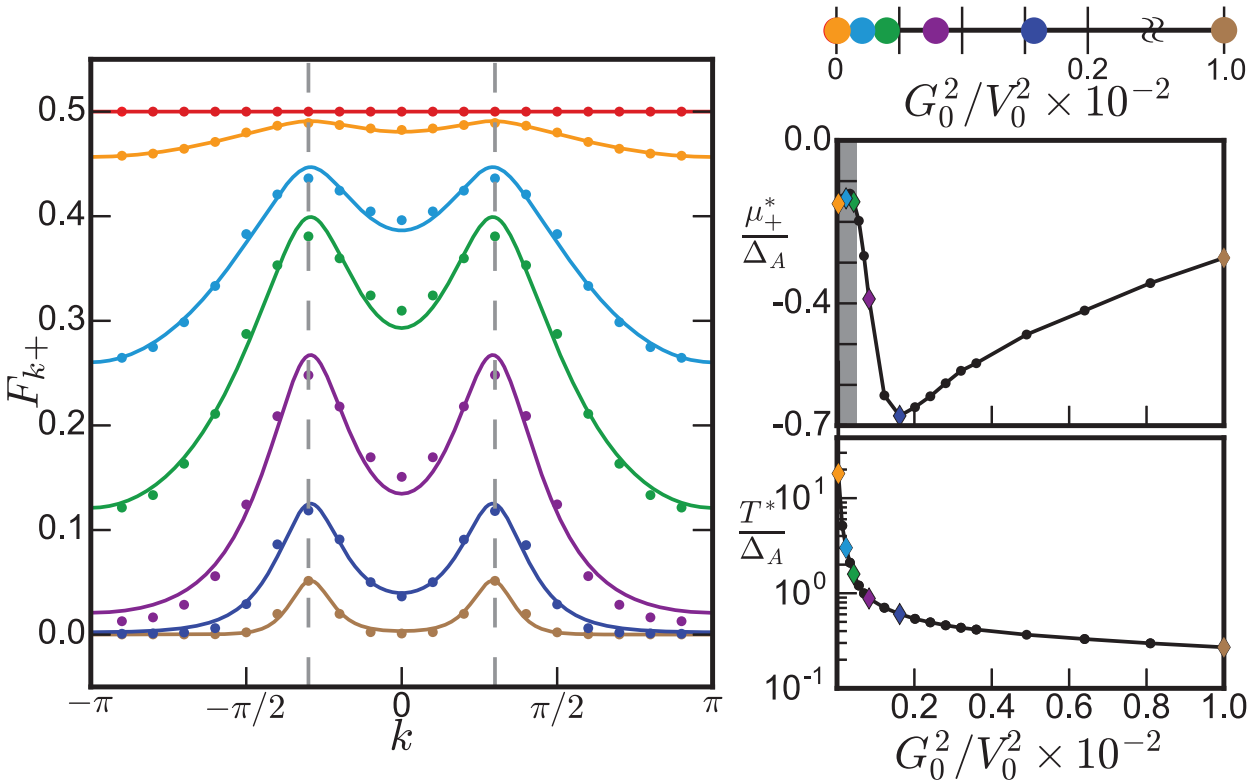


Figure 3.1: Left: Steady-state populations in the UF band, $F_{k+}$, for several values of the effective cooling strength $G_0^2/V_0^2$. Results are obtained from the FBE, Eqs. (3.5) and (3.9), with phonon bandwidth $\Omega_D/\Delta_A = 2.2$ and phonon temperature $T_{\rm ph} = \Delta_A/10$. Dashed lines indicate the crystal momentum values where the UF band minima are located. For low values of $G_0^2/V_0^2$, the steady state is "hot," with nearly uniform occupation $F_{k+} \approx 0.5$ for all $k$. For large values of $G_0^2/V_0^2$, the steady state is "cold", and features a low density of excitations concentrated around the minima of the UF band. Solid lines show fits to a Floquet-Fermi-Dirac distribution with effective chemical potential $\mu_+^*$ (with respect to $\mathcal{E} = 0$), and temperature $T^*$, taken as free parameters. Right: extracted values of $\mu_+^*$ and $T^*$ *vs.* $G_0^2/V_0^2$. When $\mu_+^* \neq 0$, the steady state is described by a "double" Floquet-Fermi-Dirac distribution, with separate chemical potentials for electrons and holes in the UF and LF bands, respectively. The gray shaded region in upper panel denotes a regime where the fits are sensitive only to the value of $T^*$ (and are insensitive to the value of $\mu_+^*$).

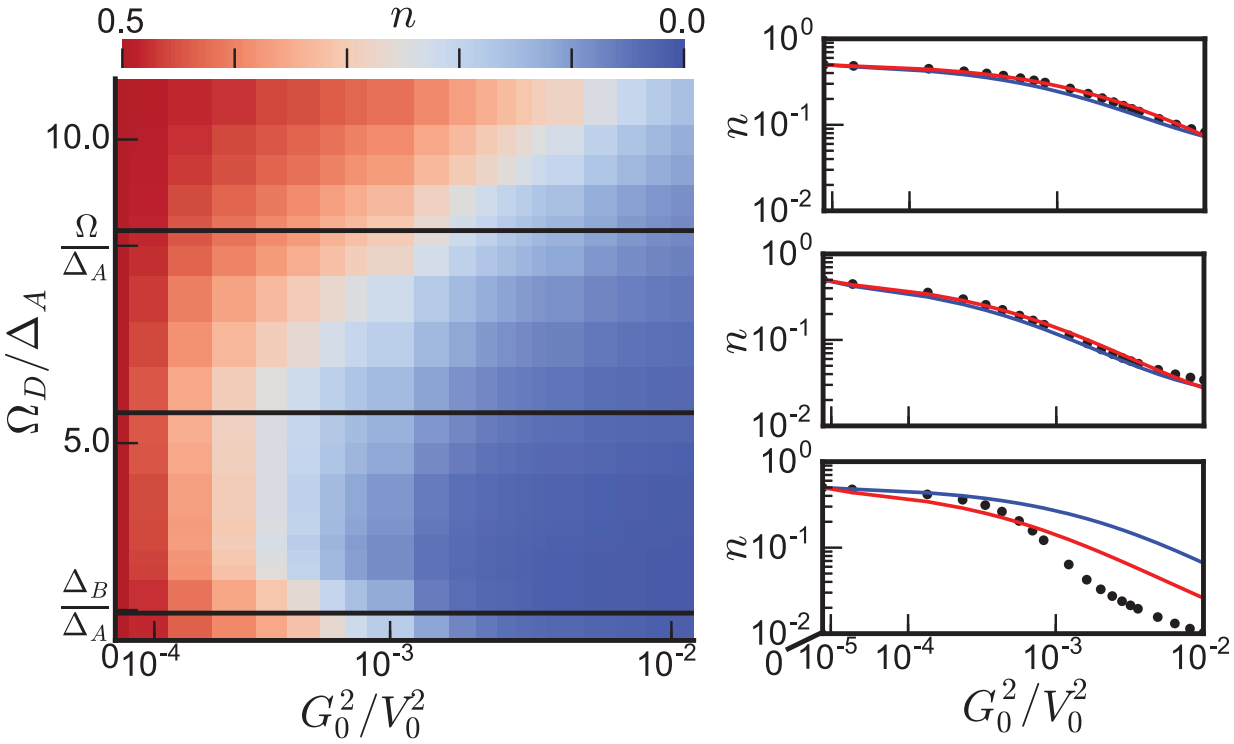


Figure 3.1: Left: Excitation density $n = n_+$, Eq. (3.6), as a function of the (normalized) phonon bandwidth $\Omega_D/\Delta_A$ and $G_0^2/V_0^2$. For large $G_0^2/V_0^2$, the phonon bath effectively cools the system, and the steady-state excitation density is low (blue color). The cutoff $\Omega_D$ controls the phase space for electron-phonon scattering; the cooling effect of the phonon bath is strongest for intermediate values of $\Omega_D$ where many relaxation processes are allowed, and heating due to phonon-mediated Floquet-Umklapp processes is relatively suppressed. Note that $\Delta_B/\Delta_A = 2.25$ and $\Omega/\Delta_A = 8.25$. Right (from top to bottom): Line cuts at $\Omega_D/\Delta_A = 8.5, 5.5, 2.2$. Blue lines show results from the effective model (Eq. 3.7) using rates computed by direct application of the uniform approximation. Red lines indicate the results of the effective model with fitted parameters (see main text). For $\Omega_D/\Delta_A = 8.5, 5.5$, the average rates are quite close to the best fit curves and also give a good approximation to the exact FBE data. For $\Omega_D/\Delta_A = 2.2$, the scattering phase space is highly restricted and the simple model does not provide a good description of the FBE results.

in the upper and lower panels on the right of Fig. 3.1. Note that without phonon-mediated Floquet-Umklapp processes and in the $V_0 = 0$ limit, the "global" Floquet-Gibbs state with populations $F_{k\alpha} = (e^{\mathcal{E}_{k\alpha}/T_{\rm ph}} + 1)^{-1}$, i.e., with $\mu_-^* = \mu_+^* = 0$, is an exact solution to the FBE (see Appendix 3.A and Refs. [12, 24, 32–34]). In particular, in this limit and for $T_{\rm ph} = 0$, the steady-state is an ideal Floquet insulator state with $F_{k-} = 1$ and $F_{k+} = 0$ for all $k$.

Going beyond the restricted scenario of Fig. 3.1, we now examine how the steady state is affected by phonon-mediated Floquet-Umklapp processes when the phonon bandwidth $\Omega_D$ is increased. The excitation density $n$ [Eq. (3.6)] as a function of $\Omega_D$ and $G_0^2/V_0^2$ is shown in Fig. 3.1. Although increasing $G_0$ increases the rates of both phonon-mediated cooling and heating processes, the blue

color on the right side of Fig. 3.1 indicates that increasing $G_0$ (for fixed $V_0$) has the overall effect of decreasing the excitation density. This can be understood by recalling that for $\Omega_D < E_{\text{gap}}$, phonon-mediated Floquet-Umklapp transition rates are suppressed with respect to direct transitions by a factor of $(S/\Omega)^4$.

The excitation density exhibits a non-monotonic dependence on $\Omega_D$, which we interpret as follows: In the regime $\Delta_A < \Omega_D < \Delta_B$, as considered in Fig. 3.1, phonon-mediated interband relaxation (cooling) is possible, but the corresponding FU processes are forbidden. However, for low values of $\Omega_D$ the scattering phase space is restricted and cooling is inefficient. As $\Omega_D$ is increased, the phase space for electron-phonon scattering increases and the bath is able to cool the system more effectively. When $\Omega_D > \Delta_B$, phonon-mediated FU processes are allowed and compete with the cooling effect of the bath. This competition leads to an optimal value $\Omega_D^{\text{opt}} > \Delta_B$ where the excitation density is minimized for a given value of $G_0^2/V_0^2$.

We now compare the results for the numerical solution of the FBE to the predictions of the simple effective model described above (right three panels of Fig. 3.1). We consider two approaches for determining the effective rate parameters in Eq. (3.7). In the first approach, we average the bare rates over momentum as per the uniform approximation in Eq. (3.17) and Eq. (3.21), and use them to predict the steady-state ($\dot{n} = 0$) for each case of $\Omega_D$ and $G_0^2/V_0^2$. The second approach builds on the first. For a given $\Omega_D$, the average rates $W_{\text{in}}^{\text{ph}}, W_{\text{out}}^{\text{ph}}, W_{31}^{\text{ee}}, and W_{22}^{\text{ee}}$ form four separate functions of $G_0^2/V_0^2$. We introduce a scaling prefactor each of these functions, which we use as fitting parameters. (Note that a global rescaling of all four functions leaves the steady state invariant; hence there are three independent fitting parameters.) These three parameters are fitted using the method of least squares for the difference between the predicted densities from the effective model and the exact densities computed from the FBE (taken over all values of $G_0^2/V_0^2$).

The simple model in Eq. (3.7) is based on a "uniform" approximation, in which the crystal momentum dependencies of the transition rates and populations are ignored. As such, we expect the simple model to work well in the "hot" regime where the distribution approaches a uniform, infinite-temperature-like form. Interestingly, when the phonon bandwidth is large, $\Delta_B < \Omega_D < E_{\text{gap}}$, we observe good agreement between the effective model and the full FBE even well outside the hot regime, where the total excitation density becomes small (see upper two line cuts in Fig. 3.1). Furthermore, in this regime, we see that the two methods for determining the effective rates in Eq. (3.7) give very similar results.For lower values of $\Omega_D$ (lowest panel, with $\Delta_A < \Omega_D < \Delta_B$), the phase space for electron-phonon scattering becomes highly restricted and we observe significant deviations between the solution of the FBE and the simplified model.

### 3.4 Discussion

Our motivation in this work was to study the applicability of Floquet band engineering in the presence of electron-electron interactions. In particular, we were interested in the situation occuring in Floquet topological insulators, where a resonant drive induces a band inversion in the Floquet spectrum. We find the regime where cooling by the phonon bath effectively counters the heating mediated by the interactions, thereby stabilizing an insulator-like steady state with a small density of excitations.

To identify the experimentally-relevant regime, we now relate our model parameters to typical time scales observed in driven semiconductors. The shortest timescale is associated with elastic electron-electron interactions, $\tau_{\mathrm{ee}}^{\mathrm{elastic}} \sim 10 - 100$ fs, while the cooling timescale due to electron-phonon scattering is on the order of $\tau_{\mathrm{ph}} \sim 0.1 - 1$ ps [35]. As discussed above, in the low-excitation-density regime, Floquet-Auger II processes dominate the heating rate. These processes are of Floquet-Umklapp type, and we thus estimate the associated time scale to be $\tau_{\mathrm{ee}}^{\mathrm{FU}} = (W_{22}^{ee})^{-1} \sim (S/\Omega)^{-2}\tau_{\mathrm{ee}}^{\mathrm{elastic}}$. Therefore, a rough estimate for the dimensionless parameter controlling the excitation density is $\kappa_{22} = (S/\Omega)^2\tau_{\mathrm{ph}}/\tau_{\mathrm{ee}}^{\mathrm{elastic}}$. For $(S/\Omega) \lesssim 0.1$, a regime of low excitation density can be reached.

To simplify the analysis in this work, we did not consider electron-hole radiative recombination processes, which also contribute to heating [32]. These processes can be straightforwardly incorporated to the model. At the level of the effective model in Eq. 3.7, recombination processes only renormalize the parameters $W_{\mathrm{out}}^{\mathrm{ph}}$, $W_{\mathrm{in}}^{\mathrm{ph}}$. The radiative recombination time scale is on the order of $\tau_{\mathrm{r}} \sim 0.1$ ns $\gg \tau_{\mathrm{ee}}^{\mathrm{elastic}}$. Thus, the contribution of radiative recombination to heating will be dominant only for $(S/\Omega)^2 \ll 1$. A further simplification in our model was the choice of band structure parameters to allow only a single-photon resonance, see Fig. 3.1. Floquet gaps resulting from an $n^{\mathrm{th}}$-order resonance would be suppressed by a factor of $(S/\Omega)^n$. Thus, in many experimental realizations, we expect these gaps to be smaller than the scattering rates in the steady state. Therefore, the primary role of the higher-order resonances would be to add additional heating channels, whose rates would be suppressed by corresponding powers of $(S/\Omega)$. Their effect would be subdominant, and would not change our results qualitatively. The effect of higher-order resonances for strong driving is an interesting direction for future work.

Our demonstration that the populations of the Floquet bands can be controlled in the presence of electron-electron interactions leaves many directions for future research: In the regime of low excitation density, an important goal is to find experimental probes for extracting the topological properties of the Floquet band structure. For higher excitation densities, we have shown that it is possible to reconstruct the results of the full FBE with a simple, nonlinear rate equation, Eq. (3.7). The effective model opens an interesting route for exploring the interplay between nonlinear phenomena such as bistability and hysteresis with the physics of Floquet-engineered

band structures.

# APPENDIX

## 3.A Floquet-Kinetic Equations

In this section, we outline the derivation of the kinetic equations for the Floquet single-particle correlation function $F^{\alpha p}_{\beta p} = \langle f^\dagger_{\alpha p}(t) f_{\beta p}(t)\rangle$, where $f^\dagger_{\alpha p}(t)$ is the creation operator for a single particle in a Floquet state with band $\alpha$ and momentum $p$ as introduced in the main text.

We begin by moving to the free Floquet basis via the transformation (same as main text) $c_{\nu p} = \sum_\alpha \langle \nu p|\psi_{\alpha p}(t)\rangle f_{\alpha p}(t) = \sum_{\alpha n} e^{-i(\mathcal{E}_{\alpha k}+n\Omega)t}\langle \nu p|\phi^n_{\alpha p}\rangle f_{\alpha p}(t)$ where, in the second equality, we have expanded the periodic piece of the Floquet state $|\phi_{\alpha p}(t)\rangle$ in terms of its harmonics. Defining $U_0(t,t')$ as the time-evolution operator from $t$ to $t'$ associated with the free part of the model, $H_0(t)$, we take note of the important property of Floquet states, $f^\dagger_{\alpha p}(t) = U_0(t,t') f^\dagger_{\alpha p}(t') U_0^\dagger(t,t')$. This immediately leads to the fact that $i\hbar\frac{\partial}{\partial t}\left(f^\dagger_{i_1}(t)...f^\dagger_{i_m}(t) f_{i_{m+1}}(t)...f_{i_{m+n}}(t)\right) = [H_0(t), f^\dagger_{i_1}(t)...f^\dagger_{i_m}(t) f_{i_{m+1}}(t)...f_{i_{m+n}}(t)]$, where $i = (\alpha, p)$ is a compressed index used for brevity. Hence, from considering both the time derivative of the state and the time derivative of the creation/annihilation operators, we obtain $i\hbar\frac{\partial}{\partial t}\langle f^\dagger_{i_1}(t)...f^\dagger_{i_m}(t) f_{i_{m+1}}(t)...f_{i_{m+n}}(t)\rangle = \langle [f^\dagger_{i_1}(t)...f^\dagger_{i_m}(t) f_{i_{m+1}}(t)...f_{i_{m+n}}(t), H - H_0(t)]\rangle$, where $H = H_0(t) + H_{\text{int}} + H_{\text{el-ph}}$ is the full Hamiltonian of the driven many-body problem. Using the above properties, we perform the cluster expansion to second order, treating doublets at the scattering level [18, 32]. The major approximation in this procedure is that we factorize higher-order correlators ("doublets") into 2-point functions ("singlets")

$$\begin{aligned}\langle f^\dagger_{i_1} f^\dagger_{i_2} f_{i_3} f_{i_4}\rangle &\approx F^{i_1}_{i_4} F^{i_2}_{i_3} - F^{i_1}_{i_3} F^{i_2}_{i_4} \\ \langle f^\dagger_{j_1} f^\dagger_{i_1} f_{j_2} f_{i_2} b^\dagger_q b_{q'}\rangle &\approx (F^{j_1}_{i_2} F^{i_1}_{j_2} - F^{j_1}_{j_2} F^{i_1}_{i_2})\langle b^\dagger_q b_{q'}\rangle. \end{aligned} \tag{3.8}$$

Furthermore, we assume that the bosons are thermal, $\langle b^\dagger_q b_{q'}\rangle \approx \delta_{qq'} N_{\omega_{\boldsymbol{q}}}$, where $N_{\omega_{\boldsymbol{q}}} = (e^{\beta_{\text{ph}}\omega_{\boldsymbol{q}}} - 1)^{-1}$ is the Bose-Einstein distribution with inverse temperature $\beta_{\text{ph}} = 1/T_{\text{ph}}$ (we set $k_{\text{B}} = 1$). Finally, we assume the bath interactions and electron-electron interactions are Markovian (and also drop principle-value terms). Non-Markovian effects are an interesting topic and beyond the scope of this work. At this level of approximation, one obtains the *Floquet-Redfield* (FRE) equation [31] which couples the kinetic equations of the off-diagonal Floquet-"polarizations" (or single-particle coherences) and the diagonal Floquet occupations. The FRE requires care in its simulation as it is explicitly time-dependent and oscillatory. Preliminary results indicate that Floquet occupations and the magnitude of the Floquet polarizations are the appropriate variables that characterize the steady state, and that the polarizations are small in comparison to the occupations in the hot and cold regimes [31]. To obtain an intuitive closed set of kinetic equations for the dominant Floquet occupations alone, we make a few more approximations and obtain the *Floquet-Boltzmann* (FBE) equation.

Keeping only the occupation terms, performing the secular approximation on the remaining explicit time-dependence, and using $\omega_{\mathbf{q}} = \omega_{-\mathbf{q}}$, we arrive at the Floquet-Boltzmann equation [1, 13, 32]. This kinetic equation is what one would obtain if considering a "Floquet-Fermi-Golden-Rule" approach where the time derivative of the occupations is given by collision integrals involving scattering of electrons with each other and with phonons:

$$\partial_t F_{\alpha p} = \mathcal{G}^{\text{Boltz}}_{\text{scat},+} + \mathcal{G}^{\text{Boltz}}_{\text{scat},-} + \mathcal{V}^{\text{Boltz}}_{\text{scat}}, \tag{3.9}$$

where $\mathcal{G}^{\text{Boltz}}_{\text{scat},+}$ and $\mathcal{G}^{\text{Boltz}}_{\text{scat},-}$ denote the two pieces of the collision integral encoding electron-phonon scattering, $I^{\text{ph}}_{k\alpha}\{F\} = \mathcal{G}^{\text{Boltz}}_{\text{scat},+} + \mathcal{G}^{\text{Boltz}}_{\text{scat},-}$, and $I^{\text{ee}}_{k\alpha}\{F\} = \mathcal{V}^{\text{Boltz}}_{\text{scat}}$ denotes the collision integral encoding electron-electron scattering. Explicitly:

$$\begin{aligned}
\mathcal{G}^{\text{Boltz}}_{\text{scat},+} &= \frac{2\pi}{\hbar} \sum_{\alpha_2 p_2 q \boldsymbol{q}_{||}} \sum_n |G^{\alpha p}_{\alpha_2 p_2 q}(n)|^2 \delta(\mathcal{E}_{\alpha p} - \mathcal{E}_{\alpha_2 p_2} - \omega_{\boldsymbol{q}} + n\Omega) \\
&\quad \Big( F_{\alpha_2 p_2}(1 - F_{\alpha p}) N_{\omega_{\boldsymbol{q}}} - F_{\alpha p}(1 - F_{\alpha_2 p_2})(1 + N_{\omega_{\boldsymbol{q}}}) \Big) \qquad (3.10) \\
\mathcal{G}^{\text{Boltz}}_{\text{scat},-} &= \frac{2\pi}{\hbar} \sum_{\alpha_2 p_2 q \boldsymbol{q}_{||}} \sum_n |G^{\alpha p}_{\alpha_2 p_2 q}(n)|^2 \delta(\mathcal{E}_{\alpha p} - \mathcal{E}_{\alpha_2 p_2} + \omega_{\boldsymbol{q}} + n\Omega) \\
&\quad \Big( F_{\alpha_2 p_2}(1 - F_{\alpha p})(1 + N_{\omega_{\boldsymbol{q}}}) - F_{\alpha p}(1 - F_{\alpha_2 p_2}) N_{\omega_{\boldsymbol{q}}} \Big) \qquad (3.11) \\
\mathcal{V}^{\text{Boltz}}_{\text{scat}} &= \frac{4\pi}{\hbar} \sum_{\alpha_2 \alpha_3 \alpha_4} \sum_{p_2 p_3 p_4} \sum_n |V^{\alpha p \alpha_2 p_2}_{\alpha_3 p_3 \alpha_4 p_4}(n)|^2 \delta(\mathcal{E}_{\alpha p} + \mathcal{E}_{\alpha_2 p_2} - \mathcal{E}_{\alpha_3 p_3} - \mathcal{E}_{\alpha_4 p_4} + n\Omega) \\
&\quad \big( (1 - F_{\alpha p})(1 - F_{\alpha_2 p_2}) F_{\alpha_3 p_3} F_{\alpha_4 p_4} - F_{\alpha p} F_{\alpha_2 p_2}(1 - F_{\alpha_3 p_3})(1 - F_{\alpha_4 p_4}) \big), \qquad (3.12)
\end{aligned}$$

where the $\alpha$ indices denote Floquet bands and the $p$ indices denote electronic momenta. As before, $q$ denotes the phonon momentum along the direction of the system, $\mathcal{E}_{\alpha p}$ denotes the quasienergy of Floquet band $\alpha$ and momentum $p$, and $n$ denotes the drive quanta exchanged in the scattering process. Moreover, $G^{\alpha p}_{\alpha_2 p_2 q}(n)$ and $V^{\alpha p \alpha_2 p_2}_{\alpha_3 p_3 \alpha_4 p_4}(n)$ are the dressed matrix elements which arise from changing basis to the Floquet states, given by

$$\begin{aligned}
G^{\alpha p}_{\alpha_2 p_2 q}(n) &= \sum_{m \nu \nu'} M^{\nu' p q}_{\nu p_2} \delta(p - p_2 - q + 2\pi l/a) \\
&\quad \langle \phi^{n+m}_{\alpha p} | \nu' p \rangle \langle \nu p_2 | \phi^{m}_{\alpha_2 p_2} \rangle \\
V^{\alpha p \alpha_2 p_2}_{\alpha_3 p_3 \alpha_4 p_4}(n) &= \sum_{\nu_1 \nu_2 \nu_3 \nu_4} \sum_{n' m m'} V^{\nu_1 p \nu_2 p_2}_{\nu_3 p_3 \nu_4 p_4} \langle \phi^{n - n' + m + m'}_{\alpha p} | \nu_1 p \rangle \\
&\quad \langle \phi^{n'}_{\alpha_2 p_2} | \nu_2 p_2 \rangle \langle \nu_3 p_3 | \phi^{m}_{\alpha_3 p_3} \rangle \langle \nu_4 p_4 | \phi^{m'}_{\alpha_4 p_4} \rangle, \qquad (3.13)
\end{aligned}$$

where $\nu, \nu'$ are the undriven band indices, and where we have assumed that the bare coupling in Eq. 3.4 does not depend on $\boldsymbol{q}_\perp$, for simplicity. Crystal-momentum conservation is explicitly shown with $l \in \mathbb{Z}$. Since we are interested in the case of a 3D bosonic bath coupled to the 1D system, we integrate out the bath degrees of freedom transverse to the system and replace the energy/momentum conservation in the FBE with a partial density of states (pDOS) defined as $\sum_{q\boldsymbol{q}_\perp} = \sum_q \int d\omega \rho(q,\omega)$. Evaluating the pDOS for the kinematic constraints yields the replacement rule $\sum_{q\boldsymbol{q}_\perp} \delta(p - p_2 - q)\delta(\omega - \Delta E) \to \rho(p - p_2, \Delta E)$ in the FBE. For the case of linear dispersion, $\omega_{\boldsymbol{q}} = C|\boldsymbol{q}|$, the pDOS is given by

$$\rho(q,\omega) = \begin{cases} \frac{2A_\perp}{(2\pi)^2}\frac{\pi\omega}{C^2} & C\sqrt{q^2} \le \omega < C\sqrt{q^2 + (\frac{\pi}{a_b})^2} \\ \frac{2A_\perp}{(2\pi)^2}\frac{2\omega}{C^2}\left(\sin^{-1}(\sqrt{\frac{(\frac{\pi}{a})^2}{(\frac{\omega}{C})^2 - q^2}}) - \sin^{-1}(\sqrt{1 - \frac{(\frac{\pi}{a})^2}{(\frac{\omega}{C})^2 - q^2}})\right) & C\sqrt{q^2 + (\frac{\pi}{a_b})^2} \le \omega < C\sqrt{q^2 + 2(\frac{\pi}{a_b})^2}, \end{cases} \tag{3.14}$$

where $a_b = 1$ is the bath lattice spacing, and $A_\perp$ is the transverse area of bath. We set $A_\perp = 1$ and understand that the rates are per unit area of the bath. With these definitions, we may define the overall electron-phonon scattering strength

$$B^{\alpha p,\pm}_{\alpha_2 p_2}(n) = |G^{\alpha p}_{\alpha_2 p_2, p-p_2}(n)|^2 \rho(p - p_2, \pm(\mathcal{E}_{\alpha p} - \mathcal{E}_{\alpha_2 p_2} + n\Omega)), \tag{3.15}$$

where the $\pm$ are associated to $\mathcal{G}^{\text{Boltz}}_{\text{scat},\pm}$ respectively.

The band matrix elements corresponding to the n.n. interaction considered in Eq. 3.2 are given by

$$\begin{aligned} V^{\nu_1 k_1 \nu_2 k_2}_{\nu_3 k_3 \nu_4 k_4} &= \mathcal{U}(1 + e^{i(k_2 - k_3)}) {R^\dagger}_{k_1,\nu_1 0} {R^\dagger}_{k_2,\nu_2 1} R_{k_3,1\nu_3} R_{k_4,0\nu_4} \\ &- \mathcal{U}(1 + e^{i(k_1 - k_3)}) {R^\dagger}_{k_1,\nu_1 1} {R^\dagger}_{k_2,\nu_2 0} R_{k_3,1\nu_3} R_{k_4,0\nu_4} \\ &- \mathcal{U}(1 + e^{i(k_2 - k_4)}) {R^\dagger}_{k_1,\nu_1 0} {R^\dagger}_{k_2,\nu_2 1} R_{k_3,0\nu_3} R_{k_4,1\nu_4} \\ &+ \mathcal{U}(1 + e^{i(k_1 - k_4)}) {R^\dagger}_{k_1,\nu_1 1} {R^\dagger}_{k_2,\nu_2 0} R_{k_3,0\nu_3} R_{k_4,1\nu_4} \end{aligned} \tag{3.16}$$

where $\mathcal{U} = \frac{V_0}{2N}\delta(k_1 + k_2 - k_3 - k_4 + 2\pi l/a)$, $N$ denotes the number of unit cells in the system, and $R_{k,a\nu} = \langle ak|\nu k\rangle$ is the rotation matrix from the sublattice to the band basis, where $a = 0, 1$ corresponds to sublattice $A, B$ in Eq. 3.1. Note the fermionic symmetries $V^{\nu_1 k_1, \nu_2 k_2}_{\nu_3 k_3, \nu_4 k_4} = -V^{\nu_2 k_2, \nu_1 k_1}_{\nu_3 k_3, \nu_4 k_4} = -V^{\nu_1 k_1, \nu_2 k_2}_{\nu_4 k_4, \nu_3 k_3} = V^{\nu_2 k_2, \nu_1 k_1}_{\nu_4 k_4, \nu_3 k_3}$. Hermiticity requires $V^{\nu_1 k_1, \nu_2 k_2}_{\nu_3 k_3, \nu_4 k_4} = (V^{\nu_3 k_3, \nu_4 k_4}_{\nu_1 k_1, \nu_2 k_2})^*$ for the interaction elements and $G^{\nu' k' q \boldsymbol{q}_\perp}_{\nu k} = (G^{\nu k (-q)(-\boldsymbol{q}_\perp)}_{\nu' k'})^*$ for the electron-phonon matrix elements.

All of the collision integrals have three main ingredients: dressed matrix elements, kinematic restrictions from the delta functions containing quasienergy (and crystal-momentum conservation

hidden in the matrix elements), and phase-space factors due to Fermi and Bose statistics (occupation functions). The kinematic restrictions give crucial insight into the structure of the FBE. The scattering of a Floquet-electron via the absorption or emission of a phonon and the $2 \rightarrow 2$ scattering of Floquet-electrons both conserve quasienergy up to multiples of the drive frequency. This kinematic structure is a signature of the fact that quasienergy is itself defined modulo $\Omega$. To understand its implications further, let us choose a gauge and define the first Floquet zone (FFZ) as shown in Fig. 3.1. As in the main text, we will, by fiat, refer to the upper band in the FFZ as the UF band and to the lower band in the FFZ as the LF band. By selecting a gauge, we have set an energetic orientation - the UF band is of higher quasienergy (positive values) than the LF band (negative values). We are now in a position to discuss the scattering processes which split into two broad categories we term "normal" and "Floquet-Umklapp" (FU), with the former encoding processes that maintain the energetic orientation and the latter that do not. Normal processes are those with $n = 0$ in the quasienergy delta functions, and FU processes are those with $n \neq 0$. This concept is best elucidated via examples for both phonon scattering and electron-electron interactions.

Let us first understand how to interpret the terms in the Floquet-Boltzmann equation beginning with the electron-phonon terms. On the left-hand side (LHS) of the equation, we have the time derivative of the occupation state $\alpha p$. The terms on the right-hand side (RHS) of the equation appearing with positive sign denote an "incoming" transition $\alpha_2 p_2 \rightarrow \alpha p$, which can be understood by looking at the occupation factors. The initial state $\alpha_2 p_2$ must have some occupation and the final state $\alpha p$ must have empty space; hence the rate is proportional to $F_{\alpha_2 p_2}(1 - F_{\alpha p})$. The $N_{\omega_q}$ factor denotes phonon absorption and the $1 + N_{\omega_q}$ factor denotes phonon emission, since at $T_{\text{ph}} = 0$, the Bose-Einstein factors vanish but the "1" term still encodes a finite rate of spontaneous emission into the "vacuum." The terms with the negative sign denote the respective hermitian conjugate processes, i.e., the "outgoing" processes with transition $\alpha p \rightarrow \alpha_2 p_2$. We will refer to each of the electron-phonon equations by their incoming terms, and so $\mathcal{G}^{\text{Boltz}}_{\text{scat},+}$ will be referred to as the phonon-absorption term, and $\mathcal{G}^{\text{Boltz}}_{\text{scat},-}$ will be referred to as the phonon-emission term.

This type of terminology is further supported by observing the delta functions. Noting that $\omega_{\boldsymbol{q}} \geq 0$, the delta function for the phonon-absorption term, for $n = 0$, can only be satisfied for $\mathcal{E}_{\alpha p} \geq \mathcal{E}_{\alpha_2 p_2}$ which is exactly what one would expect for a $\alpha_2 p_2 \rightarrow \alpha p$ transition involving absorption of energy. Similarly, the delta function for the phonon-emission term, for $n = 0$, can only be satisfied for $\mathcal{E}_{\alpha p} \leq \mathcal{E}_{\alpha_2 p_2}$, which is exactly what one would expect for a $\alpha_2 p_2 \rightarrow ap$ transition involving emission of energy. Hence, our labeling of the terms is consistent with the kinematic intuition of the scattering processes given the energy orientation we have chosen and the restriction to $n = 0$. Therefore, we refer to $n = 0$ processes as "normal," or those that preserve energy orientation. With just $n = 0$ processes, the Floquet-Fermi-Dirac solution $F_{\alpha p} = (e^{\mathcal{E}_{\alpha p}/T_{\text{ph}}} + 1)^{-1}$ for the steady state is

exact; this is mathematically the same as the case of the usual undriven Boltzmann equation, with quasienergy replacing energy.

The $n \neq 0$ are anomalous processes we term "Floquet-Umklapp" since, in analogy to Bloch theory, the scattering processes are assisted by a reciprocal lattice vector, which here is $\Omega$. In sharp contrast to the "normal" processes, these destroy the energy orientation we have chosen. Consider a process with $\mathcal{E}_{\alpha p} \geq \mathcal{E}_{\alpha_2 p_2}$. It is only possible, assuming the appropriate energy phonon exists, to satisfy this condition in two ways: in the phonon-absorption term with $n = 0$ (the normal process discussed earlier), and in the phonon-emission term with $n < 0$. The latter FU process shows that it is possible to have a transition from a lower quasienergy state, $\alpha_2 p_2$, to a higher quasienergy state, $\alpha p$, via emission of a phonon. These types of FU (or orientation-breaking) processes are manifestly nonequilibrium and are enabled due to assistance from quanta of the drive.

More generally, choosing a gauge, i.e., an energetic orientation, means to specify a preferred frame to view the Floquet bands that reside on a torus. Normal processes are those that obey kinematic intuition in the chosen frame. In contrast, FU processes are those that wrap around the torus in the opposite direction. Choosing a different gauge corresponds to choosing a different frame, and processes that are called normal and FU in one frame will correspondingly switch roles in the other. From this discussion, it is clear that with the phonons, energetic restrictions on $\Omega_D$ with respect to the gap between the bands ($\Delta_A$) and the gap at the zone edge ($\Delta_B$) can selectively populate one or both of the bands. In fact, it is perhaps better to select the frame based on which band is preferentially populated, declaring that the LF band.

Let us turn our attention to the interaction term $\mathcal{V}_{\text{scat}}^{\text{Boltz}}$. We can still segregate $n = 0$ terms as normal processes and $n \neq 0$ terms as FU processes. The normal processes just encode the usual $2 \to 2$ scattering obeying quasienergy conservation in the given frame (including Auger I processes). Since these processes do not change the total quasienergy, they only contribute to the spread of total quasienergy through the system. In contrast, the FU processes are still $2 \to 2$ scattering but with exchange of drive quanta, and, hence, are the source of quasienergy non-conservation. There are two classes of FU scattering: The Floquet-Auger I (FA-I) processes are those in which two particles start in the same Floquet band, and only one particle switches Floquet bands with an exchange of a drive quantum. Floquet-Auger II (FA-II) processes are those in which two particles start in the same Floquet band, and both switch to the other. This is only possible with the exchange of a drive quantum (see Fig. 3.1). Altogether, the quasienergy non-conservation and the spread of quasienergy through the system via normal and FU processes are the mechanisms of heating in driven weakly-interacting systems.

The last remaining ingredient of the FBE are the dressed matrix elements. The key effect of the dressing, for weak driving, is in suppressing the strength of high-$n$ scattering processes, or

in other words, those that involve the exchange of many drive quanta. This comes directly from consideration of the Floquet-band matrix elements in the undriven band basis. The chosen FFZ is primarily made from the undriven conduction band and a single drive quantum shifted undriven valence band. The higher harmonic content of the FFZ states have less weight as they are detuned significantly in energy. Scattering processes involving large $n$ involve connecting FFZ states via their higher harmonic content, and so are suppressed as $(S/\Omega)^n$. See Fig. 3.A.1 for more detailed information about the scaling of the dressed matrix elements in Eq. 3.13.

**Effective Dynamics with Bosonic Reservoir**

Here, we derive the effective model presented in the main text. Performing the "uniform" approximation on the FBE, $F_{\alpha p} \approx n_\alpha$ for all $p$, we obtain, using the half-filling condition $\sum_\alpha n_\alpha = 1$, Eq. 3.7 reproduced here for convenience:

$$\begin{aligned} \dot{n} &= W^{\mathrm{ph}}_{\mathrm{in}}(1-n)^2 - W^{\mathrm{ph}}_{\mathrm{out}} n^2 \\ &+ W^{\mathrm{ee}}_{31}((1-n)^3 n - (1-n)n^3) + W^{\mathrm{ee}}_{22}((1-n)^4 - n^4), \end{aligned}$$

with the following definitions. The electron-phonon rates are (using $\alpha = +$ for Eq. 3.7),

$$\begin{aligned} W^{\mathrm{ph},\alpha}_{\mathrm{in}} &= \frac{2\pi}{\hbar} N \sum_m \mathcal{B}^{\alpha+}_{\tilde{\alpha}}(m)\mathcal{N}_m + \frac{2\pi}{\hbar} N \sum_m \mathcal{B}^{\alpha-}_{\tilde{\alpha}}(m)(1+\mathcal{N}_m) \\ W^{\mathrm{ph},\alpha}_{\mathrm{out}} &= \frac{2\pi}{\hbar} N \sum_m (1+\mathcal{N}_m)\mathcal{B}^{\alpha+}_{\tilde{\alpha}}(m) + \frac{2\pi}{\hbar} N \sum_m \mathcal{B}^{\alpha-}_{\tilde{\alpha}}(m)\mathcal{N}_m, \end{aligned} \tag{3.17}$$

where, to make the effective model momentum-independent, we evaluate the Bose-Einstein distribution function at the gap energies relevant for the normal and FU processes:

$$\mathcal{B}^{\alpha\pm}_{\alpha_2}(m) = \frac{1}{N^2} \sum_{pp_2} B^{\alpha p,\pm}_{\alpha_2 p_2}(m), \tag{3.18}$$

$$\mathcal{N}_m = \begin{cases} N_{\Delta_A} & m = 0 \\ N_{\Delta_B} & |m| = 1. \end{cases} \tag{3.19}$$

Note that the $\mathcal{B}$ rates are just momentum averages of all the scattering strengths. Similarly, the interaction rates are

$$W^{\mathrm{ee}}_{22} = \frac{4\pi}{\hbar} N^3 V_D^2, \tag{3.20}$$

$$W^{\mathrm{ee}}_{31} = \frac{8\pi}{\hbar} N^3 V_F^2, \tag{3.21}$$

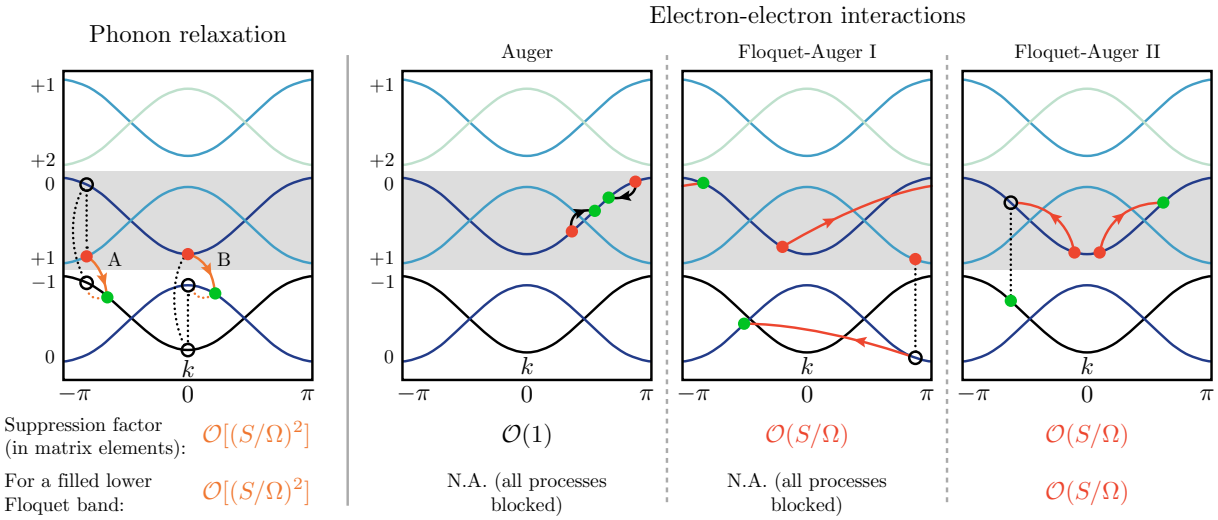


Figure 3.A.1: Dominant types of scattering processes leading to single-particle excitations across the Floquet gap, classified according to their origin: phonon relaxation and electron-electron interactions — Auger I, Floquet-Auger I, and Floquet-Auger II, as in the main text. Recall that Floquet-Auger processes of type I (II) create one (two) excitation(s) across the Floquet gap. The energy bands shown here are copies of the bands of the non-driven system (dark blue) shifted by $m\Omega$, i.e., by integer multiples of the drive frequency. Bands are labeled by $m$, and shown in different colors for distinct $m$. They can be regarded as the Floquet modes (harmonics) composing the Floquet states of the system, in the limit of a small drive amplitude $S \ll \Omega$. Here we choose our basis of Floquet states so that the latter have dominant Floquet-mode components in the Floquet zone (energy window $\Omega$) highlighted in grey. Scattering processes can be decomposed into transitions between Floquet modes (initial/final states denoted by red/green dots), and we only illustrate the dominant ones involving leading-order Floquet-mode components. Transitions between Floquet states must conserve momentum and energy, up to an integer multiple $n\Omega$ (and up to some phonon momentum and energy, for phonon-mediated processes). Normal processes are characterized by $n = 0$ (black arrows) and Floquet-Umklapp (FU) processes are characterized by $n \neq 0$ (red and orange arrows). The dotted lines indicate the virtual transitions involved in a process, with each virtual transition involving an additional power of $S/\Omega$. The suppression factors of individual processes are indicated below each panel. When the lower Floquet band is filled, Auger I and Floquet-Auger I processes are absent. Note that the "B" phonon relaxation process can be $O(1)$ if the phonon matrix elements $G^{\nu' k'}_{\nu k}(\boldsymbol{q})$ allow interband (off-diagonal in $\nu, \nu'$) transitions. This scenario exists, for example, in the case of radiative recombination.

where the momentum-averaged electron-electron scattering strengths are

$$\begin{aligned}\mathcal{S}^{\alpha\alpha_2}_{\alpha_3\alpha_4} &= \frac{1}{N^4}\sum_{pp_2p_3p_4}\sum_{n}|V^{\alpha p\alpha_2 p_2}_{\alpha_3 p_3\alpha_4 p_4}(n)|^2 \\ &\quad \delta(\mathcal{E}_{\alpha p}+\mathcal{E}_{\alpha_2 p_2}-\mathcal{E}_{\alpha_3 p_3}-\mathcal{E}_{\alpha_4 p_4}+n\Omega),\end{aligned} \tag{3.22}$$

$$\begin{pmatrix} \mathcal{S}^{00}_{00} & \mathcal{S}^{00}_{01} & \mathcal{S}^{01}_{00} & \mathcal{S}^{01}_{01} \\ \mathcal{S}^{00}_{10} & \mathcal{S}^{00}_{11} & \mathcal{S}^{01}_{10} & \mathcal{S}^{01}_{11} \\ \mathcal{S}^{10}_{00} & \mathcal{S}^{10}_{01} & \mathcal{S}^{11}_{00} & \mathcal{S}^{11}_{01} \\ \mathcal{S}^{10}_{10} & \mathcal{S}^{10}_{11} & \mathcal{S}^{11}_{10} & \mathcal{S}^{11}_{11} \end{pmatrix} = \begin{pmatrix} V_1^2 & V_F^2 & V_F^2 & V_2^2 \\ V_F^2 & V_D^2 & V_2^2 & V_F^2 \\ V_F^2 & V_2^2 & V_D^2 & V_F^2 \\ V_2^2 & V_F^2 & V_F^2 & V_1^2 \end{pmatrix}. \tag{3.23}$$

The matrix structure in Eq. 3.23 directly follows from fermionic antisymmetry, hermiticity, and particle-hole/chiral symmetry. Intuitively, this can be understood as each type of process possessing the same average strength, i.e., FA-II processes have strength $V_D$, the sum of Auger and FA-I processes together have strength $V_F$, fully intraband scattering has strength $V_1$, and interband scattering that conserves band density has strength $V_2$. As expected, only $V_F, V_D$ contribute to the effective dynamics in Eq. 3.7, since they are the only process types that change the band density. Note that since $V \sim 1/N$ (see Eq. 3.16), the interaction rates scale as $W^{\text{ee}} \sim N$, the same as phonon rates $W^{\text{ph}}$. Therefore, the steady state does not have system-size dependence, as desired for a physically meaningful effective model.

The uniform approximation treats each band as a single level disregarding all the momentum dependence of the bands. The steady-state band density is then determined “self-consistently" by solving in Eq. 3.7. Though the uniform approximation seems restrictive apriori, the effective model highlights the main processes contributing to heating/cooling and adequately captures the behavior of the band density with reasonable numerical accuracy. However, we do emphasize that for direct numerical comparison to exact FBE simulations, momentum dependence of the results are highly nonuniversal and depend on many band structure properties and coupling matrix elements. Furthermore, it is important to note that the effective dynamics is inaccurate in the restricted case of only $n = 0$ interactions. In this situation, the FBE preserves quasienergy exactly and thermalization occurs within a quasienergy manifold. Auger I processes are the only contributions to $W^{\text{ee}}_{31}$ in the effective model when both FA-I and FA-II are absent. Microscopically, Auger I processes do not change the total quasienergy, but still cause anomalous heating towards the (stable) infinite temperature fixed point in the effective model. This stems from the fact that the uniform approximation cannot differentiate an Auger I process from a FA-I process; lumping each Floquet band into a single density variable destroys information about intraband scattering. This is harmless for common $n = 0$ scattering processes $(V_1, V_2)$ which neither cause band-density changes nor quasienergy changes, but it is the crucial difference between an Auger I and a FA-I

process as shown in Fig. 3.1. This case, however, is fine-tuned and is not of physical relevance since FA-I and FA-II are usually always present. Therefore, our effective model is an appropriate minimal model with clear physical intuition that captures the dynamics of open weakly-interacting fermionic Floquet systems.

### 3.B Fermionic Reservoir

In this section, we derive the effective dynamics of the system in the presence of a static fermionic reservoir (e.g. leads) coupled to the system. We assume a local extensive tunnel coupling $\Gamma_l^{ax}$ for a lead electron $l$ tunneling into a (real-space, sublattice) system state $(x, a)$.

$$H_{\text{lead}} = \sum_l \varepsilon_l d_l^\dagger d_l, \tag{3.24}$$

$$\begin{aligned} H_{\text{el-lead}} &= \sum_{axl} \Gamma_l^{ax}(c_{xa}^\dagger d_l + d_l^\dagger c_{xa}) \\ &= \sum_{\nu kl} \Gamma_l^{\nu k} c_{k\nu}^\dagger d_l + h.c. \end{aligned} \tag{3.25}$$

where $\Gamma_l^{\nu k} = 1/\sqrt{N}\sum_{ax} e^{-ikx}\Gamma_l^{ax} R_{k,\nu a}^\dagger$ is the tunnel coupling in the band basis. The results are derived in the same fashion as in Appendix 3.A and here we just present the major results. The additional FBE contribution (RHS of Eq. 3.9) is given by

$$\mathcal{R}^{\text{Boltz}} = \frac{2\pi}{\hbar}\sum_l \sum_n |\Gamma_l^{\alpha p}(n)|^2 \delta(\mathcal{E}_{\alpha p} - \varepsilon_l + n\Omega)\left((1 - F_{\alpha p})D_l - F_{\alpha p}(1 - D_l)\right), \tag{3.26}$$

where $\Gamma_l^{\alpha k}(n) = \sum_\nu \Gamma_l^{\nu k}\langle \phi_{\alpha k}^n | \nu k\rangle$ is the dressed lead coupling and $D_l$ is the Fermi-Dirac distribution of the lead with chemical potential $\mu_{\text{res}}$ and temperature $T_{\text{res}}$.

This term encodes tunneling of a lead electron $l$ into Floquet state $(\alpha, p)$ with strength $|\Gamma_l^{\alpha p}(n)|^2$ if the lead-electron energy and the system quasienergy are matched up to a multiple of $\Omega$. Both normal and FU tunneling processes may be present based on the number of drive quanta exchanged. Detailed analysis in the context of lead engineering has been carried out in Ref. [32]. Making the uniform approximation, we obtain the lead contributions to the effective model

$$\dot{n}_\alpha = (1 - n_\alpha)\Gamma_{\text{in}}^\alpha - n_\alpha \Gamma_{\text{out}}^\alpha, \tag{3.27}$$

$$\Gamma_{\text{in}}^\alpha = \frac{2\pi}{\hbar}\sum_l D_l \bar{\Gamma}_l^\alpha, \tag{3.28}$$

$$\Gamma_{\text{out}}^\alpha = \frac{2\pi}{\hbar}\sum_l (1 - D_l)\bar{\Gamma}_l^\alpha, \tag{3.29}$$

where we have the momentum-averaged tunneling rate $\bar{\Gamma}_l^\alpha = 1/N\sum_p \sum_n |\Gamma_l^{\alpha p}(n)|^2 \delta(\mathcal{E}_{\alpha p} - \varepsilon_l + n\Omega)$. Note that the lack of particle conservation in the presence of a lead requires one to separately

consider each band density $n_\alpha$. The "in" rates favor a filled steady-state band density and "out" rates favor an empty steady-state band density.

We can gain intuition for the effect of the lead terms by considering the case where $\mu_{\text{res}} = 0$, $T_{\text{res}} = 0$, i.e., a zero-temperature lead with chemical potential set in the center of the gap between the two Floquet bands; in this case, $D_l = \Theta(\mu_{\text{res}} - \varepsilon_l) = \Theta(-\varepsilon_l)$, where $\Theta$ is the Heaviside step function. Focusing on the LF band, we find that $\Gamma^-_{\text{in}} \neq 0$ for $n \leq 0$ and $\Gamma^-_{\text{out}} \neq 0$ for $n > 0$, since $\mathcal{E}_{0p} < 0$ for all $p$. This means that tunneling into the LF band can occur as a normal or FU process. In contrast, tunneling out of the LF band can only be an FU process. With no further restrictions, the reservoir will generically heat the the system since FU tunneling processes involving exchange of drive quanta are present. However, if one considers a "filtered" lead with a bandwidth less than $\Omega$ (still centered between the bands), then FU processes are kinematically forbidden and $\Gamma^-_{\text{out}} = 0$. Hence, particles can only tunnel into the LF band. In the UF band, the situation is reversed with $\Gamma^+_{\text{in}} = 0$ and so particles may only tunnel out. Therefore, a filtered lead pushes the system toward the cold fixed point with $n_- = 1$ and $n_+ = 0$. This scenario has been analyzed in detail in Ref. [32].

The full effective model in the presence of both bosonic and fermionic reservoirs is explicitly

$$\begin{aligned}
\dot{n}_\alpha &= (1-n_\alpha)\Gamma^\alpha_{\text{in}} - n_\alpha\Gamma^\alpha_{\text{out}} + W^{\text{ph},\alpha}_{\text{in}} n_{\bar{\alpha}}(1-n_\alpha) - W^{\text{ph},\alpha}_{\text{out}} n_\alpha(1-n_{\bar{\alpha}}) \\
&+ W^{\text{ee}}_{22}\left((1-n_\alpha)^2 n_{\bar{\alpha}}^2 - n_\alpha^2(1-n_{\bar{\alpha}})^2\right) \\
&+ \frac{1}{2}W^{\text{ee}}_{31}\left((1-n_\alpha)^2 n_\alpha n_{\bar{\alpha}} - (1-n_\alpha)(1-n_{\bar{\alpha}})n_\alpha^2 + (1-n_\alpha)(1-n_{\bar{\alpha}})n_{\bar{\alpha}}^2 - (1-n_{\bar{\alpha}})^2 n_\alpha n_{\bar{\alpha}}\right).
\end{aligned} \tag{3.30}$$

One may check that Eq. 3.30 simplifies to Eq. 3.7 in the case of half-filling and no fermionic reservoir. General steady-state solutions to Eq. 3.30 can easily be found numerically by solving the system of two nonlinear equations.

### 3.C Simulation Details

We use the electronic hopping parameters $J_0 = 2$, $J_1 = -0.85$, drive parameters $\boldsymbol{S} = (1, 0, 0)$, $\Omega = 3.3$, and electronic lattice spacing $a = 1$, corresponding to gaps in the Floquet spectrum of $\Delta_A = 0.4$, $\Delta_B = 0.9$. The phonons have velocity $C = (\Omega_D/\sqrt{3})(a_b/\pi)$ (with $a_b = 1$), with spectral cutoff (bandwidth) $\Omega_D$, transverse area $A_\perp = 1$, and temperature $T = \Delta_A/10$. The interaction strength is $V_0 = 0.5$. The (quasi)energetic delta function in $\mathcal{V}^{\text{Boltz}}_{\text{scat}}$ is approximated on the finite-size system with a gaussian of finite support

$$\delta(\Delta\mathcal{E}) \approx \begin{cases} \frac{Z(r)}{\sqrt{2\pi\varepsilon^2}} e^{-\frac{(\Delta\mathcal{E})^2}{2\varepsilon^2}}, & |\Delta\mathcal{E}| \leq r\varepsilon \\ 0, & \text{o.w.} \end{cases} \tag{3.31}$$

where the standard deviation $\varepsilon = \max_k(\mathcal{E}_{\alpha,k+1} - \mathcal{E}_{\alpha,k})$ is the maximum adjacent quasienergy level spacing in a single Floquet band, $r = 1.5$ denotes the number of deviations to include in the finite support, and $Z(r = 1.5) = 1.154$ is the normalization constant ensuring that the truncated gaussian function integrates to unity. We check that the truncated gaussian does not allow any anomalous transitions across the Floquet gaps, thus strictly maintaining separation of interband and intraband processes. In the FBE simulations ($N = 20$), we scan the amplitude $G_0$ of the phonon bath and the cutoff $\Omega_D$, and perform numerical integration of the FBE until reaching a steady state.

## References


[1] Thomas Bilitewski and Nigel R. Cooper. Scattering theory for floquet-bloch states. *Phys. Rev. A*, 91:033601, Mar 2015.

[2] David Carpentier, Pierre Delplace, Michel Fruchart, and Krzysztof Gawedzki. Topological index for periodically driven time-reversal invariant 2d systems. *Phys. Rev. Lett.*, 114:106806, Mar 2015.

[3] Soonwon Choi, Joonhee Choi, Renate Landig, Georg Kucsko, Hengyun Zhou, Junichi Isoya, Fedor Jelezko, Shinobu Onoda, Hitoshi Sumiya, Vedika Khemani, Curt von Keyserlingk, Norman Y. Yao, Eugene Demler, and Mikhail D. Lukin. Observation of discrete time-crystalline order in a disordered dipolar many-body system. *Nature*, 543(7644):221–225, 2017.

[4] Luca D'Alessio and Marcos Rigol. Long-time behavior of isolated periodically driven interacting lattice systems. *Phys. Rev. X*, 4:041048, Dec 2014.

[5] Hossein Dehghani and Aditi Mitra. Optical hall conductivity of a floquet topological insulator. *Phys. Rev. B*, 92:165111, Oct 2015. doi: 10.1103/PhysRevB.92.165111.

[6] Hossein Dehghani and Aditi Mitra. Floquet topological systems in the vicinity of band crossings: Reservoir-induced coherence and steady-state entropy production. *Phys. Rev. B*, 93:245416, Jun 2016. doi: 10.1103/PhysRevB.93.245416.

[7] Hossein Dehghani, Takashi Oka, and Aditi Mitra. Dissipative floquet topological systems. *Phys. Rev. B*, 90:195429, Nov 2014. doi: 10.1103/PhysRevB.90.195429.

[8] Hossein Dehghani, Takashi Oka, and Aditi Mitra. Out-of-equilibrium electrons and the hall conductance of a floquet topological insulator. *Phys. Rev. B*, 91:155422, Apr 2015.

[9] Dominic V. Else and Chetan Nayak. Classification of topological phases in periodically driven interacting systems. *Phys. Rev. B*, 93:201103, May 2016. doi: 10.1103/PhysRevB.93.201103.

[10] Dominic V. Else, Bela Bauer, and Chetan Nayak. Floquet time crystals. *Phys. Rev. Lett.*, 117: 090402, Aug 2016.

[11] I. Esin, M. S. Rudner, G. Refael, and N. H. Lindner. Steady states and edge state transport in topological Floquet-Bloch systems. *ArXiv e-prints*, October 2017.

[12] V. M. Galitskii, S. P. Goreslavskii, and V. F. Elesin. Electric and magnetic properties of a semiconductor in the field ofa strong electromagnetic wave. *Sov. Phys. JETP*, 30:117, 1970.

[13] Maximilian Genske and Achim Rosch. Floquet-boltzmann equation for periodically driven fermi systems. *Phys. Rev. A*, 92:062108, Dec 2015.

[14] Thomas Iadecola and Claudio Chamon. Floquet systems coupled to particle reservoirs. *Phys. Rev. B*, 91:184301, May 2015. doi: 10.1103/PhysRevB.91.184301.

[15] Thomas Iadecola, Titus Neupert, and Claudio Chamon. Occupation of topological floquet bands in open systems. *Phys. Rev. B*, 91:235133, Jun 2015. doi: 10.1103/PhysRevB.91.235133.

[16] Liang Jiang, Takuya Kitagawa, Jason Alicea, A. R. Akhmerov, David Pekker, Gil Refael, J. Ignacio Cirac, Eugene Demler, Mikhail D. Lukin, and Peter Zoller. Majorana fermions in equilibrium and in driven cold-atom quantum wires. *Phys. Rev. Lett.*, 106:220402, Jun 2011. doi: 10.1103/PhysRevLett.106.220402.

[17] Vedika Khemani, Achilleas Lazarides, Roderich Moessner, and S. L. Sondhi. Phase structure of driven quantum systems. *Phys. Rev. Lett.*, 116:250401, Jun 2016.

[18] Mackillo Kira and Stephan W. Koch. *Semiconductor Quantum Optics*. Cambridge University Press, 2012. ISBN 978-0521875097.

[19] Takuya Kitagawa, Erez Berg, Mark Rudner, and Eugene Demler. Topological characterization of periodically driven quantum systems. *Phys. Rev. B*, 82:235114, 2010.

[20] Takuya Kitagawa, Takashi Oka, Arne Brataas, Liang Fu, and Eugene Demler. Transport properties of nonequilibrium systems under the application of light: Photoinduced quantum hall insulators without landau levels. *Phys. Rev. B*, 84:235108, Dec 2011. doi: 10.1103/PhysRevB.84.235108.

[21] Achilleas Lazarides, Arnab Das, and Roderich Moessner. Equilibrium states of generic quantum systems subject to periodic driving. *Phys. Rev. E*, 90:012110, Jul 2014.

[22] Achilleas Lazarides, Arnab Das, and Roderich Moessner. Periodic thermodynamics of isolated quantum systems. *Phys. Rev. Lett.*, 112:150401, Apr 2014.

[23] N. H. Lindner, G. Refael, and V. Galitski. Floquet topological insulator in semiconductor quantum wells. *Nature Physics*, 7:490–495, Mar 2011. doi: 10.1038/nphys1926.

[24] Dong E. Liu. Classification of the floquet statistical distribution for time-periodic open systems. *Phys. Rev. B*, 91:144301, Apr 2015.

[25] Takashi Oka and Hideo Aoki. Photovoltaic hall effect in graphene. *Phys. Rev. B*, 79:081406, Feb 2009. doi: 10.1103/PhysRevB.79.081406.

[26] Hoi Chun Po, Lukasz Fidkowski, Takahiro Morimoto, Andrew C. Potter, and Ashvin Vishwanath. Chiral floquet phases of many-body localized bosons. *Phys. Rev. X*, 6:041070, Dec 2016. doi: 10.1103/PhysRevX.6.041070.

[27] Hoi Chun Po, Lukasz Fidkowski, Ashvin Vishwanath, and Andrew C. Potter. Radical chiral floquet phases in a periodically driven kitaev model and beyond. *Phys. Rev. B*, 96:245116, Dec 2017. doi: 10.1103/PhysRevB.96.245116.

[28] Andrew C. Potter, Takahiro Morimoto, and Ashvin Vishwanath. Classification of interacting topological floquet phases in one dimension. *Phys. Rev. X*, 6:041001, Oct 2016. doi: 10.1103/PhysRevX.6.041001.

[29] Rahul Roy and Fenner Harper. Floquet topological phases with symmetry in all dimensions. *Phys. Rev. B*, 95:195128, May 2017. doi: 10.1103/PhysRevB.95.195128.

[30] Mark S. Rudner, Netanel H. Lindner, Erez Berg, and Michael Levin. Anomalous edge states and the bulk-edge correspondence for periodically driven two-dimensional systems. *Phys. Rev. X*, 3:031005, Jul 2013. doi: 10.1103/PhysRevX.3.031005.

[31] Karthik I. Seetharam. *Thermalization in Periodically-Driven Interacting Quantum Systems*. PhD thesis, California Institute of Technology, 2018.

[32] Karthik I. Seetharam, Charles-Edouard Bardyn, Netanel H. Lindner, Mark S. Rudner, and Gil Refael. Controlled population of floquet-bloch states via coupling to bose and fermi baths. *Phys. Rev. X*, 5:041050, Dec 2015. doi: 10.1103/PhysRevX.5.041050.

[33] Tatsuhiko Shirai, Takashi Mori, and Seiji Miyashita. Condition for emergence of the floquet-gibbs state in periodically driven open systems. *Phys. Rev. E*, 91:030101, Mar 2015.

[34] Tatsuhiko Shirai, Juzar Thingna, Takashi Mori, Sergey Denisov, Peter Hänggi, and Seiji Miyashita. Effective floquet–gibbs states for dissipative quantum systems. *New Journal of Physics*, 18(5):053008, 2016.

[35] S. K. Sundaram and E. Mazur. Inducing and probing non-thermal transitions in semiconductors using femtosecond laser pulses. *Nature Materials*, 1:217–, December 2002.

[36] Paraj Titum, Erez Berg, Mark S. Rudner, Gil Refael, and Netanel H. Lindner. Anomalous floquet-anderson insulator as a nonadiabatic quantized charge pump. *Phys. Rev. X*, 6:021013, May 2016.

[37] C. W. von Keyserlingk and S. L. Sondhi. Phase structure of one-dimensional interacting floquet systems. i. abelian symmetry-protected topological phases. *Phys. Rev. B*, 93:245145, Jun 2016. doi: 10.1103/PhysRevB.93.245145.

[38] N. Y. Yao, A. C. Potter, I.-D. Potirniche, and A. Vishwanath. Discrete time crystals: Rigidity, criticality, and realizations. *Phys. Rev. Lett.*, 118:030401, Jan 2017.

[39] J. Zhang, P. W. Hess, A. Kyprianidis, P. Becker, A. Lee, J. Smith, G. Pagano, I.-D Potirniche, A. C. Potter, A. Vishwanath, N. Y. Yao, and C. Monroe. Observation of a discrete time crystal. *Nature*, 543(7644):217–220, 03 2017.

*Chapter 4*

# STRONGLY-INTERACTING CLOSED FLOQUET SYSTEMS

Karthik Seetharam, Paraj Titum, Michael Kolodrubetz, and Gil Refael. Absence of thermalization in finite isolated interacting floquet systems. *Phys. Rev. B*, 97:014311, Jan 2018. doi: 10.1103/PhysRevB.97.014311. URL https://link.aps.org/doi/10.1103/PhysRevB.97.014311. K.I.S. participated in the conception of the project, performed numerical simulations, made primary contributions to the results, and participated in the writing of the manuscript.

## 4.1 Introduction

Periodically driven systems offer the tantalizing potential to engineer and control the collective behavior of quantum systems, which has been extremely useful in realizing novel phases of matter[31, 34, 35, 42, 51]. Often these driven systems support phases without any equilibrium analog such as time crystals and the so-called anomalous Floquet topological phases [21, 22, 28, 33, 54–56, 60–62, 67–69, 76, 78, 78, 79, 83]. Recently, novel Floquet phases have been observed experimentally in a variety of systems such as trapped ions, cold atoms, NV centers, and photonic devices[4, 7, 13, 32, 46, 52, 64, 85]. The high degree of control in these artificially engineered systems allows for precise implementation of periodically driven Hamiltonians and for easy measurements of local observables.

Predicting the long time dynamics of isolated interacting quantum systems remains a challenge. The generic behavior of such systems may be classified as thermal or non-thermal. The behavior of time-independent thermal Hamiltonians is well-described by the eigenstate thermalization hypothesis (ETH) [16, 18, 48, 66, 75]. According to the ETH, at long times and in the thermodynamic limit, all local observables asymptotically reach a value as given by a thermal density matrix with a temperature corresponding to the energy density of the initial state. An analogous claim can be made for periodically driven systems for which understanding such thermalization is not only crucial for experimental efforts, but also for realizing uniquely nonequilibrium phases. Given that energy is not conserved in such systems, the long-time thermal state is characterized by infinite temperature and maximal entropy[15, 39, 40]. This means that, in addition to being thermal, the long time dynamics of isolated interacting periodically driven systems is independent of the choice of the initial state.

Such a featureless state is uninteresting from both a theoretical and experimental point of view, so the questions remain as to when and how non-infinite-temperature behavior can be achieved and

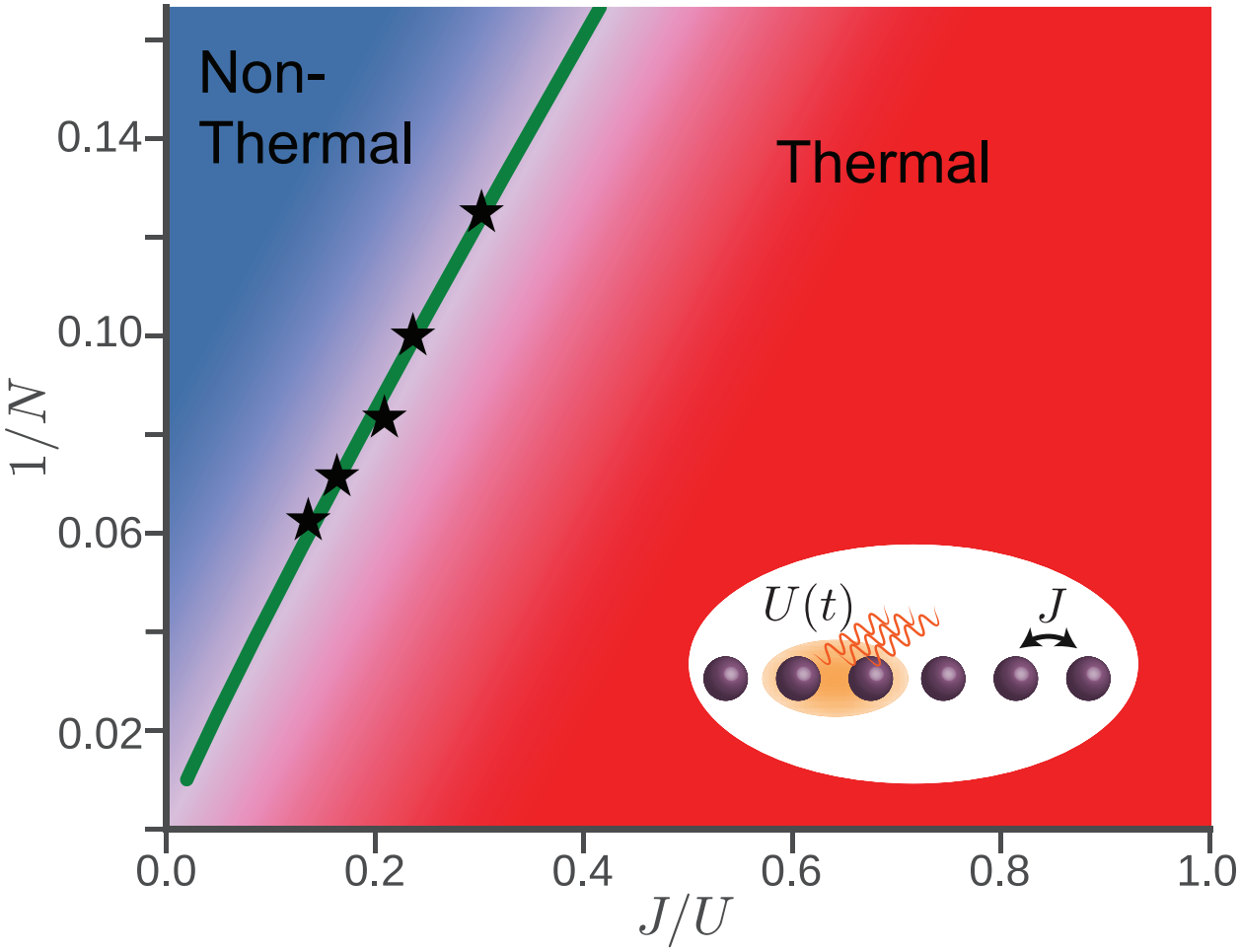


Figure 4.1: Phase diagram showing the thermal (red) and non-thermal (blue) behavior of the periodically driven model described in Eq. 4.1. We see that at finite size, $N$, and large $U/J \gg 1$, the periodically driven chain exhibits non-thermal behavior. In the thermodynamic limit, this region vanishes. The fitting points (black stars) indicate the approximate crossover region as obtained from exact diagonalization. The crossover line (green) between the thermal and non-thermal region is a power-law fit to the black stars $(\frac{J}{U})_c \approx 2.9N^{-1.1}$.

controlled. Of course, if one opens the system to engineered dissipation, it is possible to induce quasithermal steady states with finite temperature and chemical potential [17, 29, 30, 72]. However, for those systems which are well-isolated (e.g. cold atoms), alternative routes to non-thermal behavior are currently being explored. An example is quantum integrable models, which have an extensive number of local conserved quantities such that the long-time dynamics of observables are, in many cases, characterized by a generalized Gibbs ensemble (GGE)[57, 77]. Recently, it has been shown that with the appropriate choice of disorder, there is an emergent notion of integrability associated with many-body localization (MBL)[2, 48]. Furthermore, there is some evidence for partial breakdown of thermalization in translationally-invariant models[24, 74, 82]. These ideas of localization and integrability have also been extended to periodically driven systems[3, 19, 33, 41, 58, 59]. Finally, even if a system eventually thermalizes to the infinite-temperature state, it is possible that the time scale to approach such a state is quite long, and thus there exists a "prethermal" regime where interesting physics can be explored [1, 9, 23, 38, 43, 80, 84].

In this paper, we explore the effects of strong driving on an integrable model, the spinless fermionic Hubbard model with nearest-neighbor interactions. The undriven model is exactly solvable via Bethe ansatz [73]. We show that, in the thermodynamic limit, the introduction of driving leads to uncontrolled heating for all finite interaction strengths. Remarkably, at finite size, it is possible to recover non-thermal behavior for a large region in the parameter space of interactions, both for very weak and strong interactions. In both of these limits, the non-thermality is governed by a nearby (in interaction strength) integrable point that controls the behavior at finite size, a notion we will term nearly-integrable. We show that above a certain interaction scale determined by the system size, the system crosses over from non-thermal to thermal. Similar ideas about the existence of non-thermal states at finite size have been discussed in the equilibrium context in Ref. [65, 71]. We also note that recent work on integrability breaking in Floquet systems has focused on the high-frequency limit [14], studying the onset of heating as frequency is lowered. By contrast, in this work we analyze finite size scaling in regimes of highly resonant interactions as a function on interaction strength and discover nearly-integrable behavior. The complementary results provide a potential finite size scaling foundation upon which to build an analytical theory of integrability-breaking and the breakdown of the high freuqency expansion in Floquet systems.

This paper is organized as follows. In section 4.2, we introduce the model, provide a rudimentary overview of Floquet theory, describe the properties of the undriven model with a particular emphasis on finite size, and finally provide an intuitive discussion of thermalization in periodically driven systems. In section 4.3, we present the basic data of the driven model including spectral information, doublon density, and time evolution of a few representative initial states, all as a function of the interaction strength. In section 4.4, we discuss the results of finite size scaling that distinguish

the non-thermal and thermal regions. In section 4.5, we show that the origin of the non-thermal region is due to integrability and that its subsequent breakdown is responsible for the crossover to the thermal region. Finally, in section 4.6, we recapitulate the results and discuss future directions of research.

In the appendices, we further establish the robustness of our results to changes in the model. First, in appendix 4.A, we show that these results are universal in the highly resonant (i.e., low frequency) regime where $\Omega/J \sim 1$. Furthermore, we show how, at intermediate frequencies, the precise structure of the rare resonances dominates the behavior of the spectral variance of the doublon density. At sufficiently high frequencies, i.e., those above the many-body bandwidth, we recover the usual result of high frequency expansions that the dynamics are given by the time-averaged Hamiltonian, which, in our case, is just that of a free fermion static metal. In appendix 4.B, we show that the non-thermal regime exists for other waveforms. Specifically, we show that as we interpolate from a square wave to a single harmonic, the non-thermal regime exists albeit weakened by a larger crossover region. Therefore, we conclude that the non-thermal region is robust, suggesting that the general concept of near-integrability persisting at finite size occurs independent of the exact details of the model. [1]

## 4.2 Model

In this section, we first introduce a one-dimensional model for a closed periodically-driven system of spinless interacting fermions. We discuss the Floquet states which form a convenient time-dependent basis for study of a time-periodic Hamiltonian. Next, we provide some intuition for the behavior of the undriven model. Finally, we review some known results on thermalization in closed Floquet systems.

### Hamiltonian

Consider a Hamiltonian of spinless fermions interacting via nearest-neighbor Hubbard interactions,

$$\begin{aligned} H &= J\sum_i (c_i^\dagger c_{i+1} + c_{i+1}^\dagger c_i) + U(t)\sum_i n_i n_{i+1} \\ \text{with,} \qquad & U(t) = U_0 f_U(t) \end{aligned} \tag{4.1}$$

where $n_i = c_i^\dagger c_i$ is the fermion density and $U(t)$ is the time-periodic nearest-neighbor interaction coupling (see inset of Figure 4.1). Different driving protocols with angular frequency $\Omega$ are set by $f_U(t) = f_U(t + \frac{2\pi}{\Omega})$. Throughout this work, we consider the case of the lattice at half-filling and driving protocols with no static component $\int_0^T f_U(t)dt = 0$.

[1] Although, of course, the precise scaling and crossover behavior indeed should depend on model.

**Floquet Theory**

For a time-periodic Hamiltonian $H(t+T) = H(t)$, the Floquet theorem states that one may always decompose the time evolution operator as $U(t, t_0) = P(t, t_0)e^{-iH_F[t_0](t-t_0)}$ where $H_F[t_0]$ is a time-independent operator known as the stroboscopic Floquet Hamiltonian and $P(t, t_0)$, commonly called the micro-motion operator, is periodic in both arguments. The latter governs the "fast" intra-period evolution whereas the former governs the "slow" stroboscopic dynamics. Here $t_0$ is the choice of initial time for the evolution, which is equivalent to the choice of initial phase of the drive. Throughout this manuscript we use the Floquet gauge choice $t_0 = 0$ and drop the argument $t_0 = 0$ for convenience. More discussion of gauge choices can be found in appendix 4.C.

To obtain Floquet quasienergies, $\mathcal{E}$, and eigenstates, $|n_F\rangle$, throughout this manuscript we proceed by constructing $U(T, 0)$ explicitly and diagonalizing $H_F = \frac{i}{T}\log U(T, 0)$. This method is useful for periodic drives where $U(T, 0)$ can be easily written as a product of a few evolution operators, such as a square wave.

**Undriven Model**

The undriven model is integrable as it is equivalent to an XXZ chain via Jordan-Wigner transformation. In this case, one may compute the spectrum in the thermodynamic limit using Bethe ansatz. Let us, however, obtain some intuition for the simple limits of the undriven model while explicitly keeping track of finite size. For the case of pure nearest-neighbor hopping, the many-body bandwidth for a system of $M$ fermions in $N > M$ sites is $\leq 4MJ$, which, at any fixed density, scales as $NJ$. For the case of pure interaction, where for the moment we assume a nonzero static $U_0$, the many-body bandwidth is $U_0(M-1)$, which, at any fixed density, scales as $NU_0$. Note the factor of $(M-1)$ is the maximum number of doublons, defined as $\bar{n}_i = n_i n_{i+1}$, one can obtain for a finite chain system without periodic boundary conditions. With both hopping and interactions, in the case where $U_0 > NJ$, the doublon spacing $U_0$ is bigger than the bandwidth induced by hybridization, via hopping, of the doublon sectors. Hence, the doublon sectors disperse in energy but still are separated from each other. In the thermodynamic limit ($N \to \infty$) for any finite $U_0$, the doublon sectors, from a spectral point of view, merge together. The intuition gleaned from this spectral analysis is that for sufficiently large interaction $U_0$ at a given finite size, doublon character seems to persist in the eigenstates, i.e., doublons are almost conserved. This finite size persistence is a simple example of what we term as near-integrability. Indeed, in this particular case, since the undriven model is Bethe ansatz integrable [73], there is always an extensive set of conserved quantities, which, at infinite $U_0$, will again conserve doublons. However, as we will show in this work, the near-integrability behavior in the presence of strong drive is significantly different and more subtle.

**Thermalization in Floquet Systems**

Before delving into details of finite size scaling in our specific model, let us first review the generic expectations about thermalization and the role of interactions in closed systems. An undriven "thermal" system is often defined as that satisfying the eigenstate thermalization hypothesis (ETH). According to the ETH, eigenstates with similar energy will yield similar expectation values of local observables. Therefore, for an arbitrary initial state with small energy fluctuations, measurement of a local observable at late time may be replaced with measurement in the microcanonical ensemble at the same energy. As in conventional statistical mechanics, fluctuations of macroscopic conserved quantities vanish in the thermodynamic limit, leading to equivalence of ensembles.

Unlike static Hamiltonians, the presence of periodic driving destroys energy conservation and hence the "microcanonical" state is now spread over all energies; such a uniform state with no constraints is just an infinite temperature Gibbs state. Therefore, the long time steady state of a generic periodically driven interacting system is intuitively expected to be the infinite temperature diagonal ensemble [10, 15, 39, 40]. This means that the expectation value of a time-averaged local observable, $\bar{O}(t)$, starting from an arbitrary initial state, $|\psi_0\rangle$, is

$$\begin{aligned} \overline{\langle O(t)\rangle} &= \lim_{\tau\to\infty}\frac{1}{\tau}\int_0^\tau dt \langle\psi_0|U^\dagger(t)OU(t)|\psi_0\rangle \\ &= Tr[\rho_\infty O] \end{aligned} \tag{4.2}$$

where $U(t)$ is the time evolution operator and $\rho_\infty = \text{Dim}[\mathcal{H}]^{-1}\mathbb{I}$ with $\text{Dim}[\mathcal{H}]$ denoting the dimension of the Hilbert space. An important consequence of such an ensemble is that the long-time-averaged steady state value of $O$ is independent of the initial starting state.

All of these arguments about ETH and Floquet-ETH (the term we will use to characterize the infinite temperature ensemble) rely on generic and mostly unconstrained mixing of states via evolution under the Hamiltonian. This is the quantum analog of dynamical chaos leading to ergodicity in classical dynamical systems. Classically, an integrable system has an extensive number of mutually conserved quantities that destroy ergodicity; hence such systems certainly do not satisfy equilibrium statistical mechanics. In the quantum mechanical scenario, we will refer to integrability as a system with an extensive number of mutually commuting locally (additive) conserved quantities. The intuition here is the same as the classical case - the evolution of the states is highly constrained and so mixing does not really occur. With this understanding, it is clear that integrability yields non-thermal behavior.

## 4.3 Modulated Interaction

We now return to the driven case where the resonant interaction has no static value and is modulated with angular frequency $\Omega$. Unless otherwise noted, we restrict ourselves to the case where the driving frequency is much smaller than the many-body bandwidth and to a square wave drive

$$f_U(t) = \begin{cases} 1, & 0 \leq t < T/2, \\ -1, & T/2 \leq t < T, \end{cases} \tag{4.3}$$

where $T = 2\pi/\Omega$ is the period. Building upon the generic intuition developed in section 4.2, we expect that in the regime of small frequency, the periodic driving will induce a large number of resonances which allow the system to explore the full Hilbert space and result in an infinite temperature ensemble. However, as we shall show in the following, this expectation gets modified at finite size and large driving amplitude $U/J \gg 1$ where from now on we drop the subscript on $U_0$, writing $U$ for brevity.

For the special case of $J = 0$, the model is trivially solvable, as any state picks up exactly the opposite phase during the first half of the cycle as during the second half, resulting in a perfect echo with $\mathcal{E} = 0$ for all eigenstates. However, in the presence of any small but finite $J$, the $U \to \infty$ limit is actually markedly different from $J = 0$, as the perfect many-body echo is immediately destroyed. To gain simple intuition, we numerically solve for the quasienergy spectrum for $N = 10$ and $N = 12$ at half-filling. The results for both system sizes, for two limiting cases – $U \gg J$ (blue) and $U \sim J$ (red) – are shown in Figure 4.1. We have set $\Omega/J = 0.83$ which is well below the many-body bandwidth, implying we are in the highly resonant regime. Remarkably, we see that the Floquet spectrum with large driven interaction ($U/J = 100$ fixed for both sizes) shows plateau structures, which suggest that the influence of doublons is strong even when no static interaction is present. In contrast, for small interaction ($U/J = 0.59$ fixed for both sizes), the Floquet spectrum looks continuous throughout the Floquet zone. We further note that increasing the system size while keeping the interaction fixed leads to a softening of the plateaus, suggesting that these effects may be related to the fact that our system is not in the thermodynamic limit.

### Doublon Density

To systematically explore the presence of quasienergy plateaus in the Floquet spectrum, we calculate the density of doublons in each of the Floquet states.

$$\hat{D} = \frac{1}{\frac{N}{2} - 1} \sum_i n_i n_{i+1} \tag{4.4}$$

The factor $N/2 - 1$ in the denominator is the maximum number of doublons achievable for a chain of length $N$ at half-filling. This normalization factor ensures that the observable is bounded, $D \equiv \langle \hat{D} \rangle \in [0, 1]$, and is independent of system size.

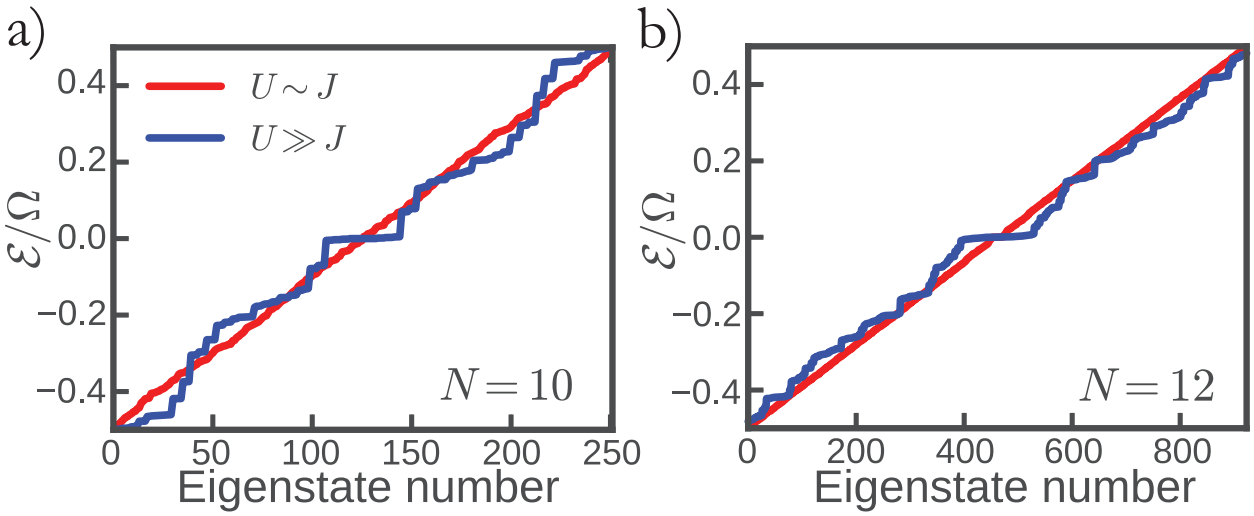


Figure 4.1: Quasienergy spectrum for $N = 10$ (a) and $N = 12$ (b) at $\Omega/J = 0.83$. Blue dots denote strong interaction $U/J = 100$ and red dots denote weak interactions at $U/J = 0.59$. We see that weak interactions give rise to a continuous spectrum. In contrast, the strong interactions yield separation of the spectrum into quasienergy plateaus reflecting the influence of doublons ($\sum_i n_i n_{i+1}$). Increasing system size softens the plateaus.

As discussed in Section 4.2, periodic driving is expected to lead to an infinite temperature ensemble, and as a result, any local observable measured in any Floquet state must yield the same value. In the infinite temperature ensemble at half-filling, one may explicitly calculate the expectation value of the doublon density

$$\begin{aligned} D &= \binom{N}{\frac{N}{2}}^{-1} \mathrm{Tr}(\hat{D}) \\ &= \frac{1}{\binom{N}{\frac{N}{2}}\left(\frac{N}{2}-1\right)} \sum_{k=1}^{\frac{N}{2}-1} k \binom{\frac{N}{2}+1}{k+1}\binom{\frac{N}{2}-1}{k} = \frac{1}{2} \end{aligned} \tag{4.5}$$

where $\binom{n}{k}$ denotes the binomial factor. Intuitively, one may understand this result as summing over $N/2$ particles with each particle having a neighbor with probability $1/2$ since the infinite temperature density matrix encodes no correlations. Hence, if we observe $D \neq 0.5$ for a Floquet state, we may conclude that the state is by definition non-thermal. It is important to note that even if a state yields $D = 0.5$, it is possible that another observable exists that can be measured which results in a value different from that given by an infinite temperature state. However, since our efforts to understand thermalization in this work focus on large $U$, we will use this observable as an indicator of non-thermality.

We examine the distribution of the doublon correlations by defining the variance of $D_n \equiv \langle n_F|\hat{D}|n_F\rangle$ over the Floquet eigenstates $|n_F\rangle$ as $\Sigma = \mathrm{var}_n(D_n)$. As we will see shortly, this spectral doublon

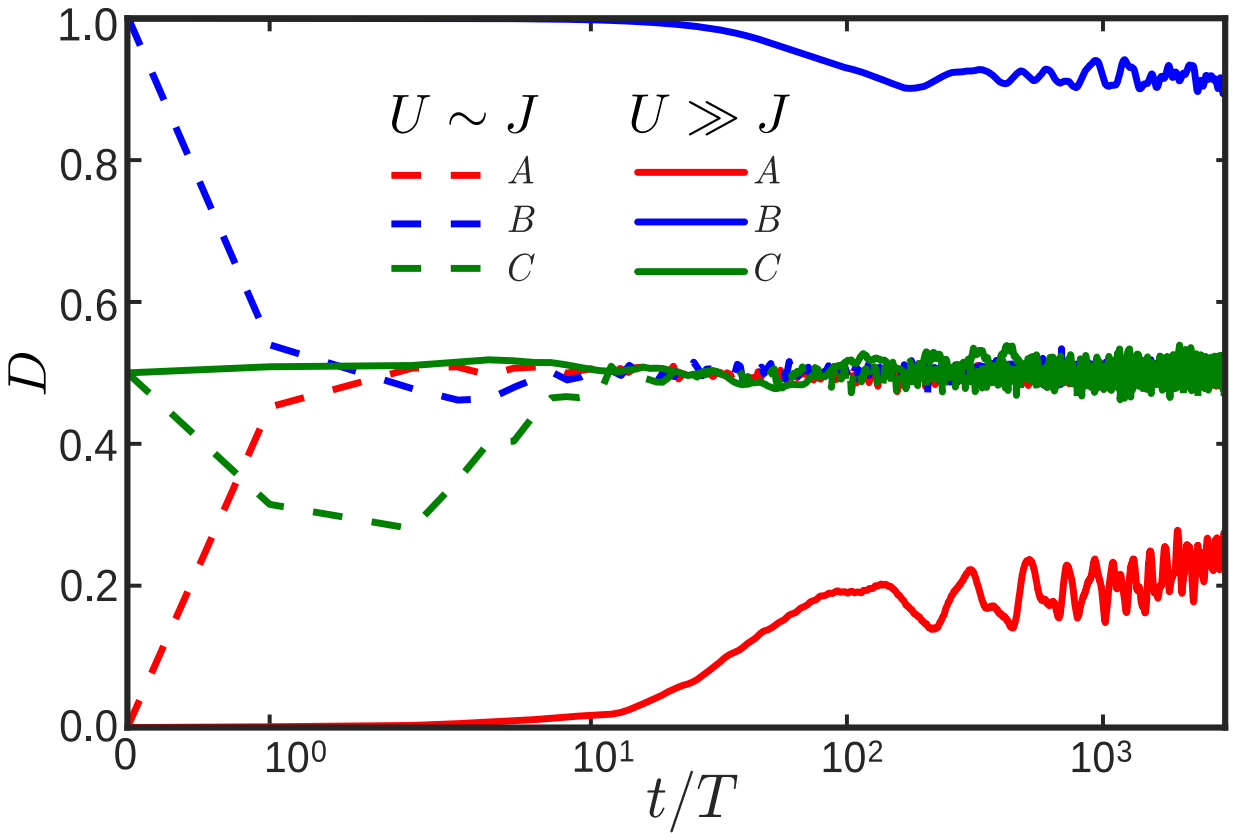


Figure 4.2: Time evolution of three initial states for weak and strong interactions ($U/J = 0.59$ and $U/J = 100$ respectively): $A = |101010...\rangle$, $B = |111...000\rangle$, and $C = (C^N_{N/2})^{-1/2} \sum_{i=1}^{C^N_{N/2}} |i\rangle$. For weak interactions all states thermalize as expected. For strong interactions, the initial states with non-thermal doublon values ($A$, $B$) maintain non-thermal values over time whereas $C$ remains thermal.

variance will be quite useful in characterizing how the the entire spectrum changes as a function of coupling and system size.

**Time Evolution**

Let us now focus on the time-dependence of the doublon density for initial states which are not Floquet eigenstates and hence not stationary. We consider three example states: $A = |101010...\rangle$, $B = |111...000\rangle$, and $C = (C^N_{N/2})^{-1/2} \sum_{i=1}^{C^N_{N/2}} |i\rangle$ which are, respectively, a no-doublon state, a maximum-doublon state, and a state composed of an even superposition of all real space occupation basis states ($C^N_{N/2} = \binom{N}{N/2}$ is the number of basis states at half-filling). Figure 4.2 shows the time dependence of $D$, at fixed system size $N = 12$ and $\Omega/J = 0.83$, for large and small values of interaction (the same as those in Figure 4.1). The $C$ state, which begins with a thermal $D$ value, stays as such during time evolution. However, the evolution of the $A$ and $B$ states, which begin

with non-thermal values of $D$, remain non-thermal at large interaction strength with quite small temporal fluctuations. This memory of the initial doublon density at long times suggests that the Floquet eigenstates have significant overlap with states of definite doublon number, although one cannot definitively conclude this on the basis of finite time data alone as the possibility of prethermalization exists. This supports our intuition that doublons are indeed an appropriate characterization of physics in this model and are a useful signature of non-thermality. In contrast, for small interaction, resonances efficiently mix doublon-like states and all initial conditions evolve to a thermal $D$ value.

### 4.4 Scaling

In this section, we explore the dependence of the doublon density on system size and interaction strength at a fixed frequency $\Omega/J = 0.83$. We show that two different regimes, characterized as non-thermal and thermal, arise, each with distinct scaling behavior of the spectral variance of the doublon density. The two regimes are separated by a crossover in interaction strength that has power-law dependence in system size.

To understand these statements, let us first consider the histogram of $D$ over all Floquet eigenstates in the spectrum as a function of the coupling $U/J$ (Figure 4.1). Interestingly, at large values of interaction, $U/J \gg 1$, the Floquet spectrum exhibits a large variance in the values of $D$ characteristic of non-thermal behavior due to integrable behavior in the $U/J \to \infty$ limit (see Section 4.5 for detailed discussion). As the interaction decreases to $U/J \sim O(1)$ , there is a tight clustering of $D$ values around 0.5. This infinite temperature thermal behavior is due to the heating and mixing expected from that of a generic closed driven interacting system. For very small values of interaction, $U/J \ll 1$, the spectrum has some doublon variance close to that of a purely static metallic spectrum ($U \to 0$). This is precisely the same type of finite-size non-thermal behavior manifesting itself around the free fermion integrable point. Near this point, however, doublons are not the ideal observable suited to gauging non-thermality and so the deviations away from the infinite temperature value are weak. We will term the situation when non-thermality arises due to finite size as near-integrability.

As the system size $N$ increases, we see that the thermal region gets more tightly centered around the infinite temperature value and persists to stronger interaction. Moreover, the near-integrability region governed by free fermions shrinks closer to $U/J = 0$. Therefore, extrapolating to the thermodynamic limit, we conclude that the entire system is likely in a thermal phase for any nonzero finite interaction strength. This is precisely the usual infinite temperature scenario for a generically non-integrable Floquet system. Regardless of the featureless thermodynamic limit, however, Figure 4.1 demonstrates that small system sizes host non-thermal regimes.

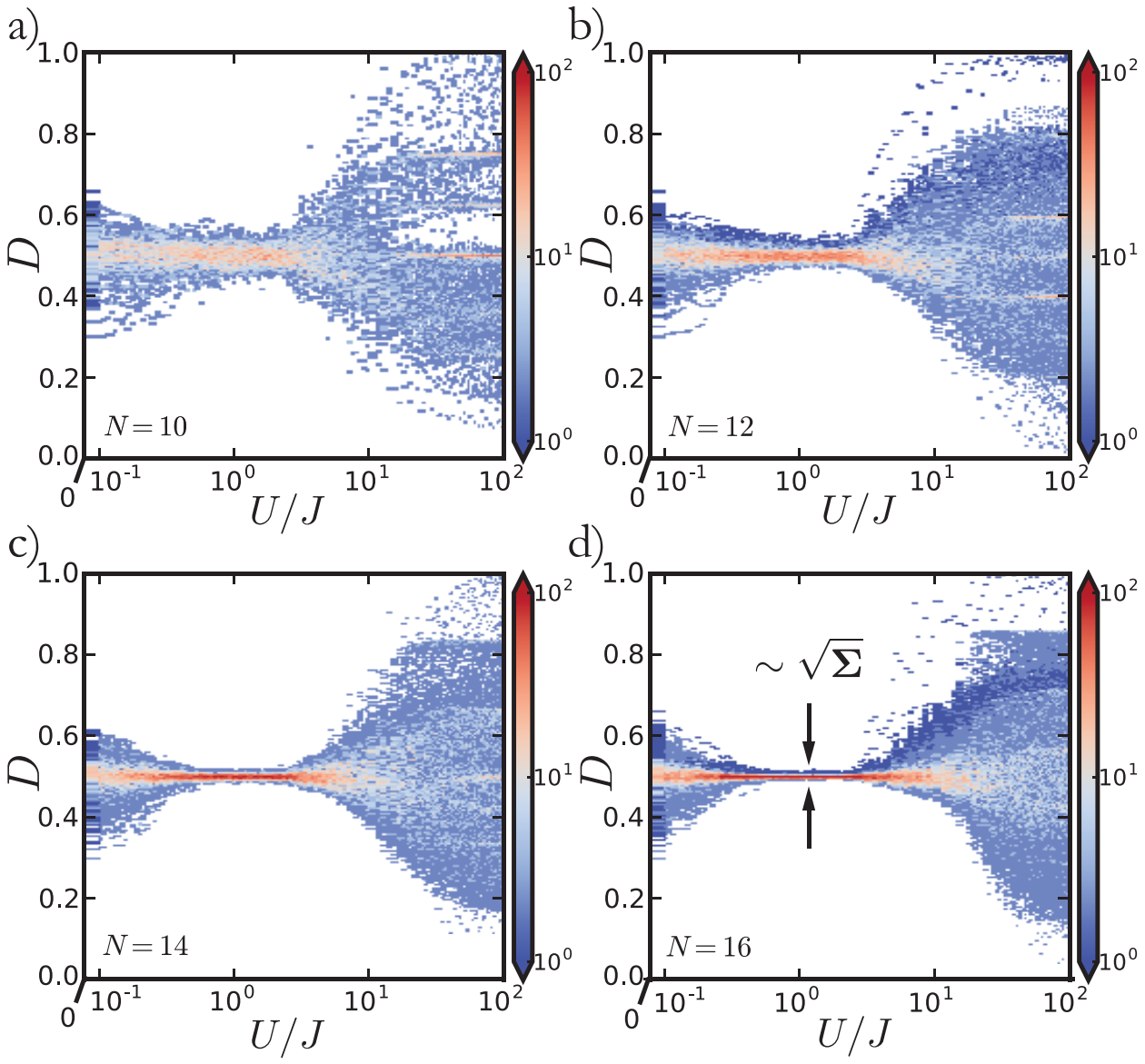


Figure 4.1: Histogram of $D_n$ measured in each Floquet eigenstate as a function of $U/J$ and system size. For $U/J \ll 1$, the spectrum displays some spread in the doublon density due to near-integrability close to the free fermion limit $U = 0$. At $U/J \sim O(1)$, however, sufficient mixing leads to a tight squeeze of $D$ around 0.5, indicating a thermal region. At strong interactions $U/J \gg 1$, there is significant spread of $D$ also indicating non-thermal behavior.

The spread of the distribution of the doublon density characterizes the non-thermality of the system at a particular interaction strength. In line with this expectation, we calculate the log spectral variance $\ln(\Sigma)$ of $D$ for various system sizes as a function of $J/U$ in Figure 4.2a. The variance clearly indicates each of the regions discussed above: the free fermion near-integrability region for $J/U \gg 1$, the thermal region for $J/U \sim O(1)$ with the smallest variances, the crossover region with midpoints denoted by black stars, and the non-thermal region $J/U \ll 1$ with the largest variances (also a near-integrability region). Note that black stars representing the crossover region are not uniquely defined. Here, we choose them to be close to the midpoint between the average log spectral variance values in the non-thermal and thermal regions.

We can distinguish the thermal and non-thermal regimes quantitatively by observing their distinct scaling forms (see Eq. 4.6). In Figure 4.2b, we see that the variance has simple exponential decay in system size with no dependence on interaction. In contrast, Figure 4.2c shows that the non-thermal regime has a non-trivial scaling function (denoted by $f$ in Eq. 4.6) with joint dependence on system size and interaction.

$$\Sigma = \begin{cases} e^{\kappa N}, (\kappa = -0.77) & \text{Thermal} \\ e^{N^{\alpha} f(N^{\beta}\frac{J}{U})}, (\alpha = 0.45, \beta = 2.0) & \text{Non} - \text{thermal} \end{cases} \tag{4.6}$$

Taking the midpoints of the crossover region as an approximate “phase boundary," we obtain the power-law

$$\left(\frac{J}{U}\right)_c \approx 2.9 N^{-1.1} \tag{4.7}$$

shown in Figure 4.1. The power-law exponent for the crossover may be understood as the intermediary behavior between the limits given by the two scaling forms - the non-thermal region suggests a crossover dependence of $N^{-\beta}$ while the thermal region suggests no system size dependence. As expected, the non-thermal region seems to vanish in the thermodynamic limit at fixed values of the couplings and drive, but there is still a non-trivial dependence on system size that suggests that heating will not take place given the appropriate order of limits.

### 4.5 Integrability and its breakdown

The source of the non-thermal regime at large interaction strength is the integrability of the system in the limit $U/J \to \infty$. Note that this integrable limit is *not* the same the $J = 0$ integrable point, a distinction that will become clear shortly. In this section, we discuss the $U/J \to \infty$ integrable

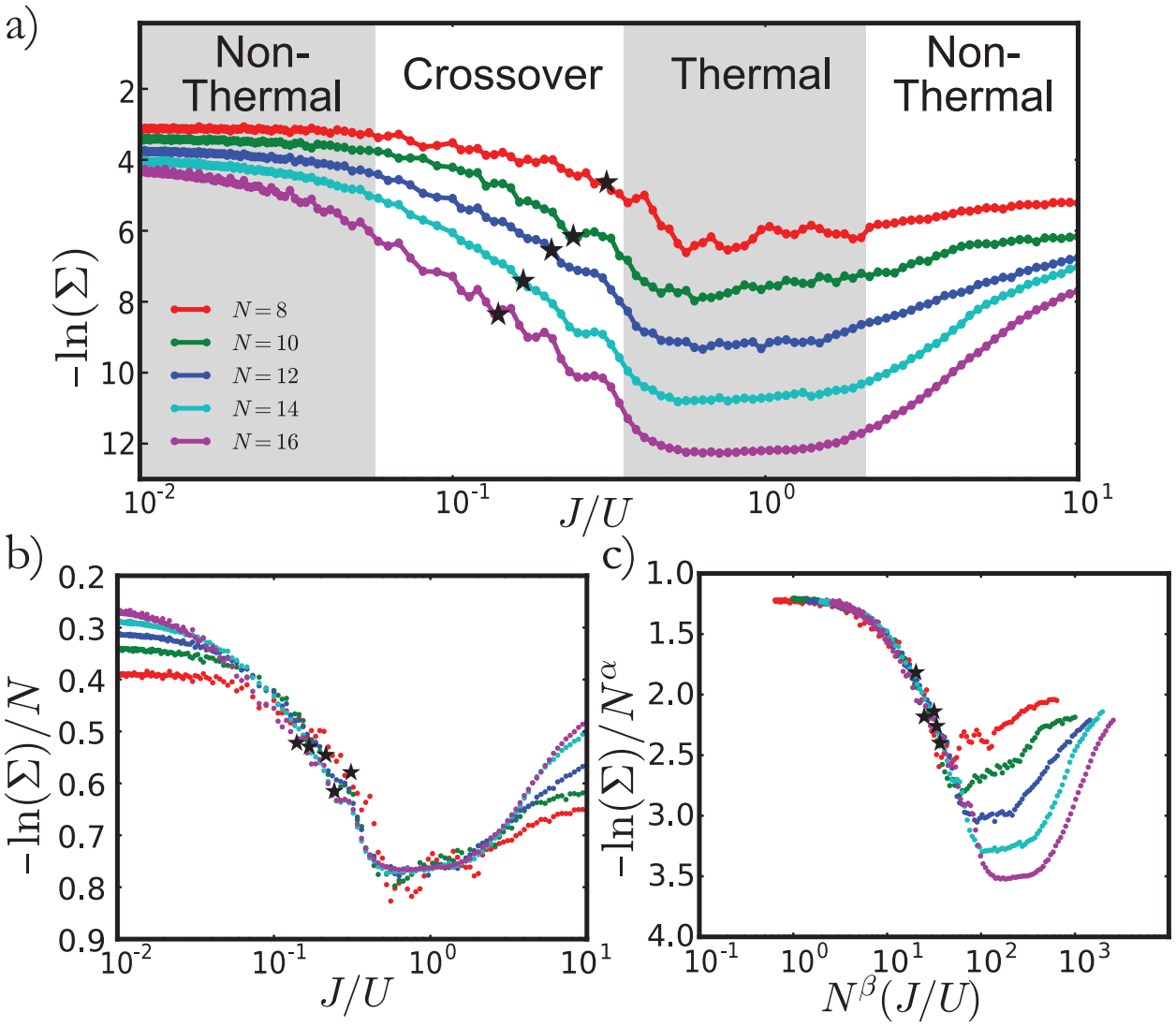


Figure 4.2: Dependence of doublon log spectral variance on coupling and and system size. Figure a) shows raw data which demonstrate the three regions clearly, near-integrability for $J/U \gg 1$, thermal for $J/U \sim O(1)$, and non-thermal (also near-integrability) for $J/U \ll 1$. The black stars indicate the approximate midpoint of the crossover region. Figure b) rescales the axes to show the scaling collapse of the thermal region indicating simple exponential behavior independent of coupling. Figure c) rescales the axes differently to show the scaling collapse of the non-thermal region with $\alpha = 0.45$ and $\beta = 2.0$.

limit of the Floquet Hamiltonian, following which we analyze the breakdown of integrability in a perturbative expansion in $J/U$. Finally, we also discuss the onset of the infinite temperature thermal phase from the perspective of this expansion.

Effective Hamiltonians for Floquet systems are often obtained by perturbative methods, treating inverse frequency, $\Omega^{-1}$, as a small parameter. In our system, we explicitly consider the highly resonant regime at strong drive strength, so direct application of high frequency expansions (HFE) such as Magnus or van Vleck is invalid. Rather, to obtain a controlled expansion in the limit of large interaction strength, it is convenient to go into a frame rotating with the driven interaction term, similar to that used for the Fermi-Hubbard model in Ref. [11, 26, 36, 45, 49]. In this rotating frame, the Fourier harmonics of the Hamiltonian come with sharply peaked coefficients, which upon use in the van Vleck expansion, yields a controlled expansion in $J/U$. Let us see how this procedure works.

Consider changing frame via the unitary transformation, $V(t) = \exp\left(-i\kappa F(\Omega t)\sum_j n_j n_{j+1}\right)$, where $F(\Omega t) = \int f_U(t) d(\Omega t)$. This drive is chosen to cancel the bare interaction term and replace it by strong oscillations of the dressed hopping term. This gives the rotated Hamiltonian $\tilde{H} = i\partial_t(V^\dagger)V + V^\dagger H V$, with

$$\tilde{H} = \sum_{m=0,\pm1} \tilde{H}_m e^{im\kappa F(\Omega t)} \tag{4.8}$$

$$\tilde{H}_0 = J\sum_j \delta_{n_{j-1},n_{j+2}}(c_j^\dagger c_{j+1} + c_{j+1}^\dagger c_j) \tag{4.9}$$

$$\tilde{H}_1 = J\sum_j \left(n_{j-1}(1-n_{j+2})c_j^\dagger c_{j+1} + n_{j+2}(1-n_{j-1})c_{j+1}^\dagger c_j\right)$$

$$\tilde{H}_{-1} = \tilde{H}_1^\dagger \tag{4.10}$$

where $\kappa = U/\Omega$ and $\delta_{n_{j-1},n_{j+2}} = (1 - n_{j-1} - n_{j+2} + 2n_{j-1}n_{j+2})$ is a constraint which allows nearest neighbor hopping only if both adjacent sites are either occupied or unoccupied. Decomposing the rotated Hamiltonian into harmonics, $\tilde{H} = \sum_l e^{il\Omega t}\tilde{H}^{(l)}$, we obtain the relation $\tilde{H}^{(l)} = \sum_{m=0,\pm1}\tilde{H}_m\alpha_l(m\kappa)$ where $\alpha_l$ are the Fourier coefficients of the rotating frame drive: $e^{im\kappa F(\Omega t)} = \sum_l e^{il\Omega t}\alpha_l(m\kappa)$. Importantly, for a square wave drive, $\alpha_l(m\kappa)$ is peaked to a constant of order 1 around $l = \pm m\kappa$ and quickly decays away from this point, a crucial property for our approach which will exist much more generally than just the square wave considered here. Performing the HFE in this frame produces an effective Hamiltonian $H_{\text{eff}} = H_{\text{eff}}^{[0]} + H_{\text{eff}}^{[1]} + H_{\text{eff}}^{[2]} + \ldots$ with terms $H_{\text{eff}}^{[n]} \sim \Omega^{-n}$ that do not seem to appear small. The fact that $\alpha_l(m\kappa)$ is sharply peaked counteracts the inverse frequency coefficient precisely in a way so as to yield an approximate $J/U$

expansion. Therefore, even though we are not in the limit of large frequency, the expansion is physically meaningful. By performing an appropriate rotation of the effective Hamiltonian computed up to $n$-th order, we obtain an approximate stroboscopic Floquet Hamiltonian $H_F^{[n]}$. More details on the rotating frame and subsequent high frequency expansion may be found in Appendix 4.C.

The leading order term of the HFE in the limit $\kappa \to \infty$ yields $H_F^{[0]} = H_{\text{eff}}^{[0]} = \tilde{H}_0$. This corresponds to the time-independent correlated hopping model arising from the aforementioned constraint. Note that this is quite interesting since the $U \to \infty$ limit yields a non-trivial correlated hopping model, quite different from the case of $J = 0$ which, in the rotated frame, would yield $\tilde{H}(J = 0) = 0$. Furthermore, the $J = 0$ Hamiltonian has locally conserved doublon numbers while the correlated hopping model in $U \to \infty$ only has a globally conserved doublon number, though as we will see shortly, it is still an integrable model. Higher order corrections such as $H_{\text{eff}}^{[2]}$ break both this global doublon number symmetry and integrability as discussed briefly below and in more detail in Appendices 4.C and 4.D.

Let us now discuss the integrability of the correlated hopping Hamiltonian, $\tilde{H}_0$ defined in Eq. 4.9. A priori it is not obvious that $\tilde{H}_0$ maps into an integrable Hamiltonian. The Hilbert space of $\tilde{H}_0$ are states with fermions at half-filling. Let us start by mapping the Hilbert space to states defined on its dual-lattice, given by the position of the domain walls which separate an occupied region from an unoccupied one. For example, on 10 sites [2],

$$|0011111000\rangle \to |0d0000d00\rangle \tag{4.11}$$

It is possible to rewrite the constrained hopping processes as nearest neighbor hopping of pairs of domain walls,

$$\begin{aligned} |\cdots 1011\cdots\rangle \leftrightarrow |\cdots 1101\cdots\rangle \equiv |\cdots dd0\cdots\rangle \leftrightarrow |\cdots 0dd\cdots\rangle, \\ |\cdots 0010\cdots\rangle \leftrightarrow |\cdots 0100\cdots\rangle \equiv |\cdots 0dd\cdots\rangle \leftrightarrow |\cdots dd0\cdots\rangle, \end{aligned}$$

with the constraint that the domain walls, $d$, are hardcore particles. Note that flipping $1 \leftrightarrow 0$ in the original fermions, maps to the same state of domain walls. This is a result of a particle-hole symmetry of $\tilde{H}_0$ in the language of the bare fermions. Also note that the correlated hopping conserves the total number of doublons. Therefore, the doublon spectral variance $\Sigma$, and indeed the full counting statistics of the doublon number, may be readily obtained in the $U \to \infty$ limit[3].

[2] We assume open boundary conditions throughout the whole paper. In this case, there is no distinction between fermions and hardcore bosons. However, if considering the system on a ring, then one must be careful about (anti-)periodic boundary conditions as exchange statistics are relevant [49].

[3] This is acheivable using the probability of finding a $k$-doublon state of a half-filled $N$ site system given by $p_N(k) = \binom{\frac{N}{2}+1}{k+1}\binom{\frac{N}{2}-1}{k}$ as in Eqn. 4.5.

This pair hopping of domain walls can be further mapped to free fermions. To do so, we map the basis states of the domain walls, denoted as a string of $d$s and 0s, into those of a new particle $\tilde{d}$ in a truncated Hilbert space as follows:

1. If a site is unoccupied, leave it alone: $0 \to 0$
2. Given a string of $d$'s, replace them pairwise by $\tilde{d}$'s: $d \to \emptyset$, $dd \to \tilde{d}$, $ddd \to \tilde{d}$, $dddd \to \tilde{d}\tilde{d}$ and so on.

This second step comes from noting that an isolated $d$ particle is essentially frozen, such that a pair of $d$s can hop right through it, or equivalently the $d$ particle reassociates into a new pair. Thus isolated $d$s play no dynamical role, and may be removed from the Hilbert space. We note here that a similar mapping to free fermions from repulsive nearest-neighbor interacting fermions has been done in Ref. [12]. However, it remains an open question as to whether more general constrained hopping models are integrable.

Interestingly, the above mapping takes several different states of $d$s to the same state of $\tilde{d}$s. This is a hidden symmetry in $\tilde{H}_0$ and gives rise to massive degeneracy in its energy spectrum. Since the $\tilde{d}$ particles behave like a pair of domain walls, the Hamiltonian $\tilde{H}_0$ in this new basis is just free particle hopping with matrix element $J$, i.e., $\tilde{H}_0 = J \sum_i \tilde{d}_i^\dagger \tilde{d}_{i+1} + h.c.$. This is the origin of the integrability when $U \to \infty$ keeping $J$ finite. We expect that the long-time limit of the non-thermal regime is smoothly connected to this $U \to \infty$ free fermion integrable point. Therefore we hypothesize that the long-time state in the non-thermal regime is well-described by a time-periodic GGE [40, 57, 70, 77] from the perspective of local observables. An explicit check is the subject of future work.

Having understood integrability of the infinite $U$ case, we can now briefly discuss its breakdown at finite $U$ and how this behavior changes as a function of system size. At finite large $U$, there are additional contributions to $H_{\text{eff}}$. For example, even at zeroth order in the HFE (see Eq. 4.19), there are additional contributions from $\alpha_0(\pm\kappa)\tilde{H}_{\pm 1}$. As discussed in Appendix 4.C, the terms in $\tilde{H}_{\pm 1}$ result in pair-creation/annihilation of $d$ particles. At second order (the first order term vanishes by symmetry of the drive), higher harmonics contribute to the effective Hamiltonian. As a result, this mapping to free $\tilde{d}$ particles breaks down. Thus, higher order terms may break integrability while keeping the HFE convergent. However, an alternative mechanism also exists. For a given finite $U$, the HFE itself may be invalid (or inaccurate), possibly at all orders, which certainly would break the infinite $U$ integrability.

In principle, the breakdown of integrability due to higher order terms and the breakdown of the HFE can occur with distinct system size dependence. One can envision two possible scenarios for

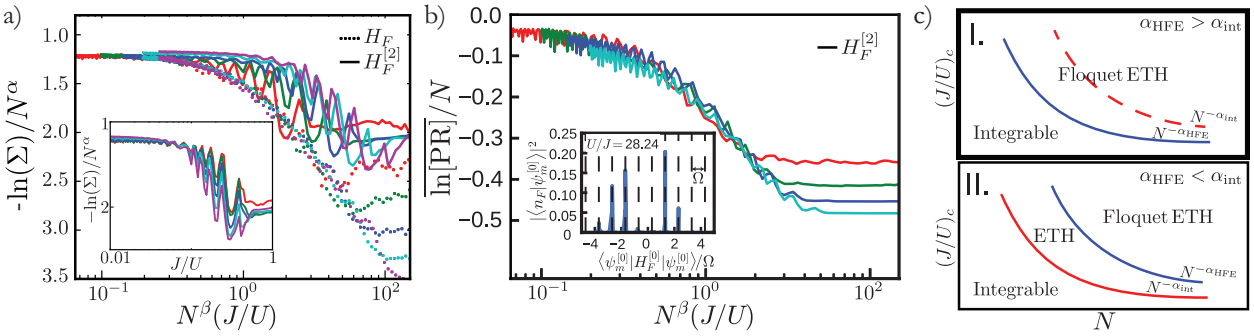


Figure 4.1: Dependence of the doublon log spectral variance on coupling and system size for both $H_F$ and $H_F^{[2]}$. Figure a) compares the data from Figure 4.2c to the same data gathered from $H_F^{[2]}$. Note that $H_F^{[2]}$ has a different scaling form as shown in the inset, displaying a much weaker dependence on system size. Breakdown of the HFE happens faster than the breakdown of integrability within the HFE, apparently resulting in a direct transition from integrability to an infinite temperature Floquet-ETH phase. Figure c) depicts this scenario in the bold top box while displaying an alternative possibility in the bottom box which contains an intermediate finite-temperature ETH phase. Figure b) displays the average log participation ratio (LPR) of exact Floquet eigenstates in the basis of zeroth-order HFE eigenstates. Note that the LPR has the same scaling form as the log spectral variance and is a good measure of delocalization (here due to resonances) of exact Floquet eigenstates in the basis of zeroth-order HFE states. An explicit example of this is shown in the inset for a representative exact Floquet eigenstate.

the crossover from integrable dynamics at $U \to \infty$ to an infinite temperature Floquet-ETH phase at finite $U$,

1. Integrable, Non-Thermal $\to$ Non-Integrable, Floquet-ETH
2. Integrable, Non-Thermal $\to$ Non-Integrable, Finite Temperature ETH $\to$ Non-Integrable, Floquet-ETH

The second scenario is plausible when a non-integrable effective Hamiltonian is obtained from a convergent HFE. With these two cases in mind, we examine the variance of the doublon density, comparing that of $H_F^{[2]}$ with that of the exact Floquet Hamiltonian. As shown in Figure 4.1a, the variance data from $H_F$ has a scaling collapse for the non-thermal plateau that breaks down at an earlier point than that of the non-thermal region predicted by $H_F^{[2]}$. In fact, as shown in the inset, $H_F^{[2]}$ exhibits a different scaling form for the non-thermal plateau. Therefore, our data indicate that the breakdown of the HFE – yielding a Floquet-ETH phase – happens first, corresponding to the first scenario. Hence, we do not observe any physics corresponding to a finite temperature ETH states. If we assume the finite-size breakdown of integrability within the HFE and of the HFE itself correspond to distinct finite-size scaling laws $(J/U)_c \sim N^{-\alpha_{\mathrm{int}}}$ and $(J/U)_c \sim N^{-\alpha_{\mathrm{HFE}}}$ respectively,

as depicted in Figure 4.1c, then our data indicates that $\alpha_{\text{HFE}} > \alpha_{\text{int}}$. If instead we had $\alpha_{\text{HFE}} < \alpha_{\text{int}}$, we would be able to achieve the second scenario where a finite temperature ETH regime emerges between the integrable and infinite temperature Floquet-ETH phases.

Finally, the breakdown of the HFE provides an explanation for the physical mechanism of thermalization. There remain two possible routes to the breakdown of the HFE. The first is the breakdown of the operator expansion, whereby the magnitude of the higher order terms relative to the zeroth order term becomes significant. In Appendix 4.D, we examine the behavior of the trace-norm of the second order term, $H^{[2]}_{\text{eff}}$ in comparison with the zeroth order term, $H^{[0]}_{\text{eff}}$. As shown in Figure 4.D.3 (Appendix 4.D), this does not capture the finite size scaling of the crossover region. While for small $J/U$ the trace-norm of $H^{[2]}_{\text{eff}}$ increases as a function $(J/U)^2$, it has no finite-size dependence which is inconsistent with the scaling observed in the distribution of the doublon density. This rules out a breakdown of the operator expansion, at least at second order.

The second route is through a proliferation of resonances [10]. This proliferation is analogous to a localization-delocalization transition in the space of many-body eigenstates of $H^{[0]}_{\text{eff}}$ (denoted by $|\psi^{[0]}_m\rangle$). When $J/U \to 0$, the exact Floquet eigenstates (denoted by $|n_F\rangle$) are identical to $|\psi^{[0]}_m\rangle$, corresponding to a localized state. As $J/U$ increases, the drive induces resonances with states energetically separated by $\Omega$ such that the eigenstates of $H^{[0]}_{\text{eff}}$ cease to faithfully represent the Floquet eigenstates due to non-perturbative instanton-like effects. It has been argued [10, 81] that in fact no finite-order HFE eigenstates capture these resonances, which is consistent with our results for $H^{[2]}_F$ (not shown). Therefore, when these resonances become active, the HFE completely breaks down. We can quantify the breakdown by viewing the proliferation of resonances as a delocalization of the exact Floquet states in the space of the zeroth-order HFE eigenstates,$\{|\psi^{[0]}_m\rangle\}$. This property is nicely characterized by the spectrum-averaged log participation ratio (LPR), $\overline{\ln[\text{PR}]} = \text{Dim}[\mathcal{H}]^{-1} \sum_{n_F} \ln\left(\sum_m |\langle n_F|\psi^{[0]}_m\rangle|^4\right)$, shown in Figure 4.1b. With increasing $J/U$, the participation ratio decreases, indicating eigenstate delocalization. The scale at which the LPR plateaus roughly agrees with the scale at which the eigenstates appear to be thermal. Furthermore, the system size scaling is consistent with that of the doublon density. This strongly indicates that in our system, the proliferation of resonances is responsible for the breakdown of the HFE. The inset in Figure 4.1b shows an explicit example of the appearance of such resonances, which are already active at a relatively strong drive $U/J = 28.24$.

In summary, we have shown that the non-thermal behavior of the driven Hamiltonian at large $U/J$ can be traced back to the integrability of the $U \to \infty$ point, where the HFE gives the effective description of the Floquet eigenstates. At finite system sizes, non-thermal behavior is observed at a large but finite $U/J$. The crossover from the integrable-to-thermal behavior of the eigenstates as a function of $U/J$ is governed by the proliferation of resonances induced by the drive. The finite

size scaling of such resonant breakdown is numerically consistent with the finite size scaling of the doublon density, a fact which remains to be understood analytically.

### 4.6 Discussion and Conclusions

We have studied a strongly-driven system of interacting spinless fermions and found an unexpected non-thermal regime at large interaction strength and finite system size. We have shown that this non-thermal regime is due to the integrability of the system at infinite $U$ that weakly persists to large but finite $U$ at finite size, a phenomenon that we call near-integrability. We found power-law scaling of the crossover region, i.e. where the system goes from integrable to non-integrable, with system size. We argued that this crossover comes from a breakdown of the high-frequency expansion leading immediately to an infinite temperature Floquet-ETH phase with no intervening finite temperature regime for our choice of parameters. Further evidence for the qualitative independence of these phenomena upon the details of the model may be found in the appendices.

Our analysis from the effective $J/U$ expansion indicates the intriguing possibility of a periodically driven system in which integrability is first broken to a finite temperature ETH phase before breaking down to the infinite temperature Floquet-ETH phase. This scenario seems plausible and is quite interesting in that it runs counter to the commonly held intuition that isolated, periodically driven interacting systems heat to infinite temperature. Reference [14] studies integrability breakdown in a driven Heisenberg chain as one moves away from high frequency limit. In a certain parameter regime, they find evidence for such a finite temperature ETH (as well as another regime where resonant breakdown occurs). In the present model, such a phase is expected to arise when $J \ll \Omega \ll U$ (or perhaps less interestingly, at even higher frequencies $\Omega \gg U \gg J$) such that resonances vanish while the interactions still strongly influence the states. Future work to explore such a intermediate phase and connect it to related finite time phenomena such as prethermalization [1, 23, 80] remains an ongoing challenge.

Our results are immediately relevant to a wide variety of engineered quantum systems, where finite system size is currently a given. Even in larger systems, our finite size scaling should provide insight into the local thermalization dynamics of finite size subsystems, which may be coarse grained towards understanding the larger-scale thermalization dynamics of the full system. This is deeply related to time scales for prethermalization, in which the dynamics is dominated by the nearby integrable point [5, 6, 20, 27, 37, 44, 47].

We can estimate the scaling of the prethermalization time $t^*$ for an infinite system by assuming that a finite subsystem appears thermal with respect to local observables when $N \geq N^*$ due to sufficient mixing. Noting that $J$ sets the characteristic velocity in the model, we may approximate the prethermalization time as $t^* \sim N^*/J = (U/J^3)^{1/2}$ using the scaling behavior at the edge of the

non-thermal region.

We expect that understanding the finite size and finite time scaling in a more rigorous way – as done in this work for one model – will allow better understanding of heating mechanisms. This in turn should allow control of heating, which is a crucial step for the experimental realization of novel Floquet phases that are able skirt their boring infinite temperature fate. While preparing this manuscript, the authors became aware of upcoming complementary work by by Peronaci et al.[53].

*Acknowledgements*. The authors would like to thank Jim Garrison, Marin Bukov, Anatoli Polkovnikov, Evert van Nieuwenburg, Yuval Baum, Min-Feng Tu and Joel Moore for insightful discussions. MK thanks funding from the Laboratory Directed Research and Development from Berkeley Laboratory, provided by the Director, Office of Science, of the U.S. Department of Energy under Contract No. DEAC02-05CH11231, and from the U.S. DOE, Office of Science, Basic Energy Sciences as part of the TIMES initiative. GR and KS are grateful for support from the NSF through DMR-1410435, the Institute of Quantum Information and Matter, an NSF Frontier center funded by the Gordon and Betty Moore Foundation, the Packard Foundation, and from the ARO MURI W911NF-16-1-0361 “Quantum Materials by Design with Electromagnetic Excitation" sponsored by the U.S. Army. KS is additionally grateful for support from NSF Graduate Research Fellowship Program. P.T. is supported by National Research Council postdoctoral fellowship, and acknowledges funding from ARL CDQI, NSF PFC at JQI, ARO, AFOSR, ARO MURI, and NSF QIS.

# APPENDIX

## 4.A Frequency Dependence

In this appendix, we consider a fixed system size $N = 12$ and study how the spectral variance changes as a function of frequency and interaction strength. Previously, we discussed the variance properties for the highly resonant case at low frequencies. In the opposite limit, at very large frequencies surpassing the many-body bandwidth, the system can be effectively described by the time-averaged Hamiltonian. For our model, the time-averaged Hamiltonian is just free fermions with nearest-neighbor hopping. Therefore, at very large frequencies, we expect the variance to be the same as that of a static metal with no dependence on interaction. Indeed, we see these two limits in Figure 4.A.1.

For intermediate frequencies, where state mixing due to resonances is weaker, the variance shows peaks at even integer values of $U/\Omega$. This is due to the fact that the square wave contains only odd harmonics of $\Omega$. At odd multiples of $\Omega$, the system has an additional resonance contributing to mixing thereby decreasing the variance closer to its thermal value. The peaks at even integer values of $U/J$ are precisely the opposite situation where these extra processes are most energetically suppressed consequently resulting in weaker mixing. We have checked that indeed choosing different waveform compositions changes this peaking phenomena accordingly (not shown). The conceptual point here is that in the intermediate frequency regime, the system is quite sensitive to the rare resonances that occur and hence the precise details of the spectrum and drive carry serious impact on its the thermalization properties. Overall, however, even if resonances are weaker, the same general onset of non-thermal behavior with increasing interaction exists.

## 4.B Waveform Dependence

In this section, we work in the highly resonant regime at fixed system size $N = 10$ and discuss how the choice of waveform can alter the behavior of the thermal to non-thermal transition. We can study this systematically by introducing a parameter $n$ that denotes the number of steps the waveform takes in approximating a single cosine harmonic over a period, i.e., we discretize the cosine function in time with $n$ steps and the amplitude of the $j$-th step given by $\cos(\frac{2\pi j}{n})$ for $j = 0, 1, \ldots, n-1$. The case of $n = 2$ corresponds to the square wave. As $n \to \infty$, we obtain a perfect cosine function. In between, we may track how continuous interpolation between a square wave and a single harmonic affects the variance.

Figure 4.B.1 shows four cases of how the variance changes with increasing $n$. Upon increasing $n$ from 2 to 4, we see a sudden drop of the variance. Again increasing $n$ from 4 to 6 results in a resurgence of the variance. Finally, at $n = 100$ where we well-approximate a cosine drive, the

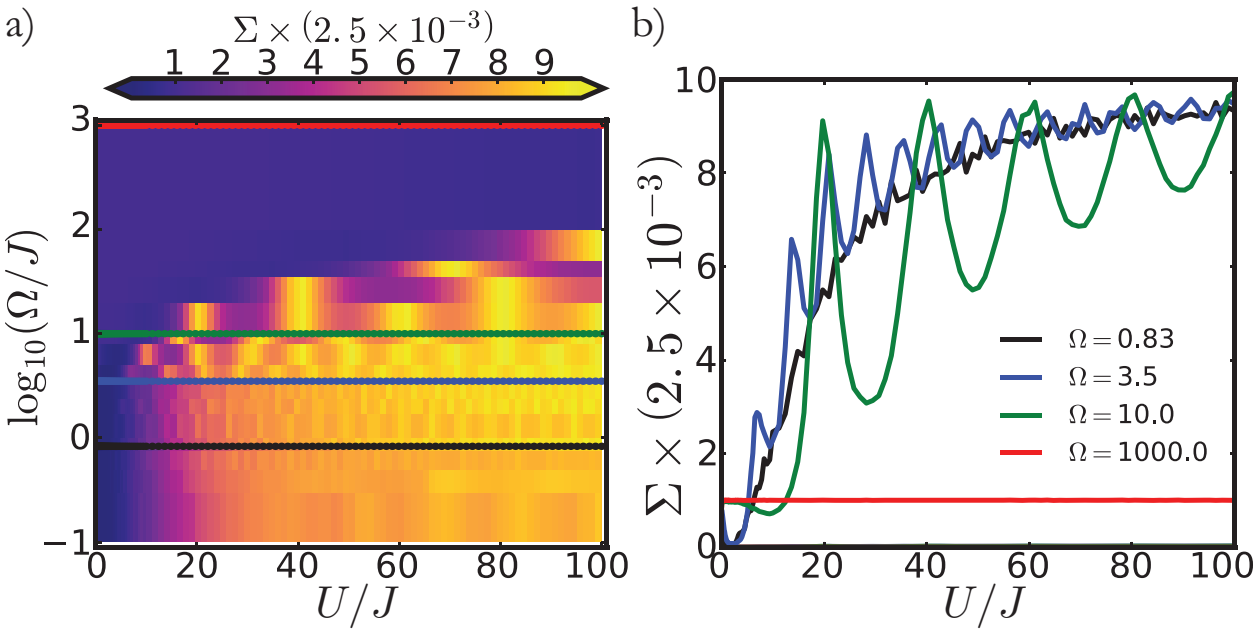


Figure 4.A.1: Frequency dependence of spectral doublon variance as a function of coupling $U/J$ at $N = 12$. Figure a) shows frequency along the y-axis and coupling along the x-axis with color denoting the variance value. Figure b) shows cuts at particular frequencies. In the high frequency limit, the system is approximated by the time-averaged lab frame Hamiltonian, leading to a variance given by static free fermions. In the low-frequency limit, we get the variance behavior discussed in the text which shows the thermal to non-thermal transition as $U/J$ gets larger. At intermediate frequencies, the rare resonances govern the precise details of the variance (e.g. peaking) and the system is quite sensitive to drive parameters.

variance grows roughly linearly as a function of interaction.

The intuition for this seemingly odd behavior is apparent by considering the time evolution operator over one period $U(T, 0)$. The unitary $U(T, 0)$ contains Hamiltonians $H_j$ constructed from the discrete cosine amplitudes. For $n = 2$, the interaction contributes terms with amplitudes $U, -U$ for time steps of $T/2$ and so $U(T, 0)$ spends all its time with the interaction at $|U/J|$. In contrast, for $n = 4$, the interaction contributes terms with $U, 0, -U, 0$ for time steps of $T/4$. In this case, we see that for half the time period, $U(T, 0)$ contains evolution due to a purely static non-interacting metal. Intuitively speaking, this severely weakens the “effective" interaction scale over a period and thus leads to a more thermal variance than the case of $n = 2$ where the $U = 0$ values are absent. Upon further increasing the sampling to $n = 6$, the interaction steps no longer contain the $U = 0$ value and hence the variance returns to a larger value. Of course, however, at fixed $U/J$, $n = 6$ indeed has a weaker effective interaction scale than that of a square wave and so the variance, while still demonstrating the same overall trend to non-thermality with increasing interaction, is dampened. This trend saturates apparently with approximately linear growth of variance with $U/J$ for a single

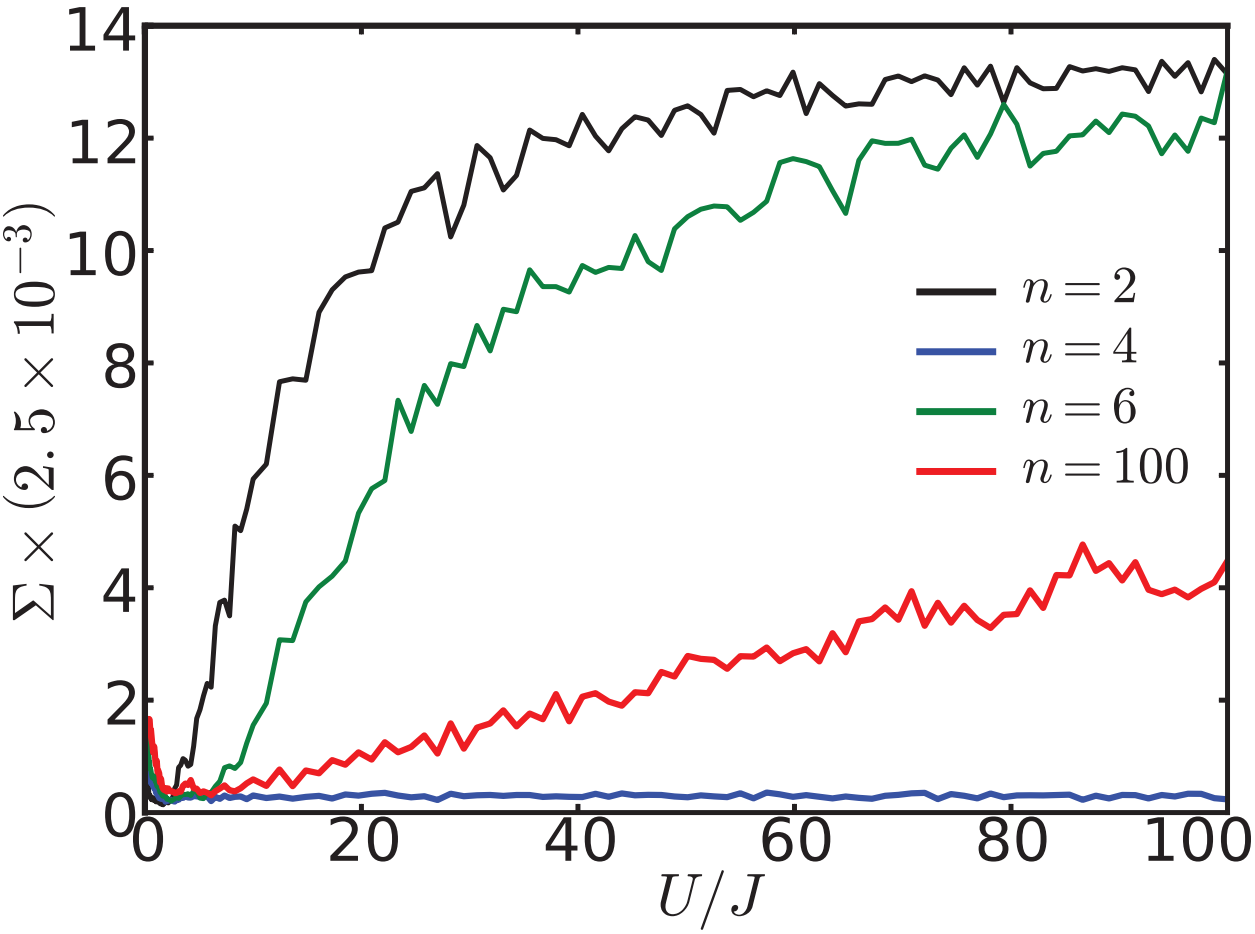


Figure 4.B.1: Waveform dependence of spectral doublon variance as a function of coupling $U/J$ at $\Omega/J = 0.83$. A square wave is given by $n = 2$ and a cosine is closely approximated by $n = 100$. In between, the discretization of sampling a waveform gives rise to dampening and resurgence effects as can be understood by considering the time-evolution operator over one period $U(T, 0)$ (see text). Overall, the thermal to non-thermal transition persists for a cosine drive but has significantly slower crossover behavior as compared to the square drive.

harmonic at $n = 100$. All of this suggests that even though a single harmonic contains contributes fewer resonances than a square wave, which apriori one might expect to lead to more non-thermal behavior, the fact that the effective interaction scale is greatly reduced at fixed $U/J$ for a single harmonic dominates the thermal to non-thermal crossover behavior.

### 4.C Derivation of the Effective $J/U$ Expansion

In this section, we provide the derivation of an effective $J/U$ expansion derived from a van Vleck high frequency expansion (HFE), though we are explicitly not working at high frequency. We move

to a rotating frame which eliminates the interaction term via the unitary transformation

$$\begin{aligned} \tilde{H} &= i\partial_t(V^\dagger)V + V^\dagger H V \\ |\tilde{\psi}\rangle &= V^\dagger|\psi\rangle \\ V(t) &= e^{-i\kappa F(\Omega t)\sum_j n_j n_{j+1}} \end{aligned} \tag{4.12}$$

where $\kappa = U/\Omega$, and $F(\Omega t)$ is the integral of the drive with respect the variable $\Omega t$. This yields the transformation of the annhilation operator $\tilde{c}_i = V^\dagger(t)c_i V(t) = e^{-i\kappa F(\Omega t)(n_{i-1}+n_{i+1})}c_i$ which can be immediately used to construct the rotated Hamiltonian

$$\begin{aligned} \tilde{H} &= J\sum_i (\tilde{c}_i^\dagger \tilde{c}_{i+1} + h.c.) \\ &= J\sum_i (e^{i\kappa F(\Omega t)(n_{i-1}-n_{i+2})}c_i^\dagger c_{i+1} + h.c.) \end{aligned} \tag{4.13}$$

Note that the time-dependence of the rotated Hamiltonian disappears if $n_{i-1} = n_{i+2}$, a property which will lead to interesting results. The above form suggests a convenient expansion $\tilde{H} = \sum_{m=0,\pm1}\tilde{H}_m e^{im\kappa F(\Omega t)}$ upon factoring out the operator content in the exponential in (4.13).

$$\begin{aligned} \tilde{H}_0 &= J\sum_j \delta_{n_{j-1},n_{j+2}}(c_j^\dagger c_{j+1} + c_{j+1}^\dagger c_j) \\ \tilde{H}_1 &= J\sum_j \left(n_{j-1}(1-n_{j+2})c_j^\dagger c_{j+1} + n_{j+2}(1-n_{j-1})c_{j+1}^\dagger c_j\right) \\ \tilde{H}_{-1} &= \tilde{H}_1^\dagger, \end{aligned} \tag{4.14}$$

where $\delta_{n_{j-1},n_{j+2}} = (1 - n_{j-1} - n_{j+2} + 2n_{j-1}n_{j+2})$ is a constraint which allows nearest-neighbor hopping only if $n_{i-1} = n_{i+2}$, i.e. the adjacent sites have the same density. This type of correlated hopping preserves total doublon number. In sharp contrast, $\tilde{H}_{\pm1}$ allows nearest-neighbor hopping only if $n_{i-1} \neq n_{i+2}$ and therefore can be understood as doublon creation and annihilation. Hence, these terms explicitly break the global doublon number symmetry. If one were to think about this correlated hopping in terms of domain wall dynamics on the bonds of the lattice, $\tilde{H}_0$ would be responsible for nearest-neighbor hopping of domain wall pairs (see section 4.5 and appendix 4.D) while $\tilde{H}_{\pm1}$ would be responsible for domain wall pair creation and annihilation. This intuitive understanding suggests that in the limit of $U \to \infty$, where only $\tilde{H}_0$ is active on average, $\tilde{H}$ is integrable. Formalizing this intuition mathematically is rather tough, but we discuss an algorithm for checking integrability in appendix 4.D.

Decomposing the rotated Hamiltonian into harmonics, $\tilde{H} = \sum_l e^{il\Omega t}\tilde{H}^{(l)}$, we obtain the relation $\tilde{H}^{(l)} = \sum_{m=0,\pm1}\tilde{H}_m\alpha_l(m\kappa)$ where $e^{im\kappa F(\Omega t)} = \sum_l e^{il\Omega t}\alpha_l(m\kappa)$ are the harmonic expansions of the time-dependent exponentials. For a square drive, we obtain

$$\alpha_l(m\kappa) = \frac{i}{2\pi}\left(\frac{e^{-i\pi(l-m\kappa)}-1}{l-m\kappa} + \frac{1-e^{i\pi(l+m\kappa)}}{l+m\kappa}\right) \tag{4.15}$$

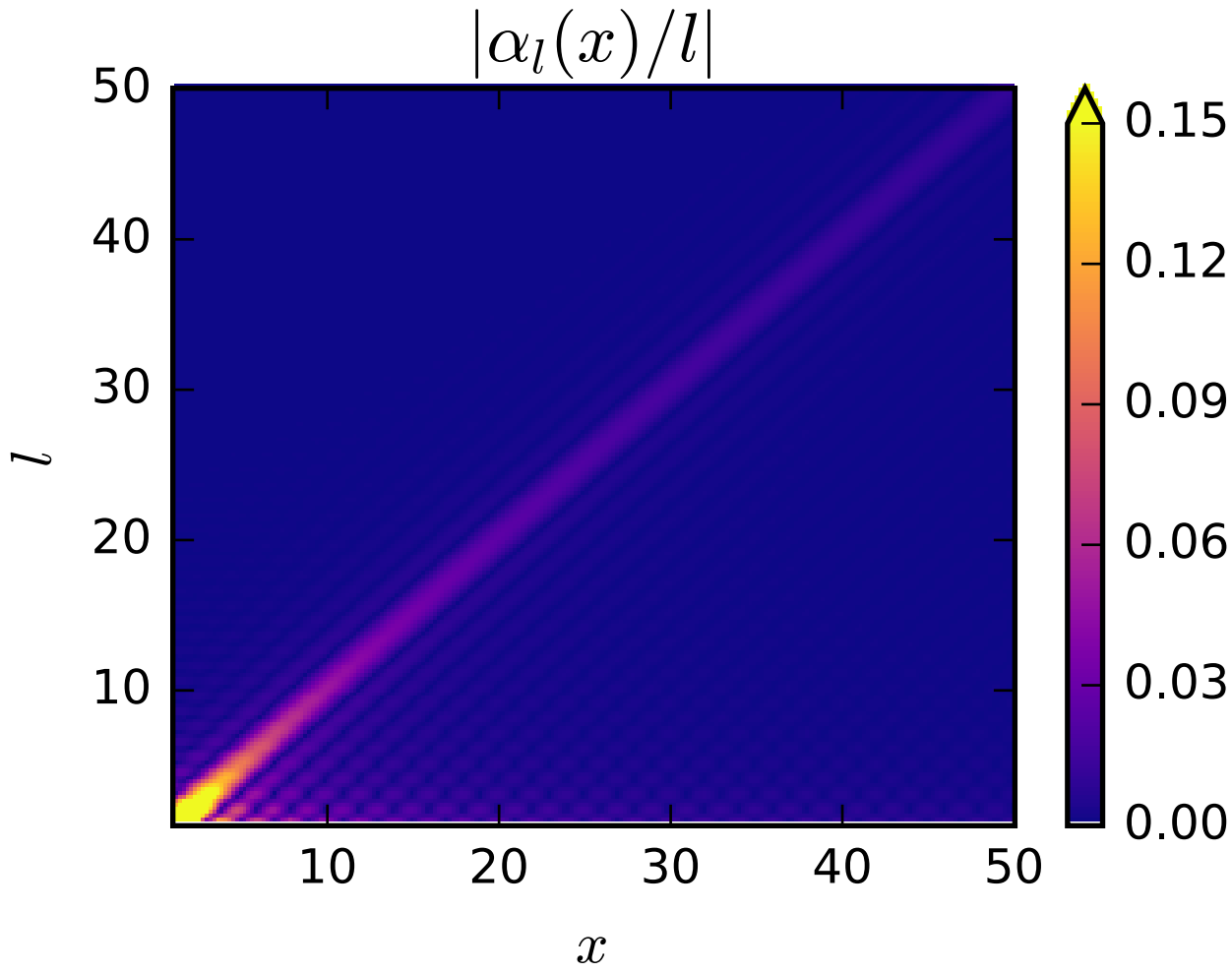


Figure 4.C.1: Harmonic coefficients of $e^{ixF(\Omega t)}$ in Eqn. 4.15 for the square wave which control the periodic time-dependence in the rotating frame. The quick decay away from the peak at $l = x$ allows for a controlled $J/U$ expansion.

and for a cosine drive, we obtain Bessel functions $\alpha_l(m\kappa) = \mathcal{J}_l(m\kappa)$. Note that in the case of a square drive, the coefficients are peaked at $l = \pm m\kappa$ with power-law decay (see Figure 4.C.1). This crucial property allows us to interpret the HFE as an effective (and approximate) $J/U$ expansion as we will see shortly.

The general evolution operator for a Floquet system [8] has a periodic piece, $P(t, t_0) \equiv e^{-iK_F[t_0](t)}$, and a static piece $H_F[t_0]$, both of which depend on a choice of gauge $t_0$. The Hermitian operator $K_F[t_0](t)$ is known as the stroboscopic kick operator. Gauge transformations between choices of initial times are implemented with the micromotion operator $H_F[\tilde{t}_0] = P(\tilde{t}_0, t_0)H_F[t_0]P^\dagger(\tilde{t}_0, t_0)$ where of course, by periodicity of $P$, initial times are only defined within a period.

Instead of choosing a single $t_0$, one might consider an alternative scenario where a symmetric gauge

choice is selected such that no $t_0$ per se is favored. This particular gauge choice is useful if one wants to discuss a single Floquet Hamiltonian, which we will call the effective Hamiltonian, without the ambiguity of which initial time point was chosen. To this end, define a unitary transformation on the stroboscopic Floquet Hamiltonian $H_{\text{eff}} = e^{iK_{\text{eff}}(t_0)} H_F[t_0] e^{-iK_{\text{eff}}(t_0)}$ such that the kick operators $K_{\text{eff}}(t_0)$ are defined to rotate a given choice of stroboscopic Floquet Hamiltonian to the effective Hamiltonian. By using the gauge change formula for $H_F[t_0]$, one finds that $P(t, t_0) = e^{-iK_F[t_0](t)} = e^{-iK_{\text{eff}}(t)} e^{iK_{\text{eff}}(t_0)}$, which immediately leads to the conclusion that the $H_{\text{eff}}$ is indeed the static Hamiltonian obtained by rotating from the original frame with $e^{-iK_{\text{eff}}(t)}$ instead of $P(t, t_0)$ which would yield $H_F[t_0]$. With these definitions, the general evolution has two representations

$$\begin{aligned} U(t_2, t_1) &= P(t_2, t_0) e^{-iH_F[t_0](t_2 - t_1)} P^\dagger(t_1, t_0) \\ &= e^{-iK_F[t_0](t_2)} e^{-iH_F[t_0](t_2 - t_1)} e^{iK_F[t_0](t_1)} \\ &= e^{-iK_{\text{eff}}(t_2)} e^{-iH_{\text{eff}}(t_2 - t_1)} e^{iK_{\text{eff}}(t_1)} \end{aligned} \tag{4.16}$$

where the kick and stroboscopic kick operators coincide if $K_{\text{eff}}(t_0) = 0$; this also means that the stroboscopic and effective Floquet Hamiltonian coincide. Quasienergy spectra are unaffected by kick operators since they are just a rotation of the Floquet Hamiltonian but measurement of observables requires one to take them into account.

In general, exact formulas for the effective Hamiltonians and kick operators are difficult to come by, so quite often one resorts to a high frequency expansion with $H_{\text{eff}}$ encoding the gauge-symmetric Floquet Hamiltonian and $K_{\text{eff}}$ encoding the explicit gauge change information. We will not rederive the results here and resort to quoting the series expansion for the effective Hamiltonian and kick operators up to second order from references [25, 63].

$$H_{\text{eff}} = H_{\text{eff}}^{[0]} + H_{\text{eff}}^{[1]} + H_{\text{eff}}^{[2]} + \ldots \tag{4.17}$$

$$K_{\text{eff}} = K_{\text{eff}}^{[0]} + K_{\text{eff}}^{[1]} + K_{\text{eff}}^{[2]} + \ldots \tag{4.18}$$

In the main text, we have considered quasienergy states and spectra obtained from $U(T, 0)$ and so kick operators used for numerical results are evaluated at $t = 0$ (the particular gauge we have chosen for the stroboscopic Floquet Hamiltonian). We define $H_F^{[n]}$ as the $n$-th order approximation to the stroboscopic Floquet Hamiltonian obtained from the HFE.

$$
\begin{aligned}
H^{[0]}_{\rm eff} &= \mathcal{H}_0 \\
H^{[1]}_{\rm eff} &= \frac{1}{\Omega}\sum_{j=1}^{\infty}\frac{1}{j}[\mathcal{V}^{(j)},\mathcal{V}^{(-j)}] \\
H^{[2]}_{\rm eff} &= \frac{1}{2\Omega^2}\sum_{j=1}^{\infty}\frac{1}{j^2}[[\mathcal{V}^{(j)},\mathcal{H}_0],\mathcal{V}^{(-j)}] \\
&\quad + \frac{1}{3\Omega^2}\sum_{j,l=1}^{\infty}\frac{1}{jl}([\mathcal{V}^{(j)},[\mathcal{V}^{(l)},\mathcal{V}^{-(j+l)}]] - [\mathcal{V}^{(j)},[\mathcal{V}^{(-l)},\mathcal{V}^{-(j-l)}]]) + \text{h.c.} \\
K^{[0]}_{\rm eff}(t) &= 0 \\
K^{[1]}_{\rm eff}(t) &= \frac{1}{i\Omega}\sum_{j=1}^{\infty}\frac{1}{j}(\mathcal{V}^{(j)}e^{ij\Omega t} - \mathcal{V}^{(-j)}e^{-ij\Omega t}) \\
K^{[2]}_{\rm eff}(t) &= \frac{1}{i\Omega^2}\sum_{j=1}^{\infty}\frac{1}{j^2}[\mathcal{V}^{(j)},\mathcal{H}_0]e^{ij\Omega t} + \frac{1}{2i\Omega^2}\sum_{j,l=1}^{\infty}\frac{1}{j(j+l)}[\mathcal{V}^{(j)},\mathcal{V}^{(l)}]e^{i(j+l)\Omega t} \\
&\quad + \frac{1}{2i\Omega^2}\sum_{j\neq l=1}^{\infty}\frac{1}{j(j-l)}[\mathcal{V}^{(j)},\mathcal{V}^{(-l)}]e^{i(j-l)\Omega t} + \text{h.c.}
\end{aligned}
\tag{4.19}
$$

where $\mathcal{H}_0 = \tilde{H}^{(0)}$ and $\mathcal{V}^{(j)} = (1-\delta_{j,0})\tilde{H}^{(j)}$. Inserting the harmonics of the rotated Hamiltonian, we obtain

$$
\begin{aligned}
H^{[0]}_{\rm eff} &= \tilde{H}_0 + \sum_{m\neq 0}\tilde{H}_m\alpha_0(m\kappa) \\
H^{[1]}_{\rm eff} &= \sum_{(m,m')\neq 0}[\tilde{H}_m,\tilde{H}_{m'}]\sum_{j=1}^{\infty}\frac{\alpha_j(m\kappa)\alpha_{-j}(m'\kappa)}{j\Omega} \\
H^{[2]}_{\rm eff} &= \sum_{(m,m')\neq 0}[[\tilde{H}_m,\tilde{H}_0],\tilde{H}_{m'}]\sum_{j=1}^{\infty}\frac{\alpha_j(m\kappa)\alpha_{-j}(m'\kappa)}{2\Omega^2 j^2} \\
&\quad + \sum_{(m,m',m'')\neq 0}[[\tilde{H}_m,\tilde{H}_{m'}],\tilde{H}_{m''}] \\
&\quad \left(\sum_{j=1}^{\infty}\frac{\alpha_j(m\kappa)\alpha_0(m'\kappa)\alpha_{-j}(m''\kappa)}{2\Omega^2 j^2} + \sum_{j,l=1}^{\infty}\frac{(1-\delta_{jl})\alpha_{-l}(m\kappa)\alpha_{-(j-l)}(m'\kappa)\alpha_j(m''\kappa)}{3\Omega^2 jl}\right. \\
&\quad \left. - \sum_{j,l=1}^{\infty}\frac{\alpha_l(m\kappa)\alpha_{-(j+l)}(m'\kappa)\alpha_j(m''\kappa)}{3\Omega^2 jl}\right) + \text{h.c.}
\end{aligned}
\tag{4.20}
$$

$$
\begin{aligned}
K_{\text{eff}}^{[0]}(t) &= 0 \\
K_{\text{eff}}^{[1]}(t) &= \sum_{m\neq 0} \tilde{H}_m \sum_{j\neq 0} \frac{\alpha_j(m\kappa)e^{ij\Omega t}}{ij\Omega} \\
K_{\text{eff}}^{[2]}(t) &= \sum_{m\neq 0} [\tilde{H}_m, \tilde{H}_0] \sum_{j=1}^{\infty} \frac{\alpha_j(m\kappa)}{i\Omega^2 j^2} e^{ij\Omega t} \\
&\quad + \sum_{(m,n)\neq 0} [\tilde{H}_m, \tilde{H}_n] \left( \sum_{j=1}^{\infty} \frac{\alpha_j(m\kappa)\alpha_0(n\kappa)}{i\Omega^2 j^2} e^{ij\Omega t} + \sum_{j,l=1}^{\infty} \frac{\alpha_j(m\kappa)\alpha_l(n\kappa)}{2i\Omega^2 j(j+l)} e^{i(j+l)\Omega t} \right. \\
&\quad \left. + \sum_{j\neq l=1}^{\infty} \frac{\alpha_j(m\kappa)\alpha_{-l}(n\kappa)}{2i\Omega^2 j(j-l)} e^{i(j-l)\Omega t} \right) + \text{h.c.}
\end{aligned}
\tag{4.21}
$$

where we have made use of the property $\alpha_l(0) = \delta_{l,0}$. Utilizing the peaking behavior of the $\alpha$ coefficients, we may understand the scaling of each term with $J/U$. We wish to compare the strength of each successive order of $H_{\text{eff}}$ to the zeroth order term which scales as $J$. The first order, $H_{\text{eff}}^{[1]}$, comes with a single commutator that yields two powers of $J$. Since each of the $\alpha$ coefficients are peaked when the subscript and arguments match (up to a sign), whenever the peaks of the two $\alpha$ coefficients overlap to give a nonzero contribution to the sum over $j$, they provide a scaling of $\kappa\Omega = U$ in the denominator, i.e. $j\Omega \to m\kappa\Omega = mU$. For a given system size $N$, the sum of the commutators provides some scaling with $N$ and so we denote the overall scaling of the first order term, relative to the zeroth order term, as $(J/U)f_1(N)$. Repeating the same arguments for the second order term gives three powers of $J$ and a denominator with two powers of $U$ for an overall relative scaling of $(J/U)^2 f_2(N)$. Each successive order gives one more power of $J$ due to an extra nested commutator and another power of $U$ in the denominator due to replacement of some $j\Omega$ term with $U$. Therefore, up to errors introduced by the power law decay of the $\alpha$ coefficients, we have constructed an approximate $J/U$ expansion from the HFE.

The convergence properties and error bounds on such an expansion are largely unknown at this point in time. Two possibilities for such an expansion are that series is convergent or that it is asymptotic with an $n$ order expansion accurately describing the dynamics for some finite period of time, although recent work suggests that the latter is more likely[81].

We delay further detailed analysis of this series and instead demonstrate the validity of our expansion by considering the large $U$ limit and comparing the exact Floquet spectrum to the spectrum of the effective Hamiltonian at various orders. Figure 4.C.2 shows the comparison of spectra between the exact Floquet Hamiltonian, zeroth (neglecting $H_{\pm 1}$ terms - valid at large $U$), and second order effective Hamiltonian. Note that the first order term vanishes identically due to the symmetry

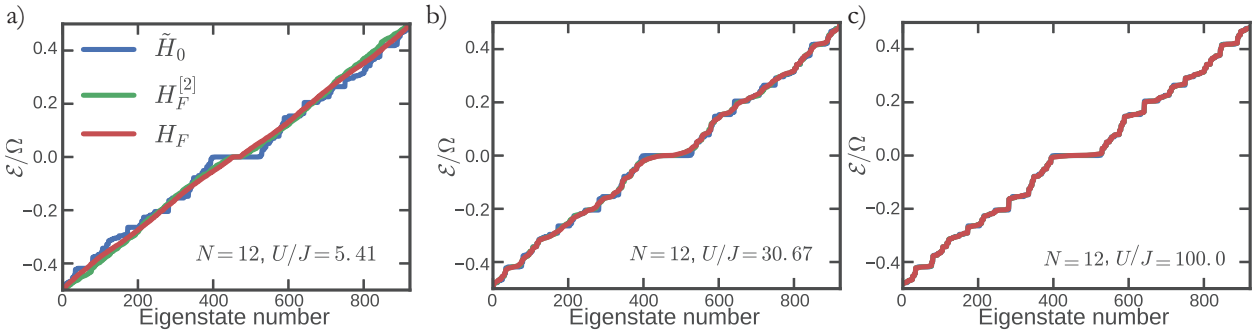


Figure 4.C.2: Quasienergies of the exact $H_F$ and the effective Hamiltonians $\tilde{H}_0$ and $H_F^{[2]}$ for three values of $U/J$. At large $U/J$, the spectra match, while away from this limit it is clear that $H_F^{[2]}$ is a good approximation over some region before the breakdown of the high frequency expansion.

$\alpha_j(m\kappa) = \alpha_{-j}(m\kappa)$ for the square wave. As expected, we see that for very large $U$, all the spectra match but as we decrease $U$, the zeroth order term deviates first before the second term which eventually also breaks down.

## 4.D Additional Evidence for Integrability and its Breaking

In this appendix, we provide additional evidence for integrability of the effective high frequency model and for integrability-breaking at finite $U$. Let us begin by showing how we numerically verify integrability of $\tilde{H}_0$. As noted in the main text, $\tilde{H}_0$ is a very unusual integrable model in the sense that multiple basis states map to the same configuration in the language of the $\tilde{d}$ fermions, leading to significant exact degeneracy. This is unlike simple free models where no exact degeneracy exists, but rather a lack of level repulsion allowing states to be close – but not the same – in energy. Therefore, level statistics is not the ideal test for integrability here.

Instead, we simply show that the spectrum may be reproduced by free fermion numerics. The procedure to generate the spectrum of $\tilde{H}_0$ is as follows:

1. Iterate through basis elements of the original model.
2. For each basis element, map it to a representation in the $\tilde{d}$-basis.
3. In the $\tilde{d}$-basis representation, count the number of fermions and the number of sites. For free one-dimensional fermions hopping on such a lattice, calculate the spectrum.
4. Impose a degeneracy on the free fermion given by the number of original basis elements that map to the same number of fermions and sites in the $\tilde{d}$ representation.

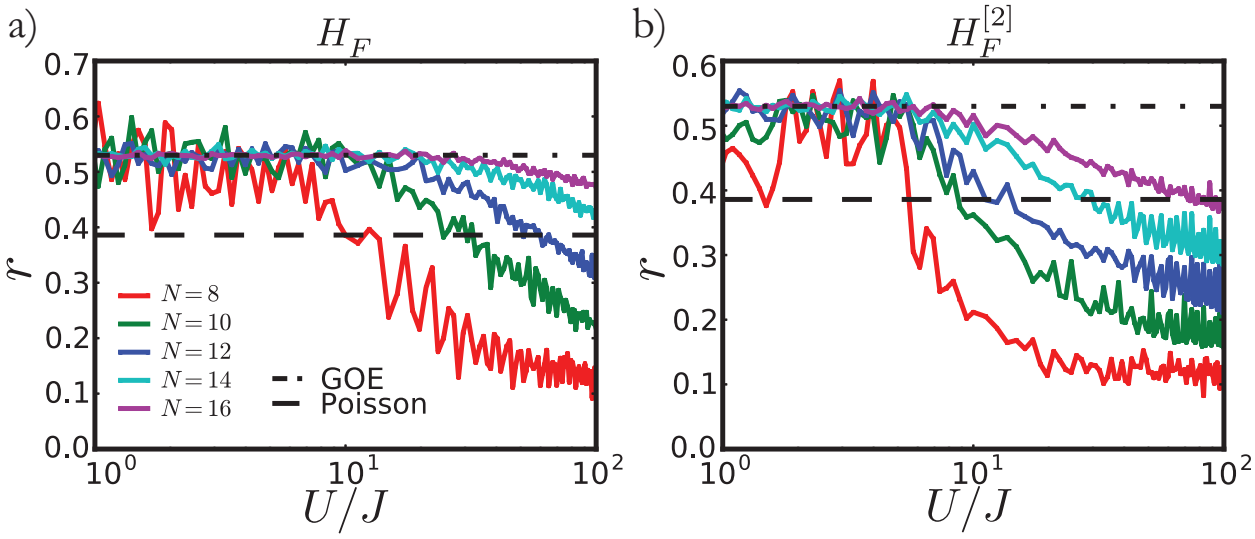


Figure 4.D.1: Level statistics of the exact $H_F$ and the effective Hamiltonian $H_F^{[2]}$. For the static Hamiltonian $H_F^{[2]}$, only the middle 50% of the spectrum is used to avoid noise from the often-anomalous high and low energy tails. For small $U/J$, the level statistic is GOE indicating non-integrable behavior of the system. As $U/J$ increases, the level statistic breaks away from GOE indicating a different spectral structure due to near-integrability. Note that this crossover is system size dependent as seen clearly in a). In b), there is a much weaker system size dependence suggesting that the HFE, at second order, does not accurately capture the crossover from integrability to non-integrability.

The spectrum obtained by this procedure is plotted as the $\tilde{H}_0$ data in Figure 4.C.2. For comparison, the spectra of $H_F$ and $H_F^{[2]}$ are obtained through exact diagonalization. The results clearly converge in the $U/J \to \infty$ limit, demonstrating the integrability of our model.

While level statistics is difficult for identifying the integrable limit of our model, it remains the smoking gun for seeing the breaking of integrability. In Figure 4.D.1 we show the level statistic $r = \min(\Delta E_n, \Delta E_{n+1})/\max(\Delta E_n, \Delta E_{n+1})$ for the exact and effective Floquet Hamiltonian, where $\Delta E_n \equiv E_n - E_{n-1}$ is the (quasi)energy difference between Floquet eigenstates $n$ and $n-1$. It has been well-studied that this object crosses over from $r \approx 0.386$ (Poisson statistics) to $r \approx 0.53$ (Gaussian orthogonal ensemble, a.k.a. GOE) as the system crosses from integrable to non-integrable [50, 59]. The non-integrable plateau is clearly seen for both $H_F$ and $H_F^{[2]}$, indicating that both obey the eigenstate thermalization hypothesis for a finite range of $U$. We also see that, due to the unusual nature of the integrable model, the Poisson limit is not reached at very large $U$. Similar to crossover behavior of $\Sigma$ in the main text, the level statistics show a system size dependent crossover for both $H_F$ and $H_F^{[2]}$ (albeit much weaker for $H_F^{[2]}$), consistent with our belief that the both $H_F$ and $H_F^{[2]}$ will thermalize for infinitesimal finite $J/U$ in the thermodynamic limit.

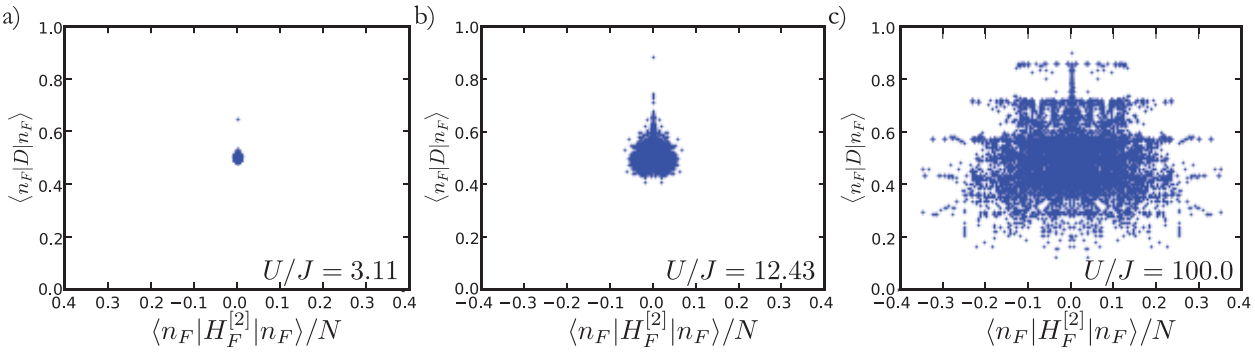


Figure 4.D.2: Expectation values of the doublon density $D$ and effective HFE Floquet Hamiltonian $H_F^{[2]} \equiv e^{-iK_{\text{eff}}^{[2]}(0)} H_{\text{eff}}^{[2]} e^{iK_{\text{eff}}^{[2]}(0)}$ in exact Floquet eigenstates of $H_F$.

Furthermore, we provide additional evidence that the crossover to thermalization of $H_{\text{eff}}$ at finite $U$ is not governed by the breaking of integrability in $H_F^{[2]}$, but rather by a direct breakdown of the high frequency expansion. In Figure 4.D.2 we plot eigenstate expectation values of two observables: the doublon density $D$ and the HFE Hamiltonian $H_F^{[2]}$. As a local observable, we expect $D$ to satisfy the Floquet-ETH for $U$ beyond the thermalization crossover, meaning that eigenstate expectation values of $D$ should be independent of quasienergy and with fluctuations exponentially suppressed in system size. This is consistent with the data shown, as $D$ compresses into a narrower region as $U$ is decreased, approaching the single value $D = 1/2$ in the thermodynamic limit. On the other hand, if $H_F^{[2]}$ were a good description of the system in this non-integrable region, we would expect that $H_F^{[2]}$ would become nearly conserved, implying that its expectation value would be extensively spread over eigenstates. Instead, we see that $H_F^{[2]}$ behaves exactly as $D$, approaching a single point in the non-integrable limit. This implies that $H_F^{[2]}$ is not a conserved quantity in the system, and thus behaves exactly the same as other non-conserved quantities such as $D$ that satisfy the Floquet-ETH.

Finally, let us see that the breakdown of the HFE is due to the resonances discussed in the main text and not directly due to a breakdown of the operator series for $H_{\text{eff}}$. For finite size systems, the expansion in (4.17) should have a well-defined convergence radius in the space of finite-dimensional matrices. We can look for the breakdown of this series by directly comparing the size of the leading correction, $H_{\text{eff}}^{[2]}$, to the zeroth order term $\tilde{H}_0$.[4] This is achieved in Figure 4.D.3 by comparing their Frobenius norms. These norms collapse amazingly well as a function of system size, such that we can immediately conclude that $H_{\text{eff}}^{[2]}$ becomes of order $\tilde{H}_0$ at fixed ratio $J/U \sim 0.5$ independent of system size. Thus we conclude that, at least to second order, there is a finite system size independent radius of convergence for the HFE, which is clearly in conflict with the breakdown of integrability in the exact $H_F$. This provides additional evidence that the breakdown of integrability is due to

[4] We have numerically confirmed that the $\tilde{H}_{\pm 1}$ corrections to $H_{\text{eff}}^{[0]}$ play a sub-leading role in all of the analyses in this paper.

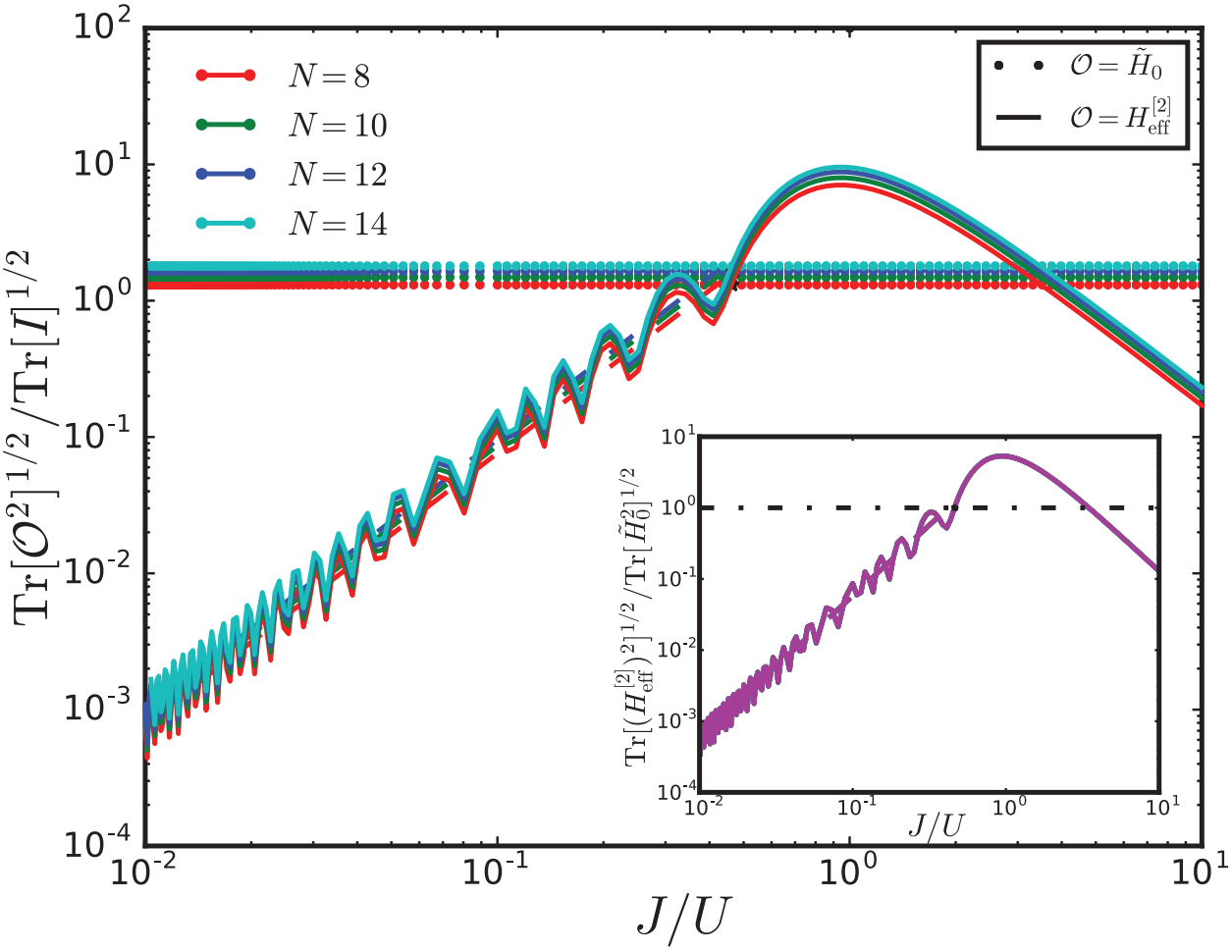


Figure 4.D.3: Frobenius norm of the integrable model $\tilde{H}_0$ and of the second order term $H_{\text{eff}}^{[2]}$ in the HFE normalized to the trace norm of the identity for each system size. As discussed in Appendix 4.C, the trace norm has $(J/U)^2$ behavior indicated by the dashed line. At $J/U \sim 0.5$, the second order term is relatively larger than the integrable part. Both zeroth order and second order terms have the same system size dependence as seen by observing the relative trace norm in the inset. This fact immediately rules out the possibility of that the breakdown of the HFE as an operator expansion is responsible for thermalization as discussed in section 4.5 and appendix 4.D, at least at second order.

non-perturbative effects for our choice of parameters, though it is possible that the direct breakdown of the HFE series expansion will be the leading effect for other models or values of the parameters.

### 4.E Alternative mapping

In this section, we present an alternative, but equivalent, mapping that demonstrates the integrability of $\tilde{H}_0$. First, define a defect as a single site that is surrounded by sites of the opposite kind. A domain wall will be two sites that are part of a sequence of occupation longer than 1. For instance: 0(01)1 is a domain wall. Now let us define the contracted lattice as a lattice where in each site we can have a hole, 0, a particle, 1, a domain wall (01) or (10) which we will call W, and a defect which is either (10) in a 111 domain or a (01) in a 000 domain which we call D. For a particular collection of these objects, we can have a lattice exemplified as follows:

$$000000111110000 \rightarrow 00000W111W000$$

and with defects:

$$001000111010000 \rightarrow 0D00W1DW000$$

A defect can move freely as long as there is no domain wall on the site it ends on. If there is a domain wall, then they switch positions:

$$1101000 = 1DW00 \rightarrow 1100100 = 1WD00$$

This means that we can write the hamiltonian as follows. We define $d$'s as annihilation operators for the defects, and $b$'s as annihilation operators for the domain walls.

$$H = d_{i+1}^{\dagger} d_i \left( (1 - n_{i+1}^{W}) + b_i^{\dagger} b_{i+1} \right) + h.c. \tag{4.22}$$

It is also clear that defects are hard-core bosons. This almost looks like free hard-core bosons except for the shift in location of the domain wall. This can be taken into account by an appropriate string operator which we now construct. First, consider the following unitary:

$$U_j = \left[ 1 + (-1)^{n_i^W + n_{i+1}^W} + 2 \left( b_i^{\dagger} b_{i+1} + b_{i+1}^{\dagger} b_i \right) \right] \tag{4.23}$$

If there is no domain wall on site $i + 1$, then this will shift a domain wall at site $i$ to site $i + 1$. We envision the chain as terminating by some domain, with no walls, so if we have a string starting operation from the farthest point, and counting to the left, this will shift all domain walls one step to the right. Alternatively, if we start from the location to the left of a domain wall, and multiply the unitaries into a string, we will shift all domain walls to the left. So if we define:

$$\tilde{d}_i = \left[ \prod_{j=N}^{i} U_j \right] d_i \tag{4.24}$$

we immediately get:

$$H = \tilde{d}^{\dagger}_{i+1}\tilde{d}_i + h.c. \tag{4.25}$$

which is the integrable model. We may further consider the creation of defects at finite $U$. This can happen only in the vicinity of a domain wall. To construct the operator we consider a $U$ energy step:

$$\begin{gathered} 111W000 = 111(10)000 \\ \downarrow \\ 11101000 = 11(10)_D(10)_W00 = 11DW00 \end{gathered}$$

with the upshot that now a site is missing. A chain with 7 effective sites, now only has 6 due to the contraction that the mapping of the defect implies. We can describe this process as originating from:

$$H_U = d^{\dagger}_{i-1}W_i b^{\dagger}_{i+1}b_i + h.c. \tag{4.26}$$

where the $W_i$ is a "warp" operator which moves everything to the left and cancels site $i$. One can write it in terms of string operator for both domain walls and defects. There is an implicit gauge choice in the above in the sense that domain walls created defects to their left, regardless of their nature.

## References


[1] Dmitry Abanin, Wojciech De Roeck, Wen Wei Ho, and Francois Huveneers. A rigorous theory of many-body prethermalization for periodically driven and closed quantum systems. *Communications in Mathematical Physics*, 354(3):809–827, September 2017.

[2] Dmitry A. Abanin and Zlatko Papić. Recent progress in many-body localization. *Annalen der Physik*, 529(7):1700169–n/a, 2017. ISSN 1521-3889. 1700169.

[3] Adhip Agarwala and Diptiman Sen. Effects of interactions on periodically driven dynamically localized systems. *Phys. Rev. B*, 95:014305, Jan 2017. doi: 10.1103/PhysRevB.95.014305.

[4] M. Aidelsburger, M. Atala, M. Lohse, J. T. Barreiro, B. Paredes, and I. Bloch. Realization of the hofstadter hamiltonian with ultracold atoms in optical lattices. *Phys. Rev. Lett.*, 111: 185301, Oct 2013. doi: 10.1103/PhysRevLett.111.185301.

[5] Ryan Barnett, Anatoli Polkovnikov, and Mukund Vengalattore. Prethermalization in quenched spinor condensates. *Phys. Rev. A*, 84:023606, Aug 2011. doi: 10.1103/PhysRevA.84.023606.

[6] J. Berges, Sz. Borsányi, and C. Wetterich. Prethermalization. *Phys. Rev. Lett.*, 93:142002, Sep 2004. doi: 10.1103/PhysRevLett.93.142002.

[7] Pranjal Bordia, Henrik Luschen, Ulrich Schneider, Michael Knap, and Immanuel Bloch. Periodically driving a many-body localized quantum system. *Nature Physics*, 13(5):460–464, 05 2017.

[8] Marin Bukov, Luca D'Alessio, and Anatoli Polkovnikov. Universal high-frequency behavior of periodically driven systems: from dynamical stabilization to floquet engineering. *Advances in Physics*, 64(2):139–226, 2015. doi: 10.1080/00018732.2015.1055918.

[9] Marin Bukov, Sarang Gopalakrishnan, Michael Knap, and Eugene Demler. Prethermal floquet steady states and instabilities in the periodically driven, weakly interacting bose-hubbard model. *Phys. Rev. Lett.*, 115:205301, Nov 2015. doi: 10.1103/PhysRevLett.115.205301.

[10] Marin Bukov, Markus Heyl, David A. Huse, and Anatoli Polkovnikov. Heating and many-body resonances in a periodically driven two-band system. *Phys. Rev. B*, 93:155132, Apr 2016.

[11] Marin Bukov, Michael Kolodrubetz, and Anatoli Polkovnikov. Schrieffer-wolff transformation for periodically driven systems: Strongly correlated systems with artificial gauge fields. *Phys. Rev. Lett.*, 116:125301, Mar 2016.

[12] Siew-Ann Cheong and Christopher L. Henley. Exact ground states and correlation functions of chain and ladder models of interacting hardcore bosons or spinless fermions. *Phys. Rev. B*, 80:165124, Oct 2009.

[13] Soonwon Choi, Joonhee Choi, Renate Landig, Georg Kucsko, Hengyun Zhou, Junichi Isoya, Fedor Jelezko, Shinobu Onoda, Hitoshi Sumiya, Vedika Khemani, Curt von Keyserlingk, Norman Y. Yao, Eugene Demler, and Mikhail D. Lukin. Observation of discrete time-crystalline order in a disordered dipolar many-body system. *Nature*, 543(7644):221–225, 2017.

[14] P. W. Claeys and J.-S. Caux. Breaking the integrability of the Heisenberg model through periodic driving. *ArXiv e-prints*, August 2017.

[15] Luca D'Alessio and Marcos Rigol. Long-time behavior of isolated periodically driven interacting lattice systems. *Phys. Rev. X*, 4:041048, Dec 2014.

[16] Luca D'Alessio, Yariv Kafri, Anatoli Polkovnikov, and Marcos Rigol. From quantum chaos and eigenstate thermalization to statistical mechanics and thermodynamics. *Advances in Physics*, 65(3):239–362, 2016.

[17] Hossein Dehghani, Takashi Oka, and Aditi Mitra. Dissipative floquet topological systems. *Phys. Rev. B*, 90:195429, Nov 2014. doi: 10.1103/PhysRevB.90.195429.

[18] J. M. Deutsch. Quantum statistical mechanics in a closed system. *Phys. Rev. A*, 43:2046–2049, Feb 1991. doi: 10.1103/PhysRevA.43.2046.

[19] Luca D'Alessio and Anatoli Polkovnikov. Many-body energy localization transition in periodically driven systems. *Annals of Physics*, 333(Supplement C):19 – 33, 2013. ISSN 0003-4916.

[20] Martin Eckstein, Marcus Kollar, and Philipp Werner. Thermalization after an interaction quench in the hubbard model. *Phys. Rev. Lett.*, 103:056403, Jul 2009. doi: 10.1103/PhysRevLett.103.056403.

[21] Dominic V. Else and Chetan Nayak. Classification of topological phases in periodically driven interacting systems. *Phys. Rev. B*, 93:201103, May 2016. doi: 10.1103/PhysRevB.93.201103.

[22] Dominic V. Else, Bela Bauer, and Chetan Nayak. Floquet time crystals. *Phys. Rev. Lett.*, 117: 090402, Aug 2016.

[23] Dominic V. Else, Bela Bauer, and Chetan Nayak. Prethermal phases of matter protected by time-translation symmetry. *Phys. Rev. X*, 7:011026, Mar 2017. doi: 10.1103/PhysRevX.7.011026.

[24] James R. Garrison, Ryan V. Mishmash, and Matthew P. A. Fisher. Partial breakdown of quantum thermalization in a hubbard-like model. *Phys. Rev. B*, 95:054204, Feb 2017. doi: 10.1103/PhysRevB.95.054204.

[25] N. Goldman and J. Dalibard. Periodically driven quantum systems: Effective hamiltonians and engineered gauge fields. *Phys. Rev. X*, 4:031027, Aug 2014. doi: 10.1103/PhysRevX.4.031027.

[26] F. Görg, M. Messer, K. Sandholzer, G. Jotzu, R. Desbuquois, and T. Esslinger. Enhancement and sign reversal of magnetic correlations in a driven quantum many-body system. *ArXiv e-prints*, August 2017.

[27] M. Gring, M. Kuhnert, T. Langen, T. Kitagawa, B. Rauer, M. Schreitl, I. Mazets, D. Adu Smith, E. Demler, and J. Schmiedmayer. Relaxation and prethermalization in an isolated quantum system. *Science*, 337(6100):1318–1322, 2012. ISSN 0036-8075.

[28] Fenner Harper and Rahul Roy. Floquet topological order in interacting systems of bosons and fermions. *Phys. Rev. Lett.*, 118:115301, Mar 2017. doi: 10.1103/PhysRevLett.118.115301.

[29] Thomas Iadecola and Claudio Chamon. Floquet systems coupled to particle reservoirs. *Phys. Rev. B*, 91:184301, May 2015. doi: 10.1103/PhysRevB.91.184301.

[30] Thomas Iadecola, Titus Neupert, and Claudio Chamon. Occupation of topological floquet bands in open systems. *Phys. Rev. B*, 91:235133, Jun 2015. doi: 10.1103/PhysRevB.91.235133.

[31] Liang Jiang, Takuya Kitagawa, Jason Alicea, A. R. Akhmerov, David Pekker, Gil Refael, J. Ignacio Cirac, Eugene Demler, Mikhail D. Lukin, and Peter Zoller. Majorana fermions in equilibrium and in driven cold-atom quantum wires. *Phys. Rev. Lett.*, 106:220402, Jun 2011. doi: 10.1103/PhysRevLett.106.220402.

[32] Gregor Jotzu, Michael Messer, Rémi Desbuquois, Martin Lebrat, Thomas Uehlinger, Daniel Greif, and Tilman Esslinger. Experimental realization of the topological haldane model with ultracold fermions. *Nature*, 515:237–240, Nov 2014. doi: 10.1038/nature13915.

[33] Vedika Khemani, Achilleas Lazarides, Roderich Moessner, and S. L. Sondhi. Phase structure of driven quantum systems. *Phys. Rev. Lett.*, 116:250401, Jun 2016.

[34] Takuya Kitagawa, Erez Berg, Mark Rudner, and Eugene Demler. Topological characterization of periodically driven quantum systems. *Phys. Rev. B*, 82:235114, 2010.

[35] Takuya Kitagawa, Takashi Oka, Arne Brataas, Liang Fu, and Eugene Demler. Transport properties of nonequilibrium systems under the application of light: Photoinduced quantum hall insulators without landau levels. *Phys. Rev. B*, 84:235108, Dec 2011. doi: 10.1103/PhysRevB.84.235108.

[36] Sota Kitamura, Takashi Oka, and Hideo Aoki. Probing and controlling spin chirality in mott insulators by circularly polarized laser. *Phys. Rev. B*, 96:014406, Jul 2017.

[37] Corinna Kollath, Andreas M. Läuchli, and Ehud Altman. Quench dynamics and nonequilibrium phase diagram of the bose-hubbard model. *Phys. Rev. Lett.*, 98:180601, Apr 2007. doi: 10.1103/PhysRevLett.98.180601.

[38] Tomotaka Kuwahara, Takashi Mori, and Keiji Saito. Floquet-magnus theory and generic transient dynamics in periodically driven many-body quantum systems. *Annals of Physics*, 367:96–124, April 2016.

[39] Achilleas Lazarides, Arnab Das, and Roderich Moessner. Equilibrium states of generic quantum systems subject to periodic driving. *Phys. Rev. E*, 90:012110, Jul 2014.

[40] Achilleas Lazarides, Arnab Das, and Roderich Moessner. Periodic thermodynamics of isolated quantum systems. *Phys. Rev. Lett.*, 112:150401, Apr 2014.

[41] Achilleas Lazarides, Arnab Das, and Roderich Moessner. Fate of many-body localization under periodic driving. *Phys. Rev. Lett.*, 115:030402, Jul 2015.

[42] N. H. Lindner, G. Refael, and V. Galitski. Floquet topological insulator in semiconductor quantum wells. *Nature Physics*, 7:490–495, Mar 2011. doi: 10.1038/nphys1926.

[43] F. Machado, G. D. Meyer, D. V. Else, C. Nayak, and N. Y. Yao. Exponentially slow heating in short and long-range interacting floquet systems. *ArXiv e-prints*, August 2017.

[44] L. Mathey and A. Polkovnikov. Light cone dynamics and reverse kibble-zurek mechanism in two-dimensional superfluids following a quantum quench. *Phys. Rev. A*, 81:033605, Mar 2010. doi: 10.1103/PhysRevA.81.033605.

[45] J. H. Mentink, K. Balzer, and M. Eckstein. Ultrafast and reversible control of the exchange interaction in mott insulators. *Nature Communications*, 6:6708–, March 2015.

[46] Hirokazu Miyake, Georgios A. Siviloglou, Colin J. Kennedy, William Cody Burton, and Wolfgang Ketterle. Realizing the harper hamiltonian with laser-assisted tunneling in optical lattices. *Phys. Rev. Lett.*, 111:185302, Oct 2013. doi: 10.1103/PhysRevLett.111.185302.

[47] Michael Moeckel and Stefan Kehrein. Crossover from adiabatic to sudden interaction quenches in the hubbard model: prethermalization and non-equilibrium dynamics. *New Journal of Physics*, 12(5):055016, 2010.

[48] Rahul Nandkishore and David A. Huse. Many-body localization and thermalization in quantum statistical mechanics. *Annual Review of Condensed Matter Physics*, 6(1):15–38, 2015.

[49] Wenxing Nie, Hosho Katsura, and Masaki Oshikawa. Ground-state energies of spinless free fermions and hard-core bosons. *Phys. Rev. Lett.*, 111:100402, Sep 2013.

[50] Vadim Oganesyan and David A. Huse. Localization of interacting fermions at high temperature. *Phys. Rev. B*, 75:155111, Apr 2007.

[51] Takashi Oka and Hideo Aoki. Photovoltaic hall effect in graphene. *Phys. Rev. B*, 79:081406, Feb 2009. doi: 10.1103/PhysRevB.79.081406.

[52] Colin Parker, Li-Chung Ha, and Cheng Chin. Direct observation of effective ferromagnetic domains of cold atoms in a shaken optical lattice. *Nature Physics*, 2013.

[53] F. Peronaci, M. Schiró, and O. Parcollet. Resonant thermalization of periodically driven strongly correlated electrons. *ArXiv e-prints*, November 2017.

[54] H. C. Po, L. Fidkowski, A. Vishwanath, and A. C. Potter. Radical chiral floquet phases in a periodically driven kitaev model and beyond. *ArXiv e-prints*, January 2017.

[55] H C Po, T. Fidkowski, A. C. Potter, and A. Vishwanath. Radical chiral floquet phases in a periodically driven kitaev model and beyond. *arXiv:1701.01440*, 2017.

[56] Hoi Chun Po, Lukasz Fidkowski, Takahiro Morimoto, Andrew C. Potter, and Ashvin Vishwanath. Chiral floquet phases of many-body localized bosons. *Phys. Rev. X*, 6:041070, Dec 2016. doi: 10.1103/PhysRevX.6.041070.

[57] Anatoli Polkovnikov, Krishnendu Sengupta, Alessandro Silva, and Mukund Vengalattore. Colloquium. *Rev. Mod. Phys.*, 83:863–883, Aug 2011. doi: 10.1103/RevModPhys.83.863.

[58] Pedro Ponte, Anushya Chandran, Z. Papić, and Dmitry A. Abanin. Periodically driven ergodic and many-body localized quantum systems. *Annals of Physics*, 353:196–204, Nov 2014. doi: 10.1016/j.aop.2014.11.008.

[59] Pedro Ponte, Z. Papić, Francois Huveneers, and Dmitry A. Abanin. Many-body localization in periodically driven systems. *Phys. Rev. Lett.*, 114:140401, 2015.

[60] A. C. Potter, A. Vishwanath, and L. Fidkowski. An infinite family of 3d floquet topological paramagnets. *ArXiv e-prints*, June 2017.

[61] Andrew C. Potter and Takahiro Morimoto. Dynamically enriched topological orders in driven two-dimensional systems. *Phys. Rev. B*, 95:155126, Apr 2017. doi: 10.1103/PhysRevB.95.155126.

[62] Andrew C. Potter, Takahiro Morimoto, and Ashvin Vishwanath. Classification of interacting topological floquet phases in one dimension. *Phys. Rev. X*, 6:041001, Oct 2016. doi: 10.1103/PhysRevX.6.041001.

[63] Saar Rahav, Ido Gilary, and Shmuel Fishman. Effective hamiltonians for periodically driven systems. *Phys. Rev. A*, 68:013820, Jul 2003. doi: 10.1103/PhysRevA.68.013820.

[64] M. C. Rechtsman, J. M. Zeuner, Y. Plotnik, Y. Lumer, D. Podolsky, F. Dreisow, S. Nolte, M. Segev, and A. Szameit. Photonic floquet topological insulators. *Nature*, 496:196–200, Apr 2013. doi: 10.1038/nature12066.

[65] Marcos Rigol and Lea F. Santos. Quantum chaos and thermalization in gapped systems. *Phys. Rev. A*, 82:011604, Jul 2010. doi: 10.1103/PhysRevA.82.011604.

[66] Marcos Rigol, Vanja Dunjko, and Maxim Olshanii. Thermalization and its mechanism for generic isolated quantum systems. *Nature*, 2008.

[67] Rahul Roy and Fenner Harper. Abelian floquet symmetry-protected topological phases in one dimension. *Phys. Rev. B*, 94:125105, Sep 2016. doi: 10.1103/PhysRevB.94.125105.

[68] Rahul Roy and Fenner Harper. Floquet topological phases with symmetry in all dimensions. *Phys. Rev. B*, 95:195128, May 2017. doi: 10.1103/PhysRevB.95.195128.

[69] Mark S. Rudner, Netanel H. Lindner, Erez Berg, and Michael Levin. Anomalous edge states and the bulk-edge correspondence for periodically driven two-dimensional systems. *Phys. Rev. X*, 3:031005, Jul 2013. doi: 10.1103/PhysRevX.3.031005.

[70] Angelo Russomanno, Alessandro Silva, and Giuseppe E. Santoro. Periodic steady regime and interference in a periodically driven quantum system. *Phys. Rev. Lett.*, 109:257201, Dec 2012.

[71] Lea F. Santos and Marcos Rigol. Localization and the effects of symmetries in the thermalization properties of one-dimensional quantum systems. *Phys. Rev. E*, 82:031130, Sep 2010. doi: 10.1103/PhysRevE.82.031130.

[72] Karthik I. Seetharam, Charles-Edouard Bardyn, Netanel H. Lindner, Mark S. Rudner, and Gil Refael. Controlled population of floquet-bloch states via coupling to bose and fermi baths. *Phys. Rev. X*, 5:041050, Dec 2015. doi: 10.1103/PhysRevX.5.041050.

[73] Jesko Sirker and Michael Bortz. The open xxz -chain: bosonization, the bethe ansatz and logarithmic corrections. *Journal of Statistical Mechanics: Theory and Experiment*, 2006(01): P01007, 2006.

[74] A. Smith, J. Knolle, D. L. Kovrizhin, and R. Moessner. Disorder-free localization. *Phys. Rev. Lett.*, 118:266601, Jun 2017. doi: 10.1103/PhysRevLett.118.266601.

[75] Mark Srednicki. Chaos and quantum thermalization. *Phys. Rev. E*, 50:888–901, Aug 1994. doi: 10.1103/PhysRevE.50.888.

[76] Paraj Titum, Erez Berg, Mark S. Rudner, Gil Refael, and Netanel H. Lindner. Anomalous floquet-anderson insulator as a nonadiabatic quantized charge pump. *Phys. Rev. X*, 6:021013, May 2016.

[77] Lev Vidmar and Marcos Rigol. Generalized gibbs ensemble in integrable lattice models. *Journal of Statistical Mechanics: Theory and Experiment*, 2016(6):064007, 2016.

[78] C. W. von Keyserlingk and S. L. Sondhi. Phase structure of one-dimensional interacting floquet systems. i. abelian symmetry-protected topological phases. *Phys. Rev. B*, 93:245145, Jun 2016. doi: 10.1103/PhysRevB.93.245145.

[79] C. W. von Keyserlingk and S. L. Sondhi. Phase structure of one-dimensional interacting floquet systems. ii. symmetry-broken phases. *Phys. Rev. B*, 93:245146, Jun 2016.

[80] Simon A. Weidinger and Michael Knap. Floquet prethermalization and regimes of heating in a periodically driven, interacting quantum system. *Scientific Reports*, 7, 2017.

[81] Phillip Weinberg, Marin Bukov, Luca D'Alessio, Anatoli Polkovnikov, Szabolcs Vajna, and Michael Kolodrubetz. Adiabatic perturbation theory and geometry of periodically-driven systems. *Physics Reports*, 688(Supplement C):1 – 35, 2017. ISSN 0370-1573. Adiabatic Perturbation Theory and Geometry of Periodically-Driven Systems.

[82] N. Y. Yao, C. R. Laumann, J. I. Cirac, M. D. Lukin, and J. E. Moore. Quasi-many-body localization in translation-invariant systems. *Phys. Rev. Lett.*, 117:240601, Dec 2016. doi: 10.1103/PhysRevLett.117.240601.

[83] N. Y. Yao, A. C. Potter, I.-D. Potirniche, and A. Vishwanath. Discrete time crystals: Rigidity, criticality, and realizations. *Phys. Rev. Lett.*, 118:030401, Jan 2017.

[84] Tian-Sheng Zeng and D. N. Sheng. Prethermal time crystals in a one-dimensional periodically driven floquet system. *Phys. Rev. B*, 96:094202, Sep 2017. doi: 10.1103/PhysRevB.96.094202.

[85] J. Zhang, P. W. Hess, A. Kyprianidis, P. Becker, A. Lee, J. Smith, G. Pagano, I.-D Potirniche, A. C. Potter, A. Vishwanath, N. Y. Yao, and C. Monroe. Observation of a discrete time crystal. *Nature*, 543(7644):217–220, 03 2017.

*Chapter 5*

# CONCLUSIONS AND OUTLOOK

In this thesis, we studied thermalization in both open and closed Floquet systems. We found that heating can be controlled by dissipation to yield a non-equilibrium steady-state that resembles the ground state of an insulator. We found that this Floquet insulator state can survive the addition of weak interactions and developed a simple effective model that captures the essence of scattering in Floquet systems. In the closed setting, we find that near-integrability of a finite size system yields intrinsic non-thermal regimes that can be exploited in small quantum systems.

Many broad questions remain open. Can one make more realistic experimental predictions about when and how the topological physics of various Floquet phases (e.g. edge states of Floquet Topological Insulator) can observed? Can one design Floquet systems that admit multi-stability (e.g. hysteresis) and is it useful? From a broader theoretical point of view, is it possible to develop effective renormalization group techniques that systematically and self-consistently capture the long-time (and perhaps time-averaged) behavior of Floquet systems in regimes of interest? This last question is an interesting direction of research riddled with difficulties as per the author's experience.

The field of Floquet engineering is nascent. As materials processing and fabrication technology develops, one can always ask if/how adding a periodic drive can induce new phases of matter. One can imagine a dreamy situation where one takes a simple, earth-abundant material, and drives it into a high temperature superconducting phase using a laser!

*Chapter 6*

# APPENDICES

## 6.1 Cluster Expansion

In this section, we derive the Floquet-Redfield equation (FRE) and simpler Floquet-Boltzmann (FBE) using the cluster expansion approach discussed in the textbook *Semiconductor Quantum Optics* by Mackillo Kira and Stephan Koch (2012).

### Clusters

The cluster expansion is a systematic decomposition of an $N$ "object" expectation value $\langle N\rangle$. An object is defined a single boson operator (e.g. $b, b^\dagger$ obeying canonical commutation relations) or a fermion bilinear operator (e.g. $c^\dagger c$ where $c, c^\dagger$ obey canonical anti-commutation relations). This definition is consistent with spin-statistics in that a fermion bilinear has bosonic properties. Fermion occupation numbers/polarizations $\langle c_i^\dagger c_j\rangle$ or single boson expectation values $\langle b_k\rangle$, $\langle b_k^\dagger\rangle$ (where $i, j, k$ index relevant degrees of freedom in the problem) are examples of singlets (single objects) which are schematically denoted $\langle 1\rangle$. Doublets (2 objects), schematically denoted $\langle 2\rangle$, include expectation values such as fermion density-density $\langle c_i^\dagger c_i c_j^\dagger c_j\rangle$, boson bilinears $\langle b_j^\dagger b_k\rangle$, and mixed terms like $\langle c_i^\dagger c_j b_k^\dagger\rangle$, etc. Triplets (3 objects), schematically denoted as $\langle 3\rangle$, include expectation values such as $\langle b_i^\dagger b_j b_k\rangle$, $\langle c_i^\dagger c_j^\dagger c_k^\dagger c_l c_m c_n\rangle$, $\langle c_k^\dagger c_l b_i^\dagger b_j\rangle$, and so on.

With this definition, one can define a "correlated cluster" of $N$ objects, $\Delta\langle N\rangle$, which measures the *unique* correlation among the $N$ objects that is not decomposable into correlations between smaller sub-clusters of $N-1, N-2, \ldots$etc. Formally, we write

$$\langle N\rangle \;=\; \sum_{J=1}^{N-1}\langle N\rangle_J + \Delta\langle N\rangle \tag{6.1}$$

where $\langle N\rangle_J$ denotes factorization of $\langle N\rangle$ into clusters of max size $J$. For example,

$$
\begin{aligned}
\langle 1\rangle &\equiv \langle 1\rangle_1 \equiv \Delta\langle 1\rangle \\
\langle 2\rangle &= \langle 2\rangle_1 + \Delta\langle 2\rangle \sim \langle 1\rangle\langle 1\rangle + \Delta\langle 2\rangle \\
\langle 3\rangle &= \langle 3\rangle_1 + \langle 3\rangle_2 + \Delta\langle 3\rangle \sim \langle 1\rangle\langle 1\rangle\langle 1\rangle + \langle 1\rangle\Delta\langle 2\rangle + \Delta\langle 3\rangle \\
\langle N\rangle &= \langle N\rangle_1 + [\langle N-2\rangle_1\Delta\langle 2\rangle + \langle N-4\rangle_1\Delta\langle 2\rangle\Delta\langle 2\rangle + ...]_2 \\
&\quad + [\langle N-3\rangle_1\Delta\langle 3\rangle + \langle N-5\rangle_1\Delta\langle 3\rangle\Delta\langle 2\rangle + ...]_3 + \sum_{J=4}^{N-1}\langle N\rangle_J + \Delta\langle N\rangle
\end{aligned}
$$

where $[\cdot]_J$ contains terms which have max size $J$. In terms of increasing complexity, singlets encode single-particle physics for fermions and coherent (classical) states of bosons, doublets encode interacting pairs/2-particle bound states, triplets encode three-particle correlated objects/bound states, and so on for higher $n$-droplets.

Explicitly, $\langle\cdot\rangle_1$ denotes factorization of the expectation value into singlets, $\langle\cdot\rangle_2$ denotes factorization of the expectation values into singlets and doublets, and so on. In this light, $\langle N\rangle_1$ is also denoted $\langle N\rangle_S$ for a singlet factorization, $\langle N\rangle_2$ is also denoted $\langle N\rangle_{SD}$ for single/doublet factorization and so on. For example, fermion/boson doublets, can be broken into singlets $\langle 2\rangle_1 \sim \langle 1\rangle\langle 1\rangle$ in a manner that respects their antisymmetry/symmetry as follows

$$
\begin{aligned}
\langle c^\dagger_{k_1} c^\dagger_{k_2} c_{k_3} c_{k_4}\rangle_1 &= \langle c^\dagger_{k_1} c_{k_4}\rangle\langle c^\dagger_{k_2} c_{k_3}\rangle - \langle c^\dagger_{k_1} c_{k_3}\rangle\langle c^\dagger_{k_2} c_{k_4}\rangle \\
\langle b^\dagger_i b^\dagger_j\rangle_1 &= \langle b^\dagger_i\rangle\langle b^\dagger_j\rangle \\
\langle c^\dagger_{k_1} c_{k_2} b_i\rangle_1 &= \langle c^\dagger_{k_1} c_{k_2}\rangle\langle b_i\rangle
\end{aligned}
$$

In general, a fully singlet factorization $\langle N\rangle_1 = \langle 1\rangle...\langle 1\rangle$ ($N$ terms of $\langle 1\rangle$) for bosons is just a product

$$
\langle b_{i_1}...b_{i_N}\rangle_1 = \langle b_{i_1}\rangle...\langle b_{i_N}\rangle \tag{6.2}
$$

and for fermions is given by a Slater determinant for fermions

$$
\begin{aligned}
\langle c^\dagger_{k_1}...c^\dagger_{k_N} c_{\tilde{k}_N}...c_{\tilde{k}_1}\rangle_1 &= \mathrm{Det}[M] \\
M_{jl} &= \langle c^\dagger_{k_j} c_{k_l}\rangle
\end{aligned} \tag{6.3}
$$

For mixed fermion/boson expectation values, one just fully anti-symmetrizes the fermion bilinears upon normal ordering as per Eq.6.3 after extracting the boson singlets as in Eq.6.2.

**Cluster Dynamics**

Given a many-body quantum Hamiltonian of interest $H$, an $N$ object expectation value (we just use $N$ as the operator representing this below), evolves under the Ehrenfest theorem as

$$i\frac{d}{dt}\langle N\rangle = \langle [N,H]\rangle + \langle \partial_t N\rangle$$

$$i\partial_t\langle N\rangle = L[\langle N\rangle] + Y[\langle N+1\rangle] \tag{6.4}$$

where $L[\langle N\rangle]$ is the functional that contains terms with same number of objects and $Y[\langle N+1\rangle]$ contains terms with an additional object, generated by any interaction/non-quadratic terms in $H$. By iterating the equations of motion for each subsequent correlation, $\langle N\rangle, \langle N+1\rangle, \langle N+2\rangle, ...$, an infinite (for thermodynamically large systems) hierarchy of differential equations appears. In general, a many-body system has nonzero initial expectation values for sets of observables in each object number sector. For example, a free-fermion system is fully determined by Slater determinant (fully-antisymmetrized) single particle states which have nonzero expectation values for any sector; higher sectors are factorizable by Wick's theorem into single particle expectations. Hence, truncating the hierarchy in Eq.6.4 arbitrarily at some $\bar{N}$ is an uncontrolled and inaccurate approximation that does not allow for physical initial conditions.

In order to overcome this, one should consider the dynamics of correlated clusters which evolve as

$$\begin{aligned} i\partial_t\Delta\langle N\rangle &= L[\Delta\langle N\rangle] + Y[\Delta\langle N+1\rangle] \\ &+ \sum_{n=1}^{N} V_1[\Delta\langle n\rangle\Delta\langle N-n\rangle] + \sum_{n=1}^{N} V_2[\Delta\langle n\rangle\Delta\langle N+1-n\rangle] \\ &+ \sum_{n=1}^{N-1}\sum_{m=1}^{N-n} V_3[\Delta\langle n\rangle\Delta\langle m\rangle\Delta\langle N+1-n-m\rangle] \end{aligned} \tag{6.5}$$

where $L, Y$ are functionals as in Eq.6.4 and $V_1, V_2, V_3$ are functionals containing *nonlinear* terms of products of various two or three cluster sizes. Clusters have initial conditions that are markedly different from $N$ object expectation values. In general, a physical system, such as weakly-interacting fermions, can begin with a physical initial condition of just singlet correlations (a gas or plasma). At this point there are no higher order correlations and so $Y$ terms do not contribute. It is the nonlinear terms $V_1, V_2, V_3$ that source doublets. After some time horizon, doublets become sizeable and their nonlinear terms source triplets and so on. Higher order clusters/correlations are developed

sequentially in time and hence truncating the cluster expansion encodes, physically, the evolution of the system upto a finite time horizon correctly described by the clusters upto the truncation size. In many physical cases, such as a weakly-interacting gas, singlets and possibly doublets accurately describe the physics even at very long times, and so the cluster expansion becomes a useful description for arbitrarily long time horizons. Note that the cluster expansion is a variant of the cumulant expansion where, in the usual scenario, cumulants are the connected correlation functions of various sizes. The cluster expansion enjoys the same spirit as the Martin-Schwinger hierarchy for nonequilibrium Green's functions.

**Scattering Approximation**

Suppose we are interested in the dynamics of singlets and doublets while excluding the formation of triplets.

$$\begin{aligned} i\partial_t \Delta\langle 1\rangle &= L[\Delta\langle 1\rangle] + Y[\Delta\langle 2\rangle] + V_2[\Delta\langle 1\rangle\Delta\langle 1\rangle] \\ i\partial_t \Delta\langle 2\rangle &= L[\Delta\langle 2\rangle] + V_1[\Delta\langle 1\rangle\Delta\langle 1\rangle] + V_2[\Delta\langle 1\rangle\Delta\langle 2\rangle] + V_3[\Delta\langle 1\rangle\Delta\langle 1\rangle\Delta\langle 1\rangle] \end{aligned}$$

where we have ignored $Y[\Delta\langle 3\rangle]$ by the assumption of no triplets. Introducing an approximation that assumes doublets are weak for the time horizon of interest,

$$L[\Delta\langle 2\rangle] + V_2[\Delta\langle 1\rangle\Delta\langle 2\rangle] \quad \rightarrow \quad (E_{MF} - i\gamma)\Delta\langle 2\rangle$$

where $E_{MF}$ is some mean-field energy and $\gamma$ is a phenomenological dephasing constant for doublets (presumably due to the formation of triplets), we get

$$i\partial_t \Delta\langle 2\rangle = (E_{MF} - i\gamma)\Delta\langle 2\rangle + V_1[\Delta\langle 1\rangle\Delta\langle 1\rangle] + V_3[\Delta\langle 1\rangle\Delta\langle 1\rangle\Delta\langle 1\rangle]$$

which is easily solved

$$\Delta\langle 2\rangle(t) = \frac{1}{i\hbar}\int_{-\infty}^{t} dz e^{\frac{i}{\hbar}(E_{MF}-i\gamma)(z-t)}(V_1[\Delta\langle 1\rangle\Delta\langle 1\rangle] + V_3[\Delta\langle 1\rangle\Delta\langle 1\rangle\Delta\langle 1\rangle])$$

Under the standard Markov approximation (see below sections for more detail),

$$\Delta\langle 2\rangle_{\text{scat}} \approx -\frac{V_1[\Delta\langle 1\rangle\Delta\langle 1\rangle] + V_3[\Delta\langle 1\rangle\Delta\langle 1\rangle\Delta\langle 1\rangle]}{E_{MF} - i\gamma}$$

This expression can be substituted into the singlet dynamics

$$i\partial_t \Delta\langle 1\rangle \;=\; L[\Delta\langle 1\rangle] + Y[\Delta\langle 2\rangle_{\rm scat}] + V_2[\Delta\langle 1\rangle\Delta\langle 1\rangle] \tag{6.6}$$

to acheive a closed differential equation in terms of pure singlets. This level of approximation, which treats doublets at the scattering level, is between the pure singlet level, and the full singlet-doublet dynamics. It takes into account the contribution of 2-singlet scattering to singlet dynamics but cannot capture the formation of true 2-object correlations (e.g. bound states).

Alternatively, one may write, using the the definition of a cluster,

$$\begin{aligned} i\partial_t \Delta\langle 2\rangle &= i\partial_t\langle 2\rangle - i\partial_t\langle 2\rangle_S \\ &\approx (i\partial_t\langle 2\rangle)_S - (i\partial_t\langle 2\rangle_S)_S \end{aligned} \tag{6.7}$$

where in the second line, we have factorized $i\partial_t\Delta\langle 2\rangle$ in terms of singlets and so this can be integrated formally to obtain $\Delta\langle 2\rangle$. We will also denote this as $\Delta\langle 2\rangle_{\rm scat}$ as it acheives a similar closed differential equation for singlets upon insertion into $i\partial_t\Delta\langle 1\rangle$ as before in Eq.6.6. Equation 6.6 may also be rewritten as

$$i\partial_t\langle 1\rangle \;=\; L[\langle 1\rangle] + Y[\Delta\langle 2\rangle_{\rm scat} + \langle 2\rangle_S] \tag{6.8}$$

using Eq.6.4. We will use this result to compute the Floquet singlet dynamics at the scattering level.

### 6.2 Time Evolution of Floquet Correlations

Floquet states are strobscopically stationary solutions to the Schrodinger equation

$$i\partial_t|\psi_i(t)\rangle = H_0(t)|\psi_i(t)\rangle$$

with the time evolution operator

$$i\partial_t U(t,t') = H_0(t)U(t,t')$$

given by the time-ordered exponential

$$\begin{aligned} U(t,t') &= \mathcal{T} e^{-i\int_{t'}^{t} H_0(z)dz} \\ &= \sum_i e^{-i\mathcal{E}_i(t-t')} |\phi_i(t)\rangle\langle\phi_i(t')| \end{aligned}$$

and so

$$|\psi_i(t)\rangle = U(t,t')|\psi_i(t')\rangle$$

Defining the creation/annihilation operators for a Floquet state $i$, in the Schrodinger picture,

$$f_i^\dagger(t)|0(t)\rangle = |\psi_i(t)\rangle$$

where $|0(t)\rangle$ denotes the Floquet single-particle vacuum state that is time-dependent (since the Floquet states are time-dependent). Hence,

$$\begin{aligned} f_i^\dagger(t)|0(t)\rangle &= U(t,t')f_i^\dagger(t')|0(t')\rangle \\ &= U(t,t')f_i^\dagger(t')U^\dagger(t,t')|0(t)\rangle \end{aligned}$$

and so we get the property

$$f_i^\dagger(t) = U(t,t')f_i^\dagger(t')U^\dagger(t,t') \tag{6.9}$$

The time evolution of the operator is given by

$$\begin{aligned} i\partial_t f_i^\dagger(t) &= i\partial_t \left(U(t,t')f_i^\dagger(t')U^\dagger(t,t')\right) \\ &= (i\partial_t U(t,t'))f_i^\dagger(t')U^\dagger(t,t') + U(t,t')f_i^\dagger(t')(i\partial_t U^\dagger(t,t')) \\ &= H_0(t)U(t,t')f_i^\dagger(t')U^\dagger(t,t') - U(t,t')f_i^\dagger(t')U^\dagger(t,t')H_0(t) \\ &= H_0(t)f_i^\dagger(t) - f_i^\dagger(t)H_0(t) \\ &= [H_0(t), f_i^\dagger(t)] \end{aligned} \tag{6.10}$$

and by extension

$$i\partial_t \left(f_{i_1}^\dagger(t)...f_{i_m}^\dagger f_{i_{m+1}}...f_{i_{m+n}}(t)\right) = [H_0(t), f_{i_1}^\dagger(t)...f_{i_m}^\dagger f_{i_{m+1}}...f_{i_{m+n}}(t)]$$

For a Hamiltonian $H = H_1 + H_0(t)$, correlation functions evolve as (where $tr$ is the trace operation)

$$
\begin{aligned}
i\frac{\partial}{\partial t}\langle f_{i_1}^\dagger(t)...f_{i_m}^\dagger f_{i_{m+1}}...f_{i_{m+n}}(t)\rangle &= i\frac{\partial}{\partial t}tr(\rho f_{i_1}^\dagger(t)...f_{i_m}^\dagger f_{i_{m+1}}...f_{i_{m+n}}(t)) \\
&= itr\left(\frac{\partial\rho}{\partial t}f_{i_1}^\dagger(t)...f_{i_m}^\dagger f_{i_{m+1}}...f_{i_{m+n}}(t)\right) \\
&\quad +itr\left(\rho\frac{\partial}{\partial t}(f_{i_1}^\dagger(t)...f_{i_m}^\dagger f_{i_{m+1}}...f_{i_{m+n}}(t))\right) \\
&= tr\left([H,\rho]f_{i_1}^\dagger(t)...f_{i_m}^\dagger f_{i_{m+1}}...f_{i_{m+n}}(t)\right) \\
&\quad +tr\left(\rho[H_0(t),f_{i_1}^\dagger(t)...f_{i_m}^\dagger f_{i_{m+1}}...f_{i_{m+n}}(t)]\right) \\
&= tr\left(\rho[f_{i_1}^\dagger(t)...f_{i_m}^\dagger f_{i_{m+1}}...f_{i_{m+n}}(t),H]\right) \\
&\quad +tr\left(\rho[H_0(t),f_{i_1}^\dagger(t)...f_{i_m}^\dagger f_{i_{m+1}}...f_{i_{m+n}}(t)]\right) \\
&= tr\left(\rho[f_{i_1}^\dagger(t)...f_{i_m}^\dagger f_{i_{m+1}}...f_{i_{m+n}}(t),H-H_0(t)]\right) \\
&= \langle[f_{i_1}^\dagger(t)...f_{i_m}^\dagger f_{i_{m+1}}...f_{i_{m+n}}(t),H-H_0(t)]\rangle \qquad (6.11)
\end{aligned}
$$

which is reminiscent of an interaction picture for a time-independent system. In the Heisenberg picture (subscript $H$ denotes Heisenberg picture),

$$
\begin{aligned}
i\frac{d}{dt}f_{H,i}^\dagger(t) &= [f_{H,i}^\dagger(t),H_H]+(i\partial_t f_i^\dagger(t))_H \\
&= [f_{H,i}^\dagger(t),H_H]+([H_0(t),f_i^\dagger(t)])_H \\
&= [f_{H,i}^\dagger(t),H_H]+[H_{0,H}(t),f_{H,i}^\dagger(t)] \\
&= [f_{H,i}^\dagger(t),H_H-H_{0,H}(t)] \\
&= ([f_i^\dagger(t),H-H_0])_H \qquad (6.12)
\end{aligned}
$$

where we have used Eq.6.10 in the second line. Using Eq.6.12, one can also determine the evolution of correlation functions for a given initial in the Heisenberg picture

$$
\begin{aligned}
i\partial_t\langle f_{H,i}^\dagger(t)\rangle_H &= i\partial_t\langle f_{H,i}^\dagger(t)\rangle_H \\
&= \langle([f_i^\dagger(t),H-H_0(t)])_H\rangle_H \\
&= \langle[f_i^\dagger(t),H-H_0(t)]\rangle \\
&= i\partial_t\langle f_i^\dagger(t)\rangle
\end{aligned}
$$

where, as expected, we obtain the same result as in the Schrodinger picture from Eq.6.11. Hence,

$$
\begin{aligned}
i\partial_t\langle f_{i_1}^\dagger(t) f_{i_2}(t)\rangle &= i\partial_t\langle f_{H,i_1}^\dagger(t) f_{H,i_2}(t)\rangle_H \\
&= \langle i\partial_t(f_{H,i_1}^\dagger(t) f_{H,i_2}(t))\rangle_H \\
&= \langle i\partial_t(f_{H,i_1}^\dagger(t)) f_{H,i_2}(t))\rangle_H + \langle f_{H,i_1}^\dagger(t) i\partial_t(f_{H,i_2}(t))\rangle_H \\
&= \langle [f_{i_1}^\dagger(t), H - H_0(t)]_H f_{H,i_2}(t))\rangle_H + \langle f_{H,i_1}^\dagger(t)[f_{i_2}(t), H - H_0(t)]_H\rangle_H \\
&= \langle [f_{i_1}^\dagger(t), H - H_0(t)] f_{i_2}(t))\rangle + \langle f_{i_1}^\dagger(t)[f_{i_2}(t), H - H_0(t)]\rangle \qquad (6.13)
\end{aligned}
$$

which easily generalizes to higher particle correlators. This means that we can just compute the single operator dynamics and then take expectation values afterwards to obtain the correct result.

## 6.3 System

### Hamiltonian in Electronic Basis

The Hamiltonian for an interacting electronic (solid-state) system (in the diagonal/band basis) coupled to bosons (e.g. phonons) and another fermionic system (e.g. a lead)

$$
H = H_0 + H_{int}
$$

$$
\begin{aligned}
H_0 &= H_0^{sys} + H_0^{bos} + H_0^{lead} \\
&= \sum_{\nu k} E_{\nu k} c_{\nu k}^\dagger c_{\nu k} + \sum_{\eta q} \omega_{\eta q} b_{\eta q}^\dagger b_{\eta q} + \sum_l \varepsilon_l d_l^\dagger d_l
\end{aligned}
$$

$$
\begin{aligned}
H_{int} &= H_{el-bos} + H_{el-el} + H_{el-lead} \\
&= \sum_{\nu\nu' k k' q q_{||}\eta} M_{\nu k}^{\nu' k' q q_{||}\eta} \delta(k' - k - q) c_{\nu' k'}^\dagger c_{\nu k} (b_{q q_{||}\eta} + b_{-q q_{||}\eta}^\dagger) \\
&+ \frac{1}{2} \sum_{k_1 k_2 k_3 k_4} \sum_{\nu_1 \nu_2 \nu_3 \nu_4} V_{\nu_3 k_3, \nu_4 k_4}^{\nu_1 k_1, \nu_2 k_2} c_{\nu_1 k_1}^\dagger c_{\nu_2 k_2}^\dagger c_{\nu_3 k_3} c_{\nu_4 k_4} + \sum_{\nu k l} \Gamma_l^{\nu k} (c_{k\nu}^\dagger d_l + h.c.)
\end{aligned}
$$

where $\nu_i$ denote electronic bands, $\eta$ denotes bosonic bands (if multiple bosonic bands are of interest), and $l$ denotes the state of the fermionic system. The variables $k_i$, $k'$, $q$ denote momenta in along the system direction and $q_{||}$ denotes any momenta (if any), transverse to the system (e.g. in the case of a 1d electronic system on a 3d substrate hosting phonons).

Note that $V_{\nu_3 k_3, \nu_4 k_4}^{\nu_1 k_1, \nu_2 k_2} = -V_{\nu_3 k_3, \nu_4 k_4}^{\nu_2 k_2, \nu_1 k_1} = -V_{\nu_4 k_4, \nu_3 k_3}^{\nu_1 k_1, \nu_2 k_2} = V_{\nu_4 k_4, \nu_3 k_3}^{\nu_2 k_2, \nu_1 k_1}$ and hermiticity requires $V_{\nu_3 k_3, \nu_4 k_4}^{\nu_1 k_1, \nu_2 k_2} = (V_{\nu_1 k_1, \nu_2 k_2}^{\nu_3 k_3, \nu_4 k_4})^*$. Momentum conservation $\delta(k_1 + k_2 - k_3 - k_4)$ is implicitly assumed inside $V$. Both

momentum conservation for interactions ($V$) and el-boson coupling ($G$) are assumed possible upto reciprocol lattice vectors $\frac{2\pi l}{a}$ for $l \in \mathbb{Z}$, where $a$ is the lattice spacing, to allow for momentum-Umklapp processes.

Furthermore, $M_{\nu k}^{\nu' k' q q_{||} \eta} = (M_{\nu' k'}^{\nu k (-q) q_{||} \eta})^*$ and $\Gamma_l^{\nu k} = (\Gamma_l^{\nu k})^*$.

**Hamiltonian in Floquet Basis**

We add a time-periodic drive to $H_0^{sys}$ such that now $H_0^{sys}(t+T) = H_0^{sys}(t)$, i.e. we drive the electrons with an external field of angular frequency $\Omega = \frac{2\pi}{T}$. The Floquet single particle states are related to the original electronic states by a unitary rotation,

$$\begin{aligned} c_{\nu k}^\dagger &= \sum_\alpha \langle \psi_{\alpha k}(t) | \nu k \rangle f_{\alpha k}^\dagger(t) \\ &= \sum_{\alpha n} e^{i(\mathcal{E}_{\alpha k} + n\Omega)t} \langle \phi_{\alpha k}^n | \nu k \rangle f_{\alpha k}^\dagger(t) \end{aligned}$$

$$\begin{aligned} c_{\nu k} &= \sum_\beta \langle \nu k | \psi_{\beta k}(t) \rangle f_{\beta k}(t) \\ &= \sum_{\beta m} e^{-i(\mathcal{E}_{\beta k} + m\Omega)t} \langle \nu k | \phi_{\beta k}^m \rangle f_{\beta k}(t) \end{aligned}$$

$$|\phi_{\alpha k}(t)\rangle = \sum_n e^{-in\Omega t} |\phi_{\alpha k}^n\rangle$$

where, $f_{\alpha k}^\dagger(t)|0(t)\rangle = |\psi_{\alpha k}(t)\rangle$ creates a one-particle Floquet state in band $\alpha$ and momentum $k$.

**El-El Term**

In the Floquet basis, the interactions become

$$\begin{aligned} H_{el-el} &= \frac{1}{2} \sum_{k_1 k_2 k_3 k_4} \sum_{\alpha \alpha' \beta \beta'} \sum_n e^{i(\mathcal{E}_{\alpha k_1} + \mathcal{E}_{\alpha' k_2} - \mathcal{E}_{\beta k_3} - \mathcal{E}_{\beta' k_4})t} e^{in\Omega t} V_{\beta k_3, \beta' k_4}^{\alpha k_1, \alpha' k_2}(n) f_{\alpha k_1}^\dagger(t) f_{\alpha' k_2}^\dagger(t) f_{\beta k_3}(t) f_{\beta' k_4}(t) \\ &= \frac{1}{2} \sum_{i_1 i_2 i_3 i_4} \sum_n e^{i(\mathcal{E}_{i_1} + \mathcal{E}_{i_2} - \mathcal{E}_{i_3} - \mathcal{E}_{i_4})t} e^{in\Omega t} V_{i_3 i_4}^{i_1 i_2}(n) f_{i_1}^\dagger(t) f_{i_2}^\dagger(t) f_{i_3}(t) f_{i_4}(t) \end{aligned}$$

$$V_{i_3 i_4}^{i_1 i_2}(n) = V_{\beta k_3, \beta' k_4}^{\alpha k_1, \alpha' k_2}(n) = \sum_{\nu_1 \nu_2 \nu_3 \nu_4} \sum_{n' m m'} V_{\nu_3 k_3, \nu_4 k_4}^{\nu_1 k_1, \nu_2 k_2} \langle \phi_{\alpha k_1}^{n - n' + m + m'} | \nu_1 k_1 \rangle \langle \phi_{\alpha' k_2}^{n'} | \nu_2 k_2 \rangle \langle \nu_3 k_3 | \phi_{\beta k_3}^m \rangle \langle \nu_4 k_4 | \phi_{\beta' k_4}^{m'} \rangle$$

with the packaged indices $i = (\alpha, k)$ and $V^{i_1 i_2}_{i_3 i_4}(n) = -V^{i_2 i_1}_{i_3 i_4}(n) = -V^{i_1 i_2}_{i_4 i_3}(n) = V^{i_2 i_1}_{i_4 i_3}(n)$ which reflects the antisymmetry of the fermions and hermiticity requires $V^{i_1 i_2}_{i_3 i_4}(n) = V^{i_3 i_4}_{i_1 i_2}(-n)^*$.

### El-Boson Term

The el-boson interaction becomes

$$\begin{aligned} H_{el-bos} &= \sum_{\alpha\beta} \sum_{kk' q q_{||} \eta} \sum_n e^{i(\mathcal{E}_{\alpha k'} - \mathcal{E}_{\beta k})t} e^{in\Omega t} G^{\alpha k'}_{\beta k, q q_{||}\eta}(n) f^\dagger_{\alpha k'}(t) f_{\beta k}(t) (b_{q q_{||}\eta} + b^\dagger_{-q q_{||}\eta}) \\ &= \sum_{i_1 i_2 j} \sum_n e^{i(\mathcal{E}_{i_1} - \mathcal{E}_{i_2})t} e^{in\Omega t} G^{i_1}_{i_2 j}(n) f^\dagger_{i_1}(t) f_{i_2}(t) (b_j + b^\dagger_{-j}) \end{aligned}$$

$$G^{i_1}_{i_2 j}(n) = G^{\alpha k'}_{\beta k, q q_{||}\eta}(n) = \sum_{m\nu\nu'} M^{\nu' k' q q_{||}\eta}_{\nu k} \delta(k' - k - q) \langle \phi^{n+m}_{\alpha k'} | \nu' k' \rangle \langle \nu k | \phi^m_{\beta k} \rangle$$

with the hermiticity requirement $G^{i_1}_{i_2 j}(n) = G^{i_2}_{i_1 (-j)}(-n)^*$ where $j = (q, q_{||}, \eta)$. Note that implicitly we understand that $-j = (-q, q_{||}, \eta)$ where applicable.

### El-Lead Term

The lead term becomes

$$\begin{aligned} H_{el-lead} &= \sum_{\alpha k l} \sum_n e^{i(\mathcal{E}_{\alpha k} + n\Omega)t} \Gamma^{\alpha k}_l(n) f^\dagger_{\alpha k}(t) d_l + h.c. \\ &= \sum_{i_1 l} \sum_n e^{i(\mathcal{E}_{i_1} + n\Omega)t} \Gamma^{i_1}_l(n) f^\dagger_{i_1}(t) d_l + h.c. \end{aligned}$$

$$\Gamma^{i_1}_l(n) = \Gamma^{\alpha k}_l(n) = \sum_\nu \Gamma^{\nu k}_l \langle \phi^n_{\alpha k} | \nu k \rangle$$

### Summary

Altogether,

$$H_0 = \sum_j \omega_j b^\dagger_j b_j + \sum_l \varepsilon_l d^\dagger_l d_l$$

$$
\begin{aligned}
H_{int} &= \sum_{i_1 i_2 j}\sum_{n} e^{i(\mathcal{E}_{i_1}-\mathcal{E}_{i_2})t} e^{in\Omega t} G^{i_1}_{i_2 j}(n) f^{\dagger}_{i_1}(t) f_{i_2}(t)(b_j + b^{\dagger}_{-j}) \\
&+ \frac{1}{2}\sum_{i_1 i_2 i_3 i_4}\sum_{n} e^{i(\mathcal{E}_{i_1}+\mathcal{E}_{i_2}-\mathcal{E}_{i_3}-\mathcal{E}_{i_4})t} e^{in\Omega t} V^{i_1 i_2}_{i_3 i_4}(n) f^{\dagger}_{i_1}(t) f^{\dagger}_{i_2}(t) f_{i_3}(t) f_{i_4}(t) \\
&+ \sum_{i_1 l}\sum_{n} e^{i(\mathcal{E}_{i_1}+n\Omega)t} \Gamma^{i_1}_{l}(n) f^{\dagger}_{i_1}(t) d_l + h.c.
\end{aligned}
$$

$$
\begin{aligned}
G^{i_1}_{i_2 j}(n) = G^{\alpha k'}_{\beta k, q q_{||} \eta}(n) &= \sum_{m\nu\nu'} M^{\nu' k' q q_{||} \eta}_{\nu k} \delta(k' - k - q) \langle \phi^{n+m}_{\alpha k'} | \nu' k' \rangle \langle \nu k | \phi^{m}_{\beta k} \rangle \\
V^{i_1 i_2}_{i_3 i_4}(n) = V^{\alpha k_1, \alpha' k_2}_{\beta k_3, \beta' k_4}(n) &= \sum_{\nu_1\nu_2\nu_3\nu_4}\sum_{n' m m'} V^{\nu_1 k_1, \nu_2 k_2}_{\nu_3 k_3, \nu_4 k_4} \langle \phi^{n-n'+m+m'}_{\alpha k_1} | \nu_1 k_1 \rangle \langle \phi^{n'}_{\alpha' k_2} | \nu_2 k_2 \rangle \langle \nu_3 k_3 | \phi^{m}_{\beta k_3} \rangle \langle \nu_4 k_4 | \phi^{m'}_{\beta' k_4} \rangle \\
\Gamma^{i_1}_{l}(n) = \Gamma^{\alpha k}_{l}(n) &= \sum_{\nu} \Gamma^{\nu k}_{l} \langle \phi^{n}_{\alpha k} | \nu k \rangle
\end{aligned}
$$

We will often refer to the boson term as the phonon term since this calculation was performed in the context of a periodically-driven semiconductor with bosons representing phonons in the lattice/substrate.

## 6.4 Floquet Kinetic Equations - Derivation

### Singlet Dynamics

We are interested in single particle correlators which evolve as per Eq. 6.11,

$$
i\hbar \frac{\partial}{\partial t} \langle f^{\dagger}_{a}(t) f_b(t) \rangle = \langle [f^{\dagger}_{a}(t) f_b(t), H^{bos}_0 + H^{lead}_0 + H_{int}] \rangle
$$

where $a, b$ are composite indices denoting the Floquet band and momentum of the state. For $a = b$, we have the Floquet state occupation and for $a \neq b$, we have the Floquet "polarization" or single-particle coherence in analogy to the $\langle \sigma^z \rangle, \langle \sigma^+ \rangle$ correlators studied in the context of a quantum-optics (Optical Bloch Equations). We compute the singlet dynamics term by term. Note the shorthand

$$
F^{a}_{b} \equiv \langle f^{\dagger}_{a}(t) f_b(t) \rangle
$$

and that $\delta_{xx'}$ denote Kronecker delta functions (1 if $x = x'$, if not 0) and similarly, $\delta(x - x')$ denote Dirac delta functions.

**Free Singlet**

The free terms yield,

$$\langle [f_a^\dagger(t) f_b(t), H_0^{bos} + H_0^{leads}] \rangle \quad = \quad 0$$

**El-Ph Singlet**

The el-boson interaction yields,

$$\begin{aligned}
[f_a^\dagger(t) f_b(t), H_{el-bos}] &= [f_a^\dagger(t) f_b(t), \sum_{i_1 i_2 j} \sum_n e^{i(\mathcal{E}_{i_1} - \mathcal{E}_{i_2})t} e^{in\Omega t} G^{i_1}_{i_2 j}(n) f^\dagger_{i_1}(t) f_{i_2}(t)(b_j + b^\dagger_{-j})] \\
&= \sum_{i_1 j} \sum_n \left( e^{i(\mathcal{E}_b - \mathcal{E}_{i_1})t} e^{in\Omega t} G^b_{i_1 j}(n) f_a^\dagger f_{i_1} - e^{i(\mathcal{E}_{i_1} - \mathcal{E}_a)t} e^{in\Omega t} G^{i_1}_{aj}(n) f^\dagger_{i_1} f_b \right) (b_j + b^\dagger_{-j})
\end{aligned}$$

Hence, we get

$$\begin{aligned}
\langle [f_a^\dagger(t) f_b(t), H_{el-bos}] \rangle &= \sum_{i_1 j} \sum_n e^{i(\mathcal{E}_b - \mathcal{E}_{i_1})t} e^{in\Omega t} G^b_{i_1 j}(n) \langle f_a^\dagger(t) f_{i_1}(t)(b_j + b^\dagger_{-j}) \rangle \\
&- \sum_{i_1 j} \sum_n e^{i(\mathcal{E}_{i_1} - \mathcal{E}_a)t} e^{in\Omega t} G^{i_1}_{aj}(n) \langle f^\dagger_{i_1}(t) f_b(t)(b_j + b^\dagger_{-j}) \rangle \\
&\equiv Ph_d
\end{aligned}$$

**El-El Singlet**

The el-el interactions yield,

$$\begin{aligned}
[f_a^\dagger(t) f_b(t), H_{el-el}] &= \sum_{i_2 i_3 i_4} \sum_n e^{i(\mathcal{E}_b + \mathcal{E}_{i_2} - \mathcal{E}_{i_3} - \mathcal{E}_{i_4})t} e^{in\Omega t} V^{bi_2}_{i_3 i_4}(n) f_a^\dagger f^\dagger_{i_2} f_{i_3} f_{i_4} \\
&+ \sum_{i_1 i_2 i_3} \sum_n e^{i(\mathcal{E}_{i_1} + \mathcal{E}_{i_2} - \mathcal{E}_a - \mathcal{E}_{i_3})t} e^{in\Omega t} V^{i_1 i_2}_{a i_3}(n) f^\dagger_{i_1} f^\dagger_{i_2} f_{i_3} f_b
\end{aligned}$$

Hence, we get

$$\begin{aligned}
\langle [f_a^\dagger(t) f_b(t), H_{el-el}] \rangle &= \sum_{i_2 i_3 i_4} \sum_n e^{i(\mathcal{E}_b + \mathcal{E}_{i_2} - \mathcal{E}_{i_3} - \mathcal{E}_{i_4})t} e^{in\Omega t} V^{bi_2}_{i_3 i_4}(n) \langle f_a^\dagger f^\dagger_{i_2} f_{i_3} f_{i_4} \rangle \\
&+ \sum_{i_1 i_2 i_3} \sum_n e^{i(\mathcal{E}_{i_1} + \mathcal{E}_{i_2} - \mathcal{E}_a - \mathcal{E}_{i_3})t} e^{in\Omega t} V^{i_1 i_2}_{a i_3}(n) \langle f^\dagger_{i_1} f^\dagger_{i_2} f_{i_3} f_b \rangle \\
&\equiv El_d
\end{aligned}$$

**Lead Singlet**

The el-leads term yields,

$$\begin{aligned}[f_a^\dagger(t)f_b(t), \sum_{ik}\sum_n e^{i\mathcal{E}_i t}e^{in\Omega t}\Gamma_k^i(n)f_i^\dagger(t)d_k + h.c.] &= \sum_k\sum_n e^{i\mathcal{E}_b t}e^{in\Omega t}\Gamma_k^b(n)f_a^\dagger(t)d_k \\ &- \sum_k\sum_n e^{-i\mathcal{E}_a t}e^{-in\Omega t}(\Gamma_k^a(n))^* f_b(t)d_k^\dagger\end{aligned}$$

Hence, we get

$$\begin{aligned}\langle[f_a^\dagger(t)f_b(t), \sum_{ik}\sum_n e^{i\mathcal{E}_i t}e^{in\Omega t}\Gamma_k^i(n)f_i^\dagger(t)d_k + h.c.]\rangle &= \sum_k\sum_n e^{i\mathcal{E}_b t}e^{in\Omega t}\Gamma_k^b(n)\langle f_a^\dagger(t)d_k\rangle \\ &- \sum_k\sum_n e^{-i\mathcal{E}_a t}e^{-in\Omega t}(\Gamma_k^a(n))^*\langle f_b(t)d_k^\dagger\rangle \\ &\equiv Ld_d\end{aligned}$$

**Summary**

In summary, the singlet dynamics are

$$\begin{aligned}i\hbar\frac{\partial}{\partial t}\langle f_a^\dagger(t)f_b(t)\rangle &= \sum_{i_1 j}\sum_n e^{i(\mathcal{E}_b-\mathcal{E}_{i_1})t}e^{in\Omega t}G_{i_1 j}^b(n)\langle f_a^\dagger(t)f_{i_1}(t)(b_j+b_{-j}^\dagger)\rangle \\ &- \sum_{i_1 j}\sum_n e^{i(\mathcal{E}_{i_1}-\mathcal{E}_a)t}e^{in\Omega t}G_{aj}^{i_1}(n)\langle f_{i_1}^\dagger(t)f_b(t)(b_j+b_{-j}^\dagger)\rangle \\ &+ \sum_{i_2 i_3 i_4}\sum_n e^{i(\mathcal{E}_b+\mathcal{E}_{i_2}-\mathcal{E}_{i_3}-\mathcal{E}_{i_4})t}e^{in\Omega t}V_{i_3 i_4}^{b i_2}(n)\langle f_a^\dagger(t)f_{i_2}^\dagger(t)f_{i_3}(t)f_{i_4}(t)\rangle \\ &+ \sum_{i_1 i_2 i_3}\sum_n e^{i(\mathcal{E}_{i_1}+\mathcal{E}_{i_2}-\mathcal{E}_a-\mathcal{E}_{i_3})t}e^{in\Omega t}V_{a i_3}^{i_1 i_2}(n)\langle f_{i_1}^\dagger(t)f_{i_2}^\dagger(t)f_{i_3}(t)f_b(t)\rangle \\ &+ \sum_k\sum_n e^{i\mathcal{E}_b t}e^{in\Omega t}\Gamma_k^b(n)\langle f_a^\dagger(t)d_k\rangle - \sum_k\sum_n e^{-i\mathcal{E}_a t}e^{-in\Omega t}(\Gamma_k^a(n))^*\langle f_b(t)d_k^\dagger\rangle \\ &= Ph_d + El_d + Ld_d \qquad (6.14)\end{aligned}$$

where we notice the appearance of 2-object expectation values as expected in the hierarchy in Eq.6.4.

**Doublet Dynamics**

We can compute the dynamics for each of the 2-object terms appearing in Eq.6.14. In this section we will use "doublet" to refer to $\langle 2\rangle$ and $\Delta\langle 2\rangle$. The distinction, when necessary, will be made clear. We shall assume thermal phonons and so $\langle b\rangle = \langle b^\dagger\rangle = 0$ (incoherence) and $\langle b_j^\dagger b_k\rangle = \delta_{jk}\frac{1}{e^{\omega_j/T_{ph}}-1} \equiv N_{\omega_j}$, i.e. phonon occupation is given by a Bose-Einstein distribution with temperature $T_{ph}$. Similarly, we assume the lead is thermal such that $\langle d_j^\dagger d_k\rangle = \delta_{jk}\frac{1}{e^{(\varepsilon_j-\mu_{res})/T_{res}}+1} \equiv D_j$, i.e. a Fermi-Dirac distribution with temperature $T_{res}$ and chemical potential $\mu_{res}$, and $\langle d\rangle = \langle d^\dagger\rangle = 0$. As a consequence, below we will see that $\Delta\langle 2\rangle = \langle 2\rangle$ for boson and lead terms since the $\langle 2\rangle_S$ terms vanish. We begin with the phonon terms.

**Phonon Doublet 1**

Consider the generic doublet $\langle f_{a_1}^\dagger(t) f_{a_2}(t) b_r\rangle$

$$i\hbar\frac{\partial}{\partial t}\langle f_{a_1}^\dagger(t) f_{a_2}(t) b_r\rangle = \langle [f_{a_1}^\dagger f_{a_2} b_r, H - H_0^{sys}]\rangle$$

Let us now compute this term by term.

**Free Part**

$$\begin{aligned}[f_{a_1}^\dagger f_{a_2} b_r, H_0^{bos} + H_0^{lead}] &= [f_{a_1}^\dagger f_{a_2} b_r, \sum_j \omega_j b_j^\dagger b_j + \sum_l \varepsilon_l d_l^\dagger d_l] \\ &= \omega_r f_{a_1}^\dagger f_{a_2} b_r\end{aligned}$$

**Phonon Part**

$$\begin{aligned}[f_{a_1}^\dagger f_{a_2} b_r, H_{el-bos}] &= [f_{a_1}^\dagger f_{a_2} b_r, \sum_{i_1 i_2 j}\sum_n e^{i(\mathcal{E}_{i_1}-\mathcal{E}_{i_2})t} e^{in\Omega t} G_{i_2 j}^{i_1}(n) f_{i_1}^\dagger(t) f_{i_2}(t)(b_j + b_{-j}^\dagger)] \\ &= \sum_{i_1 i_2 j}\sum_n e^{i(\mathcal{E}_{i_1}-\mathcal{E}_{i_2})t} e^{in\Omega t} G_{i_2 j}^{i_1}(n)[f_{a_1}^\dagger f_{a_2} b_r, f_{i_1}^\dagger f_{i_2} b_j] \\ &+ \sum_{i_1 i_2 j}\sum_n e^{i(\mathcal{E}_{i_1}-\mathcal{E}_{i_2})t} e^{in\Omega t} G_{i_2 j}^{i_1}(n)[f_{a_1}^\dagger f_{a_2} b_r, f_{i_1}^\dagger f_{i_2} b_{-j}^\dagger]\end{aligned}$$

where $-j = (\eta, -q, q_{||})$. Since we plan to factorize all clusters into singlets, we get $\langle bb\rangle_S = 0$ and so we can just drop the first term in the second equality. Taking the expectation value and factorizing the remaining term into singlets,

$$\begin{aligned}\langle [f_{a_1}^\dagger f_{a_2} b_r, H_{el-bos}]\rangle \approx \sum_{i_1 i_2 j}\sum_n & e^{i(\mathcal{E}_{i_1}-\mathcal{E}_{i_2})t} e^{in\Omega t} G_{(-r)}^{i_1}(n) \\ & \left(F_{i_2}^{a_1}(\delta_{a_2 i_1} - F_{a_2}^{i_1})(1+N_{\omega_r}) - F_{a_2}^{i_1}(\delta_{i_2 a_1} - F_{i_2}^{a_1})N_{\omega_r} + F_{a_2}^{a_1}F_{i_2}^{i_1}\right)\end{aligned}$$

where $F^{a_1}_{a_2} \equiv \langle f^\dagger_{a_1} f_{a_2}\rangle$ and $N_{\omega_r} \equiv \langle b^\dagger_r b_r\rangle$ is the boson occupation number.

**Electron Part**

$$\begin{aligned}[f^\dagger_{a_1} f_{a_2} b_r, H_{el-el}] &= [f^\dagger_{a_1} f_{a_2} b_r, \frac{1}{2}\sum_{i_1 i_2 i_3 i_4}\sum_n e^{i(\mathcal{E}_{i_1}+\mathcal{E}_{i_2}-\mathcal{E}_{i_3}-\mathcal{E}_{i_4})t} e^{in\Omega t} V^{i_1 i_2}_{i_3 i_4}(n) f^\dagger_{i_1}(t) f^\dagger_{i_2}(t) f_{i_3}(t) f_{i_4}(t)] \\ &= \frac{1}{2}\sum_{i_1 i_2 i_3 i_4}\sum_n e^{i(\mathcal{E}_{i_1}+\mathcal{E}_{i_2}-\mathcal{E}_{i_3}-\mathcal{E}_{i_4})t} e^{in\Omega t} V^{i_1 i_2}_{i_3 i_4}(n)[f^\dagger_{a_1} f_{a_2}, f^\dagger_{i_1} f^\dagger_{i_2} f_{i_3} f_{i_4}] b_r\end{aligned}$$

Applying the singlet factorization will give $\langle b\rangle = 0$ everywhere and so this term can be dropped.

**Lead Part**

$$\begin{aligned}[f^\dagger_{a_1} f_{a_2} b_r, H_{el-lead}] &= [f^\dagger_{a_1} f_{a_2} b_r, \sum_{il}\sum_n e^{i\mathcal{E}_i t} e^{in\Omega t}\Gamma^i_l(n) f^\dagger_i(t) d_l + h.c.] \\ &= \sum_{il}\sum_n e^{i\mathcal{E}_i t} e^{in\Omega t}\Gamma^i_l(n)[f^\dagger_{a_1} f_{a_2}, f^\dagger_i] b_r d_l + [f^\dagger_{a_1} f_{a_2} b_r, h.c.]\end{aligned}$$

Again this term vanishes for thermal phonons since$\langle b\rangle = 0$ upon singlet factorization.

**All together**

$$\begin{aligned}i\hbar\frac{\partial}{\partial t}\langle f^\dagger_{a_1} f_{a_2} b_r\rangle &= \omega_r\langle f^\dagger_{a_1} f_{a_2} b_r\rangle + \sum_{i_1 i_2 j}\sum_n e^{i(\mathcal{E}_{i_1}-\mathcal{E}_{i_2})t} e^{in\Omega t} G^{i_1}_{(-r)}(n) \\ &\quad \left(F^{a_1}_{i_2}(\delta_{a_2 i_1} - F^{i_1}_{a_2})(1+N_{\omega_r}) - F^{i_1}_{a_2}(\delta_{i_2 a_1} - F^{a_1}_{i_2})N_{\omega_r} + F^{a_1}_{a_2} F^{i_1}_{i_2}\right)\end{aligned}$$

We now formally integrate this differential equation from an initial time $t_0$ to later time $t$,

$$\begin{aligned}\langle f^\dagger_{a_1} f_{a_2} b_r\rangle &= \frac{1}{i\hbar} e^{-i\omega_r t}\int_{t_0}^{t} dz \sum_{i_1 i_2}\sum_n e^{i(\mathcal{E}_{i_1}-\mathcal{E}_{i_2}+\omega_r+n\Omega)z} G^{i_1}_{i_2(-r)}(n) \\ &\quad \left(F^{a_1}_{i_2}(\delta_{a_2 i_1} - F^{i_1}_{a_2})(1+N_{\omega_r}) - F^{i_1}_{a_2}(\delta_{i_2 a_1} - F^{a_1}_{i_2})N_{\omega_r} + F^{a_1}_{a_2} F^{i_1}_{i_2}\right)\end{aligned}$$

where all singlets $F$ are functions of $z$ on the RHS and the LHS is a function of $t$.

**Phonon Doublet 2**

Consider the generic doublet $\langle f^\dagger_{a_1}(t) f_{a_2}(t) b^\dagger_{-r}\rangle$

$$i\hbar\frac{\partial}{\partial t}\langle f^\dagger_{a_1}(t) f_{a_2}(t) b^\dagger_{-r}\rangle = \langle[f^\dagger_{a_1} f_{a_2} b^\dagger_{-r}, H - H^{sys}_0]\rangle$$

Let us now compute this term by term.

**Free Part**

$$\begin{aligned}[f_{a_1}^\dagger f_{a_2} b_r^\dagger, H_0^{bos} + H_0^{leads}] &= [f_{a_1}^\dagger f_{a_2} b_r^\dagger, \sum_j \omega_j b_j^\dagger b_j + \sum_l \varepsilon_l d_l^\dagger d_l] \\ &= -\omega_r f_{a_1}^\dagger f_{a_2} b_r^\dagger\end{aligned}$$

**Phonon Part**

$$\begin{aligned}[f_{a_1}^\dagger f_{a_2} b_r^\dagger, H_{el-bos}] &= [f_{a_1}^\dagger f_{a_2} b_r^\dagger, \sum_{i_1 i_2 j} \sum_n e^{i(\mathcal{E}_{i_1} - \mathcal{E}_{i_2})t} e^{in\Omega t} G_{i_2 j}^{i_1}(n) f_{i_1}^\dagger(t) f_{i_2}(t)(b_j + b_{-j}^\dagger)] \\ &= \sum_{i_1 i_2 j} \sum_n e^{i(\mathcal{E}_{i_1} - \mathcal{E}_{i_2})t} e^{in\Omega t} G_{i_2 j}^{i_1}(n)[f_{a_1}^\dagger f_{a_2} b_r^\dagger, f_{i_1}^\dagger f_{i_2} b_j] \\ &+ \sum_{i_1 i_2 j} \sum_n e^{i(\mathcal{E}_{i_1} - \mathcal{E}_{i_2})t} e^{in\Omega t} G_{i_2 j}^{i_1}(n)[f_{a_1}^\dagger f_{a_2} b_r^\dagger, f_{i_1}^\dagger f_{i_2} b_{-j}^\dagger]\end{aligned}$$

Again, we can drop the second term on the RHS due to thermal phonons ($\langle b^\dagger \rangle = 0$ and so $\langle b^\dagger b^\dagger \rangle_S = 0$). Upon factorizing the expectation values of the remaining term into singlets,

$$\begin{aligned}\langle [f_{a_1}^\dagger f_{a_2} b_r^\dagger, H_{el-ph}] \rangle &\approx \sum_{i_1 i_2} \sum_n e^{i(\mathcal{E}_{i_1} - \mathcal{E}_{i_2})t} e^{in\Omega t} G_{i_2 r}^{i_1}(n) \\ &\left( F_{i_2}^{a_1}(\delta_{a_2 i_1} - F_{a_2}^{i_1}) N_{\omega_r} - F_{a_2}^{i_1}(\delta_{i_2 a_1} - F_{i_2}^{a_1})(1 + N_{\omega_r}) - F_{i_2}^{i_1} F_{a_2}^{a_1} \right)\end{aligned}$$

**Electron Part** Disappears for same reason as the Ph Doublet 1.

**Lead Part** Disappears for same reason as the Ph Doublet 1.

**All together**

$$\begin{aligned}i\hbar \frac{\partial}{\partial t} \langle f_{a_1}^\dagger f_{a_2} b_r^\dagger \rangle &= -\omega_r \langle f_{a_1}^\dagger f_{a_2} b_r \rangle + \sum_{i_1 i_2} \sum_n e^{i(\mathcal{E}_{i_1} - \mathcal{E}_{i_2})t} e^{in\Omega t} G_{i_2 r}^{i_1}(n) \\ &\left( F_{i_2}^{a_1}(\delta_{a_2 i_1} - F_{a_2}^{i_1}) N_{\omega_r} - F_{a_2}^{i_1}(\delta_{i_2 a_1} - F_{i_2}^{a_1})(1 + N_{\omega_r}) - F_{i_2}^{i_1} F_{a_2}^{a_1} \right)\end{aligned}$$

Upon integration,

$$\begin{aligned}\langle f_{a_1}^\dagger f_{a_2} b_r^\dagger \rangle &= \frac{1}{i\hbar} e^{i\omega_r t} \sum_{i_1 i_2} \sum_n G_{i_2 r}^{i_1}(n) \int_{t_0}^t dz e^{i(\mathcal{E}_{i_1} - \mathcal{E}_{i_2} - \omega_r + n\Omega)z} \\ &\left( F_{i_2}^{a_1}(\delta_{a_2 i_1} - F_{a_2}^{i_1}) N_{\omega_r} - F_{a_2}^{i_1}(\delta_{i_2 a_1} - F_{i_2}^{a_1})(1 + N_{\omega_r}) - F_{i_2}^{i_1} F_{a_2}^{a_1} \right)\end{aligned}$$

**Summary**

Combining the two phonon doublet contributions,

$$
\begin{aligned}
Ph_d &= \frac{1}{i\hbar}\sum_{i_1 j i_1' i_2'}\sum_{mn} G^{b}_{i_1 j}(n) G^{i_1'}_{i_2'(-j)}(m) e^{i(\mathcal{E}_b-\mathcal{E}_{i_1}-\omega_j+n\Omega)t}\int_{t_0}^{t} dz e^{i(\mathcal{E}_{i_1'}-\mathcal{E}_{i_2'}+\omega_j+m\Omega)z} \\
&\quad \left(F^{a}_{i_2'}(\delta_{i_1 i_1'}-F^{i_1'}_{i_1})(1+N_{\omega_j}) - F^{i_1'}_{i_1}(\delta_{i_2' a}-F^{a}_{i_2'})N_{\omega_j} + F^{a}_{i_1}F^{i_1'}_{i_2'}\right) \\
&+ \frac{1}{i\hbar}\sum_{i_1 j i_1' i_2'}\sum_{mn} G^{b}_{i_1 j}(n) G^{i_1'}_{i_2'(-j)}(m) e^{i(\mathcal{E}_b-\mathcal{E}_{i_1}+\omega_{(-j)}+n\Omega)t}\int_{t_0}^{t} dz e^{i(\mathcal{E}_{i_1'}-\mathcal{E}_{i_2'}-\omega_{(-j)}+m\Omega)z} \\
&\quad \left(F^{a}_{i_2'}(\delta_{i_1 i_1'}-F^{i_1'}_{i_1})N_{\omega_{(-j)}} - F^{i_1'}_{i_1}(\delta_{i_2' a}-F^{a}_{i_2'})(1+N_{\omega_{(-j)}}) - F^{i_1'}_{i_2'}F^{a}_{i_1}\right) \\
&- \frac{1}{i\hbar}\sum_{i_1 j i_1' i_2'}\sum_{mn} G^{i_1}_{a j}(n) G^{i_1'}_{i_2'(-j)}(m) e^{i(\mathcal{E}_{i_1}-\mathcal{E}_a-\omega_j+n\Omega)t}\int_{t_0}^{t} dz e^{i(\mathcal{E}_{i_1'}-\mathcal{E}_{i_2'}+\omega_j+m\Omega)z} \\
&\quad \left(F^{i_1}_{i_2'}(\delta_{b i_1'}-F^{i_1'}_{b})(1+N_{\omega_j}) - F^{i_1'}_{b}(\delta_{i_2' i_1}-F^{i_1}_{i_2'})N_{\omega_j} + F^{i_1}_{b}F^{i_1'}_{i_2'}\right) \\
&- \frac{1}{i\hbar}\sum_{i_1 j i_1' i_2'}\sum_{mn} G^{i_1}_{a j}(n) G^{i_1'}_{i_2'(-j)}(m) e^{i(\mathcal{E}_{i_1}-\mathcal{E}_a+\omega_{(-j)}+n\Omega)t}\int_{t_0}^{t} dz e^{i(\mathcal{E}_{i_1'}-\mathcal{E}_{i_2'}-\omega_{(-j)}+m\Omega)z} \\
&\quad \left(F^{i_1}_{i_2'}(\delta_{b i_1'}-F^{i_1'}_{b})N_{\omega_{(-j)}} - F^{i_1'}_{b}(\delta_{i_2' i_1}-F^{i_1}_{i_2'})(1+N_{\omega_{(-j)}}) - F^{i_1'}_{i_2'}F^{i_1}_{b}\right)
\end{aligned}
$$

where all correlators are functions of $z$ on the RHS and the LHS is a function of $t$.

**Markov Approximation - Redfield Dynamics**

We make the standard Markov approximation. Assume the memory ($\tau = t - z$) depth is short as the bath contributes a dense spectrum of energies which interfere destructively once $\tau$ becomes appreciable. Assume that the correlators $F$ are time local and hence only functions of $t$. Extend the memory integral to $\infty$ and perform the resulting integration (note that we have taken $t_0 = 0$). Upon implementing these approximations and dropping principle value terms, we get

$$
\begin{aligned}
\frac{1}{i\hbar}Ph_d \;\approx\;& \frac{\pi}{\hbar}\sum_{i_1 j i_1' i_2'}\sum_{mn} G^{b}_{i_1 j}(n)G^{i_1'}_{i_2'(-j)}(m)e^{i(\mathcal{E}_b-\mathcal{E}_{i_1}+\mathcal{E}_{i_1'}-\mathcal{E}_{i_2'}+(n+m)\Omega)t}\delta(\mathcal{E}_{i_1'}-\mathcal{E}_{i_2'}+\omega_j+m\Omega)\\
&\left(F^{i_1'}_{i_1}(\delta_{i_2' a}-F^{a}_{i_2'})N_{\omega_j}-F^{a}_{i_2'}(\delta_{i_1 i_1'}-F^{i_1'}_{i_1})(1+N_{\omega_j})-F^{a}_{i_1}F^{i_1'}_{i_2'}\right)\\
+\;& \frac{\pi}{\hbar}\sum_{i_1 j i_1' i_2'}\sum_{mn} G^{b}_{i_1 j}(n)G^{i_1'}_{i_2'(-j)}(m)e^{i(\mathcal{E}_b-\mathcal{E}_{i_1}+\mathcal{E}_{i_1'}-\mathcal{E}_{i_2'}+(n+m)\Omega)t}\delta(\mathcal{E}_{i_1'}-\mathcal{E}_{i_2'}-\omega_{(-j)}+m\Omega)\\
&\left(F^{i_1'}_{i_1}(\delta_{i_2' a}-F^{a}_{i_2'})(1+N_{\omega_{(-j)}})-F^{a}_{i_2'}(\delta_{i_1 i_1'}-F^{i_1'}_{i_1})N_{\omega_{(-j)}}+F^{i_1'}_{i_2'}F^{a}_{i_1}\right)\\
+\;& \frac{\pi}{\hbar}\sum_{i_1 j i_1' i_2'}\sum_{mn} G^{i_1}_{aj}(n)G^{i_1'}_{i_2'(-j)}(m)e^{i(\mathcal{E}_{i_1}-\mathcal{E}_a+\mathcal{E}_{i_1'}-\mathcal{E}_{i_2'}+(n+m)\Omega)t}\delta(\mathcal{E}_{i_1'}-\mathcal{E}_{i_2'}+\omega_j+m\Omega)\\
&\left(F^{i_1}_{i_2'}(\delta_{b i_1'}-F^{i_1'}_{b})(1+N_{\omega_j})-F^{i_1'}_{b}(\delta_{i_2' i_1}-F^{i_1}_{i_2'})N_{\omega_j}+F^{i_1}_{b}F^{i_1'}_{i_2'}\right)\\
+\;& \frac{\pi}{\hbar}\sum_{i_1 j i_1' i_2'}\sum_{mn} G^{i_1}_{aj}(n)G^{i_1'}_{i_2'(-j)}(m)e^{i(\mathcal{E}_{i_1}-\mathcal{E}_a+\mathcal{E}_{i_1'}-\mathcal{E}_{i_2'}+(n+m)\Omega)t}\delta(\mathcal{E}_{i_1'}-\mathcal{E}_{i_2'}-\omega_{(-j)}+m\Omega)\\
&\left(F^{i_1}_{i_2'}(\delta_{b i_1'}-F^{i_1'}_{b})N_{\omega_{(-j)}}-F^{i_1'}_{b}(\delta_{i_2' i_1}-F^{i_1}_{i_2'})(1+N_{\omega_{(-j)}})-F^{i_1'}_{i_2'}F^{i_1}_{b}\right)
\end{aligned}
$$

This is the Redfield equation for a thermal bosonic bath. Note that one can acheive the same result in the standard density matrix master equation formalism by making the usual Born-Markov approximation.

**Diagonal Limit of Redfield Dynamics - Boltzmann Dynamics**

The "diagonal limit" of the Redfield equations, where we assume the Floquet polarizations vanish and only the occupations survive, is given by the simple form

$$
\begin{aligned}
\frac{1}{i\hbar}Ph_d\delta_{ab} \;=\;& \frac{2\pi}{\hbar}\sum_{i_1 j}\sum_{m}|G^{a}_{i_1 j}(m)|^2\delta(\mathcal{E}_a-\mathcal{E}_{i_1}-\omega_j+m\Omega)\left(F^{i_1}_{i_1}(1-F^{a}_{a})N_{\omega_j}-F^{a}_{a}(1-F^{i_1}_{i_1})(1+N_{\omega_j})\right)\\
+\;& \frac{2\pi}{\hbar}\sum_{i_1 j}\sum_{m}|G^{a}_{i_1 j}(m)|^2\delta(\mathcal{E}_a-\mathcal{E}_{i_1}+\omega_j+m\Omega)\left(F^{i_1}_{i_1}(1-F^{a}_{a})(1+N_{\omega_j})-F^{a}_{a}(1-F^{i_1}_{i_1})N_{\omega_j}\right)
\end{aligned}
$$

where we have assumed $\omega_j = \omega_{(-j)}$ for the boson spectrum. Additionally, we assume that $\Omega^{-1} \ll T_R$, where $T_R$ is the characteristic dissipative time scale set by $G$, and hence on any coarse-grained scale, we may take $\delta_{-n,m}$ in the Redfield dynamics. This is a Rotating-Wave (RWA)/secular approximation on the Floquet zone indices. We recover the familiar form of "Floquet-Fermi-Golden-Rule" rates giving rise to Boltzmann dynamics.

**Electron Doublet**

Consider the generic doublet $\langle f^{\dagger}_{a_1}(t)f^{\dagger}_{a_2}(t)f_{a_3}(t)f_{a_4}(t)\rangle$.

$$i\hbar\frac{\partial}{\partial t}\langle f^\dagger_{a_1}(t)f^\dagger_{a_2}(t)f_{a_3}(t)f_{a_4}(t)\rangle \;=\; \langle[f^\dagger_{a_1}f^\dagger_{a_2}f_{a_3}f_{a_4}, H-H_0^{sys}]\rangle$$

Let us now compute this term by term.

**Free Part**

$$\begin{aligned}[f^\dagger_{a_1}f^\dagger_{a_2}f_{a_3}f_{a_4}, H_0^{bos}+H_0^{leads}] &= [f^\dagger_{a_1}f^\dagger_{a_2}f_{a_3}f_{a_4}, \sum_j \omega_j b^\dagger_j b_j + \sum_l \varepsilon_l d^\dagger_l d_l]\\ &= 0\end{aligned}$$

**Phonon Part**

$$\begin{aligned}[f^\dagger_{a_1}f^\dagger_{a_2}f_{a_3}f_{a_4}, \sum_{i_1i_2j}\sum_n e^{i(\mathcal{E}_{i_1}-\mathcal{E}_{i_2})t}e^{in\Omega t}G^{i_1}_{i_2j}(n)f^\dagger_{i_1}f_{i_2}(b_j+b^\dagger_{-j})] &= \sum_{i_1i_2j}\sum_n e^{i(\mathcal{E}_{i_1}-\mathcal{E}_{i_2})t}e^{in\Omega t}G^{i_1}_{i_2j}(n)\\ &\quad [f^\dagger_{a_1}f^\dagger_{a_2}f_{a_3}f_{a_4}, f^\dagger_{i_1}f_{i_2}](b_j+b^\dagger_{-j})\end{aligned}$$

Upon singlet factorization, we would get $\langle b\rangle$ terms and again, in the thermal phonon limit, this vanishes.

**Lead Part**

Similar to the case of phonon doublets, this term vanishes since $\langle d\rangle = \langle d^\dagger\rangle = 0$ upon singlet factorization.

**Electron Part**

We are interested in $\Delta\langle 2\rangle = \langle 2\rangle - \langle 2\rangle_S$ for this doublet which we will singlet factorize as per Eq.6.7. This is given by

$$\begin{aligned}i\hbar\frac{\partial}{\partial t}\Delta\langle f^\dagger_{a_1}(t)f^\dagger_{a_2}(t)f_{a_3}(t)f_{a_4}(t)\rangle &= i\hbar\frac{\partial}{\partial t}\langle f^\dagger_{a_1}(t)f^\dagger_{a_2}(t)f_{a_3}(t)f_{a_4}(t)\rangle - i\hbar\frac{\partial}{\partial t}\langle f^\dagger_{a_1}(t)f^\dagger_{a_2}(t)f_{a_3}(t)f_{a_4}(t)\rangle_S\\ &\equiv R-W\end{aligned}$$

where

$$\begin{aligned}i\hbar\frac{\partial}{\partial t}\langle f^\dagger_{a_1}(t)f^\dagger_{a_2}(t)f_{a_3}(t)f_{a_4}(t)\rangle &= R\\ i\hbar\frac{\partial}{\partial t}\langle f^\dagger_{a_1}(t)f^\dagger_{a_2}(t)f_{a_3}(t)f_{a_4}(t)\rangle_S &= W\end{aligned}$$

Anticipating the singlet factorization of $\Delta\langle 2\rangle$, we just write the single operator evolution under only the electron-electron interaction $H_{el-el}$ as

$$i\hbar\frac{\partial}{\partial t}f_a^\dagger = \sum_{i_1 i_2 i_3}\sum_n e^{i(\mathcal{E}_{i_1}+\mathcal{E}_{i_2}-\mathcal{E}_{i_3}-\mathcal{E}_a)t}e^{in\Omega t}V_{ai_3}^{i_1 i_2}(n)f_{i_1}^\dagger f_{i_2}^\dagger f_{i_3}$$

$$i\hbar\frac{\partial}{\partial t}f_a = \sum_{i_2 i_3 i_4}\sum_n e^{i(\mathcal{E}_a+\mathcal{E}_{i_2}-\mathcal{E}_{i_3}-\mathcal{E}_{i_4})t}e^{in\Omega t}V_{i_3 i_4}^{a i_2}(n)f_{i_2}^\dagger f_{i_3} f_{i_4}$$

**Calculation of $\langle 2\rangle_S$**

The doublets are

$$\begin{aligned} El_d &= \sum_{a_2 a_3 a_4}\sum_n e^{i(\mathcal{E}_b+\mathcal{E}_{a_2}-\mathcal{E}_{a_3}-\mathcal{E}_{a_4})t}e^{in\Omega t}V_{a_3 a_4}^{b a_2}(n)\langle f_{a_1}^\dagger f_{a_2}^\dagger f_{a_3} f_{a_4}\rangle \\ &+ \sum_{a_2 a_3 a_4}\sum_n e^{i(\mathcal{E}_{a_2}+\mathcal{E}_{a_3}-\mathcal{E}_{a_1}-\mathcal{E}_{a_4})t}e^{in\Omega t}V_{a_1 a_4}^{a_2 a_3}(n)\langle f_{a_2}^\dagger f_{a_3}^\dagger f_{a_4} f_b\rangle \end{aligned}$$

where we have relabled $a \to a_1$, and $i_n \to a_n$ on the first term and $i_n \to a_{n+1}$ on the second term from Eq.6.14. Upon singlet factorization,

$$\begin{aligned} (El_d)_S &\approx \sum_{a_2 a_3 a_4}\sum_n e^{i(\mathcal{E}_b+\mathcal{E}_{a_2}-\mathcal{E}_{a_3}-\mathcal{E}_{a_4})t}e^{in\Omega t}V_{a_3 a_4}^{b a_2}(n)\left(F_{a_4}^{a_1}F_{a_3}^{a_2}-F_{a_3}^{a_1}F_{a_4}^{a_2}\right) \\ &+ \sum_{a_2 a_3 a_4}\sum_n e^{i(\mathcal{E}_{a_2}+\mathcal{E}_{a_3}-\mathcal{E}_{a_1}-\mathcal{E}_{a_4})t}e^{in\Omega t}V_{a_1 a_4}^{a_2 a_3}(n)\left(F_b^{a_2}F_{a_4}^{a_3}-F_{a_4}^{a_2}F_b^{a_3}\right) \end{aligned}$$

**Calculation of $i\hbar\partial_t\langle 2\rangle_S$ ($W$ term)**

The singlet factorization for a generic doublet is,

$$\langle f_{a_1}^\dagger f_{a_2}^\dagger f_{a_3} f_{a_4}\rangle_S = F_{a_4}^{a_1}F_{a_3}^{a_2}-F_{a_3}^{a_1}F_{a_4}^{a_2}$$

As before, in anticipation of the singlet factorization, we only keep the electron-electron contribution to the singlet kinetic equation in Eq.6.14, for each $i\partial_t F$ piece contributing to $\langle f_{a_1}^\dagger f_{a_2}^\dagger f_{a_3} f_{a_4}\rangle_S$. Therefore, for this computation,

$$
\begin{aligned}
i\hbar\frac{\partial}{\partial t}F_b^a &= \sum_{i_2 i_3 i_4}\sum_n e^{i(\mathcal{E}_b+\mathcal{E}_{i_2}-\mathcal{E}_{i_3}-\mathcal{E}_{i_4})t}e^{in\Omega t}V_{i_3 i_4}^{b i_2}(n)\langle f_a^\dagger f_{i_2}^\dagger f_{i_3} f_{i_4}\rangle \\
&+ \sum_{i_1 i_2 i_3}\sum_n e^{i(\mathcal{E}_{i_1}+\mathcal{E}_{i_2}-\mathcal{E}_a-\mathcal{E}_{i_3})t}e^{in\Omega t}V_{a i_3}^{i_1 i_2}(n)\langle f_{i_1}^\dagger f_{i_2}^\dagger f_{i_3} f_b\rangle
\end{aligned}
$$

Its dynamics are,

$$
\begin{aligned}
W &= i\hbar\partial_t(F_{a_4}^{a_1})F_{a_3}^{a_2} + i\hbar F_{a_4}^{a_1}\partial_t(F_{a_3}^{a_2}) - i\hbar\partial_t(F_{a_3}^{a_1})F_{a_4}^{a_2} - i\hbar F_{a_3}^{a_1}\partial_t(F_{a_4}^{a_2}) \\
&= \sum_{i_2 i_3 i_4}\sum_n e^{i(\mathcal{E}_{a_4}+\mathcal{E}_{i_2}-\mathcal{E}_{i_3}-\mathcal{E}_{i_4})t}e^{in\Omega t}V_{i_3 i_4}^{a_4 i_2}(n)F_{a_3}^{a_2}D_{i_3 i_4}^{a_1 i_2} + \sum_{i_1 i_2 i_3}\sum_n e^{i(\mathcal{E}_{i_1}+\mathcal{E}_{i_2}-\mathcal{E}_{a_1}-\mathcal{E}_{i_3})t}e^{in\Omega t}V_{a_1 i_3}^{i_1 i_2}(n)F_{a_3}^{a_2}D_{i_3 a_4}^{i_1 i_2} \\
&+ \sum_{i_2 i_3 i_4}\sum_n e^{i(\mathcal{E}_{a_3}+\mathcal{E}_{i_2}-\mathcal{E}_{i_3}-\mathcal{E}_{i_4})t}e^{in\Omega t}V_{i_3 i_4}^{a_3 i_2}(n)F_{a_4}^{a_1}D_{i_3 i_4}^{a_2 i_2} + \sum_{i_1 i_2 i_3}\sum_n e^{i(\mathcal{E}_{i_1}+\mathcal{E}_{i_2}-\mathcal{E}_{a_2}-\mathcal{E}_{i_3})t}e^{in\Omega t}V_{a_2 i_3}^{i_1 i_2}(n)F_{a_4}^{a_1}D_{i_3 a_3}^{i_1 i_2} \\
&- \sum_{i_2 i_3 i_4}\sum_n e^{i(\mathcal{E}_{a_3}+\mathcal{E}_{i_2}-\mathcal{E}_{i_3}-\mathcal{E}_{i_4})t}e^{in\Omega t}V_{i_3 i_4}^{a_3 i_2}(n)F_{a_4}^{a_2}D_{i_3 i_4}^{a_1 i_2} - \sum_{i_1 i_2 i_3}\sum_n e^{i(\mathcal{E}_{i_1}+\mathcal{E}_{i_2}-\mathcal{E}_{a_1}-\mathcal{E}_{i_3})t}e^{in\Omega t}V_{a_1 i_3}^{i_1 i_2}(n)F_{a_4}^{a_2}D_{i_3 a_3}^{i_1 i_2} \\
&- \sum_{i_2 i_3 i_4}\sum_n e^{i(\mathcal{E}_{a_4}+\mathcal{E}_{i_2}-\mathcal{E}_{i_3}-\mathcal{E}_{i_4})t}e^{in\Omega t}V_{i_3 i_4}^{a_4 i_2}(n)F_{a_3}^{a_1}D_{i_3 i_4}^{a_2 i_2} - \sum_{i_1 i_2 i_3}\sum_n e^{i(\mathcal{E}_{i_1}+\mathcal{E}_{i_2}-\mathcal{E}_{a_2}-\mathcal{E}_{i_3})t}e^{in\Omega t}V_{a_2 i_3}^{i_1 i_2}(n)F_{a_3}^{a_1}D_{i_3 a_4}^{i_1 i_2}
\end{aligned}
$$

where we have performed the singlet factorization, as per Eq.6.7, on the doublets arising from each $i\partial_t\langle F_b^a\rangle$ piece in $W$, and so $D_{a_3 a_4}^{i_1 i_2} \equiv \langle f_{i_1}^\dagger f_{i_2}^\dagger f_{a_3} f_{a_4}\rangle \approx F_{a_4}^{i_1}F_{a_3}^{i_2} - F_{a_3}^{i_1}F_{a_4}^{i_2}$.

**Calculation of $i\hbar\partial_t\langle 2\rangle$ ($R$ term)**

We have,

$$
\begin{aligned}
i\hbar\frac{\partial}{\partial t}\left(f_{a_1}^\dagger(t)f_{a_2}^\dagger(t)f_{a_3}(t)f_{a_4}(t)\right) &= i\hbar\left((\partial_t f_{a_1}^\dagger)f_{a_2}^\dagger f_{a_3}f_{a_4} + f_{a_1}^\dagger(\partial_t f_{a_2}^\dagger)f_{a_3}f_{a_4} + f_{a_1}^\dagger f_{a_2}^\dagger(\partial_t f_{a_3})f_{a_4} + f_{a_1}^\dagger f_{a_2}^\dagger f_{a_3}(\partial_t f_{a_4})\right) \\
&= \sum_{i_1 i_2 i_3}\sum_n e^{i(\mathcal{E}_{i_1}+\mathcal{E}_{i_2}-\mathcal{E}_{i_3}-\mathcal{E}_{a_1})t}e^{in\Omega t}V_{a_1 i_3}^{i_1 i_2}(n)f_{i_1}^\dagger f_{i_2}^\dagger f_{i_3}f_{a_2}^\dagger f_{a_3}f_{a_4} \\
&+ \sum_{i_1 i_2 i_3}\sum_n e^{i(\mathcal{E}_{i_1}+\mathcal{E}_{i_2}-\mathcal{E}_{i_3}-\mathcal{E}_{a_2})t}e^{in\Omega t}V_{a_2 i_3}^{i_1 i_2}(n)f_{a_1}^\dagger f_{i_1}^\dagger f_{i_2}^\dagger f_{i_3}f_{a_3}f_{a_4} \\
&+ \sum_{i_2 i_3 i_4}\sum_n e^{i(\mathcal{E}_{a_3}+\mathcal{E}_{i_2}-\mathcal{E}_{i_3}-\mathcal{E}_{i_4})t}e^{in\Omega t}V_{i_3 i_4}^{a_3 i_2}(n)f_{a_1}^\dagger f_{a_2}^\dagger f_{i_2}^\dagger f_{i_3}f_{i_4}f_{a_4} \\
&+ \sum_{i_2 i_3 i_4}\sum_n e^{i(\mathcal{E}_{a_4}+\mathcal{E}_{i_2}-\mathcal{E}_{i_3}-\mathcal{E}_{i_4})t}e^{in\Omega t}V_{i_3 i_4}^{a_4 i_2}(n)f_{a_1}^\dagger f_{a_2}^\dagger f_{a_3}f_{i_2}^\dagger f_{i_3}f_{i_4}
\end{aligned}
$$

Using Eq.6.13 and performing the singlet factorization as per Eq.6.7 after taking the expectation value,

$$
\begin{aligned}
R &\approx \sum_{i_1 i_2 i_3} \sum_n e^{i(\mathcal{E}_{i_1}+\mathcal{E}_{i_2}-\mathcal{E}_{i_3}-\mathcal{E}_{a_1})t} e^{in\Omega t} V^{i_1 i_2}_{a_1 i_3}(n) \left( \delta_{i_3 a_2} D^{i_1 i_2}_{a_3 a_4} - F^{i_1}_{a_4} D^{i_2 a_2}_{i_3 a_3} + F^{i_1}_{a_3} D^{i_2 a_2}_{i_3 a_4} - F^{i_1}_{i_3} D^{i_2 a_2}_{a_3 a_4} \right) \\
&+ \sum_{i_2 i_3 i_4} \sum_n e^{i(\mathcal{E}_{a_4}+\mathcal{E}_{i_2}-\mathcal{E}_{i_3}-\mathcal{E}_{i_4})t} e^{in\Omega t} V^{a_4 i_2}_{i_3 i_4}(n) \left( \delta_{i_2 a_3} D^{a_1 a_2}_{i_3 i_4} - F^{a_1}_{i_4} D^{a_2 i_2}_{a_3 i_3} + F^{a_1}_{i_3} D^{a_2 i_2}_{a_3 i_4} - F^{a_1}_{a_3} D^{a_2 i_2}_{i_3 i_4} \right) \\
&+ \sum_{i_1 i_2 i_3} \sum_n e^{i(\mathcal{E}_{i_1}+\mathcal{E}_{i_2}-\mathcal{E}_{i_3}-\mathcal{E}_{a_2})t} e^{in\Omega t} V^{i_1 i_2}_{a_2 i_3}(n) \left( F^{a_1}_{a_4} D^{i_1 i_2}_{i_3 a_3} - F^{a_1}_{a_3} D^{i_1 i_2}_{i_3 a_4} + F^{a_1}_{i_3} D^{i_1 i_2}_{a_3 a_4} \right) \\
&+ \sum_{i_2 i_3 i_4} \sum_n e^{i(\mathcal{E}_{a_3}+\mathcal{E}_{i_2}-\mathcal{E}_{i_3}-\mathcal{E}_{i_4})t} e^{in\Omega t} V^{a_3 i_2}_{i_3 i_4}(n) \left( F^{a_1}_{a_4} D^{a_2 i_2}_{i_3 i_4} - F^{a_1}_{i_4} D^{a_2 i_2}_{i_3 a_4} + F^{a_1}_{i_3} D^{a_2 i_2}_{i_4 a_4} \right)
\end{aligned}
$$

**Calculation of $\Delta\langle 2\rangle$ in the scattering approximation**

Putting the pieces together and simplifying, we obtain, in the scattering approximation

$$
\begin{aligned}
i\hbar\partial_t \Delta\langle 2\rangle &\approx R - W \\
&= \sum_{i_1 i_2 i_3} \sum_n e^{i(\mathcal{E}_{i_1}+\mathcal{E}_{i_2}-\mathcal{E}_{a_1}-\mathcal{E}_{i_3})t} e^{in\Omega t} V^{i_1 i_2}_{a_1 i_3}(n) \left( (\delta_{i_3 a_2} - F^{a_2}_{i_3}) D^{i_1 i_2}_{a_3 a_4} \right) \\
&+ \sum_{i_1 i_2 i_3} \sum_n e^{i(\mathcal{E}_{i_1}+\mathcal{E}_{i_2}-\mathcal{E}_{a_2}-\mathcal{E}_{i_3})t} e^{in\Omega t} V^{i_1 i_2}_{a_2 i_3}(n) \left( F^{a_1}_{i_3} D^{i_1 i_2}_{a_3 a_4} \right) \\
&+ \sum_{i_1 i_2 i_3} \sum_n e^{i(\mathcal{E}_{a_3}+\mathcal{E}_{i_2}-\mathcal{E}_{i_1}-\mathcal{E}_{i_3})t} e^{in\Omega t} V^{a_3 i_2}_{i_3 i_1}(n) \left( F^{i_2}_{a_4} D^{a_1 a_2}_{i_3 i_1} \right) \\
&+ \sum_{i_1 i_2 i_3} \sum_n e^{i(\mathcal{E}_{a_4}+\mathcal{E}_{i_2}-\mathcal{E}_{i_1}-\mathcal{E}_{i_3})t} e^{in\Omega t} V^{a_4 i_2}_{i_3 i_1}(n) \left( (\delta_{i_2 a_3} - F^{i_2}_{a_3}) D^{a_1 a_2}_{i_3 i_1} \right)
\end{aligned}
$$

Upon integration, we obtain $\Delta\langle 2\rangle_{\text{scat}}$,

$$
\begin{aligned}
\Delta\langle f^\dagger_{a_1} f^\dagger_{a_2} f_{a_3} f_{a_4}\rangle &= \frac{1}{i\hbar} \sum_{i_1 i_2 i_3} \sum_n \int_{t_0}^t dz e^{i(\mathcal{E}_{i_1}+\mathcal{E}_{i_2}-\mathcal{E}_{a_1}-\mathcal{E}_{i_3})z} e^{in\Omega z} V^{i_1 i_2}_{a_1 i_3}(n) \left( (\delta_{i_3 a_2} - F^{a_2}_{i_3}) D^{i_1 i_2}_{a_3 a_4} \right) \\
&+ \frac{1}{i\hbar} \sum_{i_1 i_2 i_3} \sum_n \int_{t_0}^t dz e^{i(\mathcal{E}_{i_1}+\mathcal{E}_{i_2}-\mathcal{E}_{a_2}-\mathcal{E}_{i_3})z} e^{in\Omega z} V^{i_1 i_2}_{a_2 i_3}(n) \left( F^{a_1}_{i_3} D^{i_1 i_2}_{a_3 a_4} \right) \\
&+ \frac{1}{i\hbar} \sum_{i_1 i_2 i_3} \sum_n \int_{t_0}^t dz e^{i(\mathcal{E}_{a_3}+\mathcal{E}_{i_2}-\mathcal{E}_{i_1}-\mathcal{E}_{i_3})z} e^{in\Omega z} V^{a_3 i_2}_{i_3 i_1}(n) \left( F^{i_2}_{a_4} D^{a_1 a_2}_{i_3 i_1} \right) \\
&+ \frac{1}{i\hbar} \sum_{i_1 i_2 i_3} \sum_n \int_{t_0}^t dz e^{i(\mathcal{E}_{a_4}+\mathcal{E}_{i_2}-\mathcal{E}_{i_1}-\mathcal{E}_{i_3})z} e^{in\Omega z} V^{a_4 i_2}_{i_3 i_1}(n) \left( (\delta_{i_2 a_3} - F^{i_2}_{a_3}) D^{a_1 a_2}_{i_3 i_1} \right)
\end{aligned}
$$

Note that the result here is correctly antisymmetric upon exchange of $a_1 \leftrightarrow a_2$ and $a_3 \leftrightarrow a_4$.

**Summary**

Putting the results together (using $\langle 2\rangle = \Delta\langle 2\rangle + \langle 2\rangle_S$) as per Eq. 6.8,

$$
\begin{aligned}
El_d &= \sum_{a_2a_3a_4}\sum_m e^{i(\mathcal{E}_b+\mathcal{E}_{a_2}-\mathcal{E}_{a_3}-\mathcal{E}_{a_4})t}e^{im\Omega t}V^{ba_2}_{a_3a_4}(m)D^{aa_2}_{a_3a_4} \\
&+ \frac{1}{i\hbar}\sum_{a_2a_3a_4}\sum_m e^{i(\mathcal{E}_b+\mathcal{E}_{a_2}-\mathcal{E}_{a_3}-\mathcal{E}_{a_4})t}e^{im\Omega t}V^{ba_2}_{a_3a_4}(m)\sum_{i_1i_2i_3}\sum_n \\
&\quad \int_{t_0}^{t} dz e^{i(\mathcal{E}_{i_1}+\mathcal{E}_{i_2}-\mathcal{E}_a-\mathcal{E}_{i_3})z}e^{in\Omega z}V^{i_1i_2}_{ai_3}(n)\left((\delta_{i_3a_2}-F^{a_2}_{i_3})D^{i_1i_2}_{a_3a_4}\right) \\
&+ \frac{1}{i\hbar}\sum_{a_2a_3a_4}\sum_m e^{i(\mathcal{E}_b+\mathcal{E}_{a_2}-\mathcal{E}_{a_3}-\mathcal{E}_{a_4})t}e^{im\Omega t}V^{ba_2}_{a_3a_4}(m)\sum_{i_1i_2i_3}\sum_n \\
&\quad \int_{t_0}^{t} dz e^{i(\mathcal{E}_{i_1}+\mathcal{E}_{i_2}-\mathcal{E}_{a_2}-\mathcal{E}_{i_3})z}e^{in\Omega z}V^{i_1i_2}_{a_2i_3}(n)\left(F^{a}_{i_3}D^{i_1i_2}_{a_3a_4}\right) \\
&+ \frac{1}{i\hbar}\sum_{a_2a_3a_4}\sum_m e^{i(\mathcal{E}_b+\mathcal{E}_{a_2}-\mathcal{E}_{a_3}-\mathcal{E}_{a_4})t}e^{im\Omega t}V^{ba_2}_{a_3a_4}(m)\sum_{i_1i_2i_3}\sum_n \\
&\quad \int_{t_0}^{t} dz e^{i(\mathcal{E}_{a_4}+\mathcal{E}_{i_2}-\mathcal{E}_{i_1}-\mathcal{E}_{i_3})z}e^{in\Omega z}V^{a_4i_2}_{i_3i_1}(n)\left((\delta_{i_2a_3}-F^{i_2}_{a_3})-F^{i_2}_{a_3}\right)D^{aa_2}_{i_3i_1} \\
&+ \sum_{a_2a_3a_4}\sum_m e^{i(\mathcal{E}_{a_2}+\mathcal{E}_{a_3}-\mathcal{E}_a-\mathcal{E}_{a_4})t}e^{im\Omega t}V^{a_2a_3}_{aa_4}(m)D^{a_2a_3}_{a_4b} \\
&+ \frac{1}{i\hbar}\sum_{a_2a_3a_4}\sum_m e^{i(\mathcal{E}_{a_2}+\mathcal{E}_{a_3}-\mathcal{E}_a-\mathcal{E}_{a_4})t}e^{im\Omega t}V^{a_2a_3}_{aa_4}(m)\sum_{i_1i_2i_3}\sum_n \\
&\quad \int_{t_0}^{t} dz e^{i(\mathcal{E}_{i_1}+\mathcal{E}_{i_2}-\mathcal{E}_{a_2}-\mathcal{E}_{i_3})z}e^{in\Omega z}V^{i_1i_2}_{a_2i_3}(n)\left((\delta_{i_3a_3}-F^{a_3}_{i_3})-F^{a_3}_{i_3}\right)D^{i_1i_2}_{a_4b} \\
&+ \frac{1}{i\hbar}\sum_{a_2a_3a_4}\sum_m e^{i(\mathcal{E}_{a_2}+\mathcal{E}_{a_3}-\mathcal{E}_a-\mathcal{E}_{a_4})t}e^{im\Omega t}V^{a_2a_3}_{aa_4}(m)\sum_{i_1i_2i_3}\sum_n \\
&\quad \int_{t_0}^{t} dz e^{i(\mathcal{E}_{a_4}+\mathcal{E}_{i_2}-\mathcal{E}_{i_1}-\mathcal{E}_{i_3})z}e^{in\Omega z}V^{a_4i_2}_{i_3i_1}(n)\left(F^{i_2}_{b}D^{a_2a_3}_{i_3i_1}\right) \\
&+ \frac{1}{i\hbar}\sum_{a_2a_3a_4}\sum_m e^{i(\mathcal{E}_{a_2}+\mathcal{E}_{a_3}-\mathcal{E}_a-\mathcal{E}_{a_4})t}e^{im\Omega t}V^{a_2a_3}_{aa_4}(m)\sum_{i_1i_2i_3}\sum_n \\
&\quad \int_{t_0}^{t} dz e^{i(\mathcal{E}_b+\mathcal{E}_{i_2}-\mathcal{E}_{i_1}-\mathcal{E}_{i_3})z}e^{in\Omega z}V^{bi_2}_{i_3i_1}(n)\left((\delta_{i_2a_4}-F^{i_2}_{a_4})D^{a_2a_3}_{i_3i_1}\right)
\end{aligned}
$$

Note that there are first and second order contributions in interaction coupling $V$.

**Markov Approximation - Redfield Dynamics**

Performing the same Markov approximations as earlier

$$
\begin{aligned}
\frac{1}{i\hbar}El_d &= \sum_{a_2a_3a_4}\sum_m e^{i(\mathcal{E}_b+\mathcal{E}_{a_2}-\mathcal{E}_{a_3}-\mathcal{E}_{a_4}+m\Omega)t}V^{ba_2}_{a_3a_4}(m)( \\
&\quad \frac{1}{i\hbar}D^{aa_2}_{a_3a_4} \\
&- \frac{\pi}{\hbar}\sum_{i_1i_2i_3}\sum_n V^{i_1i_2}_{ai_3}(n)\delta(\mathcal{E}_{i_1}+\mathcal{E}_{i_2}-\mathcal{E}_a-\mathcal{E}_{i_3}+n\Omega)\left((\delta_{i_3a_2}-F^{a_2}_{i_3})D^{i_1i_2}_{a_3a_4}\right) \\
&- \frac{\pi}{\hbar}\sum_{i_1i_2i_3}\sum_n V^{i_1i_2}_{a_2i_3}(n)\delta(\mathcal{E}_{i_1}+\mathcal{E}_{i_2}-\mathcal{E}_{a_2}-\mathcal{E}_{i_3}+n\Omega)\left(F^a_{i_3}D^{i_1i_2}_{a_3a_4}\right) \\
&- \frac{\pi}{\hbar}\sum_{i_1i_2i_3}\sum_n V^{a_4i_2}_{i_3i_1}(n)\delta(\mathcal{E}_{a_4}+\mathcal{E}_{i_2}-\mathcal{E}_{i_1}-\mathcal{E}_{i_3}+n\Omega)\left((\delta_{i_2a_3}-F^{i_2}_{a_3})-F^{i_2}_{a_3}\right)D^{aa_2}_{i_3i_1} \\
&\quad ) \\
&+ \sum_{a_2a_3a_4}\sum_m e^{i(\mathcal{E}_{a_2}+\mathcal{E}_{a_3}-\mathcal{E}_a-\mathcal{E}_{a_4}+m\Omega)t}V^{a_2a_3}_{aa_4}(m)( \\
&\quad \frac{1}{i\hbar}D^{a_2a_3}_{a_4b} \\
&- \frac{\pi}{\hbar}\sum_{i_1i_2i_3}\sum_n V^{i_1i_2}_{a_2i_3}(n)\delta(\mathcal{E}_{i_1}+\mathcal{E}_{i_2}-\mathcal{E}_{a_2}-\mathcal{E}_{i_3}+n\Omega)\left((\delta_{i_3a_3}-F^{a_3}_{i_3})-F^{a_3}_{i_3}\right)D^{i_1i_2}_{a_4b} \\
&- \frac{\pi}{\hbar}\sum_{i_1i_2i_3}\sum_n V^{a_4i_2}_{i_3i_1}(n)\delta(\mathcal{E}_{a_4}+\mathcal{E}_{i_2}-\mathcal{E}_{i_1}-\mathcal{E}_{i_3}+n\Omega)\left(F^{i_2}_b D^{a_2a_3}_{i_3i_1}\right) \\
&- \frac{\pi}{\hbar}\sum_{i_1i_2i_3}\sum_n V^{bi_2}_{i_3i_1}(n)\delta(\mathcal{E}_b+\mathcal{E}_{i_2}-\mathcal{E}_{i_1}-\mathcal{E}_{i_3}+n\Omega)\left((\delta_{i_2a_4}-F^{i_2}_{a_4})D^{a_2a_3}_{i_3i_1}\right) \\
&\quad )
\end{aligned}
$$

**Diagonal Limit of Redfield Dynamics - Boltzmann Dynamics**

Here we compute the explicit diagonal limit of the Redfield equations. Taking the Floquet zone index RWA-like approximation ($\delta_{mn}$ and/or $\delta_{m,-n}$) as in the phonon case,

$$
\begin{aligned}
\frac{1}{i\hbar}El_d\delta_{ab} &= \frac{4\pi}{\hbar}\sum_{a_2a_3a_4}\sum_n |V^{aa_2}_{a_3a_4}(n)|^2\delta(\mathcal{E}_a+\mathcal{E}_{a_2}-\mathcal{E}_{a_3}-\mathcal{E}_{a_4}+n\Omega) \\
&\quad \left((1-F^a_a)(1-F^{a_2}_{a_2})F^{a_3}_{a_3}F^{a_4}_{a_4}-F^a_aF^{a_2}_{a_2}(1-F^{a_3}_{a_3})(1-F^{a_4}_{a_4})\right)
\end{aligned}
$$

which is the familiar form of the Floquet-Fermi-Golden-Rule result giving rise to Boltzmann Dynamics.

**Lead Doublet 1**

The evolution of the lead doublets is

$$
\begin{aligned}
i\hbar\frac{\partial}{\partial t}\langle f_{i_1}^{\dagger}(t)d_k\rangle &= i\hbar tr\left(\frac{\partial\rho}{\partial t}f_{i_1}^{\dagger}(t)d_k + \rho\frac{\partial}{\partial t}(f_{i_1}^{\dagger}(t))d_k\right)\\
&= tr\left([H,\rho]f_{i_1}^{\dagger}d_k + \rho[H_{sys},f_{i_1}^{\dagger}]d_k\right)\\
&= tr\left(\rho[f_{i_1}^{\dagger}d_k,H] + \rho[H_{sys},f_{i_1}^{\dagger}d_k]\right)\\
&= tr\left(\rho[f_{i_1}^{\dagger}d_k,H] - \rho[f_{i_1}^{\dagger}d_k,H_{sys},]\right)\\
&= tr\left(\rho[f_{i_1}^{\dagger}d_k,H-H_{sys}]\right)\\
&= \langle[f_{i_1}^{\dagger}d_k,H-H_{sys}]\rangle\\
&= \langle[f_{i_1}^{\dagger}d_k,H_0^{ph}+H_0^{leads}+H_{int}]\rangle\\
&\rightarrow \langle[f_{i_1}^{\dagger}d_k,H_0^{leads}+H_{el-lead}]\rangle
\end{aligned}
$$

where in the last line, the terms with phonons and electron-electron interactions have been dropped preemptively since $\langle d\rangle = \langle d^{\dagger}\rangle = 0$ which would appear upon singlet factorization.

**Free part**

Computing the free part

$$
\begin{aligned}
i\hbar\frac{\partial}{\partial t}\langle f_a^{\dagger}(t)d_k\rangle &= \langle[f_a^{\dagger}(t)d_k,H_0^{leads}]\rangle\\
&= \varepsilon_k\langle f_a^{\dagger}(t)d_k\rangle
\end{aligned}
$$

we obtain the free evolution.

**Lead part**

Computing the lead part

$$
\begin{aligned}
i\hbar\frac{\partial}{\partial t}\langle f_a^{\dagger}(t)d_k\rangle &= \langle[f_a^{\dagger}(t)d_k,H_{el-lead}]\rangle\\
&\approx \sum_i\sum_n e^{-i(\mathcal{E}_i+n\Omega)t}\Gamma_k^i(n)^*\left(\langle f_a^{\dagger}(t)f_i(t)\rangle(1-D_k) - \langle f_i(t)f_a^{\dagger}(t)\rangle D_k\right)
\end{aligned}
$$

where we have used $\langle d_l^{\dagger}d_k\rangle \approx D_k\delta_{kl}$ where $D$ is the Fermi-Dirac distribution for the thermal lead, and that $\langle f^{\dagger}f^{\dagger}\rangle$ and $\langle d^{\dagger}d^{\dagger}\rangle$ are vanishing upon singlet factorization as before.

**All Together**

Putting the parts together,

$$\begin{aligned} i\hbar\frac{\partial}{\partial t}\langle f_a^\dagger(t)d_k\rangle &= \langle[f_a^\dagger d_k, H_0^{leads}+H_{el-lead}]\rangle \\ &= \varepsilon_k\langle f_a^\dagger(t)d_k\rangle + \sum_i\sum_n e^{-i(\mathcal{E}_i+n\Omega)t}\Gamma_k^i(n)^*\left(F_i^a(1-D_k)-(\delta_{ai}-F_i^a)D_k\right) \end{aligned}$$

Upon integration,

$$\langle f_a^\dagger(t)d_k\rangle = \frac{1}{i\hbar}\sum_i\sum_n\Gamma_k^i(n)^*e^{-\frac{i}{\hbar}\varepsilon_k t}\int_{t_0}^t dz e^{\frac{i}{\hbar}\varepsilon_k z}e^{-\frac{i}{\hbar}(\mathcal{E}_i+n\Omega)z}\left(F_i^a(1-D_k)-(\delta_{ai}-F_i^a)D_k\right)$$

where all correlators are functions of $z$ on the RHS.

**Lead Doublet 2**

We use the same procedure as in Lead Doublet 1.

**Free part**

Computing the free part

$$\begin{aligned} i\hbar\frac{\partial}{\partial t}\langle f_b(t)d_k^\dagger\rangle &= \langle[f_b(t)d_k^\dagger, H_0^{leads}]\rangle \\ &= -\varepsilon_k\langle f_b(t)d_k^\dagger\rangle \end{aligned}$$

we obtain the free evolution.

**Lead part**

Computing the lead part

$$\begin{aligned} i\hbar\frac{\partial}{\partial t}\langle f_b(t)d_k^\dagger\rangle &= \langle[f_b(t)d_k^\dagger, H_{el-lead}]\rangle \\ &\approx \sum_i\sum_n e^{i(\mathcal{E}_i+n\Omega)t}\Gamma_k^i(n)\left(\langle f_b(t)f_i^\dagger(t)\rangle D_k - \langle f_i^\dagger(t)f_b(t)\rangle(1-D_k)\right) \end{aligned}$$

where we have used the properties of a thermal lead as before.

**All Together**

$$\begin{aligned} i\hbar\frac{\partial}{\partial t}\langle f_b(t)d_k^\dagger\rangle &= \langle[f_b(t)d_k^\dagger, H_0^{leads} + H_{el-lead}]\rangle \\ &= -\varepsilon_k\langle f_b(t)d_k^\dagger\rangle + \sum_i\sum_n e^{i(\mathcal{E}_i+n\Omega)t}\Gamma_k^i(n)\left((\delta_{bi}-F_b^i)D_k - F_b^i(1-D_k)\right) \end{aligned}$$

Upon integration

$$\langle f_b(t)d_k^\dagger\rangle = \frac{1}{i\hbar}\sum_i\sum_n \Gamma_k^i(n)e^{\frac{i}{\hbar}\varepsilon_k t}\int_{t_0}^t dz e^{-\frac{i}{\hbar}\varepsilon_k z}e^{\frac{i}{\hbar}(\mathcal{E}_i+n\Omega)z}\left((\delta_{bi}-F_b^i)D_k - F_b^i(1-D_k)\right)$$

where all correlators are functions of $z$ on the RHS.

**Summary**

Combining the lead doublet contributions,

$$\begin{aligned} Ld_d &= \langle[f_a^\dagger(t)f_b(t), \sum_{ik}\sum_n e^{i\mathcal{E}_i t}e^{in\Omega t}\Gamma_k^i(n)f_i^\dagger(t)d_k + h.c.]\rangle \\ &= \sum_k\sum_m e^{i\mathcal{E}_b t}e^{im\Omega t}\Gamma_k^b(m)\langle f_a^\dagger(t)d_k\rangle - \sum_k\sum_m e^{-i\mathcal{E}_a t}e^{-im\Omega t}(\Gamma_k^a(m))^*\langle f_b(t)d_k^\dagger\rangle \\ &= \frac{1}{i\hbar}\sum_i\sum_k\sum_{nm} e^{i\mathcal{E}_b t}e^{im\Omega t}\Gamma_k^b(m)\Gamma_k^i(n)^* e^{-\frac{i}{\hbar}(\mathcal{E}_i+n\Omega)t} \\ &\quad \int_{t_0}^t dz e^{\frac{i}{\hbar}(\mathcal{E}_i-\varepsilon_k+n\Omega)(t-z)}\left(F_i^a(1-D_k) - (\delta_{ai}-F_i^a)D_k\right) \\ &- \frac{1}{i\hbar}\sum_i\sum_k\sum_{nm} e^{-i\mathcal{E}_a t}e^{-im\Omega t}(\Gamma_k^a(m))^*\Gamma_k^i(n)e^{\frac{i}{\hbar}(\mathcal{E}_i+n\Omega)t} \\ &\quad \int_{t_0}^t dz e^{-\frac{i}{\hbar}(\mathcal{E}_i-\varepsilon_k+n\Omega)(t-z)}\left((\delta_{bi}-F_b^i)D_k - F_b^i(1-D_k)\right) \end{aligned}$$

where the correlations are functions of $z$ on the RHS and the LHS is a function of $t$. Note that we have preemptively rewritten the $Ld_d$ in terms of $t-z$ in the integrand.

**Markov Approximation - Redfield Dyanmics**

Making the Markov approximation as before by changing variables to $\tau = t - z$, $d\tau = -dz$, $[t_0, t] \to [t - t_0, 0]$, and assuming that $F(t-\tau) \approx F(t)$ over the range $\tau$,

$$\begin{aligned}\frac{1}{i\hbar}Ld_d &= \frac{\pi}{\hbar}\sum_i\sum_k\sum_{nm}\Gamma^b_k(m)\Gamma^i_k(n)^* e^{-i(\varepsilon_k-\mathcal{E}_b-m\Omega)t}\delta(\mathcal{E}_i-\varepsilon_k+n\Omega)\left((\delta_{ai}-F^a_i)D_k-F^a_i(1-D_k)\right)\\ &+ \frac{\pi}{\hbar}\sum_i\sum_k\sum_{nm}\Gamma^a_k(m)^*\Gamma^i_k(n)e^{i(\varepsilon_k-\mathcal{E}_a-m\Omega)t}\delta(\mathcal{E}_i-\varepsilon_k+n\Omega)\left((\delta_{bi}-F^i_b)D_k-F^i_b(1-D_k)\right)\end{aligned}$$

This is the Redfield equation for a thermal lead.

**Diagonal Limit of Redfield Dynamics - Boltzmann Dynamics**

Taking the diagonal limit and making the Floquet zone RWA/secular approximation ($\delta_{nm}$) as before,

$$\frac{1}{i\hbar}Ld_d\delta_{ab} = \frac{2\pi}{\hbar}\sum_l\sum_n|\Gamma^a_l(n)|^2\delta(\mathcal{E}_a-\varepsilon_l+n\Omega)\left((1-F^a_a)D_l-F^a_a(1-D_l)\right)$$

which again gives rise to Boltzmann dynamics.

**Summary of Kinetic Equations**

**Floquet-Redfield Equation**

The Floquet-Redfield Equation (FRE) for electron-phonon coupling, electron-lead coupling, and electron-electron interaction is

$$\partial_t F^a_b = I^{FRE}_{ph}+I^{FRE}_{lead}+I^{FRE}_{ee} \tag{6.15}$$

$$
\begin{aligned}
I_{ph}^{FRE} &= \frac{\pi}{\hbar}\sum_{i_1 j i_1' i_2'}\sum_{mn} G^{b}_{i_1 j}(n) G^{i_1'}_{i_2'(-j)}(m) e^{i(\mathcal{E}_b-\mathcal{E}_{i_1}+\mathcal{E}_{i_1'}-\mathcal{E}_{i_2'}+(n+m)\Omega)t}\delta(\mathcal{E}_{i_1'}-\mathcal{E}_{i_2'}+\omega_j+m\Omega) \\
&\quad \left(F^{i_1'}_{i_1}(\delta_{i_2' a}-F^{a}_{i_2'})N_{\omega_j} - F^{a}_{i_2'}(\delta_{i_1 i_1'}-F^{i_1'}_{i_1})(1+N_{\omega_j}) - F^{a}_{i_1}F^{i_1'}_{i_2'}\right) \\
&+ \frac{\pi}{\hbar}\sum_{i_1 j i_1' i_2'}\sum_{mn} G^{b}_{i_1 j}(n) G^{i_1'}_{i_2'(-j)}(m) e^{i(\mathcal{E}_b-\mathcal{E}_{i_1}+\mathcal{E}_{i_1'}-\mathcal{E}_{i_2'}+(n+m)\Omega)t}\delta(\mathcal{E}_{i_1'}-\mathcal{E}_{i_2'}-\omega_{(-j)}+m\Omega) \\
&\quad \left(F^{i_1'}_{i_1}(\delta_{i_2' a}-F^{a}_{i_2'})(1+N_{\omega_{(-j)}}) - F^{a}_{i_2'}(\delta_{i_1 i_1'}-F^{i_1'}_{i_1})N_{\omega_{(-j)}} + F^{i_1'}_{i_2'}F^{a}_{i_1}\right) \\
&+ \frac{\pi}{\hbar}\sum_{i_1 j i_1' i_2'}\sum_{mn} G^{i_1}_{a j}(n) G^{i_1'}_{i_2'(-j)}(m) e^{i(\mathcal{E}_{i_1}-\mathcal{E}_a+\mathcal{E}_{i_1'}-\mathcal{E}_{i_2'}+(n+m)\Omega)t}\delta(\mathcal{E}_{i_1'}-\mathcal{E}_{i_2'}+\omega_j+m\Omega) \\
&\quad \left(F^{i_1}_{i_2'}(\delta_{b i_1'}-F^{i_1'}_{b})(1+N_{\omega_j}) - F^{i_1'}_{b}(\delta_{i_2' i_1}-F^{i_1}_{i_2'})N_{\omega_j} + F^{i_1}_{b}F^{i_1'}_{i_2'}\right) \\
&+ \frac{\pi}{\hbar}\sum_{i_1 j i_1' i_2'}\sum_{mn} G^{i_1}_{a j}(n) G^{i_1'}_{i_2'(-j)}(m) e^{i(\mathcal{E}_{i_1}-\mathcal{E}_a+\mathcal{E}_{i_1'}-\mathcal{E}_{i_2'}+(n+m)\Omega)t}\delta(\mathcal{E}_{i_1'}-\mathcal{E}_{i_2'}-\omega_{(-j)}+m\Omega) \\
&\quad \left(F^{i_1}_{i_2'}(\delta_{b i_1'}-F^{i_1'}_{b})N_{\omega_{(-j)}} - F^{i_1'}_{b}(\delta_{i_2' i_1}-F^{i_1}_{i_2'})(1+N_{\omega_{(-j)}}) - F^{i_1'}_{i_2'}F^{i_1}_{b}\right)
\end{aligned}
$$

$$
\begin{aligned}
I_{lead}^{FRE} &= \frac{\pi}{\hbar}\sum_{i}\sum_{l}\sum_{nm}\Gamma^{b}_{l}(m)\Gamma^{i}_{l}(n)^{*} e^{-i(\varepsilon_l-\mathcal{E}_b-m\Omega)t}\delta(\mathcal{E}_i-\varepsilon_l+n\Omega)\left((\delta_{ai}-F^{a}_{i})D_l - F^{a}_{i}(1-D_l)\right) \\
&+ \frac{\pi}{\hbar}\sum_{i}\sum_{l}\sum_{nm}\Gamma^{a}_{l}(m)^{*}\Gamma^{i}_{l}(n) e^{i(\varepsilon_l-\mathcal{E}_a-m\Omega)t}\delta(\mathcal{E}_i-\varepsilon_l+n\Omega)\left((\delta_{bi}-F^{i}_{b})D_l - F^{i}_{b}(1-D_l)\right)
\end{aligned}
$$

$$
\begin{aligned}
I_{ee}^{FRE} &= \frac{1}{i\hbar}\sum_{a_2a_3a_4}\sum_{m} e^{i(\mathcal{E}_b+\mathcal{E}_{a_2}-\mathcal{E}_{a_3}-\mathcal{E}_{a_4}+m\Omega)t}V^{ba_2}_{a_3a_4}(m)D^{aa_2}_{a_3a_4} \\
&- \frac{\pi}{\hbar}\sum_{a_2a_3a_4}\sum_{i_1i_2i_3}\sum_{mn} e^{i(\mathcal{E}_b+\mathcal{E}_{a_2}-\mathcal{E}_{a_3}-\mathcal{E}_{a_4}+m\Omega)t}V^{ba_2}_{a_3a_4}(m)V^{i_1i_2}_{ai_3}(n) \\
&\quad \delta(\mathcal{E}_{i_1}+\mathcal{E}_{i_2}-\mathcal{E}_a-\mathcal{E}_{i_3}+n\Omega)\left((\delta_{i_3a_2}-F^{a_2}_{i_3})D^{i_1i_2}_{a_3a_4}\right) \\
&- \frac{\pi}{\hbar}\sum_{a_2a_3a_4}\sum_{i_1i_2i_3}\sum_{mn} e^{i(\mathcal{E}_b+\mathcal{E}_{a_2}-\mathcal{E}_{a_3}-\mathcal{E}_{a_4}+m\Omega)t}V^{ba_2}_{a_3a_4}(m)V^{i_1i_2}_{a_2i_3}(n) \\
&\quad \delta(\mathcal{E}_{i_1}+\mathcal{E}_{i_2}-\mathcal{E}_{a_2}-\mathcal{E}_{i_3}+n\Omega)\left(F^{a}_{i_3}D^{i_1i_2}_{a_3a_4}\right) \\
&- \frac{\pi}{\hbar}\sum_{a_2a_3a_4}\sum_{i_1i_2i_3}\sum_{mn} e^{i(\mathcal{E}_b+\mathcal{E}_{a_2}-\mathcal{E}_{a_3}-\mathcal{E}_{a_4}+m\Omega)t}V^{ba_2}_{a_3a_4}(m)V^{a_4i_2}_{i_3i_1}(n) \\
&\quad \delta(\mathcal{E}_{a_4}+\mathcal{E}_{i_2}-\mathcal{E}_{i_1}-\mathcal{E}_{i_3}+n\Omega)\left(\delta_{i_2a_3}-2F^{i_2}_{a_3}\right)D^{aa_2}_{i_3i_1} \\
&+ \frac{1}{i\hbar}\sum_{a_2a_3a_4}\sum_{m} e^{i(\mathcal{E}_{a_2}+\mathcal{E}_{a_3}-\mathcal{E}_{a}-\mathcal{E}_{a_4}+m\Omega)t}V^{a_2a_3}_{aa_4}(m)D^{a_2a_3}_{a_4b} \\
&- \frac{\pi}{\hbar}\sum_{a_2a_3a_4}\sum_{i_1i_2i_3}\sum_{mn} e^{i(\mathcal{E}_{a_2}+\mathcal{E}_{a_3}-\mathcal{E}_{a}-\mathcal{E}_{a_4}+m\Omega)t}V^{a_2a_3}_{aa_4}(m)V^{i_1i_2}_{a_2i_3}(n) \\
&\quad \delta(\mathcal{E}_{i_1}+\mathcal{E}_{i_2}-\mathcal{E}_{a_2}-\mathcal{E}_{i_3}+n\Omega)\left(\delta_{i_3a_3}-2F^{a_3}_{i_3}\right)D^{i_1i_2}_{a_4b} \\
&- \frac{\pi}{\hbar}\sum_{a_2a_3a_4}\sum_{i_1i_2i_3}\sum_{mn} e^{i(\mathcal{E}_{a_2}+\mathcal{E}_{a_3}-\mathcal{E}_{a}-\mathcal{E}_{a_4}+m\Omega)t}V^{a_2a_3}_{aa_4}(m)V^{a_4i_2}_{i_3i_1}(n) \\
&\quad \delta(\mathcal{E}_{a_4}+\mathcal{E}_{i_2}-\mathcal{E}_{i_1}-\mathcal{E}_{i_3}+n\Omega)\left(F^{i_2}_{b}D^{a_2a_3}_{i_3i_1}\right) \\
&- \frac{\pi}{\hbar}\sum_{a_2a_3a_4}\sum_{i_1i_2i_3}\sum_{mn} e^{i(\mathcal{E}_{a_2}+\mathcal{E}_{a_3}-\mathcal{E}_{a}-\mathcal{E}_{a_4}+m\Omega)t}V^{a_2a_3}_{aa_4}(m)V^{bi_2}_{i_3i_1}(n) \\
&\quad \delta(\mathcal{E}_{b}+\mathcal{E}_{i_2}-\mathcal{E}_{i_1}-\mathcal{E}_{i_3}+n\Omega)\left((\delta_{i_2a_4}-F^{i_2}_{a_4})D^{a_2a_3}_{i_3i_1}\right)
\end{aligned}
$$

where, as before, $D^{12}_{34} = F^1_4F^2_3 - F^1_3F^2_4$ and $a, b, i$ are composite indices denoting all quantum numbers of the Floquet states, e.g. the discrete band indices and continuous momentum indices. Similarly, $j$ is the composite index for phonons where $(-j)$ is taken to mean flipping the sign of the momentum (along the system) of the phonon, and $l$ is the lead state (can also be a composite index if the lead has internal structure). We can use this equation for a system with any boundary condition and of any dimension.

### Floquet-Redfield Equation with Translational Invariance

If we consider translational invariance in the system such that all $k, k'$ (momentum) correlations vanish, we only have band coherences remaining. The kinetic equation is thus

$$\partial_t F^{ap}_{bp} = I^{FRE-tr}_{ph} + I^{FRE-tr}_{lead} + I^{FRE-tr}_{ee} \tag{6.16}$$

$$\begin{aligned}
I^{FRE-tr}_{ph} &= \frac{\pi}{\hbar}\sum_{i_1 i'_1 i'_2}\sum_{k_1}\sum_{j}\sum_{mn} G^{bp}_{i_1 k_1 j}(n) G^{i'_1 k_1}_{i'_2 p(-j)}(m) e^{i(\mathcal{E}_{bp}-\mathcal{E}_{i_1 k_1}+\mathcal{E}_{i'_1 k_1}-\mathcal{E}_{i'_2 p}+(n+m)\Omega)t} \\
&\quad \delta(\mathcal{E}_{i'_1 k_1}-\mathcal{E}_{i'_2 p}+\omega_j+m\Omega)\left(F^{i'_1 k_1}_{i_1 k_1}(\delta_{i'_2 a}-F^{ap}_{i'_2 p})N_{\omega_j} - F^{ap}_{i'_2 p}(\delta_{i_1 i'_1}-F^{i'_1 k_1}_{i_1 k_1})(1+N_{\omega_j})\right) \\
&- \frac{\pi}{\hbar}\sum_{i_1 i'_1 i'_2}\sum_{k_1}\sum_{j}\sum_{mn} G^{bp}_{i_1 p j}(n) G^{i'_1 k_1}_{i'_2 k_1(-j)}(m) e^{i(\mathcal{E}_{bp}-\mathcal{E}_{i_1 p}+\mathcal{E}_{i'_1 k_1}-\mathcal{E}_{i'_2 k_1}+(n+m)\Omega)t} \\
&\quad \delta(\mathcal{E}_{i'_1 k_1}-\mathcal{E}_{i'_2 k_1}+\omega_j+m\Omega)\left(F^{ap}_{i_1 p}F^{i'_1 k_1}_{i'_2 k_1}\right) \\
&+ \frac{\pi}{\hbar}\sum_{i_1 i'_1 i'_2}\sum_{k_1}\sum_{j}\sum_{mn} G^{bp}_{i_1 k_1 j}(n) G^{i'_1 k_1}_{i'_2 p(-j)}(m) e^{i(\mathcal{E}_{bp}-\mathcal{E}_{i_1 k_1}+\mathcal{E}_{i'_1 k_1}-\mathcal{E}_{i'_2 p}+(n+m)\Omega)t} \\
&\quad \delta(\mathcal{E}_{i'_1 k_1}-\mathcal{E}_{i'_2 p}-\omega_{(-j)}+m\Omega)\left(F^{i'_1 k_1}_{i_1 k_1}(\delta_{i'_2 a}-F^{ap}_{i'_2 p})(1+N_{\omega_{(-j)}}) - F^{ap}_{i'_2 p}(\delta_{i_1 i'_1}-F^{i'_1 k_1}_{i_1 k_1})N_{\omega_{(-j)}}\right) \\
&+ \frac{\pi}{\hbar}\sum_{i_1 i'_1 i'_2}\sum_{k_1}\sum_{j}\sum_{mn} G^{bp}_{i_1 p j}(n) G^{i'_1 k_1}_{i'_2 k_1(-j)}(m) e^{i(\mathcal{E}_{bp}-\mathcal{E}_{i_1 p}+\mathcal{E}_{i'_1 k_1}-\mathcal{E}_{i'_2 k_1}+(n+m)\Omega)t} \\
&\quad \delta(\mathcal{E}_{i'_1 k_1}-\mathcal{E}_{i'_2 k_1}-\omega_{(-j)}+m\Omega)\left(F^{i'_1 k_1}_{i'_2 k_1}F^{ap}_{i_1 p}\right) \\
&+ \frac{\pi}{\hbar}\sum_{i_1 i'_1 i'_2}\sum_{k_1}\sum_{j}\sum_{mn} G^{i_1 k_1}_{apj}(n) G^{i'_1 p}_{i'_2 k_1(-j)}(m) e^{i(\mathcal{E}_{i_1 k_1}-\mathcal{E}_{ap}+\mathcal{E}_{i'_1 p}-\mathcal{E}_{i'_2 k_1}+(n+m)\Omega)t} \\
&\quad \delta(\mathcal{E}_{i'_1 p}-\mathcal{E}_{i'_2 k_1}+\omega_j+m\Omega)\left(F^{i_1 k_1}_{i'_2 k_1}(\delta_{b i'_1}-F^{i'_1 p}_{bp})(1+N_{\omega_j}) - F^{i'_1 p}_{bp}(\delta_{i'_2 i_1}-F^{i_1 k_1}_{i'_2 k_1})N_{\omega_j}\right) \\
&+ \frac{\pi}{\hbar}\sum_{i_1 i'_1 i'_2}\sum_{k_1}\sum_{j}\sum_{mn} G^{i_1 p}_{apj}(n) G^{i'_1 k_1}_{i'_2 k_1(-j)}(m) e^{i(\mathcal{E}_{i_1 p}-\mathcal{E}_{ap}+\mathcal{E}_{i'_1 k_1}-\mathcal{E}_{i'_2 k_1}+(n+m)\Omega)t} \\
&\quad \delta(\mathcal{E}_{i'_1 k_1}-\mathcal{E}_{i'_2 k_1}+\omega_j+m\Omega)\left(F^{i_1 p}_{bp}F^{i'_1 k_1}_{i'_2 k_1}\right) \\
&+ \frac{\pi}{\hbar}\sum_{i_1 i'_1 i'_2}\sum_{k_1}\sum_{j}\sum_{mn} G^{i_1 k_1}_{apj}(n) G^{i'_1 p}_{i'_2 k_1(-j)}(m) e^{i(\mathcal{E}_{i_1 k_1}-\mathcal{E}_{ap}+\mathcal{E}_{i'_1 p}-\mathcal{E}_{i'_2 k_1}+(n+m)\Omega)t} \\
&\quad \delta(\mathcal{E}_{i'_1 p}-\mathcal{E}_{i'_2 k_1}-\omega_{(-j)}+m\Omega)\left(F^{i_1 k_1}_{i'_2 k_1}(\delta_{b i'_1}-F^{i'_1 p}_{bp})N_{\omega_{(-j)}} - F^{i'_1 p}_{bp}(\delta_{i'_2 i_1}-F^{i_1 k_1}_{i'_2 k_1})(1+N_{\omega_{(-j)}})\right) \\
&- \frac{\pi}{\hbar}\sum_{i_1 i'_1 i'_2}\sum_{k_1}\sum_{j}\sum_{mn} G^{i_1 p}_{apj}(n) G^{i'_1 k_1}_{i'_2 k_1(-j)}(m) e^{i(\mathcal{E}_{i_1 p}-\mathcal{E}_{ap}+\mathcal{E}_{i'_1 k_1}-\mathcal{E}_{i'_2 k_1}+(n+m)\Omega)t} \\
&\quad \delta(\mathcal{E}_{i'_1 k_1}-\mathcal{E}_{i'_2 k_1}-\omega_{(-j)}+m\Omega)\left(F^{i'_1 k_1}_{i'_2 k_1}F^{i_1 p}_{bp}\right)
\end{aligned}$$

$$
\begin{aligned}
I_{ee}^{FRE-tr} &= \frac{2}{i\hbar}\sum_{a_2a_3a_4}\sum_{p_2}\sum_{m} e^{i(\mathcal{E}_{bp}+\mathcal{E}_{a_2p_2}-\mathcal{E}_{a_3p_2}-\mathcal{E}_{a_4p}+m\Omega)t} V^{bpa_2p_2}_{a_3p_2a_4p}(m)\left(F^{ap}_{a_4p}F^{a_2p_2}_{a_3p_2}\right) \\
&- \frac{2\pi}{\hbar}\sum_{a_2a_3a_4}\sum_{i_1i_2i_3}\sum_{p_2p_3p_4}\sum_{mn} e^{i(\mathcal{E}_{bp}+\mathcal{E}_{a_2p_2}-\mathcal{E}_{a_3p_3}-\mathcal{E}_{a_4p_4}+m\Omega)t} V^{bpa_2p_2}_{a_3p_3a_4p_4}(m)V^{i_1p_4i_2p_3}_{api_3p_2}(n) \\
&\quad \delta(\mathcal{E}_{i_1p_4}+\mathcal{E}_{i_2p_3}-\mathcal{E}_{ap}-\mathcal{E}_{i_3p_2}+n\Omega)\left((\delta_{i_3a_2}-F^{a_2p_2}_{i_3p_2})F^{i_1p_4}_{a_4p_4}F^{i_2p_3}_{a_3p_3}\right) \\
&- \frac{2\pi}{\hbar}\sum_{a_2a_3a_4}\sum_{i_1i_2i_3}\sum_{p_2p_3p_4}\sum_{mn} e^{i(\mathcal{E}_{bp}+\mathcal{E}_{a_2p_2}-\mathcal{E}_{a_3p_3}-\mathcal{E}_{a_4p_4}+m\Omega)t} V^{bpa_2p_2}_{a_3p_3a_4p_4}(m)V^{i_1p_4i_2p_3}_{a_2p_2i_3p}(n) \\
&\quad \delta(\mathcal{E}_{i_1p_4}+\mathcal{E}_{i_2p_3}-\mathcal{E}_{a_2p_2}-\mathcal{E}_{i_3p}+n\Omega)\left(F^{ap}_{i_3p}F^{i_1p_4}_{a_4p_4}F^{i_2p_3}_{a_3p_3}\right) \\
&- \frac{2\pi}{\hbar}\sum_{a_2a_3a_4}\sum_{i_1i_2i_3}\sum_{p_2p_3p_4}\sum_{mn} e^{i(\mathcal{E}_{bp}+\mathcal{E}_{a_2p_2}-\mathcal{E}_{a_3p_3}-\mathcal{E}_{a_4p_4}+m\Omega)t} V^{bpa_2p_2}_{a_3p_3a_4p_4}(m)V^{a_4p_4i_2p_3}_{i_3p_2i_1p}(n) \\
&\quad \delta(\mathcal{E}_{a_4p_4}+\mathcal{E}_{i_2p_3}-\mathcal{E}_{i_1p}-\mathcal{E}_{i_3p_2}+n\Omega)\left((\delta_{i_2a_3}-2F^{i_2p_3}_{a_3p_3})F^{ap}_{i_1p}F^{a_2p_2}_{i_3p_2}\right) \\
&+ \frac{2}{i\hbar}\sum_{a_2a_3a_4}\sum_{p_2}\sum_{m} e^{i(\mathcal{E}_{a_2p}+\mathcal{E}_{a_3p_2}-\mathcal{E}_{ap}-\mathcal{E}_{a_4p_2}+m\Omega)t} V^{a_2pa_3p_2}_{apa_4p_2}(m)\left(F^{a_2p}_{bp}F^{a_3p_2}_{a_4p_2}\right) \\
&- \frac{2\pi}{\hbar}\sum_{a_2a_3a_4}\sum_{i_1i_2i_3}\sum_{p_2p_3p_4}\sum_{mn} e^{i(\mathcal{E}_{a_2p_2}+\mathcal{E}_{a_3p_3}-\mathcal{E}_{ap}-\mathcal{E}_{a_4p_4}+m\Omega)t} V^{a_2p_2a_3p_3}_{apa_4p_4}(m)V^{i_1pi_2p_4}_{a_2p_2i_3p_3}(n) \\
&\quad \delta(\mathcal{E}_{i_1p}+\mathcal{E}_{i_2p_4}-\mathcal{E}_{a_2p_2}-\mathcal{E}_{i_3p_3}+n\Omega)\left((\delta_{i_3a_3}-2F^{a_3p_3}_{i_3p_3})F^{i_1p}_{bp}F^{i_2p_4}_{a_4p_4}\right) \\
&- \frac{2\pi}{\hbar}\sum_{a_2a_3a_4}\sum_{i_1i_2i_3}\sum_{p_2p_3p_4}\sum_{mn} e^{i(\mathcal{E}_{a_2p_2}+\mathcal{E}_{a_3p_3}-\mathcal{E}_{ap}-\mathcal{E}_{a_4p_4}+m\Omega)t} V^{a_2p_2a_3p_3}_{apa_4p_4}(m)V^{a_4p_4i_2p}_{i_3p_3i_1p_2}(n) \\
&\quad \delta(\mathcal{E}_{a_4p_4}+\mathcal{E}_{i_2p}-\mathcal{E}_{i_1p_2}-\mathcal{E}_{i_3p_3}+n\Omega)\left(F^{i_2p}_{bp}F^{a_2p_2}_{i_1p_2}F^{a_3p_3}_{i_3p_3}\right) \\
&- \frac{2\pi}{\hbar}\sum_{a_2a_3a_4}\sum_{i_1i_2i_3}\sum_{p_2p_3p_4}\sum_{mn} e^{i(\mathcal{E}_{a_2p_2}+\mathcal{E}_{a_3p_3}-\mathcal{E}_{ap}-\mathcal{E}_{a_4p_4}+m\Omega)t} V^{a_2p_2a_3p_3}_{apa_4p_4}(m)V^{bpi_2p_4}_{i_3p_3i_1p_2}(n) \\
&\quad \delta(\mathcal{E}_{bp}+\mathcal{E}_{i_2p_4}-\mathcal{E}_{i_1p_2}-\mathcal{E}_{i_3p_3}+n\Omega)\left((\delta_{i_2a_4}-F^{i_2p_4}_{a_4p_4})F^{a_2p_2}_{i_1p_2}F^{a_3p_3}_{i_3p_3}\right)
\end{aligned}
$$

$$
\begin{aligned}
I_{lead}^{FRE-tr} &= \frac{\pi}{\hbar}\sum_{i}\sum_{l}\sum_{nm}\Gamma^{bp}_{l}(m)\Gamma^{ip}_{l}(n)^{*}e^{-i(\varepsilon_l-\mathcal{E}_{bp}-m\Omega)t}\delta(\mathcal{E}_{ip}-\varepsilon_l+n\Omega)\left((\delta_{ai}-F^{ap}_{ip})D_l-F^{ap}_{ip}(1-D_l)\right) \\
&+ \frac{\pi}{\hbar}\sum_{i}\sum_{l}\sum_{nm}\Gamma^{ap}_{l}(m)^{*}\Gamma^{ip}_{l}(n)e^{i(\varepsilon_l-\mathcal{E}_{ap}-m\Omega)t}\delta(\mathcal{E}_{ip}-\varepsilon_l+n\Omega)\left((\delta_{bi}-F^{ip}_{bp})D_l-F^{ip}_{bp}(1-D_l)\right)
\end{aligned}
$$

where now all $a, b, i$ indices denote bands and $p, k$ indices denote momentum.

**Floquet-Boltzmann Equation**

As before, taking the diagonal limit of the Floquet Redfield equation, assuming $\omega_j = \omega_{(-j)}$ for the phonons, and under the Floquet-secular/Floquet-RWA approximation, we get

$$
\begin{aligned}
\partial_t F^{ap}_{ap} &= \frac{2\pi}{\hbar}\sum_{i_1}\sum_{k_1}\sum_{j}\sum_{n}|G^{ap}_{i_1k_1j}(n)|^2\delta(\mathcal{E}_{ap}-\mathcal{E}_{i_1k_1}-\omega_j+n\Omega)\\
&\quad\left(F^{i_1k_1}_{i_1k_1}(1-F^{ap}_{ap})N_{\omega_j}-F^{ap}_{ap}(1-F^{i_1k_1}_{i_1k_1})(1+N_{\omega_j})\right)\\
&+ \frac{2\pi}{\hbar}\sum_{i_1}\sum_{k_1}\sum_{j}\sum_{n}|G^{ap}_{i_1k_1j}(n)|^2\delta(\mathcal{E}_{ap}-\mathcal{E}_{i_1k_1}+\omega_j+n\Omega)\\
&\quad\left(F^{i_1k_1}_{i_1k_1}(1-F^{ap}_{ap})(1+N_{\omega_j})-F^{ap}_{ap}(1-F^{i_1k_1}_{i_1k_1})N_{\omega_j}\right)\\
&+ \frac{2\pi}{\hbar}\sum_{l}\sum_{n}|\Gamma^{a}_{l}(n)|^2\delta(\mathcal{E}_a-\varepsilon_l+n\Omega)\left((1-F^a_a)D_l-F^a_a(1-D_l)\right)\\
&+ \frac{4\pi}{\hbar}\sum_{a_2a_3a_4}\sum_{p_2p_3p_4}\sum_{n}|V^{apa_2p_2}_{a_3p_3a_4p_4}(n)|^2\delta(\mathcal{E}_{ap}+\mathcal{E}_{a_2p_2}-\mathcal{E}_{a_3p_3}-\mathcal{E}_{a_4p_4}+n\Omega)\\
&\quad\left((1-F^{ap}_{ap})(1-F^{a_2p_2}_{a_2p_2})F^{a_3p_3}_{a_3p_3}F^{a_4p_4}_{a_4p_4}-F^{ap}_{ap}F^{a_2p_2}_{a_2p_2}(1-F^{a_3p_3}_{a_3p_3})(1-F^{a_4p_4}_{a_4p_4})\right) \qquad (6.17)
\end{aligned}
$$

which is known as the Floquet-Boltzmann Equation (FBE). Here again, $a, i$ indices denote Floquet bands and $p, k$ indices denote momenta. Recall that momentum conservation is hidden in the couplings $G, V$.

### 6.5 Simulation of the Floquet-Redfield Equation

In this section, we present an extension of the work in Ch. 3 that contains preliminary, unpublished results of simulating the FRE with translational invariance for the case of electron-electron interactions and a phonon bath (a lead has been omitted). As in Ch. 3, we have a low phonon temperature of $\Delta_A/10$ where $\Delta_A$ is the Floquet gap between the UF and and LF bands. Furthermore, we restrict the bandwidth ($\Omega_D$) of the acoustic phonons to $\Delta_A < \Omega_D < \Delta_B$ such that phonons strictly cool the system while interactions heat the system.

In simulating the FRE with translational invariance (Eq. 6.16), we only include the second order terms ($\mathcal{O}(V^2)$,$\mathcal{O}(G^2)$ terms) and omit the first order ($\mathcal{O}(V)$) term in the FRE which accounts for the renormalization of the quasienergies and the renormalization of the Rabi frequencies due to interactions (interactions induce non-zero Rabi frequencies in the Floquet basis).

As discussed in Ch. 3, increasing interaction strength ($V$) relative to the phonon strength ($G$) causes heating of the system as evidenced by the steady-state occupation of the lower Floquet band (Fig. 6.5) transitioning from a near Floquet-insulator state ("cold" state) to a near infinite-temperature state ("hot" state). From simulating the FRE, we also obtain information about the off-diagonal Floquet-band coherences (a.k.a. polarizations) whose magnitude is a slow/steady variable. Interestingly, the steady-state polarization magnitude (Fig. 6.5) is minimal near the cold/hot states and peaks when the system is transitioning from one to the other. This can be understood as follows. The

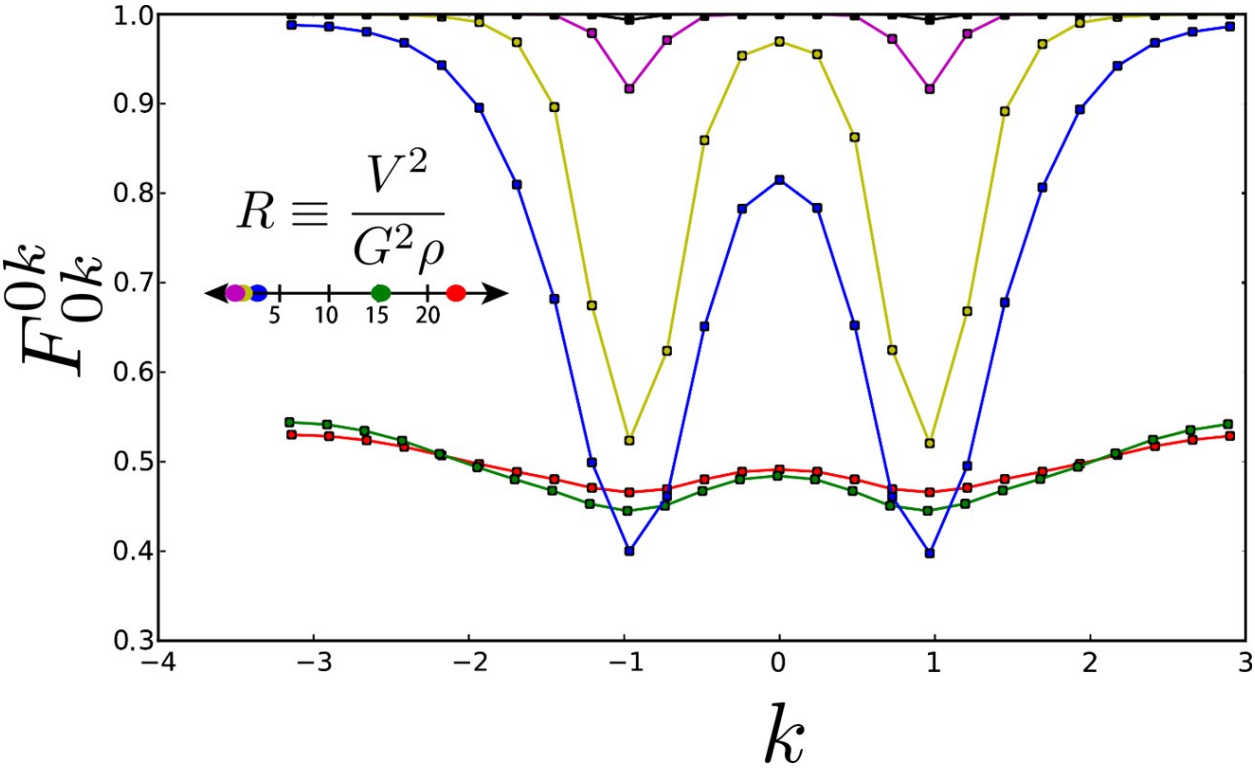


Figure 6.1: Steady-state occupation of the lower Floquet band as a function of the ratio of bare electronic interaction ($V$) and electron-phonon ($G$) couplings (scaled by $\rho$, the partial density of states for the phonon bath). As interactions get stronger relative to the phonons (which cool the system), the system heats up from a near perfect Floquet-insulator state to the an almost infinite temperature state.

cold/hot states are both thermal states with effectively small/large temperatures and so we expect that polarizations vanish when the system approaches either of the thermal points. In between, however, the system is quite far from thermal and so stronger polarizations appear. The overall magnitude of the polarizations are quite weak in comparison to the occupations and so we conclude that the effects are polarizations are negligible near steady-state. Consequently, the FBE is a good approximation for long-time dynamics near steady-state. However, this conclusion is predicated on omitting the linear interaction term which should be taken into for a more thorough analysis. Adding the linear interaction term and further analysis of the parameter space is a direction for future work.

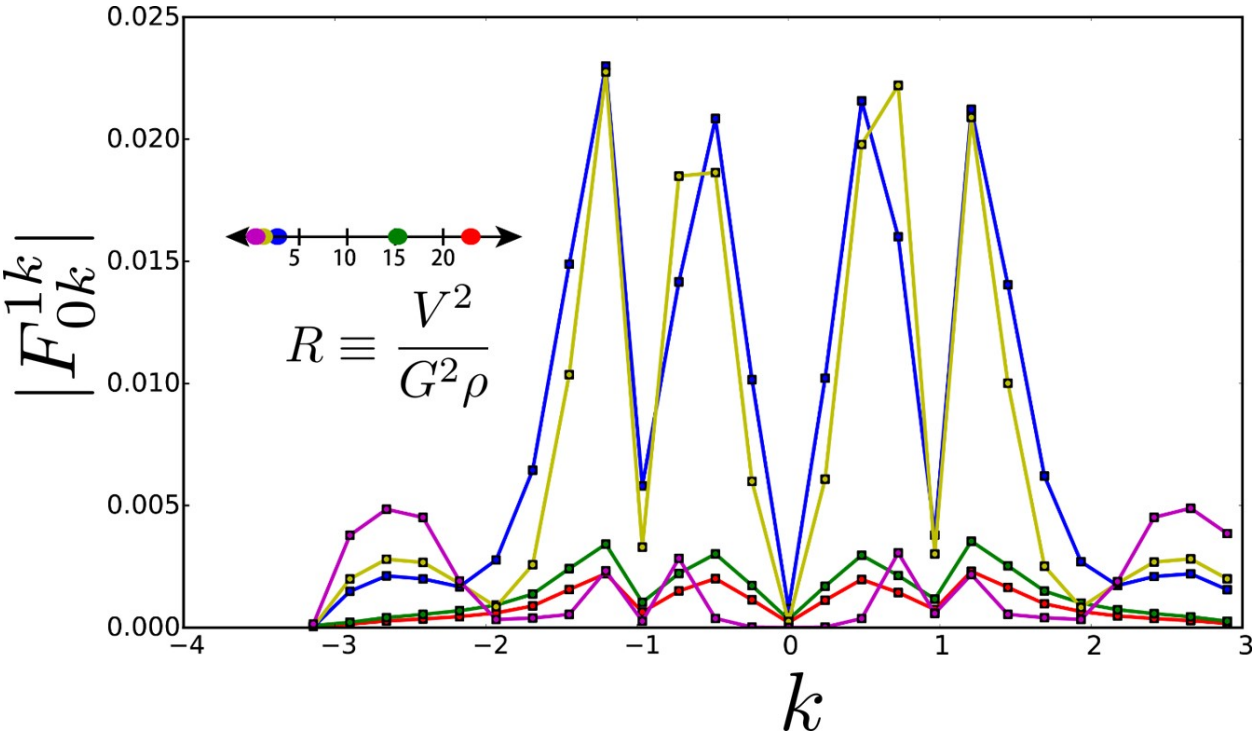


Figure 6.2: Steady-state magnitude of the off-diagonal Floquet-band polarization. We see that as a function of increasing interaction strength, the polarization is non-monotonic. Near the Floquet-insulator state (small $R$) and near the the infinite-temperature state (large $R$), there is minimal polarization. The polarization peaks when transitioning between these two cold/hot "thermal" points.